ABSTRACT

Title of Dissertation: INVESTIGATION INTO THE ROLE OF UVR8 IN BALANCING GROWTH AND ACCLIMATION TO UV-B RADIATION IN NATURAL AND TRANSGENIC *POPULUS* VARIANTS

Tiffany M. Wong, Doctor of Philosophy, 2021

Dissertation directed by: Professor Joseph Sullivan
Department of Plant Science and Landscape Architecture

Professor Edward Eisenstein
Fischell Department of Bioengineering

Research on woody plants offers promise for the development of next-generation biofuel feedstocks with reduced lignin recalcitrance and enhanced saccharification for ethanol production. Natural variants of *Populus trichocarpa* with diverse lignin content and saccharification differences, and transgenic *Populus deltoides* constructed for reduced lignin levels for improved cellulose extraction, offer clues to enhance biofuel production but with a tradeoff to overall fitness and biomass. One concern of engineering lignin relates to the protection of plants against environmental stress such as UV-B radiation. Secondary metabolite biosynthesis initiated by UV-B, particularly phenylpropanoids (lignin precursors) and flavonoids, plays an important role in managing and protection of UV

stress. Genetic modifications affecting the production of these compounds may have significant physiological consequences. Thus, the goal of this research was to develop a model for biosynthetic compensation of low-lignin *Populus* to UV-B stress. The effect of UV-B on *Populus* was evaluated by spectroscopic and metabolomic measurements on leaves. UV-B promoted shifts in physiological and metabolomic responses of natural and transgenic *Populus* with varying levels of lignin were complex, reflecting compensation from variety of biosynthetic alterations. Therefore, the impact of modulating the expression of the photoreceptor, UVR8, in regulating the response of *Populus* to UV-B was pursued. Modulation of *UVR8* expression in *Populus* hybrid was achieved by constructing transgenic plants using CRISPR and RNAi, in wild-type, and an RNAi-constructed cinnamyl alcohol dehydrogenase knockdown line. UV-B response of *UVR8* modulated *Populus* indicated that flavonoids were upregulated in *UVR8* overexpression lines, and that in a *CAD* knockdown background, these effects were slightly enhanced. Salicylates were upregulated in *UVR8* knockout poplars, suggesting metabolic flux in the pathway, but little difference was seen relative to wild-type plants in *CAD* lines, and UV-B treatment had little effect. An interesting and unexpected finding was that *UVR8* modulated *Populus* exhibited more rapid growth than wild-type plants. The findings underscore the key role of UVR8 in synchronizing protective metabolic responses to UV-B and suggest an additional function of the photoreceptor in regulating growth and development of *Populus* through shifts in the chemical equilibria of UVR8 monomers and dimers and interactions with other regulatory factors.

INVESTIGATION INTO THE ROLE OF UVR8 IN BALANCING GROWTH AND ACCLIMATION TO UV-B RADIATION IN NATURAL AND TRANSGENIC *POPULUS* VARIANTS

by

Tiffany M. Wong

Dissertation submitted to the Faculty of the Graduate School of the
University of Maryland, College Park, in partial fulfillment
of the requirements for the degree of
Doctor of Philosophy
2021

Advisory Committee:
Professor Joseph Sullivan, Chair
Professor Edward Eisenstein, Co-Chair
Professor Gary Coleman
Professor Stephen DiFazio
Professor Ganesh Sriram

Dedication

This dissertation is first and foremost dedicated to my mother, Mandy, because she made many sacrifices so that I could be across the country and achieve this degree. Additionally, this is a dedication to all underrepresented girls, women, and gender-nonconforming individuals in STEM.

Acknowledgements

There are many people without whom this dissertation may not have been completed, to which I am eternally thankful. My deepest appreciation to my advisors, Drs. Joseph Sullivan and Edward Eisenstein for continuously believing in me and this research and providing me with support and guidance to move forward. I wholeheartedly emphasize how tremendously supportive Ed has been in developing this project and taking a chance on agreeing to co-advise me throughout this academic journey. I am grateful for my committee members, Drs. Gary Coleman, Stephen DiFazio, and Ganesh Sriram, for providing individual expertise and feedback that challenged me to develop my ideas and confidence in my work. Special thanks to Dr. Wendy Peer for her contributions to this project. I would like to thank Drs. James Parsons and Ken Keefover-Ring (University of Wisconsin-Madison) for their patience in training me to use the LC-MS, Dr. Liang Hu for providing me with helpful advice in the lab, and Dr. Gen Li for his assistance in the tissue culture lab and various lab assays that was crucial for my work. I express my gratitude towards Sydney W., Meghan F., Frank C., and Caroline H. for helping me in maintaining hundreds of poplar trees over the years.

I am grateful for the support and love from my mom, Tony, Julie, Lilyan, and Ian. I would also like to thank Dr. John Matthews from the Telescope Array Project (University of Utah) and Dr. Jonathan and Pricilla Titus (SUNY Fredonia) for their encouragement because my academic background was unconventional, but these people believed in me and inspired me to continue my education. (I'm going to be this person for a moment, special shout-out to Ophelia, Oliver, and Chilly for traveling across the country multiple times and

providing a non-human source of love and companionship.) Being away from my family and making a life for myself on the East coast was not easy so, I want to specifically acknowledge those for significantly impacting my life through the various and sometimes subtle ways in showing their unconditional support, especially during the tenuous and most difficult moments: Dr. Jessica D., Andrew M. & Dr. Peter B., Kat F., Ian M., Dr. Kris N., Alex C.S., Dr. Nancy F.S., Kristin M. & Nick D., Josh A., Angie H. & Steve C., Trevor H., Clinton S., Phil V., Gabby G. & Jack G.M., Jason F., Silas N., Anders G., Jonathan T., Nic, T., Eclipse R., John S., and last but not least, Geraldine G.

Table of Contents

List of Tables

List of Figures

List of Abbreviations

CAD	Cinnamyl alcohol dehydrogenase protein
CAD	Cinnamyl alcohol dehydrogenase gene
CaMV 35S	Cauliflower mosaic virus promoter
CHI	Chalcone isomerase
COP1	CONSTITUTIVE PHOTOMORPHOGENIC 1
CRISPR	Clustered regularly interspaced short palindromic repeats
Cas9	CRISPR associated protein 9 endonuclease
CRYs	Cryptochromes
dCas9	deactivated or dead Cas9 endonuclease
E3	Ubiquitin ligase
F_v/F_m	Variable fluorescence ($F_m - F_o$) / maximum fluorescence (F_m)
GFP	Green fluorescent protein
gRNA	Guide RNA
HY5	ELONGATED HYPOCOTYL 5
KD	Gene knockdown
KO	Gene knockout
OX	Overexpression
PAR	Photosynthetically active radiation
PPFD	Photosynthetic photon flux density
Pfr	Red light active phytochrome
Pr	Far-red light inactive phytochrome
PIFs	PHYTOCHROME INTERACTING FACTOR

QE	Quercetin equivalents
RNAi	RNA interference
ROS	Reactive oxygen species
RUP1	REPRESSOR OF UV-B PHOTOMORPHOGENESIS 1
RUP2	REPRESSOR OF UV-B PHOTOMORPHOGENESIS 2
SNP	Single nucleotide polymorphism
TAC	Total anthocyanin content
UV-A	Ultraviolet radiation A
UV-B	Ultraviolet radiation B
UV-C	Ultraviolet radiation C
UVR8	UV RESISTANCE LOCUS 8 protein
UVR8	UV RESISTANCE LOCUS 8 gene
U3	Ubiquitin 3 RNA polymerase III promoter
U6	Ubiquitin 6 RNA polymerase III promoter
WT	Wild-type

Chapter 1: Background, General Knowledge, and the Effects of UV-B Radiation on Trees

Although all plants require sunlight for healthy growth and development, it can be a double-edged sword in that ultraviolet radiation in sunlight can cause significant damage to living organisms. Plants are exposed to a variety of intensities of UV radiation depending on the natural environment, and the responses can vary significantly as well. Hence, it is worthwhile to review what is known about how plants respond to UV radiation, and especially how poplar, including variants modified for use as a biofeedstock, tolerates the abiotic stress of UV radiation.

The Importance of Sunlight – Sunlight. It is hard to imagine life without it as so many biological processes are tethered to this energy in some way. It is important for our physical and mental well-being and regulates our sleep. But too much sunlight may be detrimental, with harmful effects from ultraviolet radiation ranging from a bothersome skin irritation known as 'sunburn' to various skin cancers. Plants are no different. Sunlight is critical for plant growth and development. Solar irradiance is an important source of light energy for plants. It is required for photosynthesis, the process whereby plants synthesize sugar from water and CO_2. Additionally, sunlight is utilized by plants as a signal to carry out specific physiological processes. But the ultraviolet radiation in sunlight can also be harmful to plants as it is in humans. Much of the recent mechanistic research on the effects of potentially damaging UV-B radiation (between 280 and 315 nm) from sunlight has been

conducted on model annual plants, such as *Arabidopsis thaliana*. But because so many perennial plants have considerable economic value, and because their physiology displays a number of unique attributes that reflect their life cycle, molecular studies on the effect of ultraviolet light on perennial plants, including trees, are important and research such as that described here will help fill significant gaps in our knowledge. This dissertation is focused on the molecular effects of ultraviolet radiation in the UV-B range on poplar, an important feedstock for biofuel and bioproducts. This study has uncovered a new aspect in the mechanism of the photoreceptor for UV-B radiation in poplar, UVR8, and proposes a new hypothesis for its mechanism of action in trees. These findings should be important for many next-generation applications in plant biology.

In photosynthesis, plants use light energy and the uptake of inorganic molecules, including water, carbon dioxide, and minerals, in order to synthesize organic compounds, such as carbohydrates, lipids, amino acids, and certain pigments while releasing oxygen as a byproduct through the stomata. Light quality is critical for photosynthesis, and plants respond to specific wavelengths on the electromagnetic spectrum. The spectral response of photosynthesis occurs in the region of visible light between wavelengths of 400-700 nm, which is known as photosynthetically active radiation (PAR) (Wargent and Jordan 2013). Light quantity, or irradiance levels of absorbed PAR, can affect plant growth and development. Full sunlight is considered to be approximately 2000 μmol m^{-2} s^{-1}. Increased irradiance levels of PAR can promote more photosynthesis; however, excessive light saturation can lead to photoinhibition and impairment (Demmig-Adams and Adams 2000).

Because plants rely on light quality and quantity for photosynthesis and plant productivity, the characteristics of light sources have been measured for many years and in several ways. The action spectrum of photosynthesis is calculated by the rate of carbon dioxide uptake or oxygen evolution divided by the rate of absorbed energy of a leaf (McCree 1971). Another parameter used to measure photosynthesis is quantum efficiency, which is derived from the action spectrum divided by the absorbed quanta (unit of photons) (Emerson 1958). Sunlight and other sources of light energy can be measured as photometric units (illuminance in footcandles), radiometric units (irradiance in $W \cdot m^{-2}$), and quantum units (photon flux density in $\mu mol\ m^{-2}\ s^{-1}$) as the accepted primary method of reporting data (Thimijan and Heins 1983).

The Dark Side of Sunlight – Ultraviolet Radiation – All photosynthetic organisms such as plants and algae depend on PAR to survive. However, approximately 7% of solar energy is comprised of UV radiation. Ultraviolet radiation is categorized into three classes: UV-A (315-400 nm), UV-B (280-315 nm), and UV-C (100-280 nm) (Stapleton 1992). The Earth's atmosphere contains a protective layer of ozone that exists in the stratosphere between approximately 20 to 50 km above the Earth's surface that absorbs solar ultraviolet radiation (UV) (Staehlin et al. 2001). Protection by the ozone layer is afforded by absorption of the most harmful, high-energy, short wavelength UV-C radiation, as well as most of the UV-B radiation. By contrast, longer wavelength UV-A radiation, is not attenuated by ozone and unlike UV-B and UV-C, is not sensitive to changes in stratospheric ozone levels. Approximately 95% of UV-B radiation entering the terrestrial level of the

Earth's atmosphere is absorbed by ozone, but the remaining amount that is left unfiltered can significantly affect plant productivity (Frohnmeyer and Staiger 2003, Sullivan 2005).

Ozone depletion is of concern because the stratospheric ozone column is the primary attenuator of solar UV-B radiation. A decrease in this ozone column will lead to increases in UV-B radiation, (at wavelengths above approximately 290 nm), reaching the earth's surface (Frederick et al. 1989). Spectral measurements indicate that UV-B at 300 nm increased in the twentieth century (Kerr and McElroy 1993). Zerefos et al. (1997) found that UV-B radiation was increasing at a rate of 27% per decade over northern Europe (Zerefos et al. 1997). In the southern hemisphere, Searles et al. reported that ground-based measurements showed that UV-B levels exceeded model estimates prior to ozone depletion over Tierra del Fuego (Searles et al. 1999) and McKenzie et al. found increased intensities of UV-B even at the lower latitudes of New Zealand (McKenzie et al. 1999). At mid-latitudes, data from the Smithsonian monitoring network that weighted UV-B has increased at a rate of about 1.8% percent per year in the 1980s and 1990s (Neale et al. 2004). NASA models indicate that about half of this increase can be directly attributed to loss of stratospheric ozone. These data provide alarming evidence that the increase in UV-B radiation is related to stratospheric ozone reduction since the spectral signature of the change were correlated with the absorption spectrum of ozone (Appenzeller 1993).

Although the ecological implications of ultraviolet radiation have been of interest for the past half-century (Caldwell 1968), interest in the response of plants to UV-B radiation increased with the threat of anthropogenic ozone depletion was recognized in the 1970s

(Molina and Rowland 1974). The depletion of ozone is largely driven by compounds containing chlorine and bromine that have been linked to anthropogenic emissions with dramatic depletions observed in polar regions (Molina and Rowland 1974, Programme 2014). The "Montreal Protocol" was signed by the US in 1987 following ratification by many other countries and with the cooperation of most major nations. The agreement, considered to be the first multi-national environmental treaty of its kind, has been extremely successful in transitioning society away from the use and production of chlorofluorocarbons (CFCs) and other halocarbon substances that reduce ozone (Neale et al. 2021). However, the ozone layer is still in critical condition. For example, although there has not been a recent increase in volcanic eruptions, large scale volcanic activity can have long-lasting and dramatic effects on climate patterns caused by massive release in sulfuric gases and ash into the stratosphere (Klobas et al. 2017). Additionally, halogen radicals from volcanic eruptions have been associated with the increase in UV radiation with the potential of depleting global ozone by ~20%, which predominantly affect polar regions. Although the ozone has been recovering slowly, in October of 2015, the largest ozone hole ever reported was discovered over Antarctica, resulting in an increase of over 400% in biologically active UV reaching terrestrial surfaces (Solomon et al. 2016, Brenna et al. 2019). Thus, while the use of the remaining stock of CFCs has been reduced and is being phasing out, and there has not been a dramatic release of volcanic halogens, the ozone layer is still recovering, and should continue to be monitored by a variety of approaches (Rozema et al. 2009). Importantly, these conditions portend an increase in incident UV radiation reaching the Earth's surface, thereby underpinning the importance of a study of the effects UV radiation on biological organisms, especially plants.

Satellite imaging and modeling have shown significant increases in UV-B radiation of the Earth's surface from ozone thinning between 1979-2008 (Herman 2010). The threat of increased UV-B radiation has therefore stimulated a field of research in environmental and plant responses to UV-B radiation. Although the stratosphere has been slowly recovering due to the success of the Montreal Protocol, there are other factors that contribute to increased exposure to UV-B radiation. Environmental factors that can influence UV-B exposure include aerosols, cloud albedo, deforestation and other agricultural practices that reduce canopy cover and increase ground exposure (Ballare et al. 2011, Bais et al. 2015). Particles in the atmosphere, called aerosols, can affect the atmospheric transmission of solar radiation on the terrestrial level. Aerosols may be naturally generated by the wind (dust and sea salt) or via anthropogenically derived materials (sulfates and organic particles). Aerosols can scatter and absorb UV photons in particularly polluted countries such as Russia compared to a less polluted country such as New Zealand (Palancar et al. 2013).

The angle of solar radiation is another factor that can influence the intensity of UV on the terrestrial surface. Illumination at low latitudes or on a near perpendicular 90˚ angle from the sun provides the most direct and concentrated amount of solar radiation over the smallest surface area. These effects result in warmer temperatures and higher levels of UV-B and UV-A. At higher latitudes, the solar angle is lower and the pathlength of radiation is spread over a larger area, with cooler temperatures prevailing, and UV-B being mostly attenuated by ozone (Paul and Gwynn-Jones 2003). Latitudinal, diurnal and

seasonal variation also contribute to the intensity of UV-B radiation on the terrestrial level. The position of the earth around the sun is another seasonal variation that affects intensity of solar radiation. When the Earth's elliptical orbit is closest to the sun around January 5 (perihelion) and farthest away around July 5 (aphelion), the sun-earth distance results in variation of UV intensity of about 7% and results in higher UV levels in northern hemisphere winters and southern hemisphere summers (Diffey 2002). Elevation and latitude can impact the level of UV-B radiation on plants. At low latitude, levels of biologically effective UV-B have been reported to be approximately 10.8 kJ m^{-2} at 0 m and 12.4 kJ m^{-2} at 3,000 m in Hawaii (20 °N) (Ziska et al. 1992). In Denmark (55 °N) a low-lying country at high latitude, the highest elevation peak in is 170 m receives an average annual dose of 1.9 kJ m^{-2} and in Greece (40 °N) at 2,500 m in altitude, UV-B radiation levels averages to 5.5 kJ m^{-2} annually (ONeill et al. 2016). It is clear that a variety of factors may influence environmental UV-B radiation levels and how it may affect evolutionary adaptions in plants for protection. Interestingly, it has been shown that plants which grow natively along lower latitudes and/or at higher elevation display more pronounced adaptation to UV-B radiation when compared to those at higher latitudes and/or lower elevation (Sullivan et al. 1992).

The Response of Plants to UV Radiation – Although representing only a fraction of the total solar electromagnetic spectrum, UV-B has a disproportionately large photobiological effect due to its absorption by important macromolecules such as proteins and nucleic acids (Giese 1964, Jansen et al. 1998). Therefore, it is not surprising that both plant and animal life are greatly affected by UV-B radiation. Some 400 species of plants have been screened

for sensitivity to UV-B radiation and of these, about two-thirds were found to be sensitive in some growth or physiological parameter (Sullivan and Rozema 1999). However, a wide range of responses have been found and the interpretation of these studies is hindered by the contrasting experimental conditions employed, interactive factors such as low light levels and artifacts due to the artificial experimental conditions. For instance, some plants appear quite tolerant to even high fluences of UV-B (Sullivan and Teramura 1992) while others are sensitive to even present ambient fluences (Bogenrieder and Klein 1982, Krizek et al. 1997). This variation in response to UV-B radiation makes it difficult to generalize its effects, and perhaps more importantly, implies the importance of UV-B radiation throughout the evolution of land plants.

The wide range of response differences also suggests that some plants have well-developed UV protection mechanisms (Beggs et al. 1986) in place while others may lack them to some extent. As sessile organisms, plants are restricted in their movement and have evolved unique strategies to adapt to a tremendous range of environmental conditions, including adaptation to UV-B radiation. For example, vascular plants can display salt tolerance (Volkov and Beilby 2017), and can adapt to flooding stress (Jackson and Colmer 2005), drought (Basu et al. 2016), frequent temperature fluctuation (Zheng et al. 2011), and heavy metal toxicity (Sharma and Dietz 2006). And, not only must plants generate a protective response to harmful UV radiation, and develop UV tolerance, they also utilize this energy to improve biological fitness (Jansen et al. 1998). Acclimation to UV-B radiation has been observed in many species, as rapidly as within hours after exposure to

several days after irradiation (Jansen 2002, Casati and Walbot 2004, Gruber et al. 2010, Barnes et al. 2016).

Generally, the high energy photons of UV-B radiation are absorbed by the leaf with very low levels of reflectance or transmission. This energy is readily absorbed because the biomolecules (DNA, lipids, proteins, lignin, and metabolites) found in plants contain double bonds that delocalize π electrons, rendering them receptive targets to UV-B radiation, although absorbing this energy can result in harm to cells and organelles. Prolonged exposure to UV-B radiation causes displacement of electrons from their orbitals resulting in chemical bond breakage, and subsequent formation of reactive oxygen species (Hideg and Strid 2017, Weselake et al. 2018). Consequently, new chemical bonds can form, and other cellular aberrations and genetic mutations can arise that can affect overall plant health. Even very low UV-B fluence rates can lead to at least minimal levels of damage to plant DNA (Sutherland et al. 1996, Bennett et al. 2001, Sullivan et al. 2010).

The shielding of DNA and other targets from UV damage has long been attributed to the protective effect arising from the biosynthesis of aromatic compounds particularly in the leaf epidermis that absorb much of the potentially damaging UV-B photons (Caldwell et al. 1983, Beggs et al. 1986). These compounds have also been shown to mitigate UV damage by scavenging reactive oxygen species (ROS) (Xu et al. 2008, Xuet al. 2010). Some plants treated with UV radiation increase their ability to scavenge reactive oxygen species, and even after several days post-exposure, UV-B tolerance remains (Jansen et al. 1996, Jansen et al. 1998). For example, *Spirodela oligorrhiza* treated with UV-B radiation

were found to accumulate UV absorbing pigments as well as display enhanced ROS scavenging ability, thereby providing sustained protection (Jansen et al. 1996). In addition to the induction of UV-screening compounds and ROS scavengers, other, photomorphogenic responses, such as changes in leaf anatomy and morphology or changes in internode elongation may improve tolerance to UV-B and other stressors (Kim et al. 1998, Ballare 2003).

Chemical and morphogenic changes in the leaf epidermis can reduce UV penetration through the epidermis and into the mesophyll where damage to critical membranes and macromolecules may occur (Day 1993, Day et al. 1994). Therefore, many plants are quite tolerant to UV radiation. Consequently, UV absorbing compounds can mitigate stress, and it has been proposed that damage and acclimation may be difficult to distinguish under ambient exposure (Hideg et al. 2013). Furthermore, in order to detect substantial or meaningful differences in the response of different plants to UV radiation, it may be necessary to push tolerance beyond ambient levels.

Plants have evolved a number of ways to adapt and acclimate in response to UV-B radiation, whether directly by preventing damage to photosynthetic machinery, or indirectly through photomorphogenesis. One of the main injurious effects to plants stemming from UV-B radiation damage is to photosystem II, which results in reduced chlorophyll fluorescence, a decrease in oxidative capacity of reaction centers, and attenuated carbon fixation or ribulose-bisphosphate carboxylase oxygenase (RuBisCO) activity (Sullivan and Teramura 1994). The majority of the reactive oxygen species are

produced in the mitochondria and chloroplasts stemming from electron misdirection to oxygen and the formation of superoxide (Britt 1996). Further damage to DNA can occur when it absorbs UV-B photons and forms cyclobutane pyrimidine dimers (CPDs) and pyrimidine (6-4) pyrimidinone dimers, which impede transcription and replication (Strid et al. 1994, Hideg and Vass 1996, Czégény et al. 2014). Genetic lesions that are formed from UV-B radiation can undergo base excision repair or double-strand break repair to prevent inherent mutations (Britt 1996).

Acclimation to UV-B radiation is an indirect response that involves tightly regulated biochemical and physiological processes coming together in concert to tolerate stress over time. This coordinated effort revolves around UV-B radiation as an environmental regulator that can control gene expression and cellular and metabolic processes, as well as photomorphogenesis (Jenkins 2009). Acclimation prevents the harmful effects of UV-B radiation under ambient conditions, and one might consider that when a plant is hardened to UV-B and better protected from previous stress then one might consider that a "good stress response." Thus, it can be a positive component for development by promoting acclimation to UV-B radiation (Hideg et al. 2013). For example, although acclimation can be difficult to distinguish from damage andrepair, it can be thought of as a balancing act between these functions in a dynamic environment (Jansen et al. 1998).

UV-B radiation can also play a role in plant regulatory pathways and induce the expression of genes that result in UV protection. Plants and algae have evolved a special adaptation to detect the energy from UV-B radiation via a photoreceptor known as UVR8 (UV

RESISTANCE LOCUS 8) (Brown et al. 2005). In the absence of UV-B radiation, the UVR8 receptor maintains as an inactive, homodimeric structure that resides in the cytoplasm. Upon excitation by UV-B radiation, the dimer dissociates to active monomers and translocated to the nucleus. The active, monomeric UVR8 receptor interacts with COP1 (CONSTITUTIVELY PHOTOMORPHOGENIC 1), an E3 ubiquitin ligase that regulates many transcription factors, including HY5 (ELONGATED HYPOCOTYL 5), resulting in the transcription initiation of genes promoting photomorphogenesis and UV protection (Fig. 1-1) (Favory et al. 2009, Cloix et al. 2012).

The structure of each UVR8 monomer is a seven-bladed β-propeller domain that is held together noncovalently as a dimer by a network of arginine salt bridges that are disrupted in the presence of UV-B. The dimer interface contains nine groups of aromatic residues that form a surface that includes a pyramidal arrangement of tryptophan chromophores. Excitonic coupling of this tryptophan cluster is important for disrupting interfacial salt bridges, promoting the formation of monomers as a result of sensing UV-B radiation (Christie et al. 2012). The UV-B promoted dissociation of dimers to monomers is relatively rapid, occurring within 15 minutes, and biochemical studies suggest that the reassembly of UVR8 dimers may be relatively slow *in vitro*, although it is thought to occur more rapidly *in vivo*. Reassembly is facilitated in plants by the RUP1 and RUP2 (REPRESSOR OF UV-B PHOTOMORPHOGENESIS) proteins, which bind to UVR8 monomers to accelerate their reassembly. Thus, RUP proteins provide negative feedback

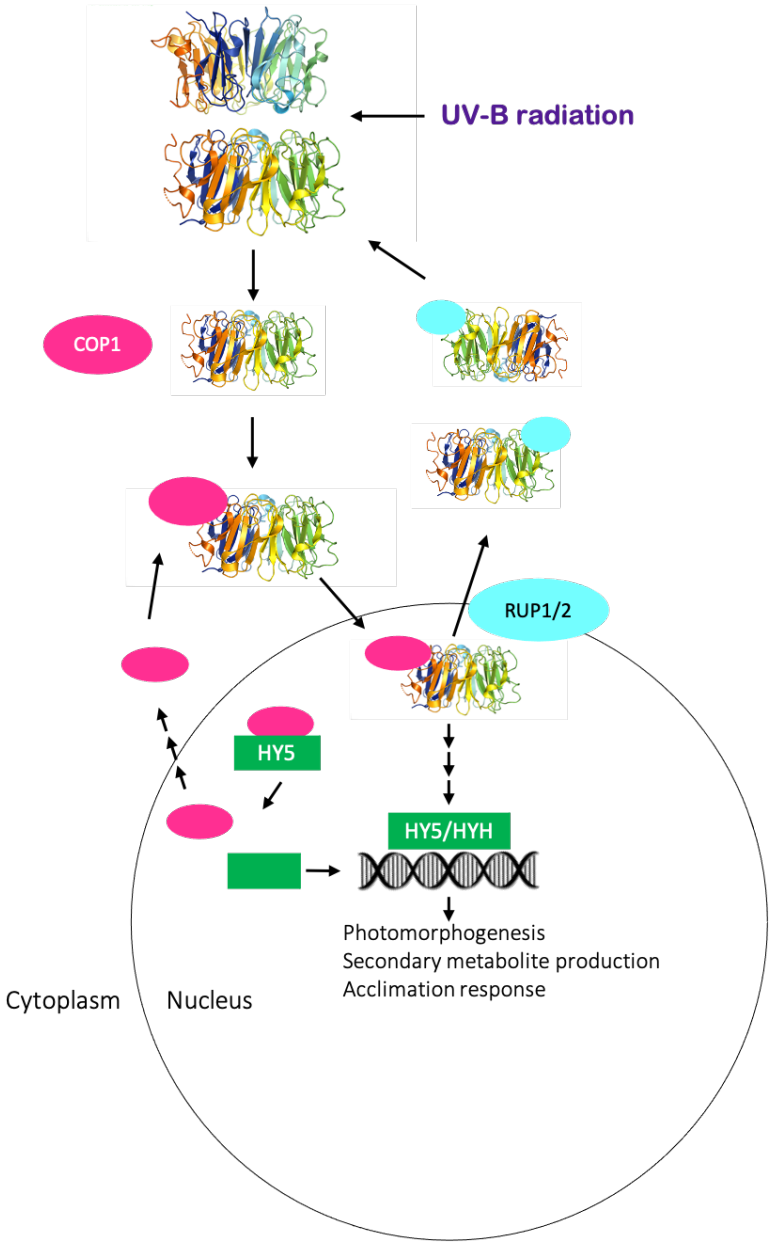

Figure 1-1. Proposed model of the UVR8 signaling pathway. In the absence of UV-B, UVR8 is mainly a dimer at rest and COP1 (pink ovals) represses photomorphogenesis by degrading HY5 (green rectangles) and other transcription factors. However, HY5 and HYH (HY5 homolog) is controlled by negative feedback from phytochromes and cryptochromes. In the presence of UV-B radiation, UVR8 monomerizes and interacts with COP1 to form the UVR8-COP-SPA complex to stabilize and promote and activate UV-B responsive genes for secondary metabolite production and acclimation. RUP1 and RUP2 (cyan ovals) compete with COP1 to interact with UVR8 to promote re-dimerization of UVR8.

on the action of the receptor by promoting dimerization (Findlay and Jenkins 2016). Research on *Arabidopsis* UVR8 has revealed it was a signaling component involved in regulating the expression of essential genes for plant protection from UV-B radiation (Brown et al. 2005). Early work showed that genes that were reduced in expression upon exposure to UV-B were identified by comparison of wild-type with *uvr8-1* knockout plants, and genes that were up-regulated were identified by a comparison of wild-type at high and low UV-B fluence rates relative to the genes found in *uvr8-1* at high and low fluence rates. The analysis yielded 72 UV-B-induced genes indirectly regulated by UVR8 (Brown et al. 2005). The regulated genes include the type II photolyase PHR1 involved in DNA repair, most of the flavonoid biosynthetic genes, as well as other secondary metabolites that play vital functions in protecting plants against UV-B radiation. However, some of the genes identified are involved in the response of *Arabidopsis* to UV stress (Brown and Jenkins 2008, O'Hara et al. 2019). Subsequent work identified the importance of the interaction of UVR8 with COP1 to promote the transcriptional response to UV-B (Favory et al. 2009), and the expression of photomorphogenic genes stemming from the increased stability of HY5 due to the formation of the UVR8-COP1 complex (Huang et al. 2013).

Transcriptional activity stemming from UVR8 activation results in the biosynthesis of UV absorbing compounds and pigments that reduce the transmission of UV-B radiation into the leaf epidermis (Shamala et al. 2020, Kliebenstein et al. 2002, Wu et al. 2016). These specialized metabolites are produced via the well-characterized phenylpropanoid pathway, which marks the divergence between primary and secondary metabolite biosynthesis in

plants (Fig. 1-2). The first step in the phenylpropanoid pathway is the conversion of L-phenylalanine into trans-cinnamic acid and ammonia via the action of phenylalanine ammonia-lyase (PAL). Cinnamate is then hydroxylated by a cytochrome-containing cinnamate 4-hydroxylase (C4H) to form p-coumaric acid (4-coumaric acid) (Fraser and Chapple 2011). In the next step, 4-coumaryl-CoA ligase converts p-coumaric acid to 4-coumaroyl-CoA, from which lignin, flavonoids, salicylates and other important phenolics are derived (Knobloch and Hahlbrock 1977). The first committed step in the production of a variety of flavonoids and anthocyanins occurs when 4-coumaroyl-CoA is converted into naringenin-chalcone via chalcone synthase (CHS) (Graham 1998, Ayabe and Akashi 2006, Mellway et al. 2009). Naringenin-chalcone is abundant and possess a wide range of biochemical activities. It contains two aromatic rings that form the base for many flavonoids. The modification of the parent compound by a variety of enzymes gives rise to six main classes of compounds: chalcones, flavones, flavonols, flavandiols, anthocyanins, and condensed tannins (Winkel-Shirley 2002).

Flavonoids have two absorption maxima in the UV range (240-280 nm and 300-380 nm) and have been known to mitigate UV-B promoted stress because the aromatic rings in flavonoids contain π electrons that absorb UV photons (Mabry et al. 1970, Kootstra 1994). Flavonoids are predominately stored in vacuoles and provide protection to the mesophyll tissue in leaves by transporting and accumulating metabolic compounds including other phenolics such as hydroxycinnamates in the epidermis (Caldwell et al. 1983, Burchard et al. 2000). Further into the pathway is the flavonoid class including anthocyanins and

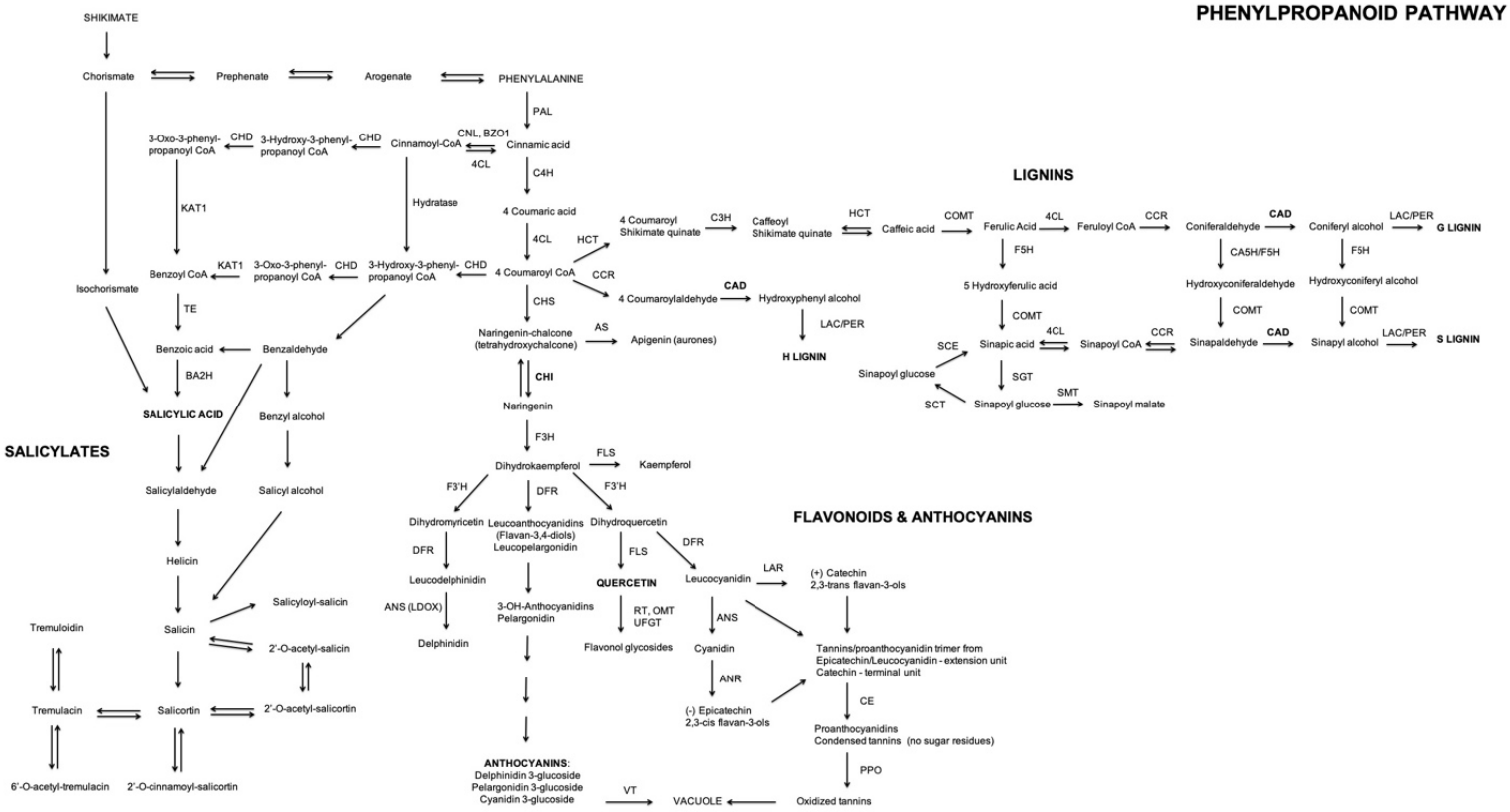
PHENYLPROPANOID PATHWAY
SHIKIMATE
Chorismate
Prephenate
Arogenate
PHENYLALANINE
PAL
Cinnamic acid
C4H
4 Coumaric acid
4CL
4 Coumaroyl CoA
Cinnamoyl-CoA
CNL, BZO1
4CL
3-Oxo-3-phenyl-propanoyl CoA
CHD
3-Hydroxy-3-phenyl-propanoyl CoA
CHD
KAT1
Hydratase
Isochorismate
Benzoyl CoA
KAT1
3-Oxo-3-phenyl-propanoyl CoA
CHD
3-Hydroxy-3-phenyl-propanoyl CoA
CHD
TE
Benzoic acid
Benzaldehyde
BA2H
SALICYLIC ACID
Benzyl alcohol
SALICYLATES
Salicylaldehyde
Salicyl alcohol
Helicin
Salicin
Salicyloyl-salicin
2'-O-acetyl-salicin
Tremuloidin
Tremulacin
Salicortin
2'-O-acetyl-salicortin
6'-O-acetyl-tremulacin
2'-O-cinnamoyl-salicortin
HCT
4 Coumaroyl Shikimate quinate
C3H
Caffeoyl Shikimate quinate
HCT
Caffeic acid
COMT
Ferulic Acid
4CL
Feruloyl CoA
CCR
Coniferaldehyde
CAD
Coniferyl alcohol
LAC/PER
G LIGNIN
F5H
CA5H/F5H
F5H
5 Hydroxyferulic acid
Hydroxyconiferaldehyde
Hydroxyconiferyl alcohol
COMT
COMT
COMT
CCR
CAD
LAC/PER
S LIGNIN
SCE
Sinapic acid
4CL
Sinapoyl CoA
Sinapaldehyde
Sinapyl alcohol
Sinapoyl glucose
SGT
SCT
Sinapoyl glucose
SMT
Sinapoyl malate
LIGNINS
CCR
CAD
4 Coumaroylaldehyde
Hydroxyphenyl alcohol
LAC/PER
H LIGNIN
CHS
AS
Naringenin-chalcone (tetrahydroxychalcone)
Apigenin (aurones)
CHI
Naringenin
F3H
FLS
Kaempferol
Dihydrokaempferol
F3'H
DFR
F3'H
Dihydromyricetin
Leucoanthocyanidins (Flavan-3,4-diols) Leucopelargonidin
Dihydroquercetin
FLAVONOIDS & ANTHOCYANINS
DFR
FLS
DFR
Leucodelphinidin
QUERCETIN
Leucocyanidin
LAR
(+) Catechin 2,3-trans flavan-3-ols
ANS (LDOX)
3-OH-Anthocyanidins Pelargonidin
RT, OMT UFGT
ANS
Delphinidin
Flavonol glycosides
Cyanidin
Tannins/proanthocyanidin trimer from Epicatechin/Leucocyanidin - extension unit Catechin - terminal unit
ANR
CE
(-) Epicatechin 2,3-cis flavan-3-ols
Proanthocyanidins Condensed tannins (no sugar residues)
PPO
ANTHOCYANINS:
Delphinidin 3-glucoside
Pelargonidin 3-glucoside
Cyanidin 3-glucoside
VT
VACUOLE
Oxidized tannins

Figure 1-2. Schematic diagram of the current knowledge of the phenylpropanoid biosynthetic pathway in *Populus.* Highlighted branches of interest include lignin, salicylates, flavonoid, and anthocyanins. Secondary metabolite derivatives produced in this pathway are involved in defense response to abiotic and biotic stress and structural support and not required for basal cellular activity in plants. Map was derived from KEGG pathway database (Kanehisa 2016).

anthocyanidins (aglycones) that are responsible for pigmentation in various organs in plants such as flowers, fruits, and leaves that can influence pollinators and also provide antioxidant protection against stress (Stommel et al. 2009).

Though flavonoids are important, other UV protective compounds are produced when 4-coumaroyl-CoA is converted to caffeic acid by the action of coumarate 3-hydroxylase (C3H), and then converted into ferulic acid by an O-methyltransferase (OMT) to yield sinapoyl malate and lignin (Rasmussen and Dixon 1999). It has been proposed that sinapoyl malate and feruloyl malate are important for UV protection when in abundance and distributed on the surface of plant leaves (Dean et al. 2014). In an HPLC analysis of UV-B treated *Arabidopsis* flavonoid mutants, the leaves of the RNAi chalcone synthase null mutant (*tt4*) possessed reduced levels of flavonoids but demonstrated an increase in sinapate esters as compared to wild-type (Li et al. 1993). However, certain sinapoyl derivatives have mostly been identified in *Brassicaceae* and it is unclear if they are produced and accumulate in other species and to the extent that they are measurable.

Upstream from phenylalanine is the shikimate pathway that produces salicylate phytohormones that are abundant in *Populus* and thought to protect against abiotic and biotic stress, and have been linked to enhanced stress tolerance (Hara et al. 2012, Abreu et al. 2011, Tsai et al. 2011). In *Populus trichocarpa*, salicortin concentration increased when treated with elevated levels of UV-B radiation, whereas other salicylates (salicin and tremulacin) showed decreased levels (Warren et al. 2003). In other *Salicaceae*, salicylates have been shown to decease when treated with elevated UV-B radiation as compared to

ambient conditions among different willow clones (Tegelberg and Julkunen-Tiitto 2001). The complexities of the shikimate and phenylpropanoid pathways and the final end products may appear to be species dependent, and it is possible that each species has a preferred substrate for pathway enzymes that produce one product relative to another. Although clearly there are merits to evaluating UV response in herbaceous plants, the response in woody plants is sufficiently dissimilar that it cannot be simplified without evaluating a range of closely related Salix.

Low Doses of Ultraviolet Radiation are Beneficial – An abundance of data suggests that all plants require at least some UV-B radiation for growth, development, and adaptation to other environmental conditions. For example, it has been suggested that early exposure to UV-B and subsequent accumulation of protective compounds in seedlings and young plants may protect plants from DNA damage and photoinhibition, essentially priming agricultural and medicinal crops when transplanted into the field (Sullivan et al. 2007, Sullivan et al. 2010, Wargent and Jordan 2013). Additionally, agriculturally important crops treated with low doses of UV-B radiation can promote the accumulation of phenolic compounds to deter insect feeding to reduce the use of herbicides and pesticides (Mazza et al. 2013).

Compounds such as ascorbic acid (vitamin C), an antioxidant involved in the stress response in plants, are essential for human nutrition and consumption is predominately from plant sources (Mittler 2002). Certain metabolites that are produced in response to UV radiation, including polyphenols such as flavonoids, are thought to scavenge oxygen

radicals to mitigate damage to plants by UV radiation (Xu et al. 2010) and therefore provide human health benefits (D'Archivio et al. 2007, Halliwell 2007, Neugart and Schreiner 2018).

Excessive Ultraviolet Radiation is Harmful – Plants exposed to an abundance of sunlight may obtain too much UV radiation, leading to photoinhibition caused by light-induced damage of chloroplasts and leaf tissue. Although UV radiation is only about 7% of emitted solar radiation, and 0.5% is UV-B radiation, it is more than sufficient to cause damage to living organisms and the affect photosynthesis (Mach 2016). The loss of photosynthetic capacity greatly reduces the efficiency of photosynthesis and can therefore affect plant growth and development (Barber and Andersson 1992). Photosynthetic pigments saturated with too much light energy can form harmful reactive oxygen species that can result in DNA damage that leads to deleterious mutations and even cell-death. Whereas DNA is the primary target in UV-induced damage by the formation of cyclobutane pyrimidine dimers (CPDs), plants have adapted mechanisms like photolyases to aid in repair (Nawkar et al. 2013).

It is clear that sunlight is important for a wide array of processes in plants, including growth and development (Demarsy et al. 2018), and plants can minimize the effects of photoinhibition by altering cellular components in the leaves and chloroplasts. For example, a systemic response to photoinhibition was observed in *Solanum lycopersicum* when leaves were treated with high light energy resulted in the transcription activation of HY5 (LONG HYPOCOTYL5) as well as the antioxidant related genes involved in

photoprotection, PGR5 (PROTON GRADIENT REGULATION5) and VDE (VIOLAXANTHIN DE-EXPOXIDASE) (Jiang et al. 2020). Some plants can avoid exposure to light by moving their leaves away from direct exposure in a process called heliotropism (Ehleringer and Forseth 1980). Another strategy involves repositioning and gathering chloroplasts perpendicularly at cell walls to avoid light (Suetsugu and Wada 2007).

It is particularly important to consider the harmful impacts of excess UV-B radiation on the photosynthetic machinery. Photosystems II (PSII) and I (PSI) are multi-protein complexes that contain pigments (chlorophylls and carotenoids); they are involved in harvesting photons, excitation energy transfer between photosynthetic subunits, and separating electric charge for the oxidation of water into O_2 (Caffarri et al. 2014). Light energy is captured in PSII and PSI by carotenoids and two types of light-absorbing chlorophylls, Chl A and Chl B. The light harvesting complex is a hollow, cylinder-like structure of Chl B and carotenoids, accessory pigments that become excited and transfer resonance energy to the next molecule towards the base in the photosystem at the reaction center. Excited Chl A in the reaction center releases electrons to the primary electron acceptor to synthesize ATP in PSII, or alternatively the electrons are transferred to other complexes and to PSI to generate NADPH (Cooper 1975). PSII is mainly targeted in excessive sunlight and by UV radiation (Bornman 1989) but some of this energy can be screened by phenolic compounds that accumulate in the leaf epidermis which leads to acclimation and prevents decreased photosynthetic activity that may lead to premature senescence (Takahashi and Badger 2011).

Although excessive UV radiation can be harmful to all living organisms especially in plants, specialized repair mechanisms allow plants to tolerate UV radiation and ameliorate damage to DNA and the photosynthetic machinery. Plants have also developed an avoidance strategy to prevent photoinhibition by moving away from direct exposure. Damaging energy from sunlight can be absorbed by the compounds that are produced in plants that are sequestered to the epidermis to protect cells and photosynthetic machinery. These methods are important for fitness and survival and part of the process in acclimating to environmental stress.

UV-B Radiation and Abiotic Stress in Plants – There are multiple stresses that plants can experience. There can be constructive or destructive stress, and the effects can be temporary or permanent. Thus, it is important to clarify this terminology in plant science. Destructive stress, or distress, experienced by plants typically relates to negative effects, that either can exhibit an elastic (reversible) response and/or a plastic (irreversible) response (Hideg et al. 2013). If a plant experiencing distress cannot avoid or repair the resulting damage, it can lead to death (Kranner et al. 2010). By contrast, eustress is a type of constructive stress that can help plants acclimate to environmental changes. Thus, mechanical stress can be considered a destructive stress that generally arises from a force that when applied to a plant results in strain from bending vegetative tissue, and though this type of stress is important, it is tangential to the main focus of this review. UV-B radiation can promote either distress or eustress in plants. For example, pre-illumination with UV-B radiation can be considered a eustress since it primes plants to acclimate to stress more rapidly by promoting the initial biosynthesis of certain metabolic compounds

(Jiang et al. 2020). On the other hand, a destructive stress has been observed with plants that have been treated with high doses of UV-B radiation and cannot overcome the ensuing cellular damage, ultimately leading to premature senescence (Ries et al. 2000).

Typically, a single plant simultaneously experiences a multitude of stressors that target a variety of organs and tissues. Plants generally manage these stresses by increasing resistance through genetic adaptation and by physiological acclimation (Hideg et al. 2013). Although plant resistance to abiotic or biotic stressors varies among species, generally there are two mechanisms to describe resistance: tolerance and avoidance (Levitt 1980). Tolerance is the resistance that is achieved when a plant reaches homeostasis or equilibrium against the stressor. By contrast avoidance is another resistance strategy to reduce exposure to the stressor by evasion (Jansen et al. 2019). Tolerance and avoidance can be distinguished by analysis of specified cells or leaf tissue.

Plants possess several defense mechanisms that enable mitigation and potential alleviation of UV-B promoted stress. For example, in response to UV-B radiation, photomorphogenic protection has been observed in many plant species with shortened root growth (Kim et al. 1998), reduced stem elongation (Barnes et al. 1996), and reduced leaf expansion and leaf thickening in many plants (Tevini and Teramura 1989). Some plant species increase trichome density and produce waxy cuticles to reflect and absorb UV from flavonoids translocated to the leaf surface as an avoidance mechanism to attenuate the impact of UV-B radiation (Liakoura et al. 1997, Jansen et al. 1998). For example, leaf tissue contains mesophyll cells that are protected against UV-B radiation by UV absorbing compounds

that accumulate in the epidermis through avoidance. Acclimation may occur simultaneously with other stress variables (eustress) and may result in heightened resistance to the stress response via both local and systemic effects (Jiang et al. 2020).

The major injurious effects of UV-B radiation on plants arise from DNA damage and the generation of reactive oxygen species (ROS) resulting in free radical damage to molecules, cells and tissues. Increased levels of DNA damage has been discovered in native plants inhabiting in the polar regions where the ozone layer is at its thinnest (Rousseaux et al. 1999, Turnbull and Robinson 2009). UV-B radiation contributes to DNA damage in all living organisms by the formation of cyclobutane pyrimidine dimers (CPD) that interfere with replication and transcription (Wang et al. 2014). DNA damage that is not repaired can cause deleterious mutations that can ultimately lead to cell death.

Reactive oxygen species (ROS) are formed in the organelles of plants as a result of aerobic metabolism under normal steady state conditions. Plants have evolved mechanisms to scavenge and thereby maintain low levels of ROS to prevent damage within the cell. However, ROS levels can increase due to abiotic and biotic stress, leading to an imbalance of ROS relative to antioxidant scavengers that can result in DNA and protein damage as well as lipid peroxidation of cellular membranes. Organelles contain enzymes such as superoxide dismutase (SOD), ascorbate peroxidase (APX) and glutathione peroxidase (GPX) that have anti-oxidative potential to quench the reactivity of ROS. Additionally, plants produce non-enzymatic ROS scavengers like ascorbate, glutathione, carotenoids, flavonoids, anthocyanins, and other metabolites to delocalize the oxygen derived radical

(Impa et al. 2012). It is well known that UV-B radiation promotes the formation of ROS in plant tissues (Hideg et al. 2013, Dai et al. 1997, Yokawa et al. 2015).

As previously mentioned, sunlight is critically important for plants, but excessive exposure may result in decreased photosynthetic efficiency. UV-B radiation may damage photosynthetic machinery in plants if received at high levels (Keren and Krieger-Liszkay 2011) and may lead to early senescence or cell death in extreme cases. High levels of UV-B energy can lead to the formation of ROS, resulting in photoinhibition and damage to the PSII and PSI machinery (Keren and Krieger-Liszkay 2011). Low PAR light can lead to a deficiency that can result in insufficient energy for photosynthesis, leading to etiolation (overgrown internodes and chlorosis) (Armarego-Marriott et al. 2020). Furthermore, extreme fluctuations in light intensities can saturate the light-harvesting antenna complexes and reduce photosynthetic efficiency by negatively impacting carbon metabolism and nitrogen assimilation (Pascual et al. 2017). Enhanced oxidative stress can be measured in plants by a variety of parameters: photosynthetic capacity, stomatal conductance, rate of transpiration, quantum efficiency of PSII (chlorophyll fluorescence), and water use efficiency (WUE) (Sharma et al. 2019).

Plant stress can be interpreted as beneficial or damaging and the effects can be transient or permanent, all of which is occurring from a variety of stressors and the response is quite complex. While some responses to cellular stress are difficult to differentiate, the biochemical and morphological responses can be characterized to some degree. In general,

plants will tolerate and simultaneously avoid stress with a host of strategies that has evolved and improved over time in order to acclimate to the environmental constraints.

The Response of Trees to UV-B Radiation – Historically, plant response to UV radiation can be traced back from fossilized spores and pollen from the End-Permian Extinction event. Palynological studies in fossils reveal UV absorbing compounds, particularly phenolic and ferulic acids, in preserved plant tissue. Reconstruction modelling of UV levels during this era suggest a thinner ozone layer compared to present-day, implying that higher UV-B irradiance is proportional to the greater production of UV absorbing compounds in plants (Rozema et al. 2009). Plants have evolved a wide range of protection and tolerance mechanisms due to adaptations to diverse and changing climates (Caldwell 1968). Historically most early studies on the response to UV-B in plants was undertaken on herbaceous annual plants with fewer studies being conducted on perennials and trees. Thus, a considerable gap remains in our understanding of the response of plants to UV radiation, and currently there is not enough information to fully explain the molecular basis of acclimation in terms of the metabolic response to UV-B in more complex woody systems.

Carbon gained from the balance of carbon increased from photosynthesis of carbon released from respiration is known as global net primary productivity (Woodward 2007). Forests account for over two thirds, and agricultural land accounts for 12% of the NPP, (Prince et al. 2001, Hicke et al. 2004), but a limited number of studies on the effects of UV-B on growth or productivity of trees have been published. For example, Basioumy

and Biggs (1975) demonstrated visual stunting of one-month-old peach seedlings under supplemental UV-B in a greenhouse whereas Semeniuk (1978) found no visual symptoms in other greenhouse studies on six ornamental species. Bogenrieder and Klein (1982), however, demonstrated in field studies that biomass accumulation in young seedlings of four tree species was increased when ambient UV-B was excluded. Two other studies (Kossuth and Biggs 1981, Sullivan and Teramura 1988) screened a total of 15 coniferous species and found that roughly half (7 of 15) exhibited reduced growth under elevated UV-B fluences in growth chambers or greenhouses. Kaufmann (1978) conducted the first outdoor UV-B radiation supplementation study of trees in the field and irradiated seedlings of *Picea engelmannii* and *Pinus contorta* in the field for one season. Although unable to detect any detrimental effects during that year, visible symptoms and increased mortality were observed during the subsequent growing season. Similarly, in a three-year field study on loblolly pine, Sullivan and Teramura (1992) found in general that growth reductions were minimal following the first growing season but increased to 12 to 20% reductions after three years. Of particular interest was the fact that after three years, the growth reductions in 2 of 4 seed sources studied were approximately equal between a simulated 16% and 25% ozone depletion scenario. These studies raise the question of whether UV-B might result in a cumulative in trees, rather than the more punctuated responses seen in annuals.

By contrast, *Arabidopsis thaliana*, has been considered a herbaceous model organism that has been used extensively for experimental research in plant physiology and biochemistry due to its small genome, short regeneration cycle, ease of transformation, and the ability to

cross parental lines to create progeny. The specific effects of UV radiation on *Arabidopsis* have been extensively studied (Jenkins 2009, Jenkins 2017, Podolec et al. 2021), and detailed hypotheses have been put forth to explain gene and metabolic activation leading to physiological adaptation to irradiation by UV-B radiation. On the other hand, trees have developed adaptations for long-term survival and tolerance of various environmental conditions due to their complex vasculature system and the development of secondary xylem tissue, wood (Taylor 2002) and, by contrast, little is known about the molecular nature of UV-B stimulated pathways for essential or protective processes. Such information is important as intensive forestry crops such as *Populus* have grown increasingly valuable as a bioenergy feedstock and as wood-based products like paper and timber. Academic, government, and private organizations have invested significantly in experimental research to engineer *Populus* for improved properties and achieved considerable progress. But managing environmental stresses remains an ongoing concern, especially for poplar in the field. However, with the availability of modern genomics approaches in addition to cutting-edge gene editing tools, there is considerable optimism for unraveling complex biological effects stemming from environmental stresses such as over-exposure to UV-B radiation, and the field is optimistic in reaching the goal of developing *Populus* as a premier biofeedstock for a variety of applications.

Several observations on conifers suggest that the impact of UV-B on tree growth are manifested at the epidermal level. UV-B transmittance through the epidermis varies widely across species (Day et al. 1994, DeLucia et al. 1992) and this is attributed to the changes in both epidermal chemistry and structure. The high degree of epidermal absorption of

UV-B as well as the inability to detect damage to the photosynthetic machinery loblolly pine and sweetgum (Sullivan et al. 1996), suggests that reduced leaf size in loblolly pine may be mediated by changes in cell wall biochemistry that leads to thickening and inhibiting cell wall extension (Dale 1988, Liu et al. 1995). This could lead to a reduction in epidermal cell size and possibly to reduced needle length (Sullivan and Teramura 1994, Sullivan et al. 1996). Consistent with this idea, Sullivan (Sullivan et al. 1996) observed epidermal thickening in response to UV-B radiation and Laakso et al. (2000) found that wall-bound phenolics and tannins increased in loblolly pine and Scots pine under supplemental UV-B radiation and that this was accompanied by a thickening of outer epidermal cell walls in these species. Other researchers have also observed changes in the epidermis and cuticle in response to UV-B radiation and suggested that these responses improved water relations in a variety of species (Petropoulou et al. 1995, Manetas et al. 1997, Tian and Sullivan 1999, Tian and Sullivan 2000).

Secondary metabolites in *Populus* and all trees highly abundant and important for growth and development as well as for protection against abiotic and biotic stress (Lindroth and Hwang 1996, Lindroth 2001, Chen et al. 2009). As previously mentioned, plants commonly accumulate epidermal phenylpropanoids that induces PAL2, CHS1, FLS4, ANR1, ANS1, and MYB134 in response to UV-B radiation to absorb potentially damaging energy in the epidermal layer (Mellway et al. 2009, Sullivan et al. 2003, Warren et al. 2003, Sullivan 2005). Meta-analysis in field studies affected by ozone depletion by Searles et al. (2001), found that the most common response to UV-B radiation was the accumulation of epidermal UV screening compounds (Searles et al. 2001). Interestingly, physiological

measurements in certain plants have revealed harmful effects of UV-B radiation, but the response can vary on leaf growth and anatomical development (Teramura and Caldwell 1981). Younger leaves may be more sensitive to UV-B radiation as compared to older leaves because there is less accumulation of UV absorbing compounds in vacuoles and cell walls (Naidu et al 1993, Dillenburg et al. 1995). However, despite an increase in UV absorbing compounds accumulating in older leaves of *Populus*, leaf thickness of mesophyll tissue (palisade parenchyma) can also protect photosynthetic machinery (Schumaker et al. 1997). *Populus* species have been modified to accumulate proanthocyanidins that regulate flavonoid genes controlled by transcription factor MYB134 (James et al. 2017). Nonetheless, it has been shown that *Populus* leaves exhibit a significant increase in UV absorbing compounds such as chlorogenic acids, salicylates, flavonoids, and proanthocyanidins when exposed to abiotic stress (Warren et al. 2003, Chen et al. 2009, Caseys et al. 2012, Gourlay and Constabel 2019).

The Potential for Engineering Enhanced UV Protection in Trees – Mankind has bred plants for over 10,000 years to domesticate and improve traits of agriculturally important crops (Shames 2007). A variety of genetic approaches have been used to improve classical breeding since the dawn of agriculture, but recently, state-of-the-art tools in molecular genetics and genome editing have revolutionized the potential to rapidly and precisely engineer plants, including economically important crops, and even trees (Allwright and Taylor 2016, Chang et al. 2018). Many of the same traits that have been the focus of traditional plant breeding have also been the focus of molecular plant engineering, including maximizing yields, improving nutritional quality, improving resistance to pests

and disease, and supporting growth on nonarable land (or at least improving tolerance to abiotic stresses). Despite increased urgency for greater access to foods and renewable bioproducts, the field is still in its infancy, and in addition there is some reluctance to embrace the potential of genetically engineered plants – especially trees (Chang et al. 2018).

The technological landscape for genetic and genome engineering of trees has improved markedly with enhanced approaches for plant transformation and genome editing (Li et al. 2013, Lowder et al. 2015, Altpeter et al. 2016). These advances, coupled with the explosion in genome sequencing information and computational tools for genome analysis, provide the foundation for improving bioenergy crops, such as poplar, to help meet society's unquenchable thirst for clean and inexpensive energy. It has long been recognized that a key barrier for the profitable use of plant feedstocks for biofuel is the removal of lignin from cellulose. Cellulose undergoes a saccharification process to enable the effective and efficient conversion of monosaccharides to ethanol. Thus, early work in lignin for paper products to improve cellulose pulp eventually led to research into the first-generation biofuel feedstocks (Wojcik et al. 2001).

Lignin is a key, indispensable polymer in plants. It provides strength for plants to grow tall in gravitropic environments, and provides a hydrophobic lining to facilitate water and nutrient transport in plant vasculature. Lignin itself is an aromatic polymer assembled via radical polymerization primarily from 'monomeric' p-hydroxycinnamyl alcohols into a complex network. The main components within lignin are derived from the monolignols

p-coumaryl alcohol, coniferyl alcohol and sinapyl alcohol, giving rise to p-hydroxyphenyl (H), guaiacyl (G) and syringyl (S) units in the lignin polymer. However, the relative abundance of these units, and others, varies among plant species, tissues, cell types and developmental stages (Boerjan et al. 2003, Ralph et al. 2004, Vanholme et al. 2010, Vanholme et al. 2012). Although lignin is an attractive target for modification by geneticists and biotechnologists, and many ingenious approaches have been applied to reducing lignin content or simplifying its composition to facilitate lignocellulosic pretreatment (Mansfield et al. 2012), advancements have been frustrated by complex negative effects of lignin modification on plant growth and development (Li et al. 2010, Gallego-Giraldo et al. 2011, Voelker et al. 2011, Baxter and Stewart 2013).

In contrast to the considerable effort in searching for improvements to the saccharification of poplar trees for improved biofuel development (Studer et al. 2011), little attention has been focused on improving the response of poplar to stress associated with increased exposure to UV-B radiation. This may be due to the considerable complexity of UV-B promoted responses in plants, and the little that is known in trees. Sensing UV-B radiation by UVR8 and subsequent signal transduction results in large scale transcriptional, metabolic and morphogenic reprogramming of plants. Yet it is clear that the main metabolites that are upregulated upon UV-B exposure are antioxidants, flavonoids, and in *Brassica* species, sinapoyl esters. Thus, given the large scale metabolic changes that can be engineered in plants by the addition of native or even exogenous transcription factors (Tohge et al. 2005, Butelli et al. 2008, Zhang et al. 2015), it be possible to reprogram plant metabolism, especially in low-lignin poplars, to withstand exposure to damaging UV-B

radiation. Metabolomic-assisted, molecular breeding may offer an attractive approach to developing low-lignin poplar variants that possess normal growth and fitness, as well as improved resistance to UV-B radiation.

Poplar is an attractive model for molecular breeding. It is considered a model for molecular studies in trees (Taylor 2002, Cronk 2005, Tuskan et al. 2006, Jansson and Douglas 2007), significant genetic and genomic resources are available, can be transformed, has broad natural variation and distribution, and is readily cultivated on plantations (Chang et al. 2018). Thus, all of the tools are available for engineering approaches to generate novel poplar genotypes for broad application.

Chapter 2: Statement of the Problem and Research Overview

The overall goal of my dissertation research is to elucidate a molecular level understanding of the impact of UV-B radiation on *Populus* species, a model for trees and an attractive biofuel feedstock. My research is multidisciplinary, guided by advisors from plant science and bioengineering, and aims to apply ecophysiology, metabolomic, computational, and molecular approaches to a collection of natural variants and in the construction of transgenic *Populus*. My work enabled me to establish the necessary groundwork to address my overarching hypothesis: that low-lignin *Populus* trees, constructed with the aim of increasing the relative ease of biofuel production, will reprogram their metabolism to compensate for reduced lignin by increasing the biosynthesis of other aromatic compounds in response to UV-B radiation. My findings will help to devise strategies for the construction of *Populus* variants that are more resistant to UV-B radiation, provide insight into the UV-B-dependent regulation of phenylpropanoid biosynthesis, and will assist efforts to engineer more robust and sustainable reduced lignin *Populus* lines for biofuel and bioproducts.

Plants acclimate to UV-B radiation through the synthesis of protective compounds that accumulate in the leaf epidermis to absorb UV-B and mitigate abiotic stress. Meta-analysis in *Arabidopsis* shows that the UVR8 photoreceptor plays a pivotal role in acclimation through transcription activation that increases the biosynthesis of UV-B protective compounds, most of which derive from the phenylpropanoid biosynthetic pathway

(Jenkins 2009, Podolec et al. 2021). Phenylpropanoids are critical for protection against UV-B radiation. Not only are phenylpropanoids important for UV-B protective metabolites, but they are also precursors of lignin. Lignin is a key biopolymer because it provides strength for plants to grow upright, and because of its aromatic character, it also contributes to protection from UV-B radiation. However, the removal of lignin is a significant barrier to the economical production of cellulose from plant feedstocks. Hence, finding natural variants or constructing transgenic plants with reduced levels of lignin has been a key target in the biofuel field to increase the relative ease of saccharification, the process of extracting and breaking down cellulose into monosaccharide molecules from lignocellulosic biomass (Van Acker et al. 2014, Lapierre et al. 2021). Unfortunately, plants that contain reduced levels of lignin often show significant deficiencies in development, growth, and protection against pests and pathogens (Li et al. 2010, Gallego-Giraldo et al. 2011, Voelker et al. 2011, Baxter and Stewart 2013). It is unknown how low-lignin plants compensate for exposure to UV-B radiation, and whether they possess auxiliary mechanisms for protection.

At the onset of my dissertation research, I examined a collection of natural variants of poplar collected at various growth elevations and that contained diverse lignin levels to assess any differences in their response to UV-B radiation. As mentioned above, lignin plays a role in protecting plants from UV-B radiation, and fluence rates are greater at higher elevation. Fluorescence measurements of chlorophyll were made on leaves from UV-B treated plants to assess 'shielding,' which reflects their global metabolic response to UV-B. As expected, plants treated with UV-B radiation have higher UV shielding compared

to plants without UV-B and acclimation was found to occur within 3 – 4 days upon exposure, with a maximal response in about 10 days. Unexpectedly, however, shielding was not directly correlated either with lignin levels or with growth elevation. These results suggested that additional factors contribute to UV-B acclimation of natural poplar variants, and further investigation is needed to elucidate the specific UV absorbing metabolites that protect plants from UV radiation.

Targeted metabolomics was used to probe the changes in the leaves that were associated with UV-B acclimation. I hypothesized that when treated with UV-B radiation, plants with different lignin levels or origin of growth at different elevations would display distinct metabolic responses by synthesizing different levels and types of UV-absorbing compounds to account for differences in UV shielding. Specific metabolites were targeted in the phenylpropanoid pathway, including quercetins and salicylates which are central to the production of a wide array of UV absorbing compounds in plants, including flavonoids and anthocyanins. Liquid chromatography coupled with electrospray ionization mass spectrometry (LC-MS) was used to identify significant increases in a number of UV absorbing metabolites in plants treated with UV-B. These observations supported my general hypothesis that poplar generates phenylpropanoid derivatives to protect against UV-B radiation, but did not reveal the underlying factors responsible for UV-B acclimation.

Based on the observations and from spectroscopic and metabolomics analyses, it became important to understand the underlying molecular signals that promote UV-B acclimation

in poplar. Because my collection of natural poplar variants exhibited diverse responses to UV-B treatment, efforts were focused on determining whether these *Populus* variants expressed UVR8 at comparable levels, or whether small differences promoted by single nucleotide polymorphisms (SNPs) in the *UVR8* locus could result in altered expression levels, thereby generating different acclimation responses. Bioinformatic tools were developed and used to analyze SNP data from the genomes of over 500 *Populus trichocarpa* natural variants. Surprisingly, no SNPs were found in cis-regulatory elements, core promoters, or *UVR8* splice sites. Although a number of non-synonymous SNPs that result in amino acid substitutions at the protein level were identified in *UVR8*, these did not appear to promote significant structure or stability alterations. These observations were surprising and suggest that there is an optimal *UVR8* expression level that is a strongly selected trait in *Populus*. Importantly, this prompted my interest in assessing the influence of UVR8 expression levels in *Populus* on the acclimation and tolerance of UV-B radiation.

To probe more deeply into the role of UVR8 expression in UV-B acclimation in poplar, I was motivated to apply genetic interventions that could manage acclimation more effectively, especially in low-lignin poplar. Thus, I redirected my efforts to focus on the UV-B photoreceptor found in plants, UVR8. I utilized genome editing tools to directly modulate *UVR8* expression in wild-type and in low-lignin *Populus*. CRISPR was used to generate knockout, up- and down-regulated *UVR8* transgenic poplar lines, which were compared to RNAi down-regulated, and 35S overexpression lines that I constructed. Additionally, transgenic lines were constructed to generate low-lignin plants by using RNAi down-regulation of cinnamyl alcohol dehydrogenase (*CAD*). CAD is the last

enzyme in monolignol biosynthesis, and down-regulated *CAD* knockdown (KD) plants result in a reduction of syringyl- and guaiacyl-lignin formation (Zhao et al. 2013). *CAD*-regulated transgenics were transformed with CRISPR constructs to generate double mutant, *UVR8* knockout or overexpression lines.

UV-B treated transgenic poplars with modulated expression of *UVR8* in wild-type or *CAD* down-regulated backgrounds were characterized physiologically and analyzed by targeted metabolomics to assess the impact of UVR8 and lignin level on UV-B acclimation. Generally, the transgenics responded as expected, exhibiting increased protective aromatic metabolite biosynthesis upon exposure to UV-B radiation. Surprisingly, an unusual, rapid and robust growth phenotype was observed for transgenic plants with modulated *UVR8* expression levels. These striking findings suggest a novel aspect in the mechanism of UVR8-promoted responses in poplar. A new and simple hypothesis was developed to account for these findings, which was consistent with previous data for *Arabidopsis* UVR8, and can be readily tested and capitalized on in future research.

Chapter 3: Spectroscopic Analysis of Low-Lignin *Populus* and UV-B Promoted Metabolomic Changes

Introduction

Plants have evolved to protect leaf mesophyll tissue from damage by UV-B radiation by producing screening compounds that can absorb UV-B radiation (Caldwell et al. 1983). Flavonoids (phenolic glycosides) and sinapate esters (hydroxycinnamates) have been implicated as UV-B screening compounds because they accumulate in the leaf epidermis and strongly absorb UV-B radiation (Kootstra 1994, Landry et al. 1995, Caldwell and Robberecht 1983). Plants have evolved accordingly to their environment, a suite of responses to protect themselves from damage caused by UV-B radiation. Numerous studies have shown that plants from high elevations or low latitudes are more adapted to UV radiation. For example, a meta-analysis investigating the relationship of elevation and the adaptation to UV-B concluded that northern latitude alpine plants experiencing increasing UV-B radiation were less well adapted to UV stress compared to southern latitude and higher elevation plants (Turunen and Latola 2005). Also, cell wall lignin has recently been considered an important factor in protection against UV-B radiation (Sadeghifar and Ragauskas 2020, Tran et al. 2021).

Lignin is the second most abundant polymer on Earth, comprising up to 30% of organic carbon in the biosphere. Lignin comprises a large network of aromatic precursors that polymerize via oxidative coupling of monolignols (hydroxycinnamyl alcohols, including coniferyl alcohol, sinapyl alcohol and p-coumaryl alcohol) via a radical mechanism. Monolignols are products of the phenylpropanoid biosynthetic pathway, which also produces the primary UV-screening phenolics and flavonoids (Boerjan et al. 2003). However, the relationship between lignin levels and composition, growth elevation, and the hierarchical synthesis of UV-screening compounds on the impact of quantitative and qualitative differences in UV tolerance or sensitivity in poplar is not known.

Poplar is an important tree to study because of its use as a source of bioenergy. *Populus* is a genus with large variation in natural lignin content and grows at a range of elevations. The bioenergy field has long recognized that lignin is a key barrier to cellulosic biofuel production from plant feedstocks. Plant secondary cell walls are important for structural integrity as they comprise a dense matrix of polymers that provide strength and rigidity and lignin is the primary complex polymer in secondary cell walls. Down-regulation of genes in the phenylpropanoid biosynthetic pathway in transgenic *Populus trichocarpa* can reduce lignin content and improve cellulosic biomass degradability for biofuel production (Tsai et al. 2006, Miller et al. 2018). Additionally, some natural variants can release unusually high sugar yields without undergoing pretreatment during cellulosic biomass conversion to fuel (Studer et al. 2011). Thus, natural variants of *P. trichocarpa* are considered a useful biofuel crop for breeding programs to improve cellulosic degradability. Moreover, *Populus deltoides* have been modified to enhance saccharification by modifying

genes in the phenylpropanoid pathway, as well as those involved in cell wall development, resulting in altered lignin levels (Macaya-Sanz et al. 2017). The monolignols coumaryl alcohol, coniferyl alcohol, and sinapyl alcohol are derived from the phenylpropanoid pathway, and serve as the source of secondary metabolites such as anthocyanins, tannins, and other aromatic compounds that function in plant signaling, defense and abiotic stress responses (Bhuiyan et al. 2009, Vogt 2010, Baxter and Stewart 2013). However, the reduction of lignin in a variety of plants including *Populus* with suppressed enzymes important in the phenylpropanoid pathway demonstrated a range of abnormal growth phenotypes with reduced fitness and may display increased sensitivity to UV-B (Hu et al. 1999, Novaes et al. 2010, Voelker et al. 2011). In order to acclimate to UV-B, *Populus* variants may compensate for low lignin levels by increasing the production of other aromatic specialized compounds to alleviate the impact of UV-B. Therefore, not only is the phenylpropanoid biosynthetic pathway important for lignin biosynthesis, but it is also of central importance to *Populus* physiology, plant defense, and health.

In this chapter, representative *Populus* collections were examined for correlations between sensitivity (or acclimation) to UV-B radiation under greenhouse and laboratory conditions, as well as poplar with different levels of lignin, whether arising from variation in natural populations that thrive under different conditions or from intentional modification of genes in transgenic lines. Noninvasive, ecophysiological measurements of chlorophyll fluorescence in UV-B treated leaves were performed and concentrations of key metabolites were determined by LC-MS.

Theory of Measurements and Hypothesis

To examine correlations between lignin levels and UV-B sensitivity, a representative collection of 25 different genotypes of natural *Populus* species was acquired and propagated with soilless potting media in the greenhouse at the University of Maryland (Table 3-1). It is important to note that although lignin plays a role in vascular and structural support, it is predominately concentrated in the shoots with some lignin in leaf tissue (Jia et al. 2015). Leaves were marked at the beginning of treatment prior to UV experimentation, and monitored throughout the duration of treatments. The same leaves were then harvested after UV experimentation for further analysis. *Populus* were maintained and grown under fluorescent lamps for 16 h at room temperature.

The various genotypes ranged from low to high syringyl (S) to guaiacyl (G) lignin ratios (S/G) as well as from low to high lignin content (%). Lignin compositions were obtained from literature results of biomass analysis of wood cores, and quantification of sugar release from a natural population of *P. trichocarpa* (Studer et al. 2011). The range of lignin content varied from 15.7% (low) to 27.9% (high), and the S/G compositional ratio from 1.0 (low) to 3.0 high. (The S/G ratio was defined in this study as low at < 2.0 and high at > 2.0.) The plants used in this study have been previously characterized by Muchero et al. (2015), and were collected from the same region, with collaborators in the same laboratory at the BioEnergy Science Center (BESC) obtaining the values describing lignin chemistry (Muchero et al. 2015). Additionally, a collection of transgenic *P. deltoides* modified in

Table 3-1. Selected genotypes of *Populus trichocarpa* varying in lignin content and composition and origin of growth elevation.

Genotype	Characteristic	Lignin (%)[A]	S/G[B]	Elevation (m)
GW-10993	High lignin	27.20	2.08	11.00
GW-9911	High lignin	27.71	1.96	60.96
CHWK-27-2	High lignin	27.94	2.00	280.00
GW-9889	High lignin	27.10	1.95	365.76
HOPF-27-5	High S/G	25.32	2.31	61.00
KTMB-12-3	High S/G	25.66	2.48	61.00
GW-9827	High S/G	26.24	2.29	76.20
VNDL-27-5	Intermediate	24.45	1.93	20.00
BESC-46	Intermediate	24.18	1.71	21.30
BESC-25	Intermediate	24.44	1.95	22.40
GW-9821	Intermediate	23.31	1.77	76.2
BESC-436	Intermediate	24.11	1.80	92.57
KLNG-20-5	Intermediate	24.28	1.83	105.00
GW-9874	Intermediate	26.32	1.98	152.40
BESC-166	Intermediate	25.65	1.72	249.77
BESC-838	Intermediate	24.39	1.58	249.77
BESC-99	Low Lignin	20.02	1.45	19.48
BESC-334	Low lignin	19.17	1.79	47.93
BESC-193	Low Lignin	19.81	1.60	249.77
GW-9791	Low Lignin	20.38	1.66	304.80
GW-10985	Low S/G	21.05	1.38	11.00
BESC-81	Low S/G	20.98	1.45	19.48
BESC-459	Low S/G	22.92	1.41	76.77
BESC-328	Low S/G	23.59	1.45	136.47
CA-01-03[C]	Unknown	Unknown	Unknown	2144.00

Table 3-1. Selected genotypes of *Populus trichocarpa* varying in lignin content and composition and origin of growth elevation. (A) Composite estimate of lignin composition from pyrolysis and molecular beam mass spectrometry (PyMB/MS), values were adjusted for variability within the plantation due to environment. A total of 15 genotypes were selected based on extreme values in lignin content (15.7-27.9%) and composition (1.0-3.0) in addition to 10 genotypes with average values. (B) Corresponds to the ratio of syringyl to guaiacyl lignin also derived from PyMB/MS. (C) Genotype does not have lignin chemistry data (Muchero et al. 2015).

cell wall development wasalso obtained and propagated in the greenhouse under the same conditions as previously described (Table 3-2). These variants were constructed by the BESC in an effort to produce more optimal variants for biofuel production. Transgenic *P. deltoides* lines were obtained from BESC that targeted genes that increased cellulose or reduced crystallinity, hemicellulose composition, or altered enzymes in the phenylpropanoid pathway in an effort to reduce recalcitrance during degradation of lignocellulosic biomass (Macaya-Sanz et al. 2017). These transgenics targeted a wide variety of genes with saccharification as the sole screening parameter. However, it seems likely that modification of genes in the early steps of phenylpropanoid biosynthesis in *P. deltoides* will affect other metabolites further downstream, and additional metabolic compensation may occur to enable acclimation to UV-B radiation. Thus, it was important to determine whether differences in key metabolites in the phenylpropanoid pathway, or in other pathways such as flavonoid and anthocyanin biosynthesis, resulted in the presence of UV-B radiation.

UV-screening and inferred epidermal shielding was measured with a portable, field pulse amplitude modulation (PAM) chlorophyll fluorometer (UV-A PAM; Gademann Instruments, Würzburg, Germany). The instrument measures the UV transmittance in the epidermis of leaves by comparing the ratio of chlorophyll fluorescence from UV-A (372 nm) divided by the chlorophyll fluorescence from blue light (470 nm) to calculate the relative extent of UV transmittance into the mesophyll. The UV-A PAM approach provides a noninvasive, sensitive, and accurate measure of UV transmittance by measuring

Table 3-2. Selected lines of *Populus deltoides* affected in lignin biosynthesis with differential transgene expression.

Gene name	**Accession number**	**Inter-line variance**	**Type**	**Annotation**
PtCAD2359	Potri.009G095800	Comparator	RNAi	Cinnamyl alcohol dehydrogenase
PtCAD2359	Potri.009G095800	TOP	RNAi	Cinnamyl alcohol dehydrogenase
PtEPSPS	Potri.002G146400	Comparator	OX	5-enolpyruvylshikimate-3-phosphate synthase
PtEPSPS	Potri.002G146400	TOP	OX	5-enolpyruvylshikimate-3-phosphate synthase
PtRWA2	Potri.010G148500	Comparator	OX	O-acetyltransferase
PtRWA2	Potri.010G148500	TOP	OX	O-acetyltransferase
PtSHMT10969	Potri.001G320400	Comparator	OX	Serine hydroxymethyltransferase
PtSHMT10969	Potri.001G320400	TOP	OX	Serine hydroxymethyltransferase
PtGAUT12	Potri.001G416800	Comparator	RNAi	Galacturonosyltransferase 12
PtGAUT12	Potri.001G416800	TOP	RNAi	Galacturonosyltransferase 12
PtVND6	Potri.015G127400	Comparator	OX	Vascular-related NAC-domain 6 TF
PtVND6	Potri.015G127400	TOP	OX	Vascular-related NAC-domain 6 TF
PtDUF266	Potri.011G009500	Comparator	OX	Protein of unknown function
PtDUF266	Potri.011G009500	TOP	OX	Protein of unknown function

Table 3-2. Selected lines of *Populus deltoides* affected in lignin biosynthesis with differential transgene expression. Identified genes involved in cell-wall development with corresponding accession numbers were targeted to alter lignin in *Populus deltoides*. A description and type of modification for each line had a comparator and top-performing line (TOP) to account for inter-variance of the transgenic lines due to genetic instability from DNA methylation and retrotransposons induced from tissue culture plants (Macaya-Sanz et al. 2017).

chlorophyll fluorescence that is proportional to UV shielding (Fig. 3-1). Transmission results can be used to correlate chlorophyll fluorescence to epidermal shielding compounds in leaf tissue (Bilger et al. 2001). However, the UV-A PAM approach only infers concentration, and in addition, screening compounds in the mesophyll may not be detected, requiring further analysis by LC-MS to provide a quantitative analysis of UV-screening compounds. The instrument uses epidermal UV-A transmittance to excite chlorophyll, with the resulting fluorescence proportional to the incident radiation. UV screening is then estimated by the ratio of fluorescence excited at 375 nm and 470 nm (Kolb et al. 2003). Chlorophyll fluorescence is normalized by exciting chlorophyll molecules with blue light at 470 nm that is not absorbed by UV-absorbing compounds in the epidermis (Kolb and Pfundel 2005, Barnes et al. 2008). UV-absorbing metabolites that are produced can reduce radiation penetration into plant tissue and the UV-A PAM instrument will measure a result that indicates a decrease in chlorophyll fluorescence. Three moderately expanded leaves were selected at the top canopy, marked, and measured with the liquid light guide at the middle section from the midrib for each pot. Ten repeated measurements were made on each leaf and averaged to calculate a single response on each plant each day.

In addition to UV acclimation, damage to photosynthetic machinery was measured by chlorophyll fluorescence (Smillie and Nott 1982). Measuring chlorophyll fluorescence offers a non-destructive approach to estimate plant stress by estimating the plant's ability to utilize light to oxidize water molecules by converting it into chemical energy in the photosynthetic reaction center (Vinyard et al. 2013). UV-B radiation has been shown to

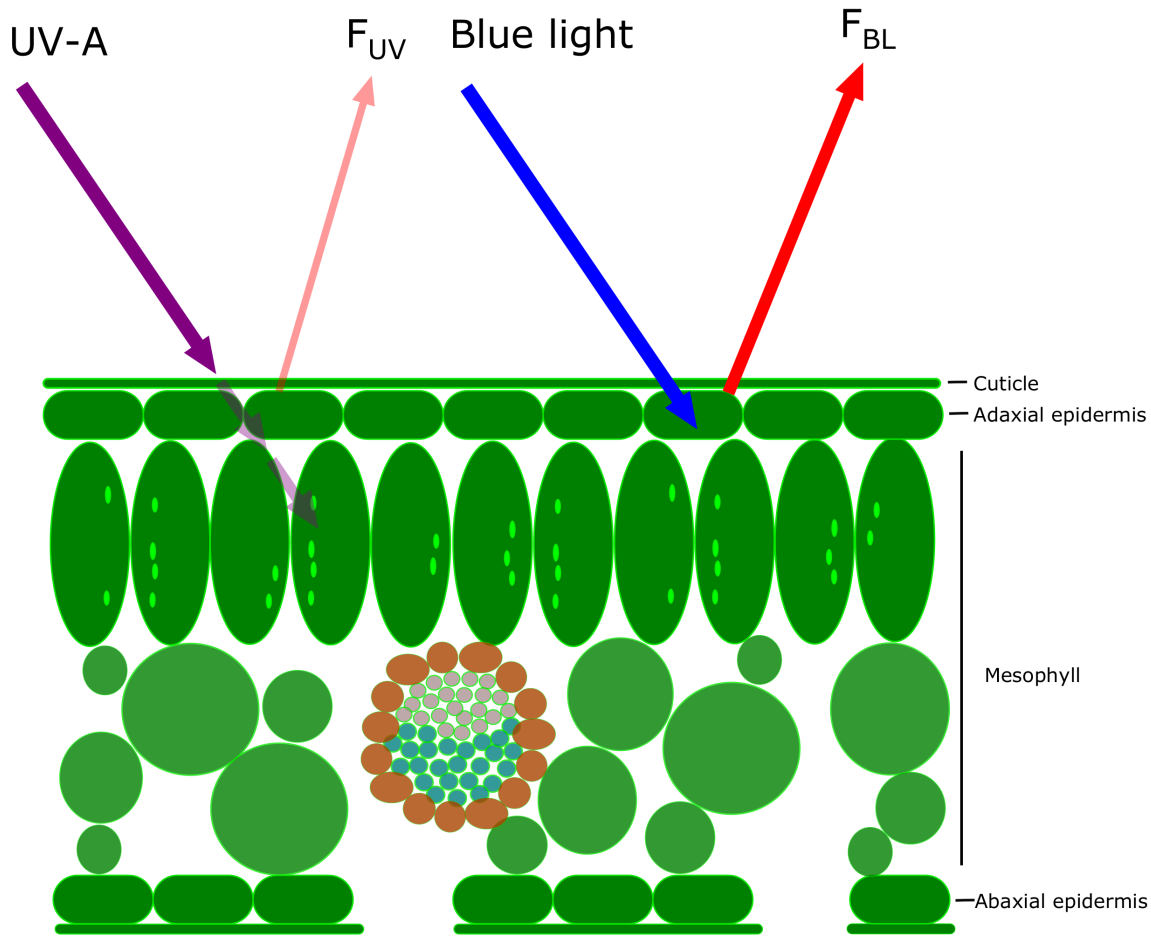

Figure 3-1. Illustration of relative epidermal UV transmittance of chlorophyll fluorescence from UV-A radiation and blue light with the UV-A PAM Chlorophyll fluorometer (Bilger et al. 1997). Excitation of chlorophyll from light-emitting diodes at 375 nm (UV-A) and 470 nm (blue light) is supplied by a 5 mm flexible tube with a liquid core light guide and a leaf clip attachment for a non-destructive measurement. A ratio is calculated by measuring chlorophyll fluorescence induced by UV (F_{UVA}) and visible blue light reference (F_{BL}) on the adaxial epidermal layer. Influence of UV-absorbing compounds accumulating in the epidermis will decrease F_{UVA} as less UV is absorbed by the leaf and re-emitted to the fluorometer. To determine the percent of UV transmittance or passing through the epidermis is calculated as UV-shielding (%) = 100 (1- F_{UVA}/F_{BL}).

affect photosynthetic efficiency (Fu et al. 2017), and this can be estimated in plants by evaluating the sensitivity to UV-B radiation, and then represented as a ratio of available open and closed reaction centers in the thylakoid membrane (Fig. 3-2). A low photosynthetic efficiency ratio arises when photosystem II (PSII) contains fewer open reaction centers due to damage and impairment of the Calvin cycle (Xiong and Day 2001). The measurement relies on estimating the energy flow through reaction centers after 20-30 minutes of dark acclimation (Schreiber 2004). A portable chlorophyll fluorometer was used to measure the minimal fluorescence (F_o) and the maximal fluorescence (F_M) of chlorophyll that is used to calculate photosynthetic efficiency (Albert et al. 2010). Two measurements were made on dark adapted leaves on opposite sides avoiding the midrib prior to experimentation and immediately following the last day of UV-B treatment.

An iterative approach was used to establish optimal conditions for detecting metabolic changes in these *Populus* collections when treated with UV-B radiation. To preserve plant specimens, a noninvasive technique was used to measure epidermal transmittance of UV. The degree of UV transmittance in leaf tissue is an indirect method that relates to the metabolic changes upon UV exposure. A decrease in UV transmittance corresponds to an increase in UV protecting compounds that accumulate in the epidermis and the percentage of chlorophyll fluorescence is decreased. Changes in the levels of any protective compounds may then be further analyzed with LC-MS. Preliminary results indicated that upon significant UV-B exposure (20 – 35 kJ m^{-2}), there was an increase in UV protecting

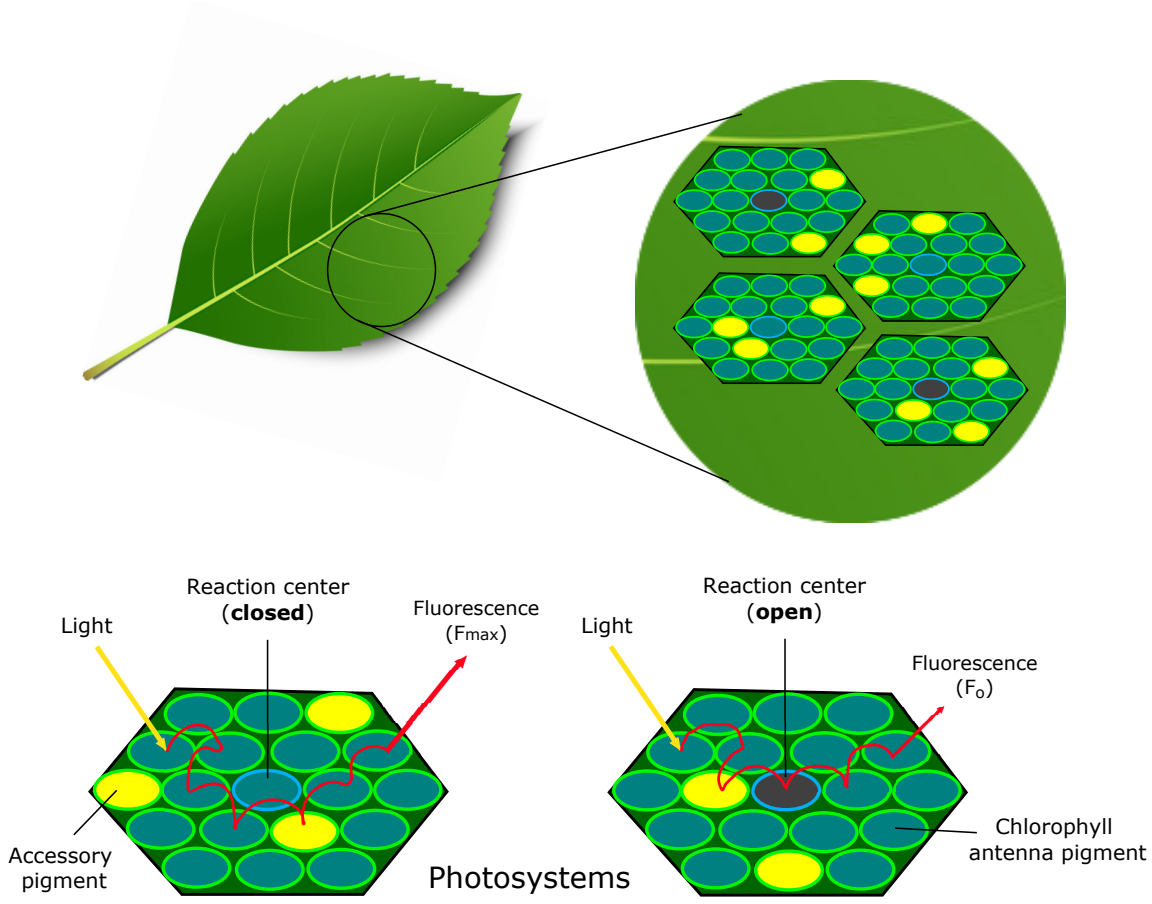

$$\Phi_{PSII,\,max} = (F_m\text{-}F_o)/F_m = F_v/F_m$$

Figure 3-2. Measurement of the maximum quantum efficiency of Photosystem II (PSII) ($\Phi_{PSII,max}$) in open reaction centers is measured with a dark-adapted chlorophyll fluorescence meter (F_v/F_m) as a parameter of plant stress. Non-destructive fluorescence measurements are performed by dark-adapting plant samples followed by exposure to the saturating excitation light source from a light emitting diode. The maximum fluorescence (F_m) represents available and oxidation state PSII reaction centers or when the level of fluorescence when the primary quinone electron acceptor has been maximally reduced and PSII reaction centers are closed. Leaf samples are exposed to saturating light intensity that closes and chemically reduces PSII reaction centers resulting in the maximum fluorescence value. The minimum fluorescence (F_o) is measured by the level of fluorescence when plastoquinone is maximally oxidized and PSII centers are open resulting in reduced fluorescence emission (Baker 2008).

compounds that varied among *Populus* genotypes. Natural variants from low and high growth elevation that possess altered lignin content suggest that UV protection is decreased in plants with lower lignin levels since lignin can absorb UV (Baxter and Stewart 2013). Further investigation with transgenic *Populus* with modifications in phenylpropanoid and lignin biosynthesis will be used to examine the hypothesis that precursors and lignin levels correlate with UV-B protection.

Materials and Methods

Plant Material – A natural population of 25 *P. trichocarpa* (Torr & Gray) genotypes were obtained from the Department of Biology at West Virginia University and the BioEnergy Science Center (currently, Center for Bioenergy Innovation). *Populus trichocarpa* trees were previously sampled along the Pacific Northwest and geographical information was recorded. Transformation of *P. deltoides* (Marsh.) clone, WV94 from Issaquena County., MS. was performed by ArborGen LLC. as described previously (Karve et al. 2012) and obtained from the Department of Biology at West Virginia University. *Populus* cuttings were propagated and planted in 6.0 L pots filled with soilless growing media (Sunshine LC1) and maintained in the greenhouse at the University of Maryland (College Park, MD) at 25 °C with 16 h photoperiod. Photosynthetic photon flux was between (PPF) 400-700 nm at about 1000 μmol m^{-2} s^{-1}. Temperatures were controlled by an evaporative cooling system and heating element to maintain 25°C. Representative plants (n = 3) similar in

height and appearance was based on availably and used for experimentation for each genotype and treatment condition.

UV-B Treatments – Lamp banks of UV-B fluorescent tubes were suspended above greenhouse benches. The lamp bank contained twelve Q-lab UVB-313 QFS40W fluorescent sunlamps (Q-panel Inc., Westlake, OH). Lamps were wrapped with 0.038 mm cellulose acetate film to absorb radiation below 290 nm (UV-B treatment) or 0.051 mm clear Mylar polyester film to absorb radiation below 315 nm (control treatment) following the general procedure outlined in Sullivan and Teramura (1988). Each fluorescent UV-B tube was measured with a broadband Solarmeter Digital Ultraviolet Meter 6.2 UV-B meter (Solartech, Harrison Township, MI) in μW cm^{-2} and recorded values were converted to kJ m^{-2} at 30 or 60 cm. UV-B experiments involved UV-B dosage ranging from 10 – 35 kJ m^{-2} for 6 – 8 h centered around solar noon for 10 – 14 days.

Epidermal UV Transmittance – The leaf plastochron index (LPI) range was used to assign an arbitrary age based on a morphological time scale rather than chronological time (Dickson et al. 1974). Adaxial surfaces of leaves at LPI 2 – 3 or LPI 7 – 8 correspond to approximately younger and older leaves, respectively. The same leaves were marked and selected for UV transmittance measurements with a pulse amplitude modulation (PAM) chlorophyll fluorometer (UV-A PAM; Gademann Instruments, Würzburg, Germany). UV-A PAM chlorophyll fluorescence was from UV-A radiation (375 nm) and visible blue light (470 nm). The UV-A PAM has been compared to UV transmittance in epidermal peels and was found to be highly correlated with intact leaf samples and allows for data collection

throughout experimentation (Markstädter et al. 2001). UV-A PAM measurements were taken at the beginning of UV-B experimentation and every other day. Ten repeated measurements were made on the same three leaves throughout experimentation and averaged with standard error calculation.

Chlorophyll Fluorescence Measurements – Maximum potential quantum efficiency of PSII was measured by the normalized ratio of variable fluorescence divided by maximum fluorescence (F_v/F_m). The measurement determines if photosynthetic efficiency is affected by plant stress such as UV-B radiation. Previously selected leaves from the UV epidermal transmittance measurements were dark adapted for 20 minutes and multiple locations were measured with a chlorophyll fluorometer (OS30p+, Opti-Sciences Inc., Hudson, NH). The instrument uses red light emitting diodes between 700-750 nm that detects low noise fluorescence in minimal fluorescence (F_o) and saturating light levels for s maximum fluorescence (F_m).

Metabolomic Analysis – Metabolite detection was performed on leaves previously selected for analysis using a UPLC-MS (Acquity Ultra Performance Liquid Chromatography system coupled with an LCT Premier XE Time-of-Flight Mass Spectrometer) system (Waters Corporation, Milford, MA). Leaf tissue was flash frozen in liquid nitrogen, ground into a fine powder with a mortar and pestle and stored at -80°C until analysis. Secondary metabolites were extracted from 4 mg/leaf of ground tissue with 1.5 ml with HPLC-grade MeOH at room temperature for 30 minutes, centrifuged for 10 minutes at 2100 x g, and filtered through microcentrifuge filtration units. Sample extracts were introduced into 12 x

32 mm screw neck glass vials with bonded preslit PTFE/silicone septa for automatic injection into a Waters Acquity C18 BEH 1.7 μm, 2.1x 50 mm UPLC column at 30°C. The column mobile phase consisted of solvent A (water + 0.1% formic acid) and solvent B (acetonitrile + 0.1% formic acid) at a flow rate of 0.4 mL/min. Time of flight (TOF) mass spectrometry was set to negative electrospray mode with V resolution. Capillary and cone voltage was set to 2800 V and 80 V, respectively, and the scan range was between 150 to 800 *m*/*z*. All samples were analyzed with an internal reference lock mass using leucine enkephalin (200 ng/mL) at a flow rate of 2.0 μL/min.

Chromatography and mass spectra were processed with the MassLynx 4.1 software package (Waters Corporation). Identification of signature compounds was achieved by comparison with internal and external standards (Millipore Corporation, St. Louis, MO). Identification of compounds for which standards are unavailable was determined with LC-MS molecular weights and retention times from previous work (Caseys et al. 2012, Babst et al. 2014) and the database within MassLynx. Using the mass of the deprotonated [M-H] ion, single ion chromatograms were integrated to calculate peak areas and normalized to an internal standard, vanillic acid. Quercetin glucoside and salicin external standards were used to generate a standard curve to determine concentration of each metabolite within a sample.

Results

UV Sensitivity of Leaves at Different LPI – As a first step, optimal conditions needed to be established to determine the impact of UV-B radiation in *Populus* based on plant leaf age (LPI), time of exposure, and radiation intensity. For this series of experiments, both *P. trichocarpa* and *P. deltoides* were used interchangeably since their responses to UV-B were so similar.

Due to the complexity of higher plants, and a gap in knowledge regarding the influence of leaf age on acclimation to UV-B in low-lignin *Populus*, leaves at different growth stages were evaluated to determine the impact of UV-B treatment. Leaves at LPI 2-3 and 7-8 leaves of low-lignin *P. trichocarpa* were treated with UV-B radiation for seven days and epidermal transmittance was measured during the initial (I) and final (F) day of experimentation (Fig. 3-3).

It was determined that on the final day of treatment, leaves at LPI 2-3 and 7-8 treated with ~10 kJ m^{-2} of UV-B radiation showed no difference from one another in epidermal transmittance, but differed from leaves without UV-B treatment. In general, after 3 – 4 days of UV-B exposure, UV epidermal transmittance increased compared to the control group in both *P. trichocarpa* and *P. deltoides,* and a maximal response was observed at approximately 10 days of UV-B irradiation. Similarly, the maximum quantum efficiency of PSII in the dark-adapted state showed an increase in F_v/F_m in *P. deltoides* treated with

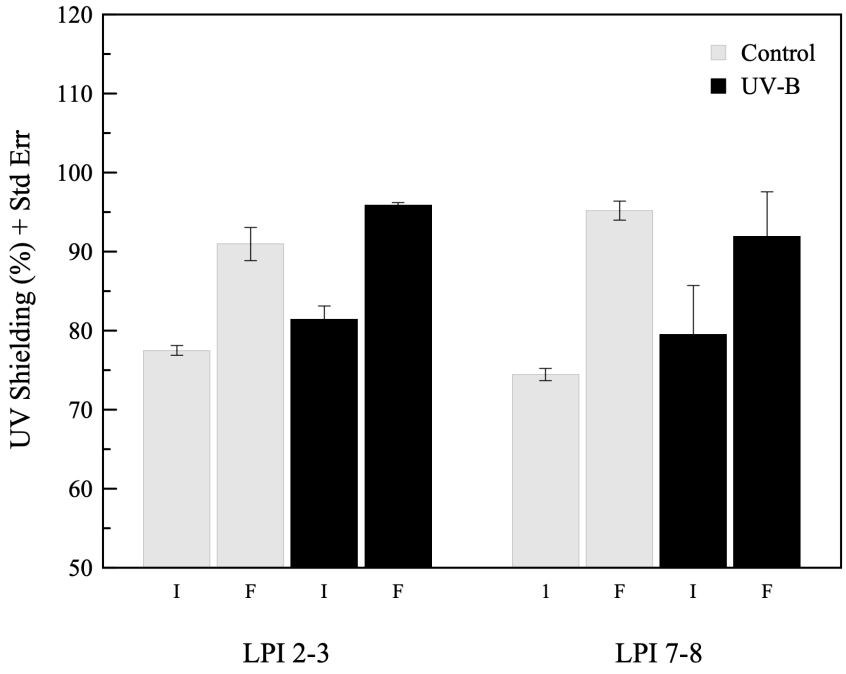

Figure 3-3. Initial and final epidermal transmittance in leaves at LPI 2-3 and 7-8 of *Populus trichocarpa* treated with low UV-B radiation. The effect of UV-B radiation in leaf tissue at different stages of growth in *P. trichocarpa* for 7 days. *Populus trichocarpa* was grown to about 30 cm, young leaves were marked and sampled from LPI 2-3 and leaves were marked and sampled from LPI 7-8 with the UV-A PAM fluorometer for epidermal transmittance. F_{UVA}/F_{BL} ratio was converted into percent with standard error bars. To further parameterize the effect of UV-B radiation in *P. trichocarpa* variants, leaf sampling at different growth stages determined no difference in preliminary screening of epidermal transmittance in day 1 for the initial (I) and day 7 for the final (F) measurement between leaves at LPI 2-3 and 7-8.

UV-B compared to the control (Fig. 3-4). These preliminary experiments determined that *Populus* leaves at LPI 3-4 could be marked and then analyzed on an average of 10 days after exposure to UV-B radiation at ~35 kJ m^{-2}.

Chlorophyll Fluorescence Response to UV-B in Populus Variants – Further characterization was necessary to find a correlation between lignin content or composition, growth of elevation, and UV-B acclimation. The observed acclimation response in the *Populus* variants provided some insight, but to determine if UV protection was related to elevation or low or high-lignin content, selected variants in the collection were analyzed for 14 days, with UV transmittance recorded every other day to calculate relative change (%) from the first measurement. For variants obtained at low growth elevation, the relative change in chlorophyll fluorescence was measured in a high-lignin variant (GW-10993, 27.20%, filled squares) showed a decrease in UV shielding compared to a low-lignin (BESC-99, 20.02%, open squares) (Fig. 3-5). This observation is consistent with the idea that lignin helps protect the plants from UV-B radiation and therefore is an important component to the rate and/or extent of acclimation. The low elevation-high lignin plants displayed a lower response to UV shielding of radiation, indicating that low-lignin plants are less well adapted to UV-B radiation and, accordingly, displayed a more robust response. However, the results contrasted in *P. trichocarpa* obtained from higher growth elevation that were treated under the same conditions. The relative change in chlorophyll fluorescence in a low-lignin variant (GW-9791; 20.38%, open triangles) variant decreased compared to a high-lignin variant (GW-9889, 27.10% filled triangles) variant (Fig. 3-6).

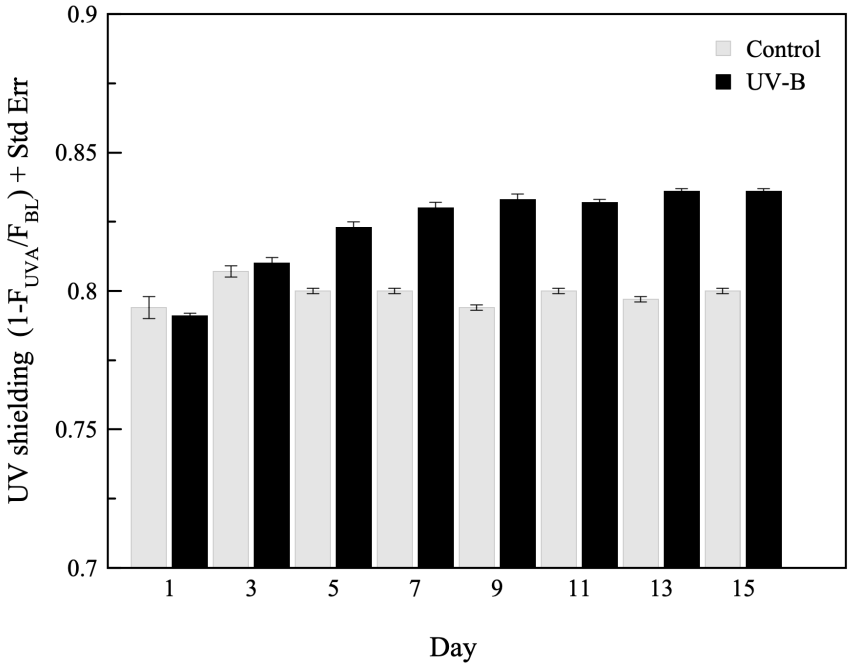

Figure 3-4. Increased UV epidermal absorbance and acclimation in leaves of UV-B treated *Populus deltoides* over a 15-day interval. Relative UV screening using the UV-A PAM fluorimeter was used to measure epidermal excitation radiation of chlorophyll in the mesophyll (n = 3). Chlorophyll fluorescence using UV-A radiation at 375 nm, F_{UVA}, was divided by the fluorescence from visible blue light at 470 nm, F_{BL} and this ratio corresponds to the extent of penetration of UV radiation into the mesophyll. UV induced chlorophyll fluorescence will decrease as increased UV absorbing compounds accumulate in the epidermis and further calculation to determine the percent of UV passing through the epidermis is calculated as UV-shielding (%) = 100 (1- F_{UVA}/F_{BL}). *Populus deltoides* was treated with UV-B radiation for 15 days and chlorophyll fluorescence was measured each day to determine that UV-B treated plants decreased in transmittance that is inversely proportional to increased UV protection compared to the control.

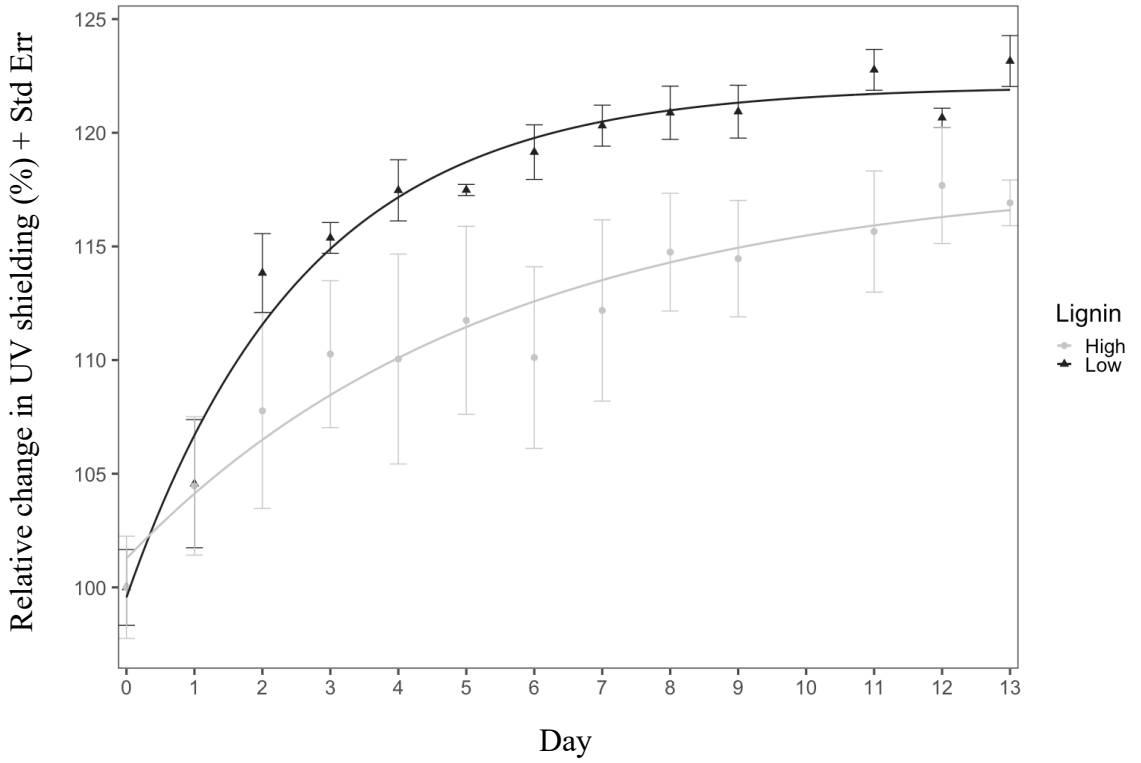

Figure 3-5. Relative change in epidermal screening in *Populus trichocarpa* variants with low and high lignin content at low origin of growth elevation over 14 days. Data show maximal response to UV (acclimation) within 9-10 days of UV-B radiation. Leaves of *P. trichocarpa* variants were measured with the UV-A PAM fluorometer and values were converted to percent change relative to control to represent the increase in UV-absorbing compounds for acclimation. The low-lignin variant (BESC-99, black line) showed increased change compared to the high lignin variant (GW-10993, gray line). Though latitude can affect UV-B radiation intensity, UV-B intensity is lower at low elevation compared to high elevation. These data suggests that less protected low-lignin *P. trichocarpa* from low elevation treated with UV-B, required greater change in UV-protective compounds for acclimation.

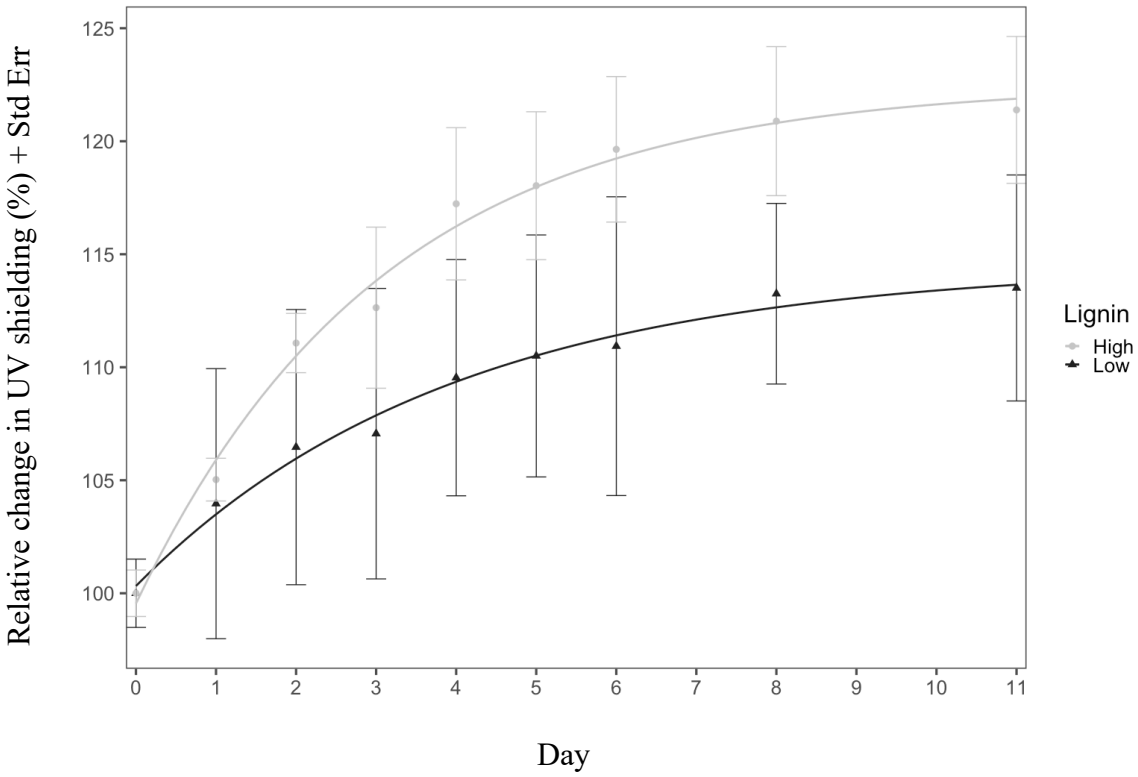

Figure 3-6. Relative change in epidermal screening in *Populus trichocarpa* variants with low and high lignin content at high origin of growth elevation over 12 days. Data show maximal response to UV (acclimation) within 9-10 days of UV-B radiation. Leaves of *P. trichocarpa* variants were measured with the UV-A PAM fluorometer and values were converted to percent change relative to control to represent the increase in UV-absorbing compounds for acclimation. The high-lignin variant (GW-9889, gray line) showed increased change compared to the low lignin variant (GW-9791, black line). Though latitude can affect UV-B radiation intensity, UV-B intensity is higher at high elevation compared to low elevation. These data suggests that though high-lignin *P. trichocarpa* have more lignin, it still required a greater increase in UV-protective compounds to compensate for acclimation. Additionally, low-lignin *P. trichocarpa* from high elevation may be predisposed for better protection metabolically.

In the case for high elevation poplars, higher levels of lignin appear less well adapted to UV-B radiation and therefore display a greater response to radiation, whereas plants with low-lignin levels seem better adapted with a lower response.

Generally, UV-B radiation levels are typically higher at high elevation compared to low elevation, however, latitude, weather conditions, and ozone concentration can contribute to the variation of radiation intensity. Thus, to further probe the contrasting shielding results of poplars obtained from high and low elevation, data for the growth elevation of each *P. trichocarpa* genotype was compared to respective lignin chemistry data. These data were obtained for the natural variants of *P. trichocarpa* in the collection of plants previously characterized with respect to lignin chemistry from wood cores and geographical information (Studer et al. 2011). Analysis of the composition of lignin (syringyl and guaiacyl ratio) showed no relationship to growth elevation (Fig. 3-7). Additionally, no clear correlation was found between the lignin content and growth elevation in *P. trichocarpa* (Fig. 3-8). In this light, a simple correlation observed between UV shielding and low and high lignin plants from low and high elevations cannot be made because although lignin can provide protection and absorb UV-B radiation, lignin data was obtained from wood cores and not sampled from leaves.

Metabolomic Analysis in Low-Lignin P. deltoides – The *Populus deltoides* collection obtained from the BESC included several lines that targeted a variety of genes to alter lignin levels or cellulose availability (Table 3-2). One specific line targeted the *CAD*

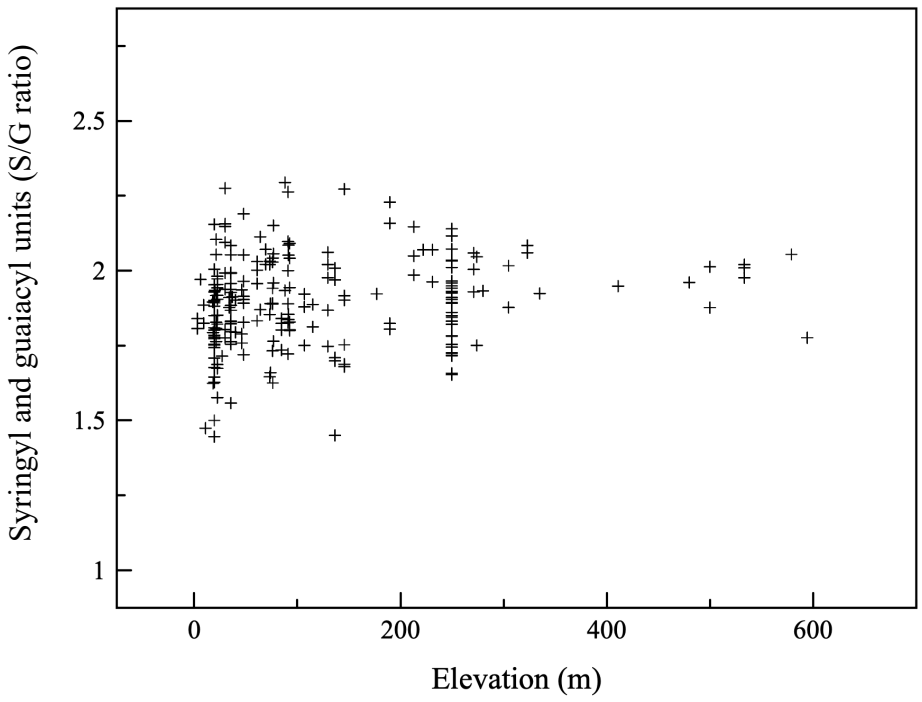

Figure 3-7. Relationship in lignin composition and origin of growth elevation. A dataset of natural variants of *Populus trichocarpa* analyzed for lignin content (%) and S/G ratio composition (Studer et al. 2011) was obtained to establish if the geographical information influenced the abundance of syringyl or guaiacyl units. The S/G ratio was plotted with origin of growth elevation (m) and a relationship was not determined.

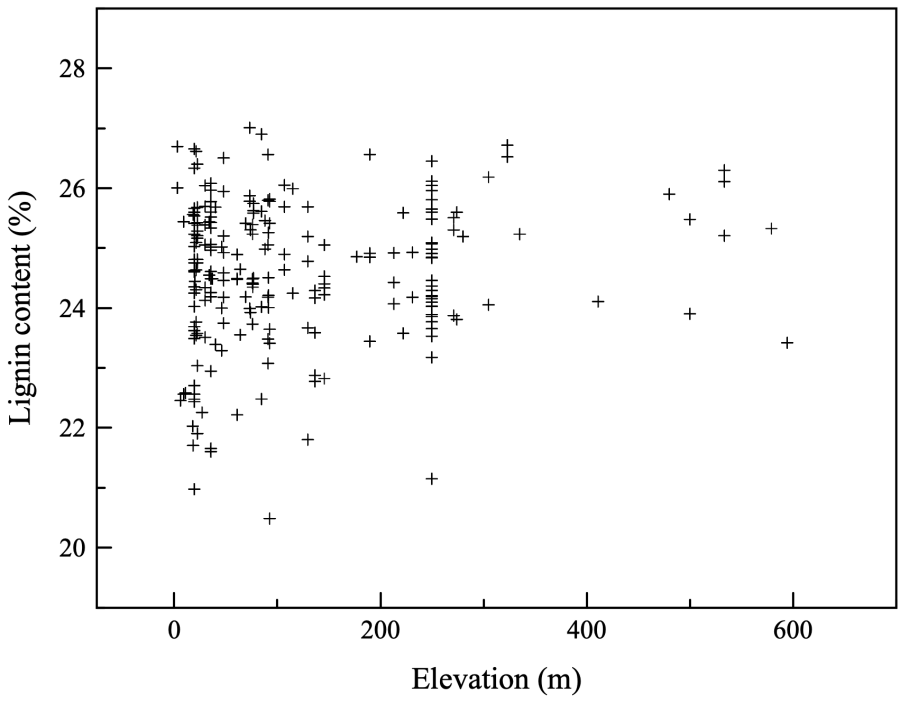

Figure 3-8. Relationship in lignin content and origin of growth elevation. A dataset containing the lignin chemistry from a population of natural variants of *Populus trichocarpa* was obtained from Studer et al. (2011). The lignin content (%) was plotted against the elevation (m) gradient of the natural population, however, a relationship was not determined.

(cinnamyl alcohol dehydrogenase) gene, which encodes the last enzyme in the phenylpropanoid pathway involved for lignin precursor biosynthesis. This line, with an attenuated copy of the single *CAD* gene, was used to assess the impact of UV-B radiation both ecophysiologically and metabolically. Ideally, one might expect a relatively straightforward outcome resulting from a block in this biosynthetic step. In *CAD* knockdown plants, with compromised lignin, it was expected that specific changes in metabolite levels could be readily targeted for analysis. The BESC used RNAi technology to attenuate the expression the single *CAD* allele in *P. deltoides*. Inter-variance of the transgenic RNAi *CAD* lines were categorized as either comparator (low transgene expression), or a top performing (TOP – high transgene expression) line (Macaya-Sanz et al. 2017). These plants were propagated in the greenhouse at College Park and used in UV-B acclimation experiments. Strikingly, UV-B treated *P. deltoides* lines downregulated in *CAD* showed remarkable anthocyanin hyper-pigmentation in newly emerging and fully expanded leaves throughout the stems, petioles, and veins as well as the leaf margin compared to the control (Fig. 3-9a-d). Based on this simple visual readout of UV-B acclimation, LC-MS analysis was used to determine the levels of key phenylpropanoid metabolites in these plants upon exposure to UV-B radiation. Quercetin glucoside and 4-coumaroyl glucoside were selected for analysis were based on the branch points that may affect UV-B protection in the phenylpropanoid pathway (Fig. 3-10). Quercetin glucoside is an abundant flavonoid that increased in normalized intensity in the TOP line compared to the comparator in the control and in UV-B treated plants (Fig. 3-11). The phenolic glycoside and a major branchpoint, 4-coumaroyl glucoside, showed an increase in the

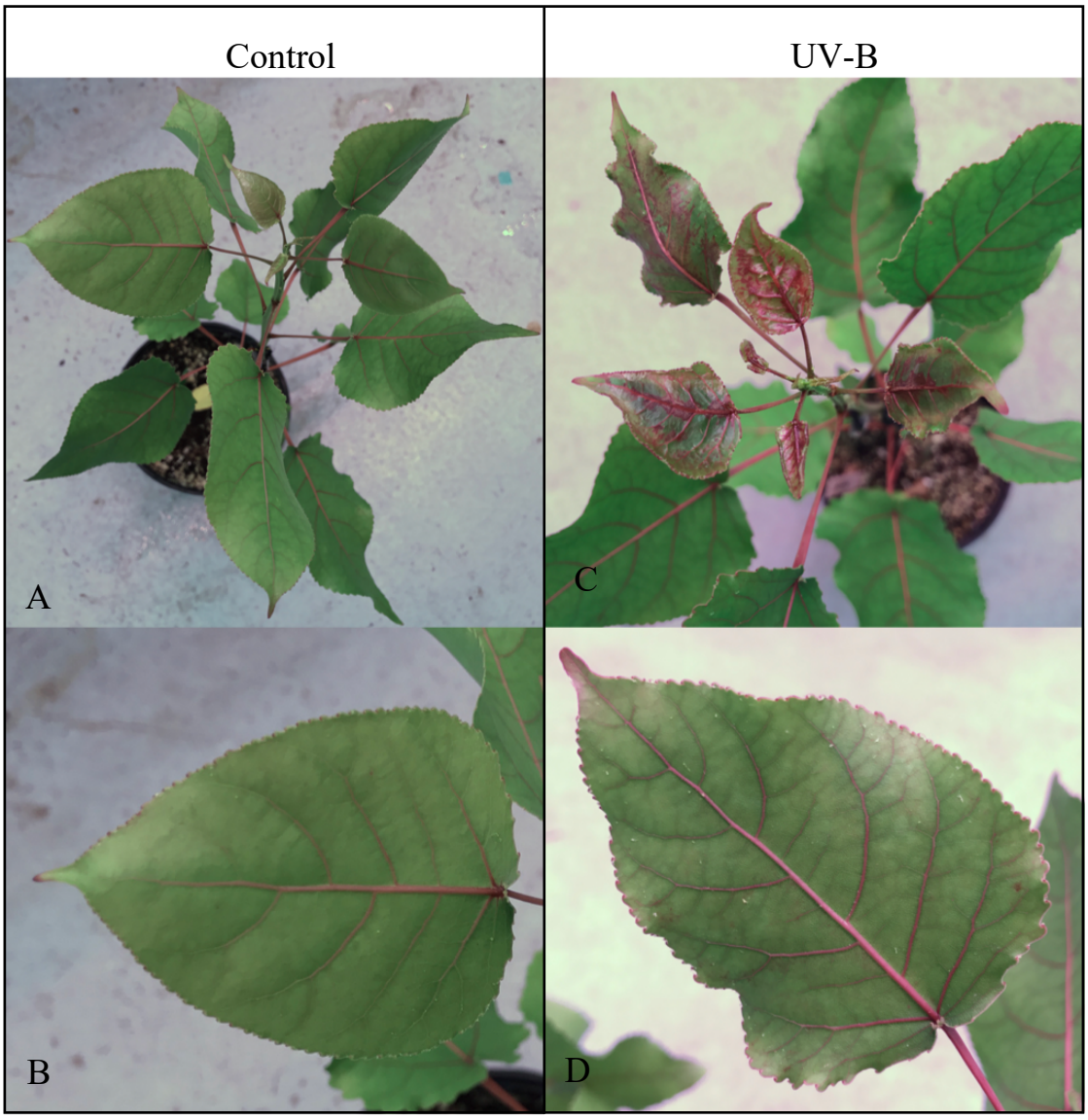

Figure 3-9. Low-lignin *Populus deltoides* show increased anthocyanin accumulation with UV-B exposure. (A) UV-B experiment showed low-lignin *P. deltoides* control group with red pigmentation in the stems and petioles and through part of the (B) midrib and veins. (C) Low-lignin *P. deltoides* showed increased accumulation in the newer leaves treated with UV-B radiation. (D) The older leaves show increasing anthocyanin accumulation through the veins and on the leaf margins.

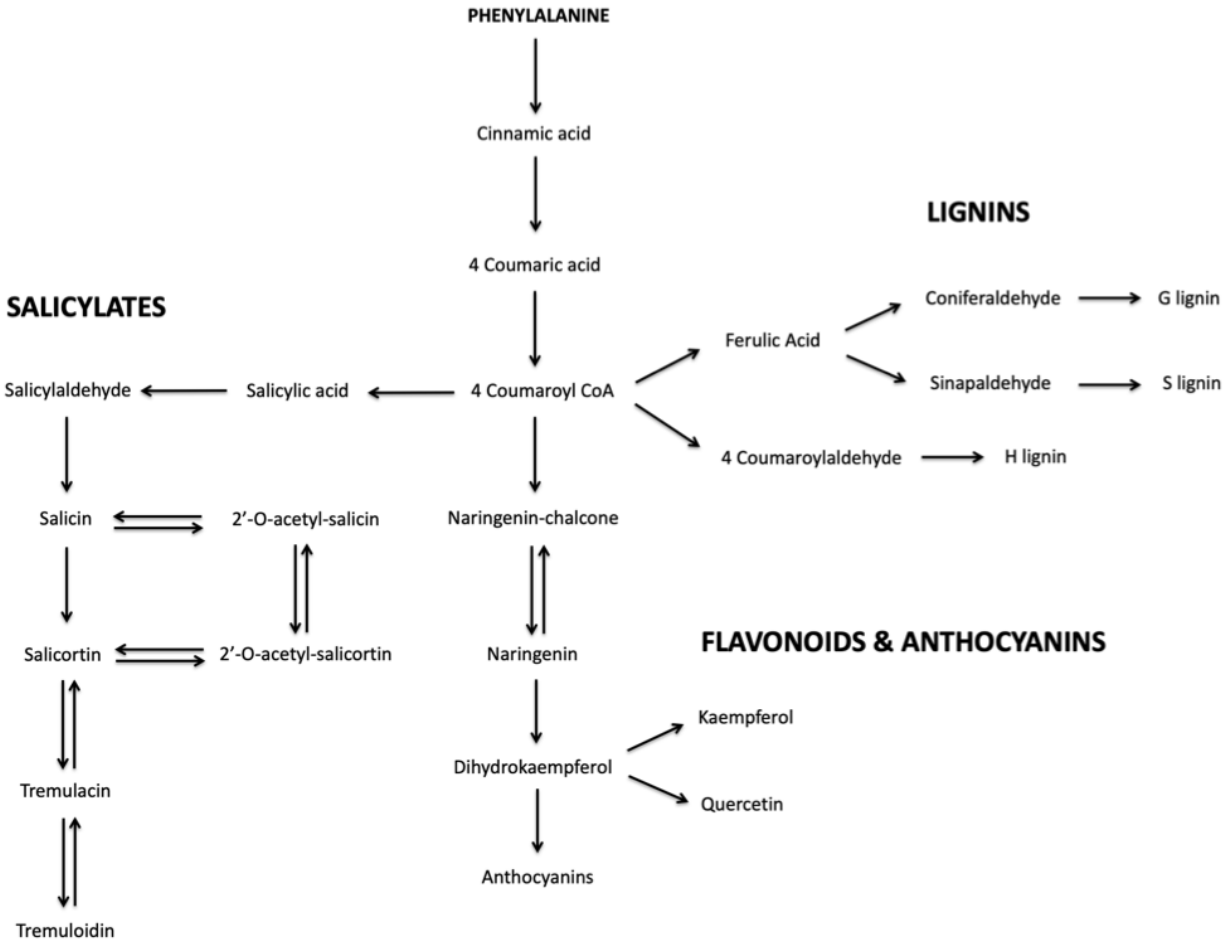

Figure 3-10. An abridged map of the phenylpropanoid pathway to highlight major branches of interest including: lignin, flavonoid, anthocyanin, and salicylate biosynthesis. Targeted metabolomic analysis was used to identify compounds in these pathways to measure changes in key metabolites after UV-B radiation treatments.

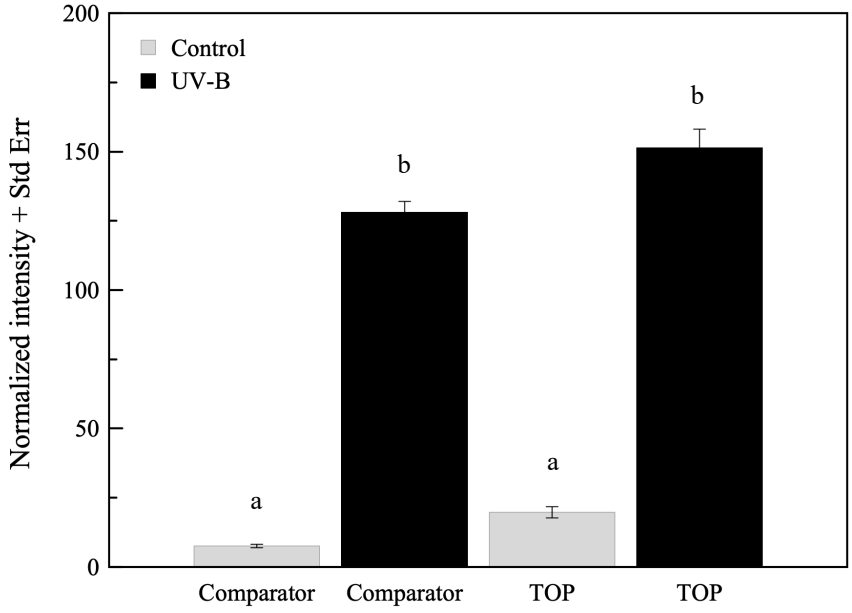

Figure 3-11. Measurement of quercetin glucoside in *P. deltoides* with differential transgene expression of *CAD*. Metabolomic analysis using LC-MS in differential transgene expression (comparator or TOP) of *CAD* (cinnamyl alcohol dehydrogenase) RNAi lines in *P. deltoides* were treated with UV-B radiation (n = 3). The results show increased levels of quercetin glucoside in the comparator (b) and TOP (b) lines treated with UV-B ($p < 0.00$) compared to Comparator and TOP controls (a) that showed no difference ($p < 0.79$ and 0.31). Statistically significant differences in normalized intensity values between Comparator and TOP lines are indicated by different letters (a and b: analysis of variance with post hoc Tukey's HSD test, $p < 0.05$). Inferential error bars denote the standard error in the variability of the mean.

comparator and TOP lines treated with UV-B compared to the control (Fig. 3-12). The TOP line in the controls showed slightly higher levels of 4-coumaroyl glucoside compared to the comparator. Additionally, salicylate levels were affected by UV-B radiation with similar trends in 2-acetylsalicortin, HCH-salicortin, and salicortin (Fig. 3-13-15). The comparator line showed an increase in salicylate after UV-B exposure compared to the controls, however, there was no difference in the TOP lines in either control or UV-B treatment.

Discussion

The UV-B treatment on leaves at LPI 2-3 and 7-8 over seven days did not reveal any meaningful relationship between leaves at different growth stages and UV-B acclimation at low doses of radiation. It has been reported in literature that there are some minor metabolic differences in both *Brassica* species and in *P. trichocarpa* between leaves at LPI 2-3 and 7-8 when treated with UV-B radiation for long periods, including changes in the concentration of phenolics, including salicylates and flavonoids (Warren et al. 2003, Reifenrath and Müller 2007). Despite these interesting observations, given the minor differences reported, as well as the increased extent of investigation required to address the challenge of analyzing the developmental and physiological response of individual leaves for each genotype, this direction was not pursued and deemed beyond the scope of the project. UV-B intensity can be more accurately annotated if applying a biological spectral

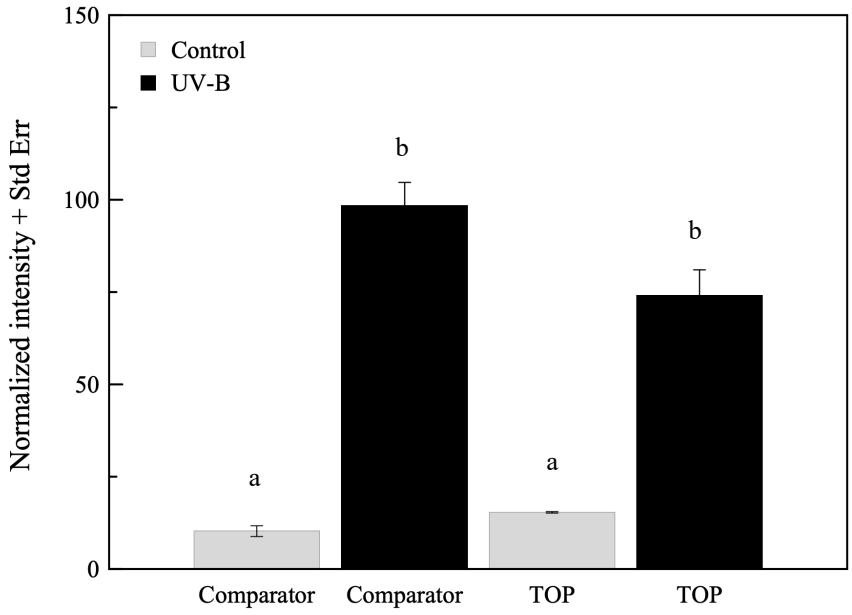

Figure 3-12. Measurement of 4-coumaroyl glucose in *P. deltoides* with differential transgene expression of *CAD*. Metabolomic analysis using LC-MS in differential transgene expression (comparator or TOP) of *CAD* (cinnamyl alcohol dehydrogenase) RNAi lines in *P. deltoides* were treated with UV-B radiation (n = 3). The results show increased levels of 4-coumaroyl glucose in the comparator (b) and TOP lines treated with UV-B (b) compared to Comparator and TOP controls (a) ($p < 0.00$). Control poplars showed no difference ($p < 0.98$ and $p < 0.25$). Statistical significance in normalized intensity values between Comparator and TOP lines are indicated by different letters (a, b: analysis of variance with post hoc Tukey's HSD test, $p < 0.05$). Inferential error bars denote the standard error in the variability of the mean.

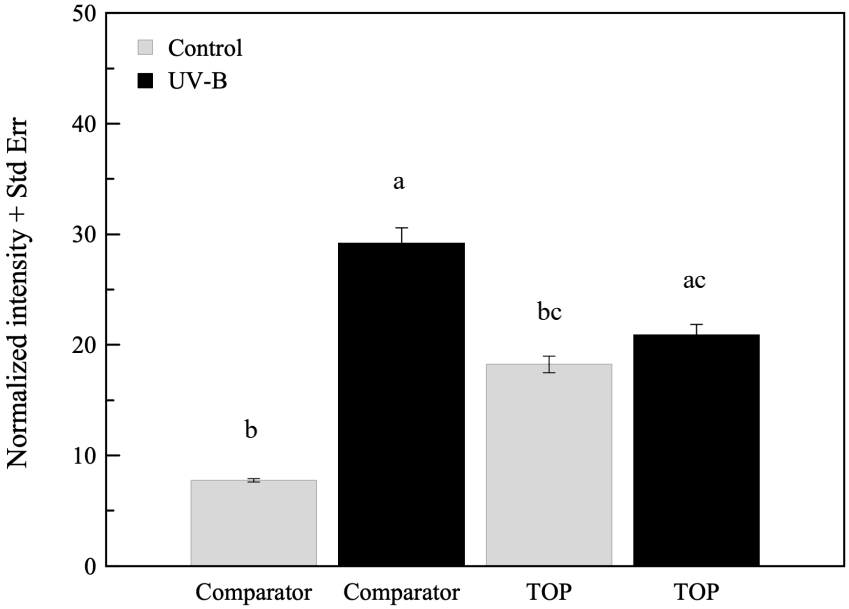

Figure 3-13. Measurement of 2'-acetylsalicortin in *P. deltoides* with differential transgene expression of *CAD.* Metabolomic analysis using LC-MS in differential transgene expression (comparator or TOP) of *CAD* (cinnamyl alcohol dehydrogenase) RNAi lines in *P. deltoides* were treated with UV-B radiation (n = 3). Control Comparator (b) is statistically different than UV-B treated Comparator (a) ($p < 0.00$); control TOP (bc) is statistically identical to UV-B treated TOP (ac) ($p < 0.91$). Statistically significant differences in normalized intensity values between Comparator and TOP lines are indicated by different letters (a, b, and c: analysis of variance with post hoc Tukey's HSD test, $p < 0.05$). Inferential error bars denote the standard error in the variability of the mean.

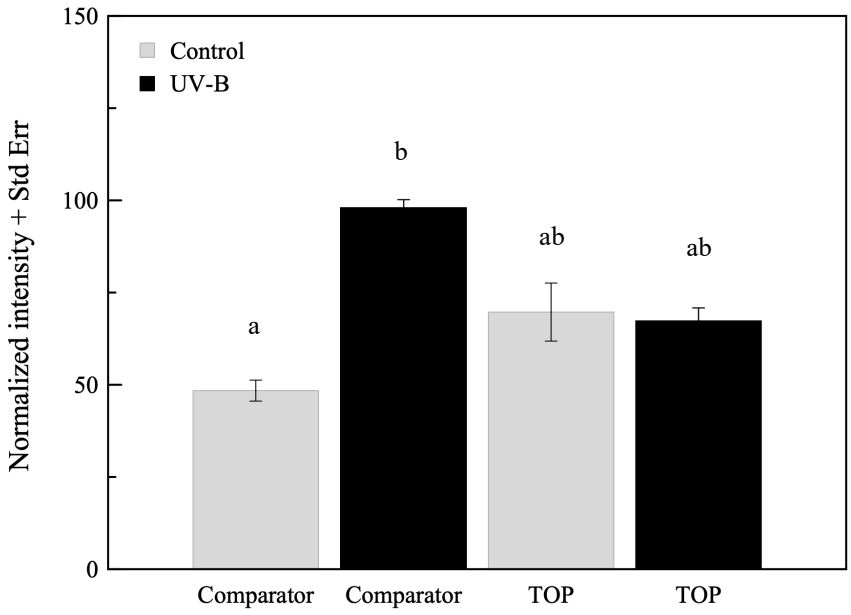

Figure 3-14. Measurement of HCH-salicortin in *P. deltoides* with differential transgene expression of *CAD*. Metabolomic analysis using LC-MS in differential transgene expression (comparator or TOP) of *CAD* (cinnamyl alcohol dehydrogenase) RNAi lines in *P. deltoides* were treated with UV-B radiation (n = 3). The results show increased levels of HCH-salicortin only in the comparator line with UV-B treatment (b) compared to the control (a) ($p < 0.01$) but no difference in the TOP lines (ab) ($p < 1.00$). Additionally, no significance in between the control poplars and no difference between the UV-B treated poplars. Statistical significance in normalized intensity values between Comparator and TOP lines are indicated by different letters (a and b: analysis of variance with post hoc Tukey's HSD test, $p < 0.05$). Inferential error bars denote the standard error in the variability of the mean.

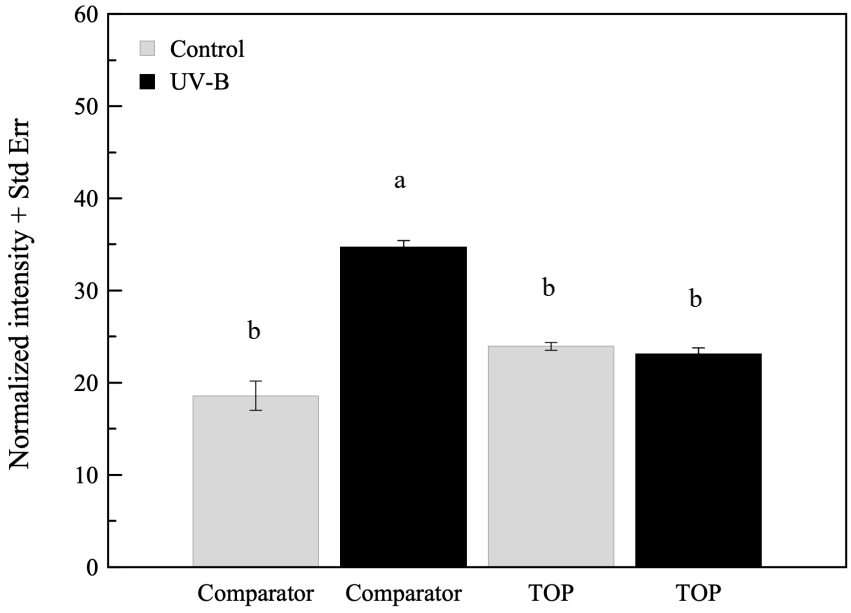

Figure 3-15. Measurement of salicortin in *P. deltoides* with differential transgene expression of *CAD*. Metabolomic analysis using LC-MS in differential transgene expression (comparator or TOP) of *CAD* (cinnamyl alcohol dehydrogenase) RNAi lines in *P. deltoides* were treated with UV-B radiation (n = 3). The results indicate increased levels of salicortin in the comparator line with UV-B treatment (a) compared to the control (b) and TOP line ($p < 0.04$ and 0.02) but no difference in the TOP lines with or without UV-B treatment (b). Normalized intensity values between Comparator and TOP lines are indicated as statistically significant by different letters (a and b: analysis of variance with subsequent Tukey's HSD test, $p < 0.05$). Inferential error bars denote the standard error in the variability of the mean.

weighting function in assessing the effectiveness of varying wavelengths that may affect the biological response in plants (Flint and Caldwell 2003). To further simplify experimental conditions and due to the high doses of UV-B radiation, a weighting function was not used because the level is not biologically relevant and would only occur in severe stratospheric ozone reduction. *Populus* treated with higher doses of UV-B radiation (20-35 kJ m^{-2}) showed an increase in epidermal UV transmittance and increased photosynthetic efficiency (F_v/F_m) compared to low dose exposure (10 kJ m^{-2}). Both measurements consistently showed the initial acclimation response within a few days and a maximal response in approximately 10 days. This response may be due to the accumulation of UV-B absorbing compounds in the epidermis as well as protection from lignin that is also produced from metabolites originating from the phenylpropanoid pathway. In the natural population, low elevation genotypes showed results that were consistent with the rationale that low-lignin *P. trichocarpa* are less protected from UV-B radiation because of reduced absorption of UV-B stemming from the lignin deficiency. The low-lignin genotype showed greater change in acclimation by producing more UV-absorbing compounds compared to the low elevation with high-lignin variants. The results from the low-lignin poplars at low elevation may indicate a level of photoprotection from metabolic compensation that could be more useful compared to high-lignin poplars. However, the high elevation variants responded inversely: the high-lignin plants showed a greater change in relative chlorophyll fluorescence over time than the low-lignin variant. The results from the high elevation variants showed an unexpected response compared to the low elevation variants that may be attributed to the committed allocation of certain metabolites. It is possible that lignin precursors are abundant in low-lignin plants and other UV-absorbing

compounds are synthesized, which would require more extensive metabolite analysis for corroboration. The chemical complexities and functional roles of secondary metabolites are complicated: many metabolites not only absorb UV in the epidermis and thereby attenuate transmission of radiation into the mesophyll, but some metabolites also protect photosynthetic machinery or mitigate reactive oxygen species during stress (Burchard et al. 2000, Hideg et al. 2013). A comprehensive, non-targeted analysis of the metabolome of well-defined *Populus* variants would be needed to fully characterize the metabolic flux through the phenylpropanoid pathway within contexts such as modified levels or composition of lignin and UV-B stress. However, this approach would require specific, additional expertise and more sophisticated instrumentation, both beyond those immediately available. Nonetheless, a targeted metabolomics approach would still provide a framework to understand the acclimation of low-lignin *Populus* to UV-B radiation.

In spite of the complexities that underlie lignin content and composition, growth elevation, and the influence on acclimation to UV-B, it is clear that metabolic changes occur in *Populus* leaves in response to UV-B radiation. Lignin is abundant in vascular transport structures but it can be detected via spectroscopy in fresh leaves from various species (Martin and Aber 1994). However, the response of these measurements were made in leaves and not wood cores but altered lignin levels can affect secondary metabolite precursors in the phenylpropanoid pathway (Dauwe et al. 2007). Therefore, a broad interpretation can be made that is supported by results from epidermal UV transmittance, photosynthetic efficiency and targeted metabolomic analyses. Increases in key UV-absorbing compounds, such as flavonoids and salicylates were detected in *Populus* treated

with UV-B. However, the increase in salicylates in Comparator and TOP lines regardless of UV-B treatments, were most likely due to the metabolome alteration in lignin biosynthesis (Dauwe et al. 2007). Furthermore, metabolic flux has been demonstrated in down-regulated *CAD* that affected other phenylpropanoids that resulted in red pigmentation from anthocyanins in *Populus* (Baucher et al. 1996). To account for differences in salicylate levels in *P. deltoides CAD* knockdown Comparator and TOP lines, total salicylate levels should be measured because the compounds are labile and may accumulate in leaves, stems, and shoot tips (Ruuhola and Julkunen-Titto 2000). These results suggest that the metabolites in these major branches are an important component to the acclimation response in *Populus*. Future modification of these metabolic pathways in *Populus* with the purpose of increasing certain metabolites for additional UV-B protection in low-lignin plants, may provide additional insight into developing new biofuel feedstocks.

Chapter 4: Analysis of the *Populus trichocarpa UVR8* Locus for Polymorphisms that Alter Expression or Structure and Function of the Photoreceptor

Introduction

The poor correlation between lignin levels and ecophysiological properties in the environmentally diverse *Populus* collection described in Chapter 3 suggests that natural genetic variation was insufficient to drive significant enough changes to phenylpropanoid and flavonoid biosynthesis for easily analyzing with metabolic acclimation to UV-B radiation. Therefore, more dramatic alterations that resulted in large metabolic changes when poplar was exposed to UV-B radiation were sought. Thus, I focused on genetic alterations that would alter the expression levels of *UVR8*, which would be expected to result in pronounced downstream physiological changes relative to wild-type plants when treated with UV-B. If a down-regulated UVR8 variant could be identified, it might simplify the analysis of low-lignin *Populus* response to UV-B. Given the significant genomic resources available for poplar, single nucleotide polymorphisms were investigated in the *UVR8* locus.

The most common type of genetic variation arises from single nucleotide polymorphisms (SNPs). SNPs are germline substitutions at one nucleotide position at a specific location

in a genome. The frequency with which SNPs occur in the human genome is approximately 1/1000 bp, but in plants SNPs can be more abundant, occurring with a frequency of 1/100-300 bp (Gupta et al. 2005, Kharabian 2010). The explosion of sequences in public genome databases provides a significant opportunity for identifying SNPs to understand genetic diversity, to indicate susceptibility to disease, and to discover useful alleles to improve economically important crops and enhance performance. Although polymorphisms can lead to phenotypic diversity in plant yield, size, and color, they can also lead to a variation in response and tolerance to various abiotic and biotic stresses (Huq et al. 2016).

SNPs can have multiple effects on gene expression and regulation. For example, SNPs can influence the activity of the control regions involved in gene expression. Additionally, SNPs can alter splice sites and lead to alternative processing of mRNA and therefore non-native protein expression. SNPs that occur in the coding regions of genes can be synonymous, which do not result in a change in the amino acid coding sequence, or they can be non-synonymous, that can lead to either amino acid substitutions or a stop codon that alters the function or structure of a protein. Analyzing with these polymorphisms in gene loci will lead to a better understanding of genetic variation on plant traits under normal and adverse environmental conditions and thus provide opportunities for agronomic improvement.

The identification of SNPs in the gene for the UVR8 photoreceptor, which affect receptor expression and/or function, would be of particular interest because of its role in the perception of UV-B radiation and in initiating the response to UV-B exposure. Therefore,

SNPs within the *UVR8* gene locus in natural variants of *P. trichocarpa* were analyzed computationally to provide information on changes in gene expression, splicing patterns, and/or receptor function. Ideally, a goal would be to identify polymorphisms that indicate a poplar line with a bias in photoreceptor structure, stability or expression, that would be useful for ecological physiology and metabolomic studies to better understand the molecular basis of UV-B perception, signal transduction, acclimation and tolerance to UV-B radiation. Importantly, almost 18 million SNPs have been identified in the whole genome sequences of 461 accessions of *P. trichocarpa,* with between 4 to 20 clonal replicates, totaling 883 natural variants (Evans et al. 2014). Therefore, an analysis of SNPs associated within the *UVR8* gene locus was examined to determine whether any nucleotide variation would predict altered UVR8 expression, structure, or function.

Three computational and bioinformatic approaches were utilized to examine high frequency SNPs in the *UVR8* locus that could result in several important outcomes. First, a sequence profile was generated for transcription activation motifs (Liu et al. 2014, Porto et al. 2014, Liu and Stewart Jr 2016) and SNPs in the *UVR8* control region that disrupt or more closely align with ideal sequence motif were identified to glean clues on changes in gene expression and therefore protein levels. Second, the splice junctions (donor and acceptor splice sites) of the 11 intron sequences within the *UVR8* gene locus were identified and scanned for SNPs that could result in incorrect or alternative splicing, that would affect wild-type UVR8 levels available for sensing and downstream activation (Dogan et al. 2007). Third, SNPs were identified in the protein coding regions of URV8 that result in amino acid changes, leading to possible structure or function change. The results showed

a surprisingly low number of SNPs that may affect UVR8 expression and function, and support the hypothesis that UVR8 is under positive selection to maintain a regulated expression level. The data suggest that altering expression of *UVR8* may lead to significant metabolic effects upon exposure of *Populus* to UV-B radiation and may therefore yield clues on the molecular basis for acclimation and tolerance.

Materials and Methods

BLAST Search and UVR8 Paralogs – The gene model for *UVR8* was obtained from *Arabidopsis thaliana* and the protein sequence (accession number AT5G63860) was used to locate the homologous sequence in the *Populus trichocarpa* genome v3.0 using the Phytozome v12.1 database. The gene with the lowest expect value was used for SNP analysis: Potri.007G100200. Additionally, Potri.007G100200 was used to identify the gene family of UVR8 using a plant comparative genomic database, Plaza 3.0. Based on the homologous sequence of *UVR8* in *P. trichocarpa*, 23 *UVR8* paralogs were found. A list of accession numbers in Plaza 3.0 were used to cross reference *UVR8* sequences in Phytozome 12.1 to determine functional copies. Additionally, an expression profile was created using the Bio-Array Resource (BAR) database that displays an electronic fluorescent pictograph to visualize gene expression patterns across homologous sequences (http://bar.utoronto.ca) (Waese and Provart 2016). Each paralog of UVR8 was compared to analyze the global patterns of gene expression in different tissues and organs of interest.

A phylogenetic analysis by maximum likelihood (PAML) program was used to analyze DNA and protein sequences with amino acid substitutions (Goldman and Yang 1994). K_a/K_s ratios in single-copy genes was performed with PAL2NAL online software (http://www.bork.embl.de/pal2nal/) that utilizes codeml, a PAML package used to calculate maximum likelihood (Suyama et al. 2006). Genomic and peptide sequences of selected single-copy gene models used for analysis was obtained from Phytozome and BioMart.

SNP Identification in the UVR8 Promoter Region – A sequence profile was generated in the promoter region at 500 bp from the start codon of UVR8 in *P. trichocarpa*. Because there is no information on the transcriptional regulation of *UVR8*, a promoter database was used to determine putative transcription factor binding sequences upstream of the gene. Promoter elements were predicted with consensus sequences using a plant *cis*-acting regulatory element database, PlantCARE (Zwaenepoel and Van de Peer 2019). Three classes of binding sites for transcription factors were selected for identification within the *UVR8* gene locus. These included the core promoter region, response to stress and the light responsive element (Porto et al. 2014).

SNP Identification within UVR8 Splice Junctions – Intron and exon organization of *UVR8* in *P. trichocarpa* was determined in Phytozome. Analysis of the 11 introns revealed 22 splice junction sites in the reference sequence of *P. trichocarpa*. These regions were compared across 883 sequenced individuals of *P. trichocarpa* natural variants. Sequence data was obtained from Phytozome to target genomic regions in the gene of interest

(Goodstein et al. 2012). Splice motifs were predicted using web-based software, SplicePort (https://spliceport.cbcb.umd.edu/), that scans candidate acceptor and donor splice site sequences (Dogan et al. 2007). A profile was created by listing SNPs found in splice junctions to determine potential splicing variants in UVR8.

SNP Identification in the UVR8 Structural Gene (Exons and Introns)– To determine possible amino acid changes that could lead to altered structure or function of the photoreceptor, non-synonymous amino acid substitutions were retrieved from Phytozome and identified in the coding region of *P. trichocarpa* UVR8. Substitutions were analyzed within the context of the three-dimensional structure (PDB ID: 4D9S) of *A. thaliana* UVR8 (Christie et al. 2012) by visualization in PyMOL.

Results

The sequence of *Arabidopsis thaliana UVR8* was used to probe the *P. trichocarpa* in Phytozome to identify homologs using a BLAST search. This approach yielded 23 paralogous genes in *P. trichocarpa* that were similar to the *UVR8* gene of *Arabidopsis* and are listed in Table 4-1. All 23 sequences were aligned, and the five sequences that showed the most homology to the *Arabidopsis* UVR8 sequence are shown in Fig. 4-1. The alignment was visually inspected to identify the essential UV-B sensing mechanism in UVR8, composed of residues W233, W285 and W337 (highlighted in red in Fig. 4-1), as

Table 4-1. *Arabidopsis thaliana UVR8* gene ID with *Populus trichocarpa* paralogs.

Gene ID (PLAZA)	**Strand**	**Chromosome**	**Accession Number (Phytozome)**	**Alignment ID**	**Amino acid length**
AT5G63860	-	Chr05	AT5G63860.1	AT*	441
PT01G02690	-	Chr01	Potri.001G026900.1	PT1	1101
PT01G27690	+	Chr01	Potri.001G276900.1	PT2	1116
PT02G07030	+	Chr02	Potri.002G070300.1	PT3	1115
PT03G19760	+	Chr03	Potri.003G197600.1	PT4	1115
PT04G00060	-	Chr04	Potri.004G000600.1	PT5	448
PT04G08090	+	Chr04	Potri.004G080900.1	PT6	1079
PT04G10180	+	Chr04	Potri.004G101800.1	PT7	390
PT05G06880	+	Chr05	Potri.005G068800.1	PT8	60
PT05G07100	-	Chr05	Potri.005G071000.1	PT9	420
PT05G19000	-	Chr05	Potri.005G190000.1	PT10	1115
PT06G08990	+	Chr06	Potri.006G089900.1	PT11	135
PT07G10020	-	Chr07	Potri.007G100200.1	PT12	443
PT08G05980	+	Chr08	Potri.008G059800.1	PT13	486
PT08G16750	+	Chr08	Potri.008G167500.1	PT14	1110
PT09G07180	+	Chr09	Potri.009G071800.1	PT15	1105
PT10G19910	-	Chr10	Potri.010G199100.2	PT16	483
PT11G02370	-	Chr11	Potri.011G023700.1	PT17	183
PT14G17250	+	Chr14	Potri.014G172500.1	PT18	446
PT14G19830	-	Chr14	Potri.014G198300.1	PT19	446
PT15G10700	+	Chr15	Potri.015G107000.5	PT20	391
PT16G10170	+	Chr16	Potri.016G101700.1	PT21	477
PT17G11320	-	Chr17	Potri.017G113200.1	PT22	393
PT17G13960	-	Chr17	Potri.017G139600.1	PT23	1083

**Arabidopsis thaliana UVR8* gene model was aligned with *Populus trichocarpa* amino acid sequences.

Table 4-1. *Arabidopsis thaliana UVR8* gene ID with *Populus trichocarpa* paralogs. The amino acid sequence from *At*UVR8 was used to identify the paralogous gene models in *P. trichocarpa*.

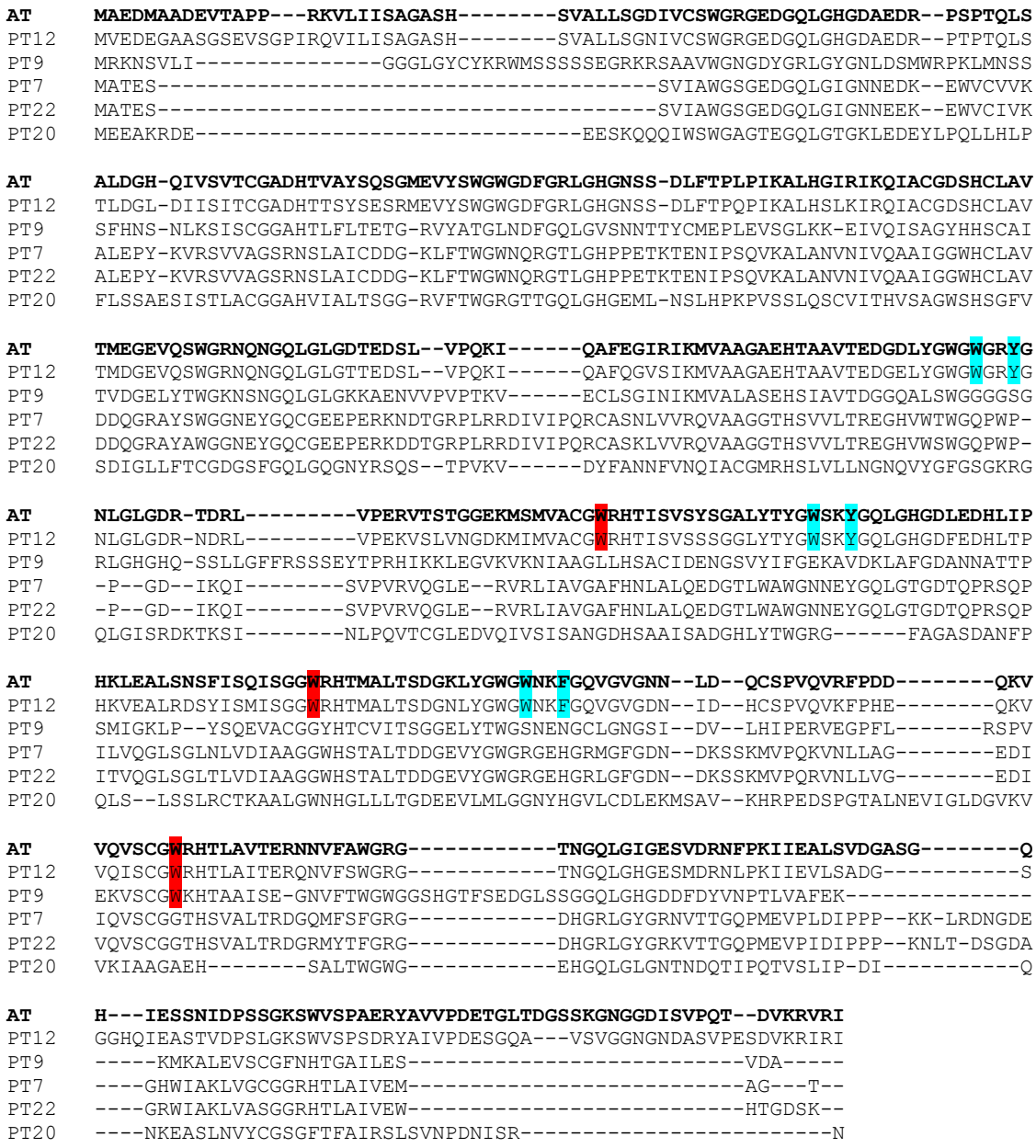

Figure 4-1. Sequence alignment in *UVR8* gene models in *Populus trichocarpa.* All gene models found in *P. trichocarpa* (Table 4-1) were aligned in the same manner using AtUVR8 as the reference sequence. Highlighted in red indicates important residues (W233, W285, and W337) that form the tryptophan pyramid chromophore that is essential for UV-B perception. Three aromatic pairs form the perimeter to protect the tryptophan pyramid (W198, Y201; W250, Y253; and W302, F305) highlighted in cyan. The only candidate sequence that contains all the mentioned aromatic residues is PT12 (Potri.007G100200.1) indicating the only functional UV-B sensing photoreceptor.

well as conserved aromatic residues that surround the tryptophan pyramid chromophore (highlighted in cyan in Fig. 4-1). As can be seen in the alignment, only a single gene model (Potri.007G100200) contains the conserved regions and therefore is consistent with a single-copy of *UVR8* in *Populus trichocarpa*. Interestingly, the sequences missing the key functional residues found in UVR8 show striking similarity to human RCC1, a guanine nucleotide releasing factor involved in chromatin condensation in S phase, which displays a similar seven-bladed β-propeller domain structure, but which assembles as a trimer, rather than a dimer like UVR8 (Rizzini et al. 2011, Duanmu et al. 2017). Thus, it was concluded that *Populus trichocarpa* contains one functional copy of the UVR8 photoreceptor.

The assembled and annotated genome sequences of *Populus trichocarpa* (Phytozome v3.0) were used to identify SNPs in the upstream control region, in splice sites and in the coding region of the *UVR8* gene. Both synonymous and non-synonymous SNPs were identified in the *UVR8* gene model to obtain K_a/K_s ratios to evaluate whether selective pressure is acting on UVR8 structure, function and expression. K_a/K_s ratios are typically used in population genetics to glean information on the selective forces acting on a gene. Ka is related to the number of nonsynonymous substitutions, and Ks relates to the number of synonymous substitutions (Hurst 2002). The genome sequence in the control region contains motifs for transcription factor binding that activate or repress gene expression, and SNPs in these regions could result in altered level of UVR8 expression. However, the regulatory and core promoter elements that are recognized by transcription factors and serve as binding sites for transcription of a gene have not been characterized in *UVR8*.

Therefore, the PlantCARE database was used to predict regulatory elements 500 bp upstream from the start codon in *UVR8* that may be involved in transcription. Regulatory sites were predicted based on transcription factor classes that function as part of the core promoter, response to stress, and light-responsive elements (Table 4-2) (Porto et al. 2014). Although the locations of regulatory sequences are typically given relative to the transcription start site, since the start site for transcription is unknown for *UVR8*, the distances are provided from the start codon.

A gene expression profile was generated using eFP to show tissue specific expression of UVR8 and paralogous gene models in *P. trichocarpa.* The *UVR8* gene (Potri.007G100200) appears to strongly express in male catkins and young leaves as compared to the female catkins and roots, and mature leaves and xylem show moderate expression (Fig. 4-2A). Selected gene models for this analysis show contrasting expression in various organs and tissue types. Paralogous gene models of *UVR8* (Potri.005G071000 and Potri.009G071800) display contrasting gene expression in the catkins and roots (Fig. 4-2B, C).

Six sequence motifs were predicted for control of *UVR8* expression. First, the TATA box promoter element was identified. This site, comprising a binding site for transcription factors and which is involved in the initiation of transcription, was found 112 bp upstream from the start codon. The TATA box sequence, TATTATA, was found 112 nucleotides upstream of the ATG start codon of *UVR8*. An analysis of Phytozome revealed two SNPs,

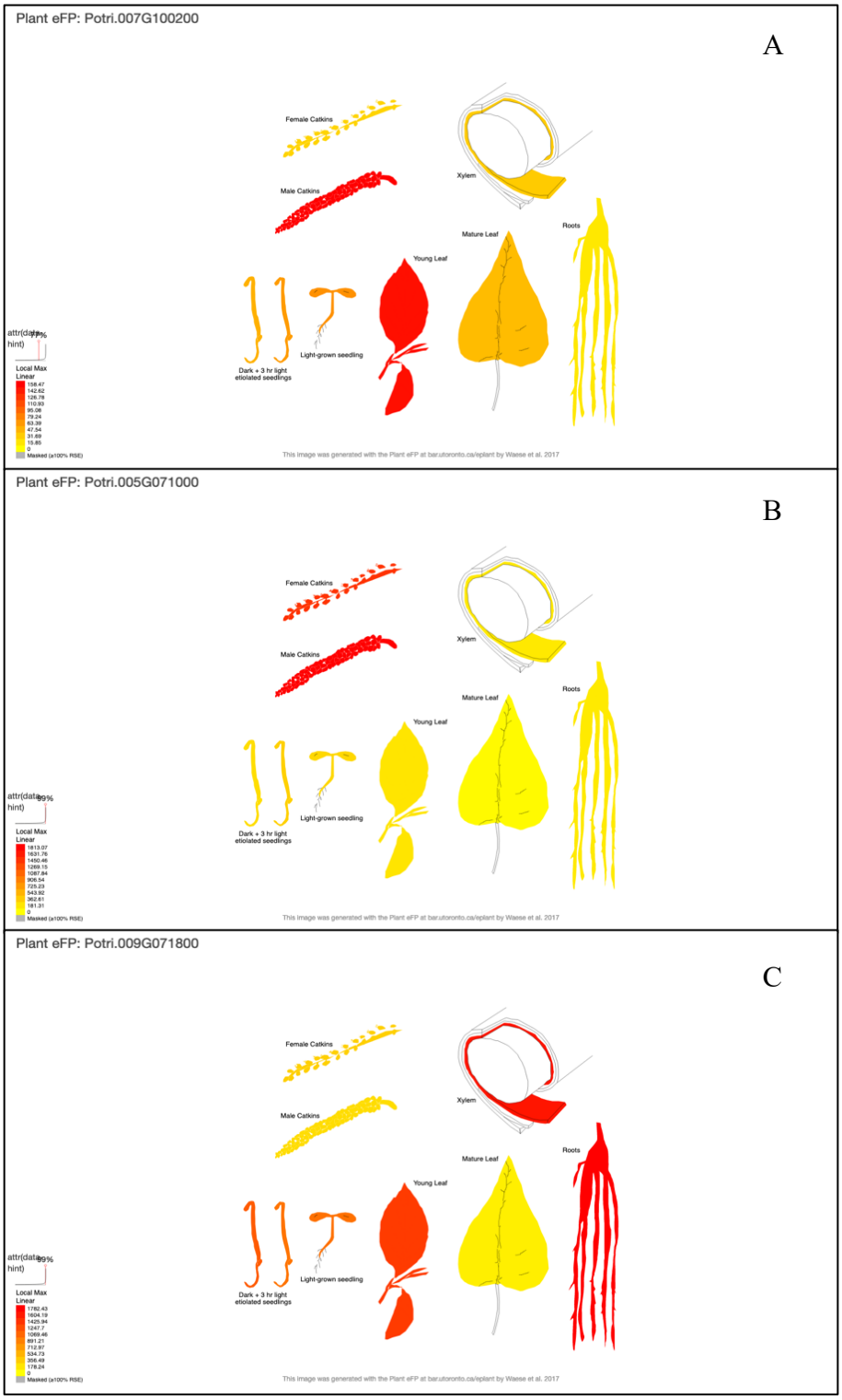
Plant eFP: Potri.007G100200
A
Female Catkins
Male Catkins
Xylem
Mature Leaf
Roots
Young Leaf
Dark + 3 hr light etiolated seedlings
Light-grown seedling
Local Max
Linear
156.47
142.62
126.78
110.93
95.08
79.24
63.39
47.54
31.69
15.85
0
Masked (a>100% RSE)
This image was generated with the Plant eFP at bar.utoronto.ca/eplant by Waese et al. 2017
Plant eFP: Potri.005G071000
B
Female Catkins
Male Catkins
Xylem
Mature Leaf
Roots
Young Leaf
Dark + 3 hr light etiolated seedlings
Light-grown seedling
Local Max
Linear
1813.07
1631.76
1450.46
1269.15
1087.84
906.54
725.23
543.92
362.61
181.31
0
Masked (a>100% RSE)
This image was generated with the Plant eFP at bar.utoronto.ca/eplant by Waese et al. 2017
Plant eFP: Potri.009G071800
C
Female Catkins
Male Catkins
Xylem
Mature Leaf
Roots
Young Leaf
Dark + 3 hr light etiolated seedlings
Light-grown seedling
Local Max
Linear
1782.43
1604.19
1425.94
1247.7
1069.46
891.21
712.97
534.73
356.49
178.24
0
Masked (a>100% RSE)
This image was generated with the Plant eFP at bar.utoronto.ca/eplant by Waese et al. 2017

Figure 4-2. Plant eFP Brower output showing expression profile of *UVR8* gene in selected paralogs. (Waese and Provart 2016). (A) The *UVR8* gene identified as Potri.007G100200, shows strong expression (denoted in red) in the male catkins and young leaves compared to the female catkins, mature leaves, and roots with minimal expression (denoted in yellow). (B) Potri.005G071000 paralog of *UVR8* shows high expression in the catkins compared to the other tissue types. (C) The paralog Potri.009G071800 shows minimal expression in the catkins and high expression in the xylem and roots as well as young leaves.

at positions TATTA(T/A)(A/T), (Fig. 4-3). However, TATA box variation has been observed in several plant species and consensus sequences such as: TATTTATT or TATTAAA are recognizable elements (Joshi 1987, Vogel 1994). The other classes of regulatory sequences that were predicted to occur in the *UVR8* upstream region included stress response elements, light response elements and core and proximal promoter sequences. The sequence for these motifs along with their location in the upstream region are given in Table 4-2. Interestingly, no SNPs in any of these regions were identified in Phytozome. Thus, assuming that the consensus motifs gathered from PlantCARE that correspond to transcriptional control sites are indeed operational in *UVR8*, it appears that there are no SNPs that affect *UVR8* transcription among the 883 natural variants that have been sequenced.

The *Populus trichocarpa UVR8* gene contains 12 exons and 11 introns (Fig. 4-4A), so it is likely that proper RNA splicing is important for accurate expression of the receptor. Thus, the 22 splice junctions within the *UVR8* gene model were analyzed for SNPs. Splice junctions were identified by GT and AG nucleotide sequences at the 3'- and 5'-splice sites, and SNPs were obtained from Phytozome. A summary, shown in Fig. 4-4B, shows exon sequences highlighted in green and SNPs highlighted in cyan. The only deviation from the canonical splice junction sequence was found in the intron 8 donor sequence. This polymorphism, consisting of a GT to AG change, is not thought to be a significant influence on splicing efficiency because mismatching can be tolerated at either end of the 5' or 3' splice site, however SNPs occurring on both cleavage sites would result in splicing

Figure 4-3. Sequence analysis of the upstream region of the *UVR8* promoter in *Populus trichocarpa*. Predicted regulatory elements present in the 500 bp region upstream of the ATG start codon for *UVR8* are shown in bold text. Underlined nucleotides represent high-frequency SNPs from the sequenced genome of *P. trichocarpa* dataset (Tuskan et al. 2006). Text in red indicate intergenic SNP base change in the TATA box promoter element.

Table 4-2. Description of predicted promoter elements found in *UVR8* in *Populus trichocarpa.*

Function	Motif	Sequence	Position from start codon
Stress response	ABI4	CACCT	-339
Proximal promoter	GC Box	GGGCGG	-301
Light responsive element	L Box	CCACCCACTCTCT	-134
Core promoter	TATA box	TATTATA	-112
Core promoter	CAAT box	CAAT	-94
Stress response	ABRE	TGGTTT	-61

Table 4-2. Description of predicted promoter elements found in *UVR8* in *Populus trichocarpa.* The precise mechanisms of transcriptional regulation of *UVR8* and cognate sequences in the control region are unknown. However, a computational predicting software and database (PlantCARE) was used to locate putative promoter elements based on DNA binding motifs. Promoter elements are characterized by function and position from start codon.

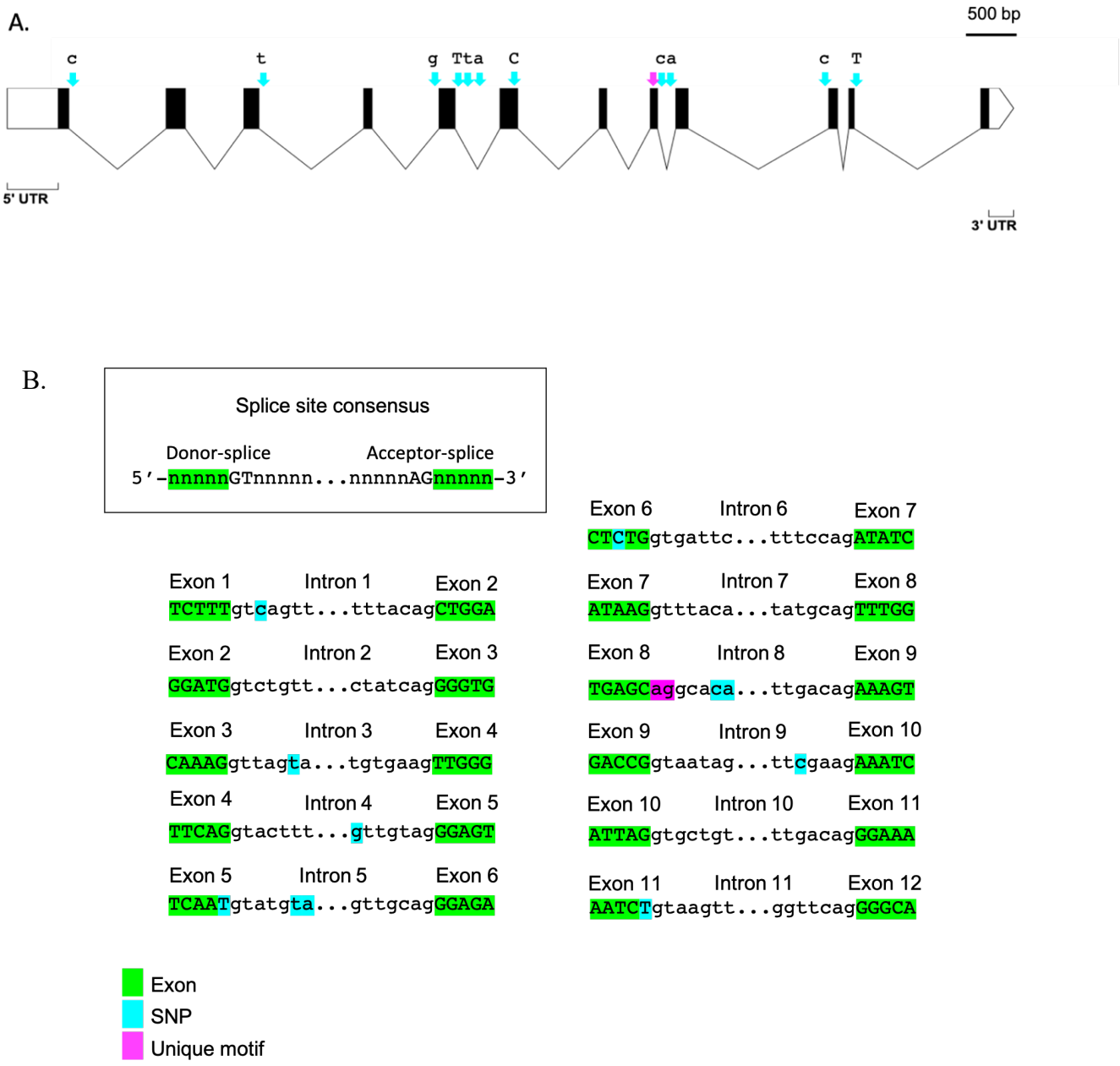

Figure 4-4. Schematic map of the *UVR8* gene and splice junction sites in *UVR8* from *Populus trichocarpa* were predicted by using SplicePort (Dogan et al. 2007). (A) Map of the exon and introns with arrows highlighting SNPs in cyan and the unique splice site motif in magenta. (B) Splice sites have a consensus motif for RNA splicing. Nucleotides highlighted in cyan indicate SNPs that are not predicted to affect the recognition of the splice sites and thereby lead to alternative splicing. A single, unique splice motif highlighted in magenta, was found at the donor site of exon 8.

mutations (Abramowicz and Gos 2018). Thus, similar to the analysis of the *UVR8* promoter, there seems to be little effect of SNPs on proper *UVR8* splicing, and therefore photoreceptor expression.

Analysis of SNPs in the model for the structural gene (exons and introns) for *Populus trichocarpa UVR8* revealed 489 SNPs. However, only 22 non-synonymous SNPs (and 19 synonymous SNPS) were identified in the protein coding region (exons) of *UVR8* from the 883 natural variants sequenced (Table 4-3). The allele frequency of the variant shown in Table 4-3 is represented as a ratio of the fraction of individuals that possess the variant nucleotide relative to the fraction that are homozygous for the reference nucleotide. The alleles are also annotated as to whether they are homozygous or heterozygous.

To evaluate the possible impact of non-synonymous SNPs on the structure of *Populus trichocarpa* UVR8, their locations were examined on the structure of *Arabidopsis thaliana* UVR8 since the two proteins exhibit 80% identity and 95% similarity over 440 residues (Table 4-4 and Fig.4-5). The locations of non-synonymous amino acid changes on *P. trichocarpa* UVR8 are illustrated on the structure for *A. thaliana* UVR8 (Fig. 4-5). At rest, the three-dimensional structure of the UVR8 photoreceptor is arranged as two doughnut-shaped homodimers which dissociate upon UV-B perception into two active monomers (Christie et al. 2012). As can be seen in Fig. 4-6, most of the non-synonymous SNPs, shown as cyan spheres on a ribbon backbone, are located the outside of the photoreceptor, remote from the dimer interface. Thus, it is unlikely that they would have

Table 4-3. List of non-synonymous SNPs in the coding region of *UVR8* in *Populus trichocarpa* were identified in the Phytozome database

Position location (bp)	Reference sequence	Variant sequence	Reference amino acid	Variant amino acid	Substitution	Exon	Allele frequency (%)
12609389	A	G	Valine	Alanine	V2A	1	0.2 Hom
12609384	C	T	Aspartic acid	Asparagine	D4N	1	0.2 Hom
12609360	C	T	Glutamic acid	Lysine	E12K	1	0.1 Hom
12609347	G	A	Proline	Leucine	P16L	1	0.1 Hom
12609345	T	C	Isoleucine	Valine	I17V	1	0.1 Hom
12608256	T	C	Threonine	Alanine	T60A	2	0.4 Hom
12608184	A	C	Serine	Alanine	S84A	2	24.33 Het
12607427	T	A	Glutamine	Lycine	Q145L	3	0.1 Hom
12604932	T	A	Glutamine	Lycine	Q257L	6	0.1 Hom
12604876	G	A	Arginine	Tryptophan	R277W	6	0.3 Hom
12604858	T	G	Methionine	Lycine	M283L	6	24.5 Het
12604032	T	A	Methionine	Lycine	M291L	7	24.4 Het
12604023	T	C	Threonine	Alanine	T295A	7	0.3 Hom
12604017	C	T	Aspartic acid	Asparagine	D297N	7	0.4 Hom
12603998	C	G	Tryptophan	Serine	W302S	7	0.3 Hom
12603533	T	C	Isoleucine	Valine	I317V	8	0.1 Hom
12603268	T	C	Valine	Glycine	V346G	9	24.3 Het
12603243	G	T	Serine	Tyrosine	S353Y	9	0.1 Hom
12603204	T	C	Glutamic Acid	Glycine	E361G	9	0.1 Hom
12601799	A	G	Valine	Alanine	V379A	10	24.2 Het
12601773	G	A	Histidine	Tyrosine	H388Y	10	0.1 Hom
12600327	A	T	Valine	Aspartic acid	V423D	12	0.2 Hom

Table 4-3. List of non-synonymous SNPs in the coding region of *UVR8* in *Populus trichocarpa* were identified in the Phytozome database. The position location (bp) is along the forward strand of the reference sequence of *UVR8*. The genotypes are represented by the ratio of individuals possessing the variant allele, the fraction of the homozygous reference allele and by the number of individuals that are different from the reference position. The relative allelic frequency (%) is the percentage of the *P. trichocarpa* population that contains the specific allele as homozygous (hom) or heterozygous (het).

Table 4-4. Homologous UVR8 peptide sequences in *Arabidopsis thaliana* and *Populus trichocarpa.*	
AT5G63860	MAEDMAADEVTAPPRKVLIISAGASHSVALLSGDIVCSW GRGEDGQLGHGDAEDRPSPTQLSALDGHQIVSVTCGADH TVAYSQSGMEVYSWGWGDFGRLGHGNSSDLFTPLPIKAL HGIRIKQIACGDSHCLAVTMEGEVQSWGRNQNGQLGLG DTEDSLVPQKIQAFEGIRIKMVAAGAEHTAAVTEDGDLY GWGWGRYGNLGLGDRTDRLVPERVTSTGGEKMSMVAC GWRHTISVSYSGALYTYGWSKYGQLGHGDLEDHLIPHKL EALSNSFISQISGGWRHTMALTSDGKLYGWGWNKFGQV GVGNNLDQCSPVQVRFPDDQKVVQVSCGWRHTLAVTER NNVFAWGRGTNGQLGIGESVDRNFPKIIEALSVDGASGQ HIESSNIDPSSGKSWVSPAERYAVVPDETGLTDGSSKGNG GDISVPQTDVKRVRI*
Potri.007G100200	MVEDEGAASGSEVSGPIRQVILISAGASHSVALLSGNIVCS WGRGEDGQLGHGDAEDRPTPTQLSTLDGLDIISITCGADH TTSYSESRMEVYSWGWGDFGRLGHGNSSDLFTPQPIKAL HSLKIRQIACGDSHCLAVTMDGEVQSWGRNQNGQLGLG TTEDSLVPQKIQAFQGVSIKMVAAGAEHTAAVTEDGELY GWGWGRYGNLGLGDRNDRLVPEKVSLVNGDKMIMVAC GWRHTISVSSSGGLYTYGWSKYGQLGHGDFEDHLTPHK VEALRDSYISMISGGWRHTMALTSDGNLYGWGWNKFGQ VGVGDNIDHCSPVQVKFPHEQKVVQISCGWRHTLAITER QNVFSWGRGTNGQLGHGESMDRNLPKIIEVLSADGSGGH QIEASTVDPSLGKSWVSPSDRYAIVPDESGQAVSVGGNG NDASVPESDVKRIRI*

Table 4-4. Homologous UVR8 peptide sequences in *Arabidopsis thaliana* and *Populus trichocarpa.* *Arabidopsis thaliana* sequence was obtained from TAIR and used to BLASTP search for the homologous sequence in the *Populus trichocarpa* genome in Phytozome.

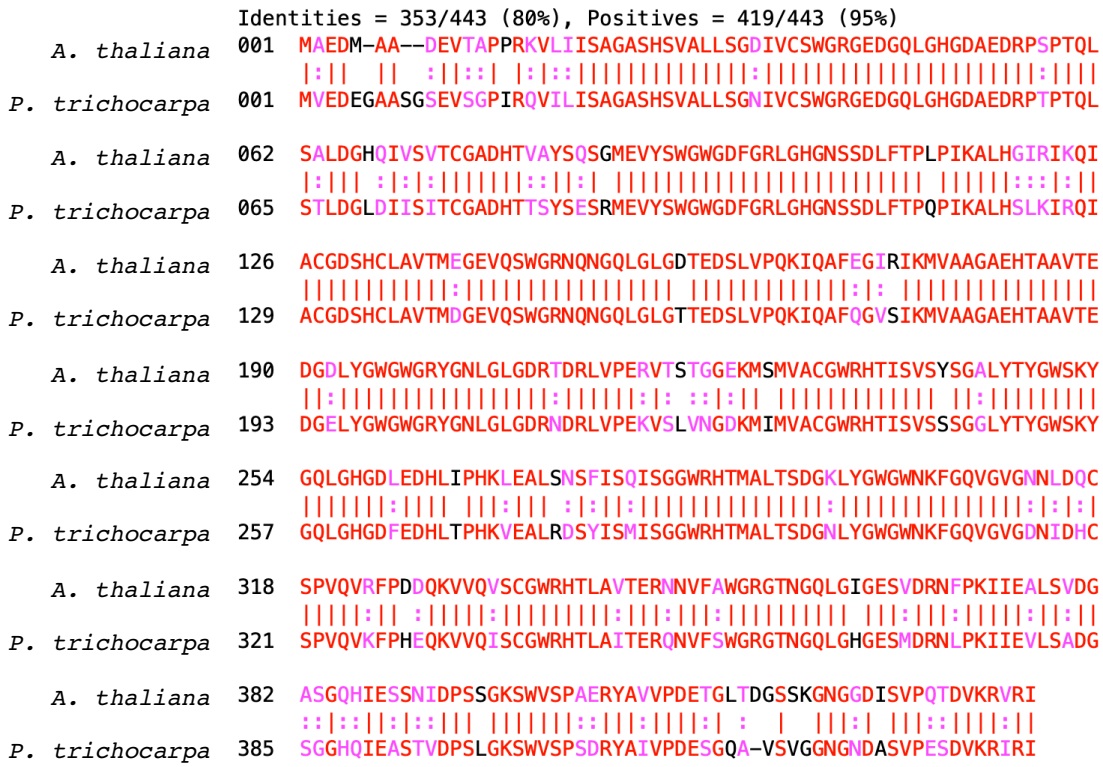

Figure 4-5. Pairwise sequence alignment of AtUVR8 with homolog in *Populus trichocarpa*. The *A. thaliana* sequence used as the reference and the queried *P. trichocarpa* sequence was aligned using the BLOSUM62 scoring matrix performed in MATLAB that resulted in a 80% sequence identity in red text and a 95% positive similarity in pink text.

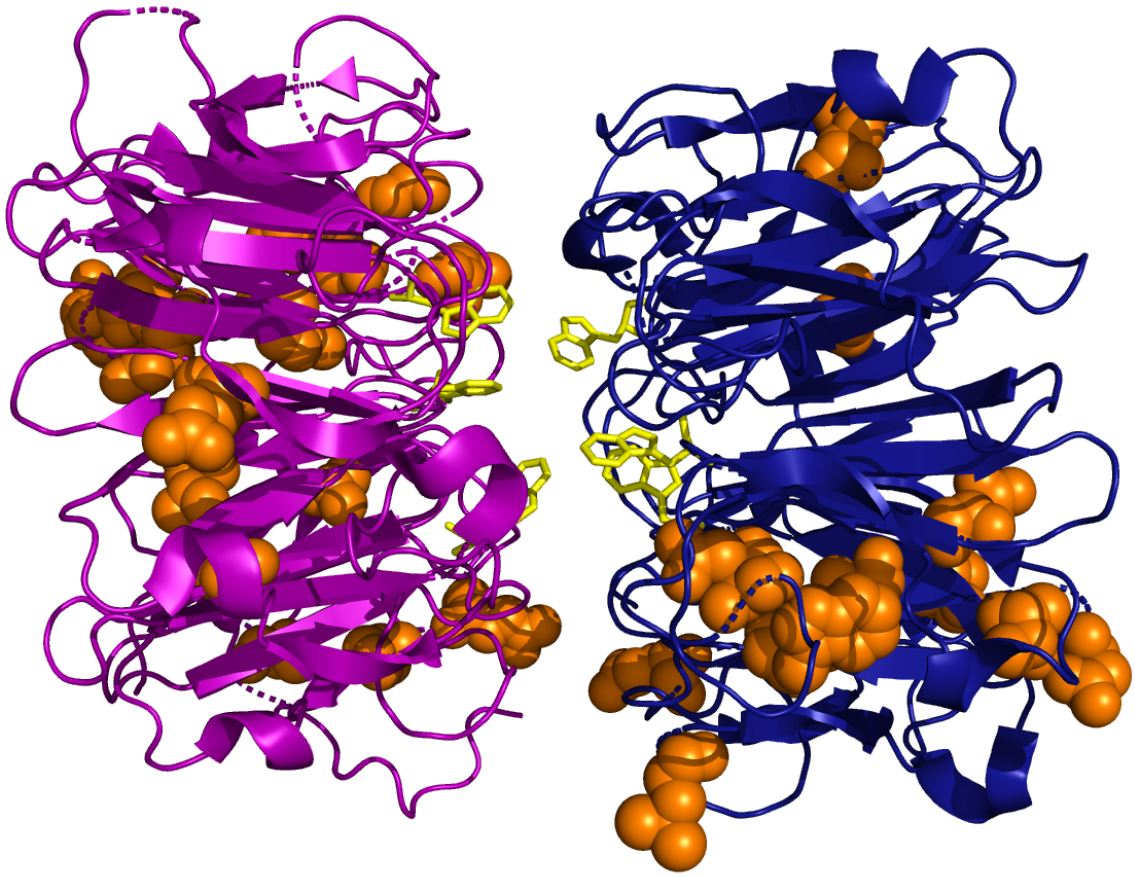

Figure 4-6. Crystal structure of *At*UVR8 (4D9S) dimer from x-ray diffraction (Christie et al. 2012). Non-synonymous SNPs were rendered as orange spheres indicating location outside of the interface of the sensing region. The location of the tryptophan pyramid, the proposed sensing mechanism of UVR8, is located at the interface of each monomer and is shown as yellow stick residues. The dimer is held together by a network of salt bridges.

a significant impact on the structure of UVR8, or the monomer-dimer interconversion. Additionally, the UVR8 photoreceptor contains a set of UV-B absorbing residues consisting of W233, W285, and W337, which is surrounded by a perimeter of aromatic amino acid pairs W198-Y201, W250-Y253, and W302-F305 (Christie et al. 2012). No SNPs were found in any of these locations. Interestingly, three non-synonymous SNPs, yielding the amino acid substitutions Q257L, M291L and W302S, were identified in a domain that might influence the structure of UVR8. These residues are packed tightly together in the UVR8 dimer and located adjacent to the tryptophan pyramid which functions as the UV-B chromophore (Fig. 4-7A-B). Additionally, no specimens contain two or more of the potentially disruptive SNPs.

The lack of SNPs and the minimally anticipated effects on the possible expression, structure, or function of UVR8 may be significant evolutionarily. UVR8 is an essential protein expressed from a single-copy gene in *Populus* that orchestrates the response and acclimation of plants upon exposure to UV-B radiation. It is possible that there are selective forces that maintain wild-type levels of UVR8 in plant cells. To explore this possibility, a simple analysis was performed on the occurrence of SNPs in single-copy and multi-copy gene families.

In order to undertake this analysis, a collection of single-copy genes in *P. trichocarpa* was needed. This was not a straightforward requirement since many genes have related though non-identical copies that are annotated with the same functional terms. Indeed, this is the

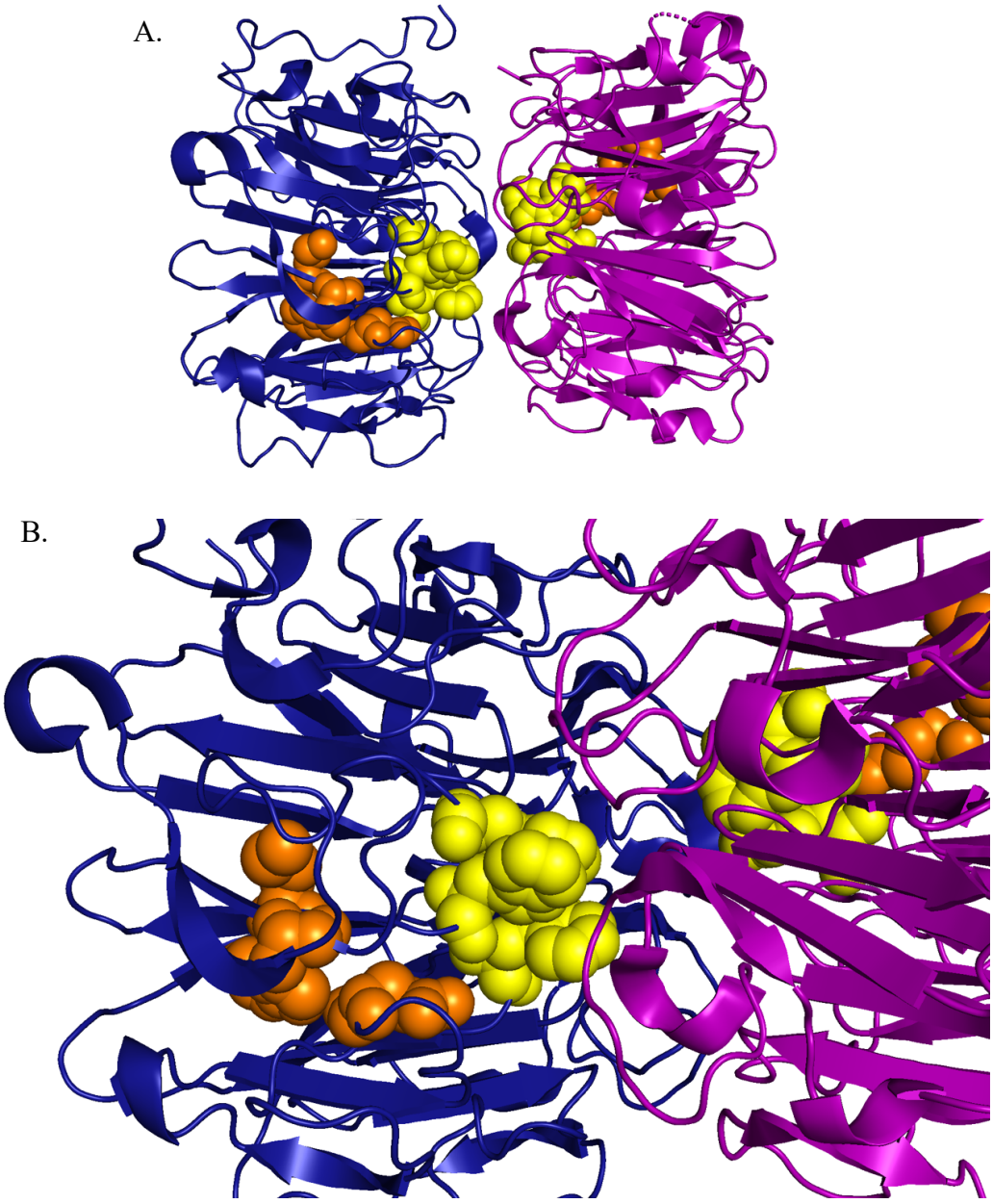

Figure 4-7. (A) UVR8 crystal structure from *A. thaliana* with *P. trichocarpa* notable non-synonymous SNPs. (B) Close-up image of the three non-synonymous SNPs that were identified to be potentially disruptive, Q257L, M291L, and W302S highlighted in orange spheres. The tryptophan pyramid consisting of W233, W285, and W337 residues are clustered to form the chromophore highlighted in yellow spheres. X-ray crystallography structure was obtained from Christie et al. 2012.

case for *UVR8* in *P. trichocarpa*. Thus, the first step was to evaluate a small set of candidates as single-copy genes in *P. trichocarpa*. A list of single-copy genes shared between *Arabidopsis, Populus, Vitis,* and *Oryza* was obtained from previous work (Duarte et al. 2010). The list was filtered to contain only single-copy genes in *Arabidopsis* and cross referenced with the database in Phytozome to verify single-copy status in *P. trichocarpa* and recording exon and gene sizes. With these six genes in hand, another set of multi-copy genes were identified from literature and used for the analysis.

Using the same approach as applied to *UVR8*, synonymous and non-synonymous SNPs were identified in the genomic regions of the single- and multi-copy gene families, in both intron and exon sequences. The distribution of SNPs in five single-copy genes in addition to *P. trichocarpa UVR8* were analyzed using Phytozome. The gene models included *TPL8* (TUBBY LIKE PROTEIN 8), *PDE316* (PIGMENT DEFECTIVE EMBRYO 316), *BIOF* (BIOTIN F), *ACS5* (ACC SYNTHASE 5), and *URED* (UREASE ACCESSORY PROTEIN D). The non-synonymous and synonymous SNPs were identified in exon regions to compute approximate K_a/K_s ratios. K_a/K_s ratios for *UVR8*, *BIOF*, *ACS5* and *URED* were calculated to be 0.3847, 0.3294, 0.3294, 0.4757, 0.2085, and 0.2512, respectively (Table 4-5). These values are lower than 1.0, and though the calculation suggests that the SNPs exert some purifying selective pressure on these genes, it is likely that none of the substitutions are highly advantageous. Further analysis that compares single-copy genes to multi-copy gene families in *P. trichocarpa* would be necessary to

Table 4-5. Calculated K_a/K_s ratios in gene models, *TPL8*, *PDE316*, *BIOF*, *ACS5*, and *URED*

Gene	K_a (Non-synonymous)	K_s (Synonymous)	K_a (d_n)	K_s (d_s)	Gene size	K_a/K_s
UVR8	1011.7	314.3	0.0236	0.0612	9128	0.3847
BIOF	1080.7	344.3	0.0244	0.0742	4917	0.3294
ACX5	1495.4	493.6	0.0262	0.0666	7729	0.3941
URED	651.3	230.7	0.0316	0.0664	3236	0.4757
TLP8	932.0	289.0	0.0174	0.0834	5227	0.2085
PDE316	1762.3	568.7	0.0134	0.0533	4168	0.2512

Table 4-5. Calculated K_a/K_s ratios in gene models, *TPL8*, *PDE316*, *BIOF*, *ACS5* and *URED*. The non-synonymous and synonymous SNPs were identified in exon regions, d_N and d_S substitution rates were calculated using online software, PAL2NAL, by a multiple sequence alignment of proteins and the corresponding cDNA sequence. K_a/K_s ratios for *UVR8*, *BIOF*, *ACS5* and *URED* were calculated to be 0.3847, 0.3294, 0.3294, 0.4757, 0.2085, and 0.2512, respectively. These values were lower than 1.0 and may suggest that the SNPs exert purifying selective pressure on these genes and therefore unlikely that the substitutions are highly advantageous (Suyama et al. 2006, Goldman and Yang 1994).

fully characterize the regulation of important single-copy genes. However, because these values are less than 1.0 the SNPs are tentatively considered to be purifying variations that stabilize selection against changes.

Discussion

In an effort to identify poplar variants with altered expression of the UVR8 photoreceptor, an analysis of SNPs within the *Populus trichocarpa UVR8* gene model was undertaken. Initially, it was hoped that SNPs would be identified that dramatically influenced photoreceptor expression, structure or function, which would result in significant downstream effects on metabolic pathways responsible for UV-B acclimation and tolerance. Little is known about the transcriptional regulation of UVR8, however, expression of UVR8 was analyzed using an eFP brower for visualization in various organs and tissue types in *P. trichocarpa.* Strong expression of UVR8 in the young leaves and male catkins compared to the other organs is consistent for UV sensing and subsequent UV-B protection. Therefore, a set of canonical sequences that regulate gene transcription in poplar were used to scan for SNPs that may affect *UVR8* expression. Surprisingly, no SNPs were detected in these regions, suggesting that expression of *UVR8 in planta* must be tightly regulated. Because *UVR8* contains 12 exons and 11 introns, stringent pressure must select against splicing variants in this essential gene. Accordingly, no deleterious SNPs were detected in splice junctions within the *UVR8* gene. Finally, there are very few SNPs in the coding region of *UVR8*, and based on an examination of its location on the

three-dimensional structure of the highly homologous UVR8 receptor from *Arabidopsis*, it is unlikely that any have a significant effect on receptor stability or function. Future analysis of transcriptome datasets might provide evidence of alternative splicing that could change the structure and/or function of UVR8, however at this time, alternative transcript information in Phytozome is unavailable. These results were surprising, and suggested at least a cursory analysis be undertaken to establish whether expression modulation of *UVR8* would be a useful approach to investigate the mechanism of UV-B acclimation in poplar.

An important consideration with respect to these findings is that *UVR8* is a single-copy gene in *Populus trichocarpa*. Although BLAST analysis of the *Arabidopsis* UVR8 amino acid sequence revealed 23 paralogs, manual inspection of each of these genes revealed that only one was a close match to a bona fide UVR8. Analysis to evaluate SNPs and expression data may be useful to characterize each UVR8 paralog since the other genes fall within the seven-bladed β-propeller domain protein family that characterizes UVR8. However, the other paralogs lack the key amino acids that make up the chromophore domain are therefore cannot be functional UV-B receptors. Thus, there may be selective pressure to maintain optimal expression of a functional copy of the single *P. trichocarpa UVR8* gene.

In a groundbreaking study, De Smet and colleagues (De Smet et al. 2013) found that a large set of genes in flowering plants undergo convergent gene loss to single-copy following genetic duplication events. The findings were supported by the fact that many single-copy genes are not randomly distributed in genomes but instead are involved in essential

functions that are highly conserved, including functions related to DNA damage and repair. The investigators concluded that there is selective pressure that preserves some genes as singletons. It is tempting to speculate that similar selective pressure is exerted at the level of single nucleotide polymorphisms (SNPs), and that single-copy genes display lower frequencies of non-synonymous SNPs in their coding regions, as well as a reduction of SNPs in transcriptional and splicing control regions. At this stage, I hypothesize that mechanisms such as dosage balance or dominant negative effects that maintain some genes as singletons also regulate the frequency and distribution of SNPs in *UVR8* and other single-copy genes, and may account for the patterns of SNPs observed.

Obviously, a significant limitation of this analysis is that it was performed on a limited set of genes and rigorous statistical tests were not performed to ensure that the estimated K_a/K_s ratios are significantly different, although they do appear to significantly differ from 1.0. Another limitation of the analysis is that the upstream control region of *UVR8* has not been fully characterized in poplar, and little is known about the factors that regulate and promote transcription. The motifs gleaned from literature and PlantCARE may be involved in the transcriptional regulation of many genes, but may not apply to poplar *UVR8*.

On the other hand, the graphical and heuristic analysis of the impact of SNPs on the structure and function of the UVR8 photoreceptor are interesting, though they too require further investigation. Nonetheless, the M291L substitution is present at a relatively high frequency (24.4%), although it is heterozygous for the variation. Moreover, the substitution of leucine for methionine at position 291 should be relatively isosteric, and

therefore play little role in the stability of the chromophore regions. Alternatively, the Q257L and W302S are homozygous, though they are present at low frequency, 0.1% and 0.3%, respectively. Interestingly, these variations occur in specimens collected at low elevation, and contain high levels of lignin. Thus, it is possible that if there was any effect of these substitutions on the structural integrity or functional performance of UVR8, the response of these *Populus* plants to UV-B radiation, albeit lower levels at their local growth elevation, would be bolstered by their high lignin levels.

Taken together, the observations in this chapter suggest that there may be selective pressure that controls the level of *UVR8* expression in *Populus* and future work that analyzes SNPs additional single copy genes, multi-gene families, and in the remaining 22 *UVR8* paralogs may substantiate these interpretations. However, if *UVR8* expression in poplar is under specific control, then modulating its expression may promote significant effects on downstream processes that result in UV-B acclimation and tolerance. These findings and interpretation motivated me to explore expression regulation using modern genome engineering as described in the next chapter.

Chapter 5: Generation of Transgenic *Populus* Lines for Molecular Studies on the Acclimation to UV-B Radiation

Introduction

Genome editing technology has transformed our ability to investigate and understand plants. Revolutionary, simple yet highly precise and powerful approaches to specifically alter plant genomes is finding use not only as an indispensable research tool, but is also being used to enhance favorable traits in many agricultural crops (Jaganathan et al. 2018, Chen et al. 2019, Razzaq et al. 2019, Zhang et al. 2019, Wada et al. 2020, Zhu et al. 2020, Nasti and Voytas 2021). The modification of a genome can involve gene disruption, gene replacement, and insertion of sequences to control expression of a gene or protein function. Some methods are time-consuming and cost prohibitive, and in addition, a significant barrier to the widespread use of genome editing technology is our limitation in the ability of many plant species (Altpeter et al. 2016), or to advance techniques in plant tissue culture in order to transfer transgenic, regenerated shoots for subsequent acclimation to a greenhouse environment.

Traditional methods of modifying genes in organisms usually rely on the random insertion of sequences to produce silenced or knockout mutants and activation tagging. One approach, RNA interference (RNAi), is a mechanism adapted from eukaryotic organisms that utilizes double stranded RNA (dsRNA) molecules of about 20-22 bp to directly control

gene activity. Homology-dependent degradation of mRNA occurs when the Dicer enzyme, an RNAase III endonuclease, recognizes the two nucleotide overhangs on the 3' end of dsRNA. Dicer forms a complex with RNA-binding proteins to process dsRNA into small-interfering RNAs (siRNAs). The siRNAs are bound to RNA-induced silencing complexes (RISC) to promote single-stranded RNA molecules that specifically bind directly to mRNA targets by base paring with the homologous sequence. Gene silencing results when the enzyme, Argonaute ("Slicer"), recognizes and degrades the siRNA/mRNA complex (Hammond 2005). However, RNAi is not always reliable, and often results in off-target control, leaky transgene expression, low transformation efficiency, and difficulty in generating positive clonal replicates (Osakabe et al. 2016).

An even more common approach to modify gene expression in plants is to overexpress a gene via transient or stable transformation. A commonly used promoter from the cauliflower mosaic virus (CaMV), the 35S promoter, is a robust, constitutive promoter that drives transgene expression and promotes high levels of RNA transcripts in a variety of plants (Fromm et al. 1985). However, CaMV 35S promoter has the potential to become inhibitory over time, and thus the use of constitutive promoters that display moderate levels of expression may be more effective depending on the desired outcome (Park et al. 2010, Chen et al. 2013).

The CRISPR/Cas9 (clustered regulatory interspaced short palindromic repeat/CRISPR-associated protein 9) gene editing system has been predominately used for molecular breeding in herbaceous plants due to the extensive characterization, short growth times,

relative ease of transformation (Lowder et al. 2015, Razzaq et al. 2019, Zhang et al. 2019, Wada et al. 2020, Pan et al. 2021, Pan et al. 2021). CRISPR/Cas9 was discovered in bacteria where it functions as part of an adaptive immunity response to viruses, and with the ability of cells to perform non-homologous end joining (NHEJ) repair, modifications can be introduced into genomic DNA (Doudna and Charpentier 2014). The elements of CRISPR include an endonuclease, such as Cas9, and a short, 20-22 bp guide RNA that is homologous to a region in the genome to be cleaved, which also includes a short, three bp protospacer adjacent motif (PAM) sequence. Co-expression of the Cas9 endonuclease with a single guide RNA (gRNA) containing the protospacer adjacent motif (PAM) sequence results in a site-directed, double-strand break in DNA near the three bp protospacer adjacent motif, thereby inducing the NHEJ repair pathway. NHEJ repair at the break is often error prone. Frequently, indels result, which can lead to single or biallelic gene disruptions. These changes often result in translational alterations that disrupt protein formation, such as a premature stop codon. CRISPR can also be used for transcription regulation. Engineering Cas9 to produce a catalytically deactivated nuclease (dCas), and linking dCas9 with transcriptional enhancers or repressors, can be used with gRNA for transcriptional regulation of a gene by activation or interference. For example, dCas9 can be linked with VP64 domains to provide a CRISPRa system that recruits transcriptional machinery during initiation or elongation to up-regulate transcription. VP64 is a herpes simplex virus transcription factor of four tandem monomers of VP16 fused to the C-terminal region of the deactivated endonuclease (Beerli et al. 1998, Lowder et al. 2015). Alternatively, a commonly used CRISPRi system utilizes three copies of the EAR motif repressor domain (SRDX) fused to dCas9 to target the promoter region for transcriptional

repression by sterically inhibiting the binding site for transcriptional machinery (Moradpour and Abdulah 2020).

CRISPR has been used extensively to genetically modify herbaceous plants, providing tremendous insight into a number of fundamental processes in plants. However, there have been relatively few studies in woody perennials such as *Populus* species that have employed CRISPR (Fan et al. 2015, Liu et al. 2015, Zhou et al. 2015, Muhr et al. 2018, An et al. 2020, Wang et al. 2020, Azeez and Busov 2021, Bae et al. 2021, de Vries et al. 2021, Triozzi et al. 2021). The limited number of studies stems from the difficulty in obtaining stable and high efficiency transformation in many *Populus* species. Additionally, it is possible to generate chimeric transgenic plants when the modified gene is expressed in plant tissue in transformed and non-transformed cells. High frequency SNPs that occur in outcrossing species may impede gRNA specificity and limit the ability of genome editing in poplar. Most importantly, *Populus* are dioecious outcrossing species, which furthers the challenge of backcrossing with a parental line and segregating the endonuclease for transgene-free plants (Zaidi et al. 2018). However, despite these limitations, through several cycles of clonal propagation, stable transformants using CRISPR-Cas9/dCas9 can be produced (Bewg et al. 2018). Thus, a comparison of conventional and modern approaches to genome editing in poplar would be useful to assess efficiency and thereby adopt the best approach to achieve the desired response and phenotype.

Populus is a good model for trees and has useful advantages for gene editing studies; it was the first tree with a full genome sequence (Tuskan et al. 2006), many species within the

Populus genera have been sequenced as well as a number of variants within natural populations (Evans et al. 2014), and an effective and highly efficient transformation system that allows for the facile construction of transgenic lines (G.D. Coleman, personal communication). INRA 717-1B4 (717) is a hybrid female clone from a cross between female *Populus tremula* and male *Populus alba* trees (Mader et al. 2016), and because of its relative ease in cultivation and transformation, 717 has been used for many years in research as an attractive model for trees. Moreover, there is considerable economic importance to enhancing poplar traits for the sustainable use as a feedstock for wood and timber, paper products, and biofuel.

It would be interesting to apply traditional or modern genome editing approaches to study UV-B acclimation and tolerance. It has been shown in a variety of plants that UV-B radiation can reduce biomass and increase flavonoid and anthocyanin accumulation and decrease chlorophyll content in herbaceous perennials and in complex species (Gao et al. 2004, Singh et al. 2011, León-Chan et al. 2017). Under low fluence of UV-B radiation, plants respond photomorphogenically and metabolically in order to mitigate stress and damage to photosynthetic machinery and plant cells (Tossi et al. 2019). UVR8 promotes UV-B acclimation and tolerance in plants by inhibiting hypocotyl elongation and accumulating flavonoids and anthocyanins in various plant organs including leaf tissue and reproductive structures (Peer et al. 2001).

The UVR8 (UV RESISTANCE LOCUS 8) photoreceptor is a member of the seven-bladed β-propeller protein family that perceives UV-B radiation to promote signaling and

activation of pathways that are important for acclimation, tolerance, and response to stress. UVR8 has been extensively studied in *Arabidopsis thaliana* (Rizzini et al. 2011, Wargent and Jordan 2013) *Chlamydomonas reinhardtii* (Tilbrook et al. 2013), *Marchantia polymorpha* (Clayton et al. 2018), and *Zea mays* (Belén et al. 2019). Comprehensive phylogenetic analysis suggests that UVR8 is well conserved and functional among photosynthetic plants from green algae to higher plant species (Fernandez et al. 2016). Although UVR8 is conserved in green algae to higher plants, it has not been characterized in complex woody perennials such as *Populus* species.

In this chapter, the application of genome editing approaches will be described for the modulated expression of the UVR8 photoreceptor in normal and phenylpropanoid deficient *Populus* variants, and as a probe of the molecular basis for UV-B acclimation and tolerance.

Materials and Methods

Plant Materials and Growth Conditions – *Populus deltoides* was acquired from the BioEnergy Science Center (renamed Center for Bioenergy Innovation) (Oak Ridge, TN, USA) and maintained at the University of Maryland – College Park Research Greenhouse Complex (College Park, MD, USA). Hybrid clone INRA 717-1B4 (*Populus tremula* x *P. alba*) was propagated and grown at the University of Maryland – College Park, Research Greenhouse Complex and at the Plant Sciences building. Acclimation of tissue culture

plants into greenhouse conditions was performed at the University of Maryland and at the Institute for Bioscience and Biotechnology Research (IBBR) (Rockville, MD, USA). Tissue culture to greenhouse acclimation consisted of transferring plantlets at approximately 5 cm in height from culture vessels to planting in trays with potting media. Plants were kept in a moist environment with a flat dome cover and placed on growing racks with fluorescent lamps for a 16 h photoperiod at 25°C. Over two weeks, the dome was removed for 5 mins, sprayed generously with water, and the length in time without the cover was gradually increased until the plants could withstand wilting beyond 30 minutes. Plants were then transferred to pots and used for UV-B experimentation.

Populus Transformation and Tissue Culture – Plant transformation consisted of co-cultivating petiole and stem explants from INRA 717-1B4 and *P. deltoides*. Petioles were gently wounded with plyers and grown on callus inducing media with 5.32 g/L DKW medium, 30 g/L sucrose, and growth regulators 1.5 mg/L 1-naphthaleneacetic acid (NAA), 0.25 mg/L 6-benzylaminopurine (BA), and 2.2 μg/L thidiazuron, 1.5 g/L Gelzan, and 5.0 g/L agar with pH adjusted to 5.7 ± 0.2 (Leple et al. 1992). *Agrobacterium* strains containing plasmids with the gene editing components were grown in the presence of selection agent(s): kanamycin, hygromycin, and Basta (Table 5-1) and supplemented with acetosyringone. Colonies were selected and inoculated in 5 mL in media containing the appropriate antibiotics. The overnight culture was harvested and resuspended in 25 mL liquid callus inducing media and adjusted to concentration at OD_{600} at 0.3. Petiole explants were co-cultivated overnight in *Agrobacterium* in deep dish petri dishes in a dark box with gentle shaking and then transferred on solid callus inducing media with no antibiotics in a

Table 5-1. Organization of antibiotic and herbicide selectable markers in the construction of transgenic lines targeting *UVR8* or *CAD* genes in *E. coli* and *A. tumefaciens* transformations.

Line ID	Gene	Gene editing tool	*E. coli* selection (μg/mL)	*A. tumefaciens* selection (μg/mL)	Plant selection (μg/mL)
1	*CAD*	RNAi	Spectinomycin 100	Rifampicin 50, gentamicin 20	Basta 5
2,3	*UVR8*	RNAi	Spectinomycin 100	Rifampicin 50, gentamicin 20	Hygromycin 20
4,5	*UVR8*	RNAi	Spectinomycin 100	Rifampicin 50, gentamicin 20	Basta 5
10-12	*UVR8*	CRISPR KO	Kanamycin 100	Rifampicin 50, gentamicin 20	Hygromycin 20
13	*UVR8*	CRISPRa	Kanamycin 100	Rifampicin 50, gentamicin 20	Hygromycin 20
14	*UVR8*	CRISPRi	Kanamycin 100	Rifampicin 50, gentamicin 20	Hygromycin 20
20, 21	*UVR8*	35S	Spectinomycin 100	Rifampicin 50, gentamicin 20	Kanamycin 100
28-30	*CAD* *UVR8*	RNAi CRISPR KO			Basta 5, Hygromycin 20
33, 34	*CAD* *UVR8*	RNAi 35S			Basta 5, Kanamycin 100

Table 5-1. Organization of antibiotic and herbicide selectable markers in the construction of transgenic lines targeting *UVR8* or *CAD* genes in *E. coli* and *A. tumefaciens* transformations. *Populus* explant material used for transformations was selected on media based with the appropriate selectable marker(s) and maintained in tissue culture vessels with LS media (0.5 X Linsmaier & Skoog Basal medium), indole butyric acid, and nutrients.

dark box for two days. Explants were disinfected with 200 mg/L vancomycin, 250 mg/L cefotaxime, and 25 mg/L tetracycline in sterile water and rinsed three times following another rinse with callus inducing media using the same antibiotics. Explants were blotted dried and plated on callus inducing media for two weeks. Explants were transferred to shoot inducing media on plates containing 5.32 g/L DKW media, 30 g/L sucrose, 1.5 mg/L 1-naphthaleneacetic acid (NAA), 0.25 mg/L 6-benzylaminopurine (BA), 2.2 ug/L thidiazuron, 1.5 g/L Gelzan, 5.0 g/L agar, containing 250 mg/L cefotaxime, 200 mg/L timentin with selection agent(s): kanamycin, hygromycin, and Basta until shoots were regenerated. Selected shoots were micropropagated and maintained in rooting media containing 2.2 g/L Linsmaier and Skoog (LS) media supplemented with 15 g/L sucrose, 0.1 mg/L indole-3-butyric acid (IBA), 200 mg/L timentin, and selection agent(s): kanamycin, hygromycin, and Basta. Micropropagated shoots were assigned a number that corresponds to the targeted gene (*CAD* and *UVR8*) and the method of gene modification (RNAi, CRISPR, and 35S promoter) and the letter represents the subculture as an independent event.

Construction of RNAi-Regulated UVR8 Populus Lines – Two regions of the *UVR8* genes from *P. deltoides* and INRA 717-1B4 were targeted and amplified using high fidelity KOD Hot Start DNA Polymerase (Novagen, Madison, WI, USA). The first segment was located at the beginning of the 5'-sequence of *UVR8* in *P. deltoides* and was amplified using the forward primer, (5'-CACCGAGGATGAAGGAGCTGCTAGTGG-3'), and the reverse primer, (5'-CCCCAACTATAGACCTCCATTCGTG-3'), to generate a 281 bp fragment. The second segment in *P. deltoides* was amplified using the forward primer, (5'-

CACCGTCAACTGGGACATGGGGACTTTG-3'), and the reverse primer, (5'-TCAAATCCGTATCCGTTTGACATCACT-3'), to generate a 560 bp fragment towards the 3'-end of the cDNA sequence. In a similar manner, the first UVR8 segment from INRA 717-1B4 was amplified using the forward primer, (5'-TGTGGTCTCACTTAATGGCCGAGGATGGACGAG-3'), and the reverse primer, (5'-TGTGGTCTCGGGTTCCCCAACTATAGACCTCCATTCGTG-3'), to generate a 281 bp fragment and a second region was targeted to generate a 560 bp fragment further downstream that was amplified using the forward primer, (5'-TGTGGTCTCACTTAGTCAACTGGGACATGGGGACT-3'), and the reverse primer, (5'-TGTGGTCTCGGGTTTCAAATCCGTATCCGTTTGACATCACT-3'). The *UVR8* amplicons for use in RNAi regulation in *Populus* are referred as fragment 1 and fragment 2 (Table 5-2), and the complete list of primers used in all RNAi suppression lines are presented in Table 5-3.

Construction of RNAi-Regulated CAD Populus Lines – *Populus deltoides* lines with RNAi-regulated *CAD* were previously constructed by ArborGen and obtained from the Department of Biology, West Virginia University (S. Difazio, personal communication). However, to recapitulate the genotype in INRA 717-1B4, and to construct a *CAD*- and *UVR8* regulated poplar line, additional constructs were needed. The INRA 717-1B4 RNAi-regulated *CAD* lines targeted an identical region as referenced in the literature (Macaya-Sanz et al. 2017). A 234 bp amplicon of INRA 717-1B4 *CAD* (Table 5-2) was generated using the forward primer (5'-

Table 5-2. Nucleotide sequences from the cDNA in INRA 717-1B4 for overexpression of *UVR8* or RNA silenced *UVR8* and *CAD*.

Gene	**Sequence (5'- 3')**
*UVR8**	ATGGCCGAGGATGGACGAGCTGCTAGTGGTAGTGAAGTTAGTGGTCCAATTCGTCAAGT TATTCTTATTTCTGCCGGTGCTAGTCACTCTGTTGCTCTTCTTTCTGGAAACATCGTTT GCTCCTGGGGACGAGGAGAGGATGGGCAGTTAGGCCATGGGGATGCTGAGGATAGACCC ACTCCAACTCAATTGAGTACATTGGATGGCCTTGATATAATATCAATTACTTGCGGTGC TGATCATACAACTGCGTATTCTGAGTCACGAATGGAGGTCTATAGTTGGGGATGGGGTG ATTTTGGGAGGCTAGGACATGGAAATTCTAGTGATTTGTTCACTCCTCAGCCAATTAAG GCTTTGCACAGTTTAAAGATAAGGCAAATTGCTTGTGGGGATAGCCATTGTCTGGCAGT CACCATGGATGGTGAGGTGCAAAGTTGGGGGCGGAATCAAAATGGTCAACTTGGTCTTG GCACCACCGAGGACTCCCTTGTGCCTCAGAAAATTCAAGCTTTTCAGGGAGTCTCTATT AAAATGGTTGCTGCTGGTGCTGAACATACTGCAGCTGTCACAGAAGATGGAGAGCTCTA TGGATGGGGTTGGGGCCGATATGGGAACTTGGGACTAGGTGACAGAAATGATCGCCTAG TTCCTGAAAAAGTTTCACTTGTCAAAGGAGACAAGATGATAATGGTTGCATGTGGGTGG CGGCATACAATATCTGTTTCCTCTTCTGGTGGATTGTACACTTATGGATGGAGCAAATA TGGTCAACTGGGACATGGGGACTTTGAGGATCACCTGACTCCTCACAAGGTGGAAGCCT TGCGGGATAGTTACATTTCTCTGATATCAGGTGGCTGGAGACACACCATGGCATTGGCT TCTGATGGAAAACTTTATGGCTTGGGATGGAATAAGTTTGGACAGGTTGGAGTTGGTGA CAACATTGATCATTGCTCTCCTGTGCAAGTTAAATTTCCACATGAGCAGAAAGTAGTCC AGATCTCATGTGGATGGAGGCACACGCTTGCTGTTACTGAACGACAAAATGTATTTTCT TGGGGAAGAGGCACAAATGGACAACTTGGTCATGGAGAGTCTATGGACCGAAATCTACC GAAAATCATAGAAGCTCTGAGTGCTGATGGATCTGGTGGCCATCAGATTGAAGCTTCAA CTGTTGATCCGTCATTAGGGAAAAGCTGGGTTTCGCCATCTGATAGATACGCTATTGTT CCTGATGAATCTGGGCAAACTGTTTCAGTTGGGGGAAATGGGAATGATGCAAGTGTCCC GGAGAGTGATGTCAAACGGATACGGATTTGA
UVR8 Fragment 1	GCTGGTAGCAAGCTTATTCCCTGAACGACAATGCTATTCATATTCGAAAAAACACTATA TACATTCATACTTGTTTCAGACGTGACTTTATTTTCGAGTGACGTGTTTTGTGGTTCAA ATGTGACAGTTTGTCTTTGCTTTTAAAATAAATAAAAAGTTGAGTTGTTTTTTATTTTT CACAAATGGGTATGAGTTACATTGTAATTGAATGCGCTGTGCATCTGGTGATCTGTC
UVR8 Fragment 2	GTCAACTGGGACATGGGGACTTTGAGGATCACCTGACTCCTCACAAGGTGGAAGCCTTG CGGGATAGTTACATTTCTCTGATATCAGGTGGCTGGAGACACACTATGGCATTGACTTC CGATGGAAACCTTTATGGCTGGGGATGGAATAAGTTTGGACAGGTTGGAGTTGGTGACA ACATTGATCATTGCTCTCCTGTGCAAGTTAAATTTCCACATGAGCAGAAAGTAGTCCAG ATCTCATGTGGATGGAGGCACACACTTGCTGTTACTGAACGACAAAATGTATTTTCTTG GGGAAGAGGCACAAATGGACAACTTGGTCATGGAGAGTCTATGGACCGAAATCTACCAA AAATCATAGAAGCTCTGAGTGCTGATGGATCTGGTGGCCATCAGATTGAAGCTTCGACT GTTGATCCGTTATTAGGGAAAAGCTGGGTTTCGCCATCTGATAGATATGCTATTGTTCC TGATGAATCTGGGCAAACTGTTTCAGTTGGGGGAAATGGGAATGATGCAAGTGTCCCGG AGAGTGATGTCAAACGGATACGGATTTGA
CAD	GCTGGTAGCAAGCTTATTCCCTGAACGACAATGCTATTCATATTCGAAAAAACACTATA TACATTCATACTTGTTTCAGACGTGACTTTATTTTCGAGTGACGTGTTTTGTGGTTCAA ATGTGACAGTTTGTCTTTGCTTTTAAAATAAATAAAAAGTTGAGTTGTTTTTTATTTTT CACAAATGGGTATGAGTTACATTGTAATTGAATGCGCTGTGCATCTGGTGATCTGTC
* Overexpression constructs were made using reporter gene fusion to *UVR8* with or without stop codon.	

Table 5-2. Full-length *UVR8* coding sequence with or without stop codon was used for the overexpression line with *GFP* reporter gene fusion at the C-terminus. Four lines of *UVR8* RNAi were developed using either fragment 1 or fragment 2 cloned into a Gateway vector, pB7GWIWG2 or pH7GWIWG2, and selected on media containing either Basta or hygromycin, respectively. The *CAD* RNAi sequence targeted the ORF (in red) and the 3' UTR to improve binding sites for RISC complexes (Sigoillot and King 2011, Wei et al. 2012).

Table 5-3. Primers used for PCR amplification targeting *UVR8* or *CAD* genes in INRA717-1B4 for Golden Gate assembly

Gene	Direction	Sequence (5' - 3')	PCR purpose
UVR8	Forward	CACCGAGGATGAAGGAGCTGCTAGTGG	RNAi, fragment 1, *P. deltoides*
	Reverse	CCCCAACTATAGACCTCCATTCGTG	
UVR8	Forward	CACCGTCAACTGGGACATGGGGACTTTG	RNAi, fragment 2, *P. deltoides*
	Reverse	TCAAATCCGTATCCGTTTGACATCACT	
UVR8	Forward	TGTGGTCTCACTTAATGGCCGAGGATGGACGAG	RNAi, fragment 1, INRA 717-1B4
	Reverse	TGTGGTCTCGGGTTCCCCAACTATAGACCTCCATTCGTG	
UVR8	Forward	TGTGGTCTCACTTAGTCAACTGGGACATGGGGACT	RNAi, fragment 2, INRA 717-1B4
	Reverse	TGTGGTCTCGGGTTTCAAATCCGTATCCGTTTGACATCACT	
UVR8	Forward	TGTGGTCTCACTTAATGGCCGAGGATGGACGAG	OX no stop, *P. deltoides*
	Reverse	TGTGGTCTCGGGTTAATCCGTATCCGTTTGACATCACTCTC	
UVR8	Forward	TGTGGTCTCACTTAATGGCCGAGGATGGACGAG	OX with stop, *P. deltoides*
	Reverse	TGTGGTCTCGGGTTTCAAATCCGTATCCGTTTGACATCACT	
UVR8	Forward	TGTGGTCTCACTTAATGGCCGAGGATGGACGAG	OX no stop, INRA 717-1B4
	Reverse	TGTGGTCTCGGGTTAATCCGTATCCGTTTGACATCACTCTC	
UVR8	Forward	TGTGGTCTCACTTAATGGCCGAGGATGGACGAG	OX with stop, INRA 717-1B4
	Reverse	TGTGGTCTCGGGTTTCAAATCCGTATCCGTTTGACATCACT	
CAD	Forward	TGTGGTCTCACTTAGCTGGTAGCAAGCTTATTCCCTG	RNAi, INRA 717-1B4
	Reverse	TGTGGTCTCGGGTTGACAGATCACCAGATGCACAGC	

Table 5-3. Primers used for PCR amplification targeting *UVR8* or *CAD* genes in INRA717-1B4 for Golden Gate assembly. Primers contain overhangs (in red) with type IIS endonuclease, *Bsa*I site that cleaves outside of the recognition sequence for multiple fragment and directional assembly.

TGTGGTCTCACTTAGCTGGTAGCAAGCTTATTCCCTG-3'), and the reverse primer (5'-TGTGGTCTCGGGTTGACAGATCACCAGATGCACAGC -3') (Table 5-3).

Populus deltoides UVR8 and INRA 717-1B4 *UVR8* (Fig. 5-1) and *CAD* (Fig. 5-2) amplicons were separated by 0.8% agarose gel electrophoresis, bands were excised, and purified using the Wizard SV gel and PCR clean-up system (Promega Corp., Madison, WI, USA). *UVR8* fragments were cloned into entry vectors pENTR/D-TOPO (Invitrogen, Carlsbad, CA, USA) or pLA3 and inserted into destination vectors pH7GWIWG(II) and pB7GWIWG(II) by using the Gateway™ LR Clonase™ II enzyme (Karimi et al. 2002). Destination vectors containing *UVR8* fragment 1 or 2, or the *CAD* fragment, were transformed into *Agrobacterium tumefaciens* strain C58/PMP90 (Table 5-4). Positive clones were selected with the appropriate selectable markers (Table 5-1), confirmed by DNA sequencing, and used for co-cultivation with *P. deltoides* or INRA 717-1B4 explants.

Construction of Populus Lines with CRISPR-Mediated Disruptions of UVR8 – Based on the high identity between *UVR8* from *Populus deltoides* and INRA 717-1B4, it was possible to design guide RNAs (gRNAs) based on location and PAM sequences that were compatible in either species. The exon and intron organization in the *UVR8* gene, with the region selected for the gRNAs used for CRISPR knockout, CRISPRa and CRISPRi, is shown in a schematic diagram (Fig. 5-3). Three gRNAs were designed to be used with the active Cas9 endonuclease in a multiplex construction to generate a *UVR8* knockout. The three gRNA target the coding region. The DNA fragment encoding the first gRNA was

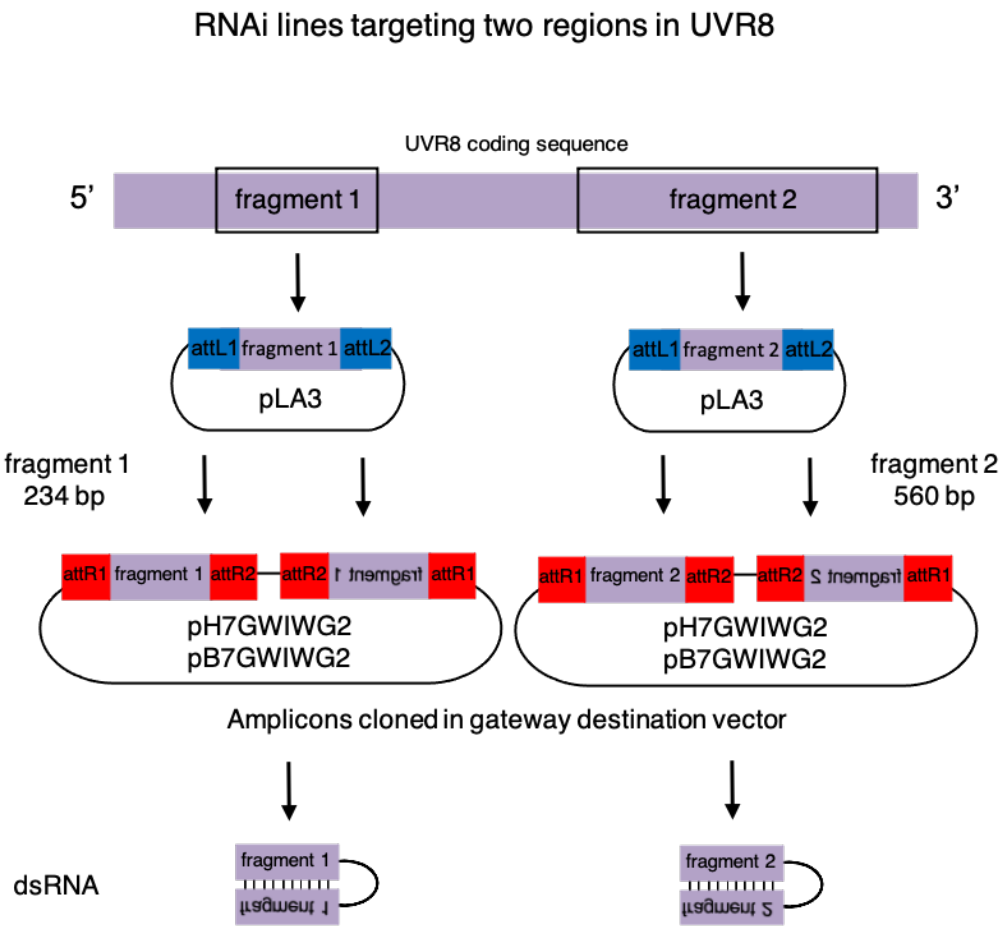

Figure 5-1. Schematic representation of *UVR8* RNAi vector construction. Due to RNAi lacking in specificity, two different regions were selected for the *UVR8* RNAi vectors in the coding region. Fragment 1 or fragment 2 was cloned in pLA3 with attL1 and attL2 sites for recombination of *UVR8* fragments into the expression vector (pB7GWIWG2 or pH7GWIWG2). The Gateway destination vectors with directional attR1 and attR2 sites to generate RNAi lines allow the insertion of inverted *UVR8* sequences to generate a hairpin double-stranded RNA.

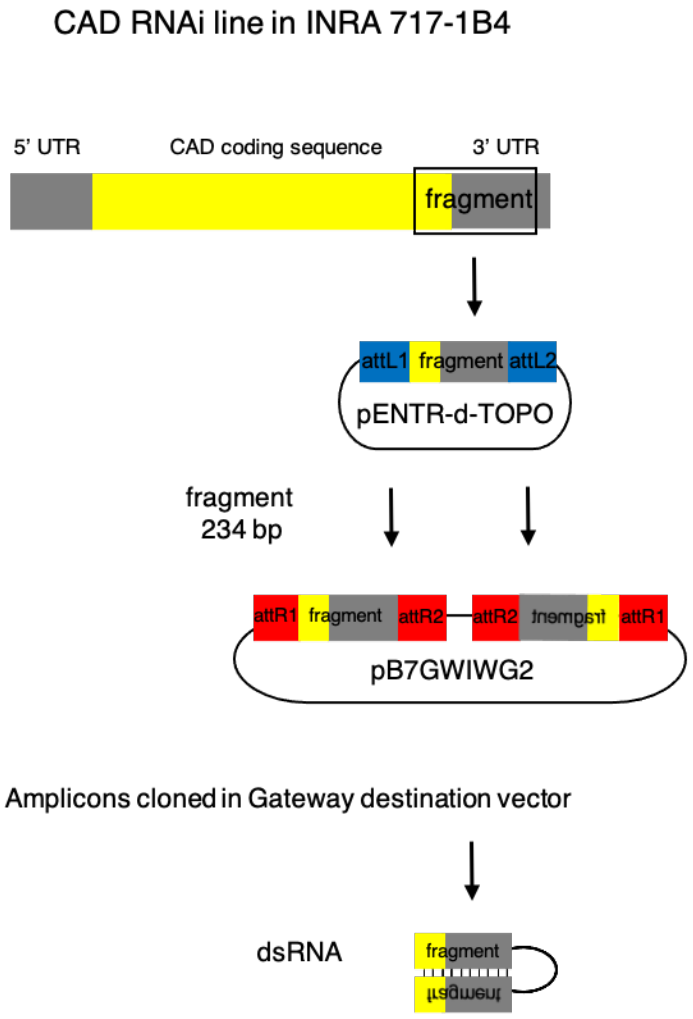

Figure 5-2. Schematic representation of *CAD* RNAi vector construction. *CAD* RNAi vectors in includes the coding region and 3' UTR. *CAD* fragment was cloned in pENTR-d-TOPO with attL1 and attL2 sites for recombination of *CAD* fragments into the expression vector (pB7GWIWG2). The Gateway destination vectors with directional attR1 and attR2 sites generate the RNAi line that allows the insertion of inverted *CAD* sequences to generate dsRNA.

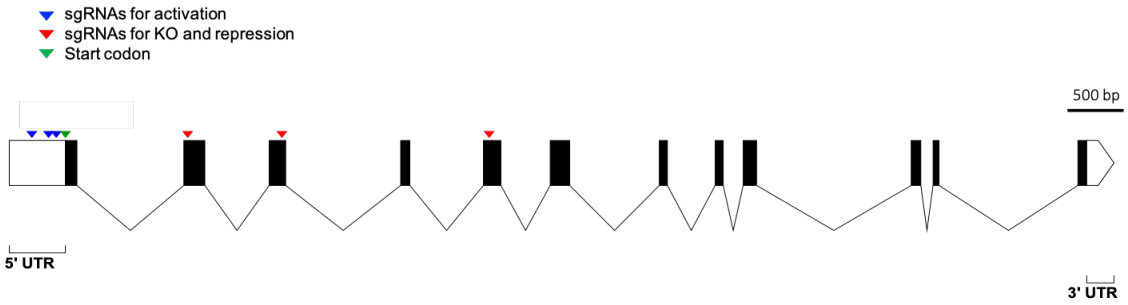

Figure 5-3. Schematic diagram of the genomic structure of *UVR8* in INRA 717-1B4 showing exon and intron locations as of CRISPR single guide RNAs (gRNA). Three gRNA sequences were selected in the promoter region for CRISPRa and CRISPRi (blue triangle). Three CRISPR KO gRNA sequences were selected in exons 2, 3, and 5 (red triangle). The organization of the exons and introns in *UVR8* was obtained from the genomic sequence available in Aspen DB (sPta717 v1.1) and illustrated using a graphic tool maker (http://wormweb.org/exonintron).

Table 5-4. Description of *UVR8* and *CAD* RNAi lines in *Populus.*

ID	Line	Purpose	Entry vector	Gateway destination vector	*E. coli* strain	*A. tumefaciens* strain
1	717-*CAD*	*CAD* RNAi	pENTR-d-TOPO	pB7GWIWG2	DH5α or Top10	C58/pMP90
2, 3	717 H+1, 717 H+2	*UVR8* RNAi Fragment 1, 2	pLA3	pH7GWIWG2	DH5α or Top10	C58/pMP90
4, 5	717 B+1, 717 B+2	*UVR8* RNAi Fragment 1, 2	pLA3	pB7GWIWG2	DH5α or Top10	C58/pMP90
6, 7	Pdel H+1, Pdel H+2	*UVR8* RNAi Fragment 1, 2	pENTR-d-TOPO	pH7GWIWG2	DH5α or Top10	C58/pMP90
8, 9	Pdel B+1, Pdel B+2	*UVR8* RNAi Fragment 1, 2	pENTR-d-TOPO	pB7GWIWG2	DH5α or Top10	C58/pMP90

Table 5-4. Description of *UVR8* and *CAD* RNAi lines in *Populus*. *UVR8* RNAi transgenic lines targeted two different regions of the gene in INRA 717-1B4 and *P. deltoides* and designated as fragment 1 or fragment 2. A single RNAi *CAD* line was generated in INRA 717-1B4. UVR8 fragments 1 and 2 and *CAD* fragment were cloned into a Gateway compatible destination hairpin vector pB7GWIWG2 or pH7GWIWG2 using the LR Clonase reaction for ligation. Each line was positively selected with either hygromycin (H) or Basta (B). Destination vectors were transformed into *A. tumefaciens* for plant transformation in *Populus*.

constructed by annealing two primers: (Forward: 5'-GATTGGATGGGCAGTTAGGCCATG-3') and (Reverse: 5'-AAACCATGGCCTAACTGCCCATCC-3'). The DNA fragment for the second gRNA utilized the primers: (Forward: 5'-GATTGTCTGGCAGTCACCATGGA-3') and (Reverse: 5'-AAACTCCATGGTGACTGCCAGAC-3'). And the DNA fragment for the third gRNA utilized the primers (Forward: 5'- GGTCACAGAAGATGGAGAGCTCTA-3') and (Reverse: 5'- AAACTAGAGCTCTCCATCTTCTGT-3'). The gRNA primers used to construct the multiplex expression cassettes are listed in Table 5-5.

CRISPRa and CRISPRi lines were also generated by using three gRNAs, but instead of cloning with a gene for active Cas9, a deactivated variant of the Cas9 endonuclease (dCas9) was used. In this way, the dCas9 acts as a site-specific DNA binding protein, with sites within approximately the first 100 bp upstream of the *UVR8* translational start site, for the purposes of repressing or activating *UVR8*. The primers used for multiplexed cloning were (Forward 1: 5'-GATTGCATCATCAATGCCGTTGTTT-3') and (Reverse 1: 5'-AAACAAACAACGGCATTGATGATGC-3'), (Forward 2: 5'-GATTGCATCACTGCCACCCACTCTC-3') and (Reverse 2: 5'-AAACGAGAGTGGGTGGCAGTGATGC-3'), and (Forward 3: 5'-GGTCAGAAACATCTTCTAGACTT-3') and (Reverse 3: 5'-AAACAAGTCTAGAAGATGTTTCT-3'. Destination vectors containing *UVR8* gRNAs and either the deactivated or activated Cas9 endonuclease were transformed into the pMDC32 vector using the Gateway LR Clonase II enzyme (Fig. 5-4). Transformed

Table 5-5. Multiplex CRISPR gRNA primers for *UVR8* in *Populus*.

Species	gRNA	Direction	Sequence 5'-3'	Function
717, *P. deltoides*	gRNA1	Forward	GATTGGATGGGCAGTTAGGCCATG	KO, CRISPRi
		Reverse	AAACCATGGCCTAACTGCCCATCC	
717, *P. deltoides*	gRNA2	Forward	GATTGTCTGGCAGTCACCATGGA	KO, CRISPRi
		Reverse	AAACTCCATGGTGACTGCCAGAC	
717, *P. deltoides*	gRNA3	Forward	GGTCACAGAAGATGGAGAGCTCTA	KO, CRISPRi
		Reverse	AAACTAGAGCTCTCCATCTTCTGT	
717, *P. deltoides*	gRNA4	Forward	GATTGCATCATCAATGCCGTTGTTT	CRISPRa
		Reverse	AAACAAACAACGGCATTGATGATGC	
717	gRNA5	Forward	GATTGATCACTGCCACCCACTCTC	CRISPRa
		Reverse	AAACGAGAGTGGGTGGCAGTGATC	
P. deltoides	gRNA5	Forward	GATTGCATCACTGCCACCCACTCTC	CRISPRa
		Reverse	AAACGAGAGTGGGTGGCAGTGATGC	
717	gRNA6	Forward	GGTCGTGAAACATCTTCTAGACTT	CRISPRa
		Reverse	AAACAAGTCTAGAAGATGTTTCAC	
P. deltoides	gRNA6	Forward	GGTCAGAAACATCTTCTAGACTT	CRISPRa
		Reverse	AAACAAGTCTAGAAGATGTTTCT	

Table 5-5. Multiplex CRISPR gRNA primers for *UVR8* in *Populus*. Three gRNAs were chosen 19 – 20 bp upstream from NGG PAM sequences for *UVR8* KO, *UVR8* activation, and *UVR8* interference. Overhangs (in red) were included in for cloning based on the expression cassette promoter. *Arabidopsis* U6 promoter overhang for the forward oligo is (5'-GATT-3') and reverse (5'-AAAC-3'). *Arabidopsis* U3 promoter overhang for the forward oligo is (5'-GGTC-3') and reverse (5'-AAAC-3'). To optimize U6 and U3 promoters, if the first nucleotide in the gRNA sequence is not a guanine (G) or adenine (A), an extra G is added to the 5' end of the overhang (Wang et al. 2019).

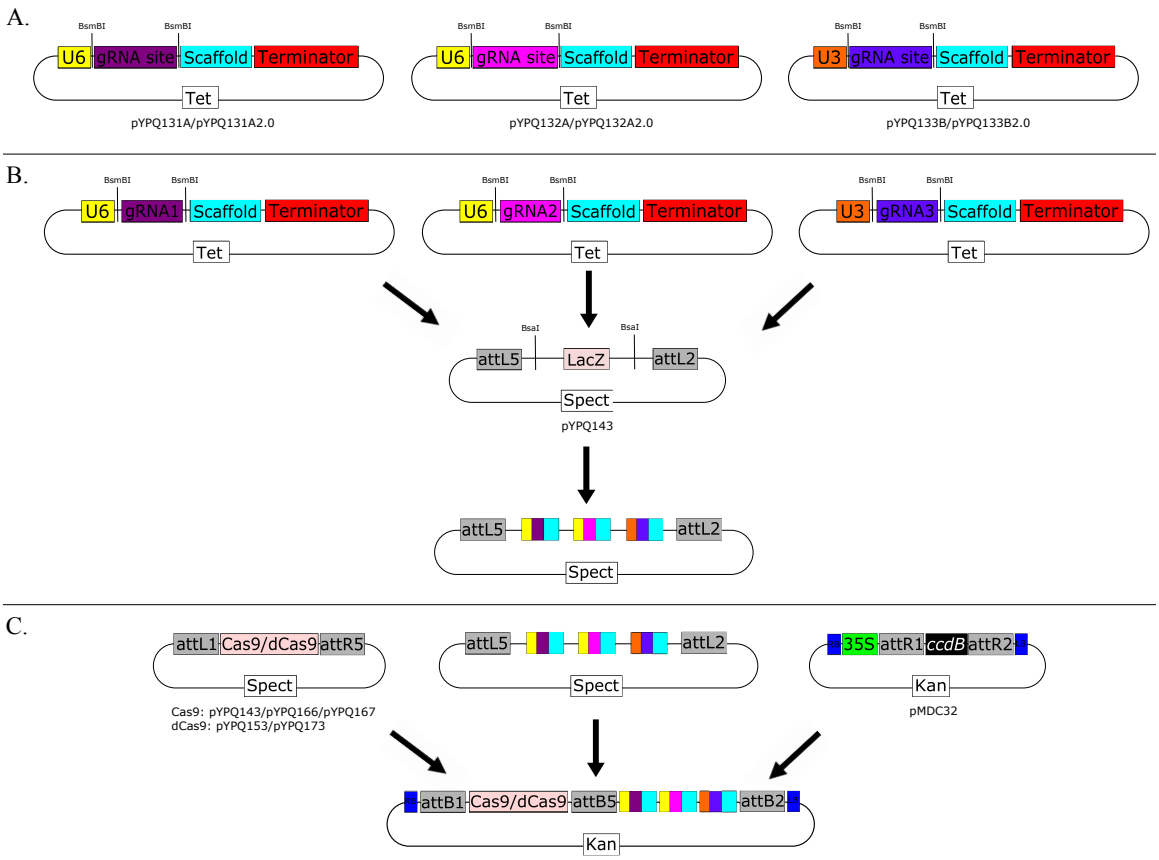

Figure 5-4. Schematic representation of multiplex CRISPR-Cas9 and CRISPR-dCas9 vector construction. (A) Three gRNA expression plasmids with either the *A. thaliana* U6 or U3 promoters were linearized by digesting with type IIS restriction enzyme *BsmB*I. Phosphorylated gRNA oligonucleotides were annealed and ligated to entry vectors. (B) Golden gate recipient plasmid was linearized with restriction enzyme *Bsa*I. The gRNA cassettes were cloned into the recipient plasmid by Golden Gate reaction. (C) Multiplex CRISPR vector was constructed by Gateway recombination with entry vectors with gRNA cassettes, Cas9 or dCas9 vector, and T-DNA binary vectors. Assembled plasmids were transformed into *E. coli* and subsequently transformed into *A. tumefaciens*.

plants were generated as described above, and selected and maintained on LS media containing hygromycin or Basta (Table 5-1). A list of the transgenic poplar lines and vectors used in the construction via CRISPR is presented in Table 5-6.

Construction of UVR8 Overexpression Populus Lines– Homologous sequences of *Arabidopsis thaliana UVR8* were identified in *P. deltoides* and in INRA 717-1B4 by using TAIR, Phytozome, and the URGI INRA databases (Huala et al. 2001, Goodstein et al. 2012, Mader et al. 2016). These sequences were used to synthesize full-length cDNA copies of the respective *UVR8* genes for overexpression constructs (Table 5-2). Primers used to amplify the full-length *UVR8* sequence in *P. deltoides*, with a stop codon were, (Forward: 5'-TGTGGTCTCACTTAATGGCCGAGGATGAAGGAGC-3') and (Reverse: 5'-TGTGGTCTCGGGTTTCAAATCCGTATCCGTTTGACATCACT-3'). Primers used to amplify the full-length *UVR8* gene from *P. deltoides* but without a stop codon were (Forward: 5'- CACCATGGCCGAGGATGAAGGAGC-3') and (Reverse: 5'-AATCCGTATCCGTTTGACATCACTCTC-3') (Table 5-3). Full-length *UVR8* with or without stop codon was cloned into Gateway vector pK7FWG2 as a C-terminal GFP fusion (Table 5-7). Transformed plants were generated as described and selected and maintained on LS media containing hygromycin or Basta (Table 5-1).

Construction of RNAi-Regulated CAD and UVR8 Knockout and UVR8 Overexpression Populus Lines – INRA 717-1B4 lines that suppressed expression or knockdown of *CAD* by RNAi were micropropagated and used as the starting material for the generation of *UVR8* knockout (KO) and overexpression (OX) lines derived from CRISPR and expression

Table 5-6. CRISPR generated transgenic lines developed in *Populus*.

ID	Line	Purpose	Gateway entry vector	Golden Gate recipient and expression cassettes	Gateway destination vector	*E. coli* strain	*A. tumefaciens* strain
10	717-21	CRISPR- *Arabidopsis* codon optimized Cas9 (KO)	pYPQ154	pYPQ143, pYPQ131A, pYPQ132A, pYPQ133B	pMDC32	DH5α or Top10	C58/pMP90
11	717-22	CRISPR- *Maize* codon optimized Cas9 (KO)	pYPQ166	pYPQ143, pYPQ131A, pYPQ132A, pYPQ133B	pMDC32	DH5α or Top10	C58/pMP90
12	717-23	CRISPR- Plant codon optimized Cas9 (KO)	pYPQ167	pYPQ143, pYPQ131A, pYPQ132A, pYPQ133B	pMDC32	DH5α or Top10	C58/pMP90
13	717-24	CRISPR- dCas9 VP64 (activation)	pYPQ173	pYPQ143, pYPQ131A2.0, pYPQ132A2.0, pYPQ133B2.0	pMDC32	DH5α or Top10	C58/pMP90
14	717-25	CRISPR-dCas9 SRDX (repressor)	pYPQ153	pYPQ143, pYPQ131A, pYPQ132A, pYPQ133B	pMDC32	DH5α or Top10	C58/pMP90
15*	Pdel-21	CRISPR- *Arabidopsis* codon optimized Cas9 (KO)	pYPQ154	pYPQ143, pYPQ131A, pYPQ132A, pYPQ133B	pMDC32	DH5α or Top10	C58/pMP90
16*	Pdel-22	CRISPR- *Maize* codon optimized Cas9 (KO)	pYPQ166	pYPQ143, pYPQ131A, pYPQ132A, pYPQ133B	pMDC32	DH5α or Top10	C58/pMP90
17*	Pdel-23	CRISPR- Plant codon optimized Cas9 (KO)	pYPQ167	pYPQ143, pYPQ131A, pYPQ132A, pYPQ133B	pMDC32	DH5α or Top10	C58/pMP90
18*	Pdel-24	CRISPR- dCas9 VP64 (activation)	pYPQ173	pYPQ143, pYPQ131A2.0, pYPQ132A2.0, pYPQ133B2.0	pMDC32	DH5α or Top10	C58/pMP90
19*	Pdel-25	CRISPR-dCas9 SRDX (repressor)	pYPQ153	pYPQ143, pYPQ131A, pYPQ132A, pYPQ133B	pMDC32	DH5α or Top10	C58/pMP90

Table 5-6. CRISPR generated transgenic lines developed in *Populus*. CRISPR KO lines produced from Gateway entry vectors containing either *Arabidopsis* codon optimized Cas9 (pYPQ154), *Maize* codon optimized Cas9 (pYPQ166), and plant codon optimized Cas9 (pYPQ167). gRNA expression cassettes (pYPQ131A, pYPQ132A, pYPQ133B) with different promoters (*At*U6, *At*U6, *At*U3, respectively) were cloned into a Golden Gate recipient (pYPQ143). Cas9 plasmids, Gateway entry vector containing gRNA expression cassettes were assembled though Gateway recombination with the T-DNA binary vector (pMDC32). CRISPRa lines contain a Gateway vector with dCas9 and MS2-VP64 fusion protein (pYPQ173). Expression cassettes each with four MS2 binding sites (pYPQ131A2.0, pYPQ132A2.0, pYPQ133B2.0) were driven with various promoters (*At*U6, *At*U6, *At*U3, respectively) and cloned into pYPQ143. Entry vector and Golden Gate recipient were recombined with Gateway binary vector. CRISPRi was generated by using a dCas9-SRDX entry vector, pYPQ153. Expression cassettes from the KO lines were cloned into pYPQ143 and recombined through Gateway reaction using pYPQ153 and pMDC32. * *Populus deltoides* failed to generate sufficient plant material required for transformation.

Table 5-7. Organization of the *UVR8-GFP* overexpression lines using CaMV35S constitutive promoter in INRA 717-1B4 and *Populus deltoides* and using Gateway destination vector, pK7FWG2.

ID	Line	Purpose	Entry vector	PCR Product	Gateway destination vector	*E. coli* strain	*A. tumefaciens* strain
20	717 *UVR8-GFP*	*UVR8* OX cDNA no stop with *GFP*	pENTR-d-TOPO	717 *UVR8* cDNA no stop	pK7FWG2	DH5α or Top10	C58/pMP90
21	717 *UVR8*-stop-*GFP*	*UVR8* OX cDNA with stop with *GFP*	pLA3	717 *UVR8* cDNA with stop	pK7FWG2	DH5α or Top10	C58/pMP90
22	Pdel *UVR8-GFP*	*UVR8* OX cDNA no stop with *GFP*	pLA3	Pdel *UVR8* cDNA no stop	pK7FWG2	DH5α or Top10	GV3101
23	Pdel *UVR8*-stop-*GFP*	*UVR8* OX cDNA with stop with *GFP*	pLA3	Pdel *UVR8* cDNA with stop	pK7FWG2	DH5α or Top10	C58/pMP90

Table 5-7. Organization of the *UVR8-GFP* overexpression lines using CaMV35S constitutive promoter in INRA 717-1B4 and *Populus deltoides* and using Gateway destination vector, pK7FWG2. Full-length *UVR8* (with and without stop codon) cDNA was amplified and cloned into pK7FWG2. *GFP* gene was fused to the C-terminal region of *UVR8* and transformed.

from the 35S promoter. The vectors and plant transformation protocol were as described above. The list of double mutant poplar lines is provided in Table 5-8.

Isolation of RNA and cDNA Synthesis – RNA was obtained from wild-type or transgenic *Populus* leaf tissue that was flash frozen in liquid N_2 and finely ground with a mortar and pestle. RNA was extracted and purified from ground leaf material using the RNeasy Plant Mini Kit (Qiagen, Valencia, CA, USA) according to manufacturer's protocol. An alternative, phenol and guanidine isothiocyanate based extraction method was also used to extract RNA. TRIzol reagent (Invitrogen, Carlsbad, CA, USA) was added to 50 mg of ground material in a tube. Samples were incubated for 10 minutes and centrifuged at 14,000 g x 15 minutes. The supernatant was transferred to a new tube with chloroform and centrifuged for phase separation. The aqueous phase was obtained, and RNA was precipitated by adding isopropanol and incubating at -20°C. Samples were centrifuged, supernatant was discarded and washed with 75% ethanol multiple times. Decanted and dried pellets were resuspended in TE. Following isolation of RNA, cDNA was synthesized using SuperScript™ IV Reverse Transcriptase (ThermoFisher Scientific, Marietta, OH, USA) and used as a template for PCR.

Transgene Validation Using RT-PCR – Relative transcript levels were quantified to determine specificity of transgene targets from expression modulation using RNAi, the 35S promoter, and CRISPR-based tools. Synthesized cDNA was constructed using 1 µg of total RNA in a 20 µL mixture using SuperScript™ IV Reverse Transcriptase. Gene

Table 5-8. Generation of several double mutant lines with low-lignin *UVR8* KO and *UVR8* OX lines in INRA 717-1B4.

ID	LINE	Purpose	PCR Product or Entry Vector
28	717 *CAD-UVR8*-CRISPR 21	RNAi *CAD* and *UVR8* KO	CRISPR- *Arabidopsis* codon opt Cas9 (KO)
29	717 *CAD-UVR8*-CRISPR 22	RNAi *CAD* and *UVR8* KO	CRISPR- *Maize* codon optimized Cas9 (KO)
30	717 *CAD-UVR8*-CRISPR 23	RNAi *CAD* and *UVR8* KO	CRISPR- Plant codon optimized Cas9 (KO)
33	717 *CAD-UVR8:GFP*	RNAi *CAD* and OE *UVR8:GFP*	Overexpression *UVR8* cDNA no stop
34	717 *CAD-UVR8*stop:*GFP*	RNAi *CAD* and OX *UVR8*	Overexpression *UVR8* cDNA with stop

Table 5-8. Generation of several double mutant lines with low-lignin *UVR8* KO and *UVR8* OX lines in INRA 717-1B4. Cinnamyl alcohol dehydrogenase (CAD) is the last enzyme in lignin monomer (coumaryl alcohol, caffeyl alcohol, coniferyl alcohol, and sinapyl alcohol) biosynthesis, which provides structural support in trees and protection against pathogens. RNA silenced *CAD* with *UVR8* CRISPR KO or 35S *UVR8* overexpression lines were created to further understand metabolic acclimation.

specific primers targeting a region of *UVR8* mRNA was amplified using a forward (F: 5'-CTCTGAGTGCTGATGGATCTGGTG-3') and reverse primer (R: 5'-ATCCGTTTGACATCACTCTCCGG-3'). *CAD* mRNA was amplified using a forward (F: 5'-CCTGATGGGATGTCACCAGAACA-3') reverse primer (R: 5'-CTCTTAGCCCACTCTGTTTCAGTCC-3') (Table 5-9). RT-PCR reactions were performed in a 20 µL mixture containing 1 µL cDNA, 10 µL 1x SYBR Green reaction buffer, 7 µL H_2O, and 1 µL of each primer diluted to 10 µM. Amplification of *UVR8* and *CAD* genes consisted of the following cycling conditions; 50°C for 2.00 min, 95°C for 10.00 min, followed by 40 cycles at 95°C for 15 s, 60°C for 1:00 min. The reference genes used to normalize relative expression in each reaction were *CDC2* and *CYC063* with the primers used taken from the literature (Pettengill et al. 2012). All experiments were performed three times and relative expression levels were calculated using the $2^{-\Delta\Delta C_T}$ Livak Method (Livak and Schmittgen 2001).

Validation of CRISPR KO Populus Lines– Fragments encompassing the targeted gRNA regions and with restriction enzyme sites in close proximity were amplified by PCR and screened for the loss of the restriction enzyme site to initially verify biallelic mutagenesis of *UVR8* using CRISPR/Cas9. To confirm these results, genomic DNA was extracted from the candidate INRA 717-1B4 *UVR8* KO lines using the cetyltrimethylammonium bromide (CTAB) and sodium dodecyl sulfate (SDS) method as previously described (Infante 2002). PCR with the high fidelity KOD Hot Start DNA Polymerase was used to generate fragments flanking the region of *UVR8* targeted for disruption by CRISPR/Cas9. PCR

Table 5-9. Primer sets for RT-PCR gene expression analysis and sequencing in INRA 717-1B4.			
Gene	Direction	Sequence (5' - 3')	PCR purpose
UVR8	Forward	GAGGATGGACGAGCTGCTAGTG	RT-PCR, set 1
	Reverse	GTGGGTCTATCCTCAGCATCCC	
UVR8	Forward	GCTTGTGGGGATAGCCATTGTC	RT-PCR, set 2
	Reverse	CAGCTGCAGTATGTTCAGCACC	
UVR8	Forward	GATGGAGAGCTCTATGGATGGGG	RT-PCR, set 3
	Reverse	CCACCCACATGCAACCATTATCATC	
UVR8	Forward	GATATCAGGTGGCTGGAGACACAC	RT -PCR, set 4
	Reverse	CCTCCATCCACATGAGATCTGGAC	
UVR8	Forward	CTCTGAGTGCTGATGGATCTGGTG	RT -PCR, set 5
	Reverse	ATCCGTTTGACATCACTCTCCGG	
CAD	Forward	CCTGATGGGATGTCACCAGAACA	RT-PCR, set 1
	Reverse	CTCTTAGCCCACTCTGTTTCAGTCC	
CAD	Forward	GGTGCTGATGAATACTTGGTCAGC	RT -PCR, set 2
	Reverse	CACCCATCAAGATCAGCTTGCC	
CHI	Forward	ATGTCTCCTGCAGTGCCTCTC	RT -PCR, set 1
	Reverse	CTCCAAGTACACTCCTATAGCCGTG	
CHI	Forward	ATGTCTCCTGCAGTGCCTCTC	RT -PCR, set 2
	Reverse	CTCCAAGTACACTCCTATAGCCGTG	
CDC2	Forward	ATTCCCCAAGTGGCCTTCTAAG	Reference gene
	Reverse	ATTCCCCAAGTGGCCTTCTAAG	
CYC063	Forward	ATTCCCCAAGTGGCCTTCTAAG	Reference gene
	Reverse	CACAACTCTTCCGAACACCAC	
PT1	Forward	GCGGAAAGAAAAACTGCAAG	Reference gene
	Reverse	TGACAGCACAGCCCAATAAG	
TIP4-like	Forward	GCTGATAATGGGGTGTCG	Reference gene
	Reverse	CAACTCTAAGCCAGAATCGC	

Table 5-9. Primer sets for RT-PCR gene expression analysis and sequencing in INRA 717-1B4. Primers targeted multiple regions of *UVR8*, *CAD*, and *CHI* and several reference genes were used for normalization. Stable reference genes were selected based on PCR efficiency and dissociation curves to ensure homogeneity of PCR products (Pettengill et al. 2012). Transcript levels were measure based on Ct values and calculated using the $2^{-\Delta\Delta CT}$ method (Livak and Schmittgen 2001).

products at either 465, 571, and 728 bp were gel purified from 1% agarose, and the DNA was purified using Wizard Plus SV Minipreps DNA Purification Kit (Promega, Madison, WI, USA). About 200 ng of the DNA was subjected to restriction enzyme digestion using NcoI or *Sac*I for visual confirmation of the initial results on 1% agarose gels. The DNA segments that were amplified by PCR were sent for Sanger sequencing with appropriate forward and reverse primers to verify *UVR8* sequence disruptions (Table 5-10).

Localization of Transiently Expressed UVR8:GFP *–Populus deltoides UVR8* as a C-terminal GFP fusion from the CaMV 35S promoter was transiently expressed in *Nicotiana benthamiana. UVR8* or control sequences were cloned into pK7FWG2, a binary vector that expresses target genes from the 35S promoter as for C-terminal GFP fusions. Expression vectors were transformed into *Agrobacterium tumefaciens* (GV3101) using electroporation. Colonies were selected and streaked on solid Luria Broth (LB) supplemented with spectinomycin (100 µg/ml) and grown at 28 °C for 2 days. Colonies were then used to inoculate 3-5 ml YEP medium supplemented with 100 µg/ml spectinomycin, 25 µg/ml rifampicin and 10 µg/ml gentamicin, and grown overnight in a shaker at 250 RPM at 28°C. Cells were collected by centrifugation at 4,000 x g for 10 min and resuspended in buffer containing 10 mM 2-(N-morpholino) ethane sulfonic acid (MES), pH 5.7, 10 mM $MgCl_2$, and 200 µM acetosyringone, and adjusted to final density of 0.5-1.0 OD_{600}. The top canopy leaves of 5-week-old *Nicotiana benthamiana* were selected for infiltration. *Agrobacterium* suspensions containing the various *UVR8* constructs were mixed with *Agrobacterium* suspensions that contained the turnip crinkle

Table 5-10. Restriction site loss primers used to amplify regions in *UVR8* surrounding each gRNA INRA 717-1B4.			
Gene	Direction	Sequence (5' - 3')	PCR purpose
UVR8	Forward	CGGTAAGCTATGGCCTTGATGG	*Nco*I restriction site loss for gRNA1 region
	Reverse	GACCATCCCCAACTATAGACCTCC	
UVR8	Forward	CTCGACTGGATTTCATGTGTAGCC	*Nco*I restriction site loss for gRNA2 region
	Reverse	CTGCTGAATTGGACTCCTCAACC	
UVR8	Forward	GATGCTTCCTCTGTGACATGCTG	*Sac*I restriction site loss for gRNA3 region
	Reverse	CTTGTCTCCCTGCAACTACCATG	

Table 5-10. Restriction site loss primers used to amplify regions in *UVR8* surrounding each gRNA INRA 717-1B4. Amplicons were digested with either *Nco*I or *Sac*I restriction endonucleases. Digested patterns were analyzed by 1% agarose gel electrophoresis to screen transgenic lines for Cas9 activity in the gRNA regions.

virus (TCV) suppressor of RNA silencing (Qu et al. 2003) and then used to infiltrate leaves abaxially using a 1 ml plastic needleless syringe. Agro-infiltrated plants were incubated for two days on a growing rack supplemented with fluorescent lights for 16 hours. Leaves were harvested and visualized by light microscopy at five days post infiltration.

Confocal Laser Scanning Microscopy – Live imaging of transgenic INRA 717-1B4 leaves with pavement cells was observed under single or multiple channels with a confocal microscope (LSM710 Zeiss) as previously described in (Berkey et al. 2017). Images were processed using Zen 2009 Light Edition.

UV-B Treatments – Lamp banks of UV-B fluorescent tubes were suspended above growing rack at IBBR. The lamp bank contained four Q-lab UVB-313 QFS40W fluorescent sunlamps (Q-panel Inc., Westlake, OH). Lamps were wrapped with 0.038 mm cellulose acetate film to absorb radiation below 290 nm (UV-B treatment) or 0.051 mm clear Mylar polyester film to absorb radiation below 320 nm (control treatment). The output of each fluorescent UV-B tube was measured in μW cm^{-2} with a broadband Solarmeter Digital Ultraviolet Meter 6.2 UV-B meter (Solartech, Harrison Township, MI) and recorded values were converted to kJ m^{-2} at 30 or 60 cm. UV-B experiments involved UV-B dosages ranging from 20 – 35 kJ m^{-2} for 8 to 16 h for 1 to 10 days duration.

Assay for Total Anthocyanins – Extracts containing anthocyanins were prepared by collecting approximately 0.2 g of leaf discs in scintillation vials containing 5 mL of acidified methanol (1% HCl v/v). Samples were placed on a shaker and incubated at 4°C

for 24 h in darkness to prevent degradation. Extracts were transferred into tubes and clarified by centrifugation at 16,000 x g for 5 minutes to pellet debris. Absorbance was read at 530 nm and corrected for chlorophyll at 657 nm as previously described (Rabino and Mancinelli 1986, Gamon and Surfus 1999). Total anthocyanin content (TAC) was calculated using absorbance values and fresh weight (FW) of leaf discs using the equation:

$$TAC = A_{530} - \frac{(0.25\ x\ A_{657})}{FW}$$

Determination of Total Flavonoid Content – Total flavonoid content (TFC) was determined by a colorimetric method and using quercetin as a standard for construction of a calibration curve (Chang et al. 2002). Flavonoid extracts were prepared by collecting approximately 0.2 g of leaf discs in scintillation vials containing 5 mL of methanol. 10% $AlCl_3$ (w/v) and 1M potassium acetate stock solutions were prepared. Extracts were diluted with methanol, 10% $AlCl_3$, and 1M potassium acetate and incubated at room temperature in the dark for 30 minutes. Absorbance was measured at 430 nm and concentrations were calculated based on a quercetin calibration curve at using 25, 50, 75, 100, and 200 µg/mL standards.

Metabolomic Analysis – Metabolite detection was performed on a UPLC-MS (Acquity Ultra Performance Liquid Chromatography system coupled with an LCT Premier XE Electrospray Time-of-Flight Mass Spectrometer) system (Waters Corporation, Milford, MA). Leaf tissue was flash frozen in liquid nitrogen, ground into a fine powder with a mortar and pestle and stored at -80 °C until analysis. Secondary metabolites were extracted

from 4 mg/leaf of ground tissue with 1.5 ml of HPLC-grade MeOH at room temperature for 30 minutes, centrifuged for 10 minutes at 2,100 x g, and filtered through microcentrifuge filtration units. Sample extracts were introduced into 12 x 32 mm screw neck glass vials with bonded preslit PTFE/silicone septa for automatic injection into a Waters Acquity C18 BEH 1.7 μm, 2.1x 50 mm UPLC column at 30°C. The column mobile phase consisted of solvent A (water + 0.1% formic acid) and solvent B (acetonitrile + 0.1% formic acid) at a flow rate of 0.4 mL/min. TOF Mass spectrometry was set to negative electrospray mode with V resolution. Capillary and cone voltage was set to 2800 V and 80 V, respectively, and the scan range was between 150 to 800 *m*/*z*. All samples were analyzed with an internal reference lock mass using leucine enkephalin (200 ng/mL) at a flow rate of 2.0 μL/min.

Chromatography and mass spectra were processed with the MassLynx 4.1 software package (Waters Corporation). Identification of signature compounds was achieved by comparison with internal and external standards (Millipore Corporation, St. Louis, MO). Identification of compounds for which standards are unavailable was determined with LC-MS molecular weights and retention times from previous work (Caseys et al. 2012, Babst et al. 2014) and the database within MassLynx. Using the mass of the deprotonated [M-H] ion, single ion chromatograms were integrated to calculate peak areas and normalized to an internal standard, vanillic acid. Quercetin glucoside and salicin external standards were used to generate a standard curve to determine concentration of each metabolite within a sample.

Determination of Plant Morphological Parameters – Before irradiation treatments, initial height and UV transmittance was measured for all plants. Upon the completion of UV-B treatment, final height and bud count was recorded. Approximate internode length was calculated by dividing final height and node count for each plant. Leaves at LPI 5–7 were harvested and placed on a scanning bed with LED detectors to digitize the length, area, and width of each leaf to measure total leaf area (cm^2) (Li-3100, LICOR, Lincoln, NE).

Results

In order to evaluate the effects of altered *UVR8* expression in normal plants and a variant that was disrupted in phenylpropanoid biosynthesis, a number of transgenic poplar lines were constructed. RNAi was used to down-regulate the expression of *UVR8* and *CAD*. In an effort to compare the established RNAi technology to newer gene editing techniques, CRISPR was also used to generate knockout, down- and up-regulated *UVR8* transgenic lines. Additionally, a *UVR8* overexpression line was constructed with the gene transcribed from the CaMV 35S promoter. Once these lines were generated, double mutant lines were constructed by using the RNAi-regulated *CAD* transgenic line as starting material for the introduction of vectors to effect either *UVR8* overexpression or a *UVR8* knockout. In this way, it would be possible to examine the effect of altered *UVR8* expression in a plant line with disrupted phenylpropanoid biosynthesis. Thus, considerable effort was spent on the construction and characterization of transgenic poplar lines with modulated *CAD* and *UVR8* expression.

Construction and Characterization of RNAi-Regulated UVR8 and CAD Transgenic Populus Lines – Four *Populus deltoides* and four INRA 717-1B4 plants were transformed with two plasmid vectors (pB7GWIWG2 or pH7GWIWG2) with different selection markers (Basta or hygromycin) to generate RNAi-regulated *UVR8* transgenic *Populus* lines targeting two regions of the *UVR8* gene (Fig. 5-1). Unfortunately, transformation efficiencies in the *P. deltoides UVR8* RNAi lines were very low and resulted in the loss of the cultures. However, transformation of INRA 717-1B4 was more successful and resulted in shoot regeneration in abundance. After cultivation and several rounds of micropropagation of the transgenic lines, relative transcript levels were measured using RT-PCR for several subcultures. A range of *UVR8* levels expression was observed for the lines, with several subcultures showing lower transcript levels than the wild-type control, some subcultures showing no difference, and even one subculture with increased expression (Fig. 5-5). The subcultures with low transcript levels were selected and propagated for UV-B experimentation. Similarly, vectors for RNAi-regulated *CAD* were used to transform INRA 717-1B4 and *P. deltoides*, with only the INRA 717-1B4 surviving. The analysis of transcript levels by RT-PCR showed lower levels of *CAD* mRNA relative to the wild-type control in multiple subcultures (Fig. 5-6).

Construction and Characterization of a UVR8 Overexpression (OX) Transgenic Populus Line – A transgenic poplar line that overexpresses the *UVR8* gene was constructed by cloning the gene under the control of the CaMV 35S promoter. Two different constructs

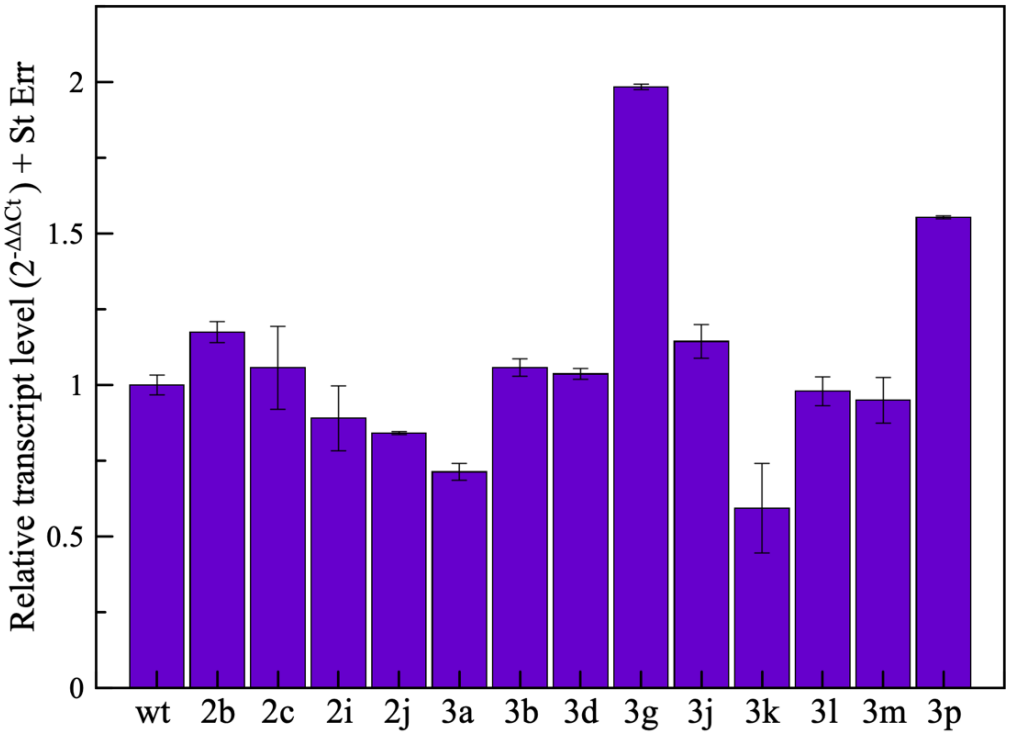

Figure 5-5. Relative transcript levels of WT and *UVR8* RNAi lines were used to screen candidates. RNA was extracted from frozen ground leaf material from INRA 717-1B4, reverse transcribed, and analyzed for *UVR8* transcripts by RT-PCR. Stably expressed reference genes, *CDC2* and *CYC063*, were used for data analysis (Pettengill et al. 2012). Subcultures showing the lowest transcript levels were used for UV-B experimentation.

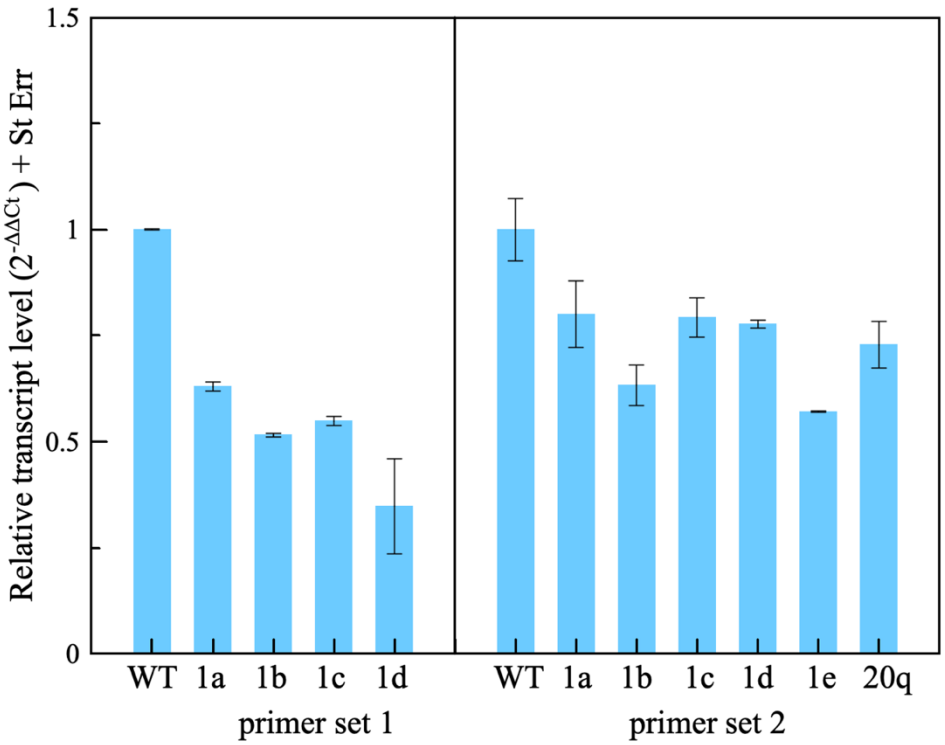

Figure 5-6. *CAD* RNAi lines have reduced cinnamyl alcohol dehydrogenase, the last enzyme used for monolignol biosynthesis. Two different primer sets targeting *CAD* in INRA 717-1B4 revealed decreased transcript levels from compared to the wild-type. Relative mRNA levels were normalized to *CDC2* and *CYC063* housekeeping genes. Subcultures showing the lowest transcript levels were used for UV-B experimentation and as explant tissue for *A. tumefaciens* transformation.

were used: one construct contained the INRA 717-1B4 *UVR8* gene with a stop codon; another construct contained the *UVR8* gene expressed as a C-terminal fusion to GFP. As was observed with the RNAi constructs described above, only INRA 717-1B4 cultures were able to grow under propagation conditions, and the *P. deltoides* cultures did not survive. RT-PCR was used to quantify the efficiency of *UVR8* expression in the two different overexpression lines that were generated in INRA 717-1B4. The peptide sequence for UVR8 in transgenic line 20 lacks the stop codon and is fused to GFP, whereas transgenic line 21 contains *UVR8* with a stop codon (Table 5-7). The relative transcript levels were only measured in line 20, and several subcultures showed strong promoter activity with up to 50-fold increases in mRNA (Fig. 5-7). The subcultures, 20Q and 20R were used for UV-B experimentation.

Construction and Characterization of a UVR8 Knockout (KO) Transgenic Populus Line Using CRISPR – The CRISPR/Cas9 system was used to generate a *UVR8* KO transgenic line in INRA 717-1B4 (Lowder et al. 2015). Three gRNAs were used for multiplexed targeting to improve efficiency in affecting the coding region of *UVR8*. The plasmid systems for CRISPR utilized the *Arabidopsis* U6 and U3 promoters for gRNA expression in order to screen for an optimal promoter for use in poplar.

Additionally, CRISPR vectors were chosen to screen three codon-optimized versions of Cas9 for their efficiency in poplar: an *Arabidopsis* construct (line 10), a *Maize* construct (line 11), and a generic plant construct (line 12) (Table 5-6). *UVR8* KO subcultures

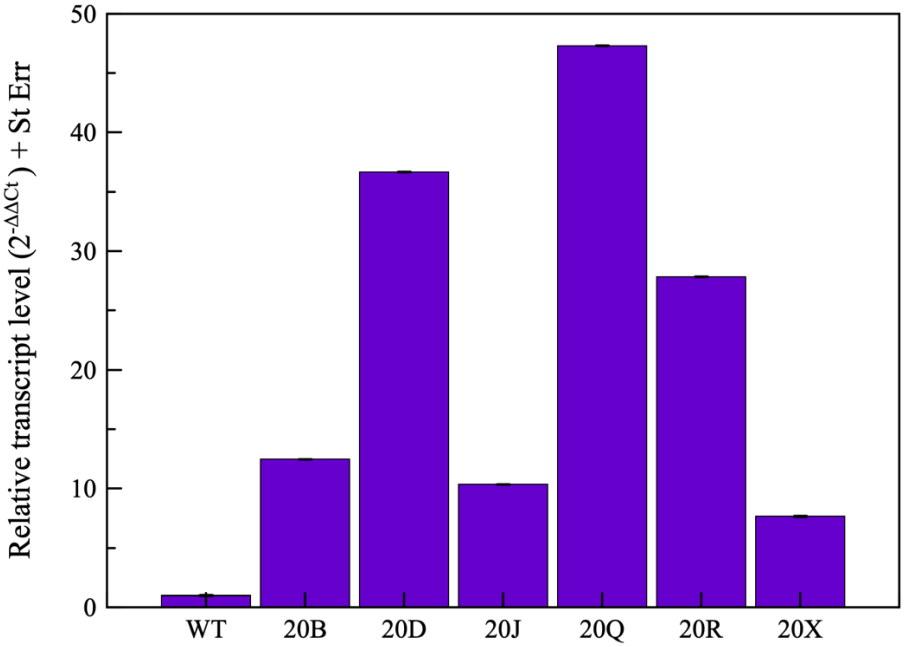

Figure 5-7. Relative transcript levels were measured in *UVR8* OX lines and normalized to reference genes, *CDC2* and *CYC063*. Expression levels in INRA 717-1B4 were compared to WT and several subculture independent events. Subcultures showing the highest transcript levels were used for UV-B experimentation.

screened by analyzing relative transcript levels using RT-PCR, showed a decrease in expression for each of the different lines screened compared to the wild-type (Fig. 5-8). Interestingly, reduced *UVR8* mRNA was detected regardless of which Cas9 variant was expressed, suggesting that codon-optimization of the nuclease had little effect on expression and DNA cleavage. In lines 10 and 11, there were several subcultures that showed the lowest transcript levels of *UVR8*, notably, 10Q, 10R, 11W, and 11Z. Line 12 showed some differences but not as low as the lines 10 and 11. Subcultures 10Q, 10R, and 12K were selected for experimentation.

Confirmation of Biallelic Mutagenesis in UVR8 Knockout Lines – Screening and verification of targeted gene disruption in transgenic subcultures are necessary to ensure that the cleavage by the Cas9 endonuclease was specific and resulted in a double-stranded break in the genomic DNA. Because non-homologous end joining in the repair process is error-prone, indels often result in the gene of interest and can lead to frameshifts with potential loss of function. A multi-step approach was used to determine whether monoallelic or biallelic mutants were obtained in the *UVR8* knockout lines in INRA 717-1B4. First, a restriction site loss assay was performed. Genomic DNA (gDNA) flanking the gRNA binding site from candidate lines was amplified by PCR and screened for the loss of a specific restriction enzyme site (Table 5-10). As can be seen in Fig. 5-9, amplified gDNA comprising binding sequences for the three gRNAs are compared to amplicons digested with restriction enzymes whose sites would be eliminated upon *UVR8* disruption.

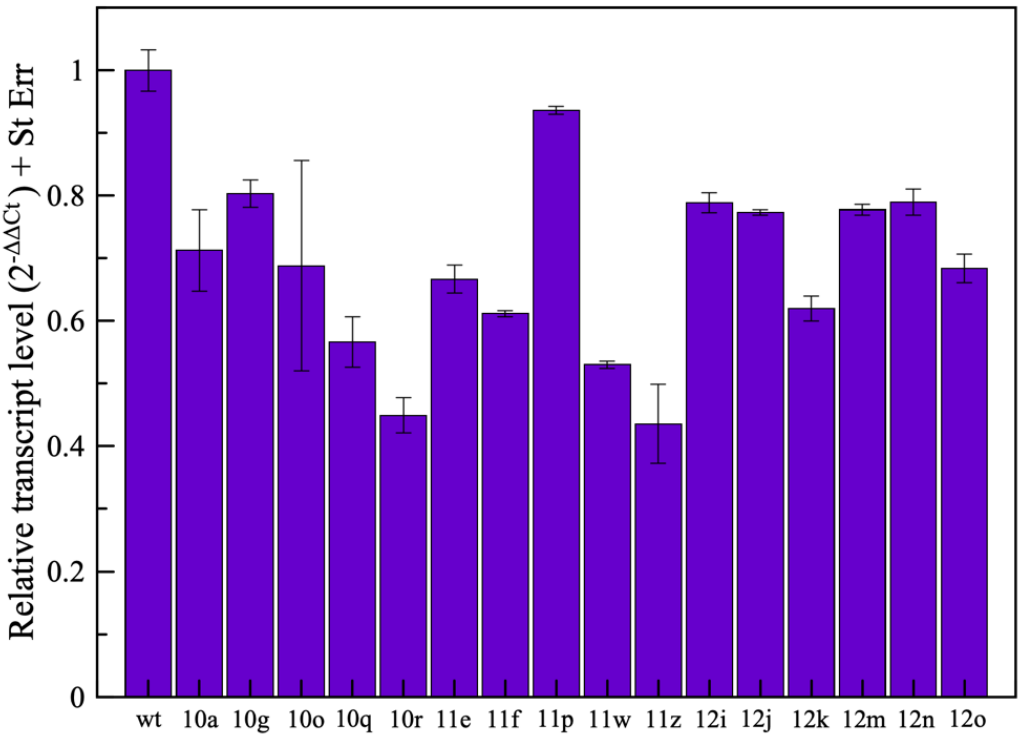

Figure 5-8. Relative transcript levels of *UVR8* in different CRISPR KO lines. Activity of various Cas9 endonucleases were evaluated and screened by measuring gene expression levels of *UVR8* in INRA 717-1B4. Subcultures with the lowest relative transcript levels were selected for UV-B experimentation. Numbers 10-12 represent the lines created by the different Cas9 endonuclease and the letters correspond to independent events within those lines. Reference genes, *CDC2* and *CYC063*, were used to normalize fold expression. Subcultures showing the lowest transcript levels were used for UV-B experimentation.

For the region containing the binding site for gRNA1, an amplified fragment of 465 bp is observed, and digestion with *Nco*I results in the formation of two fragments of 334 and 131 bp. It can be seen that four of the five candidates do not contain a disruption to *UVR8*, but one chimeric variant is observed, 11Z (Fig 5-9a). For the second amplicon containing the binding sequence for the second gRNA, a fragment of 571 bp is observed, which upon digestion with *Nco*I yields fragments of 394 and 177 bp. Again, the majority of candidates do not exhibit a disruption to *UVR8*, but one biallelic mutant was found, 11P and one chimeric variant as well, 11Z (Fig. 5-9b). For the region containing the binding site for the third gRNA, an amplicon of 728 bp is observed, that when digested with *Sac*I yields fragments of 541 and 187 bp for wild-type genomic DNA. However, in these candidates, in which the third gRNA, expressed from the *Arabidopsis* U3 promoter, all lines yielded a fragment of approximately 728 bp, suggesting that biallelic mutants resulted from CRISPR/Ca9 treatment (Fig. 5-9c).

Final confirmation of biallelic mutagenesis in the *UVR8* knockout lines was obtained by performing Sanger sequencing on the three amplicons analyzed by the restriction site loss assay. Nucleotide sequences of the amplified gDNAs were aligned with a reference sequence for *UVR8* for wild-type INRA 717-1B4 obtained for from Aspen DB. Sequences shown in Fig. 5-10 include the gDNA binding regions for gRNA1 and gRNA2 highlighted in cyan, and the PAM sequence highlighted in magenta. The underlined sequences in the gRNA indicate the restriction enzyme site *Nco*I for both regions. It can be seen that disruption to *UVR8* was minimally efficient from these gRNAs, presumably due to poor expression.

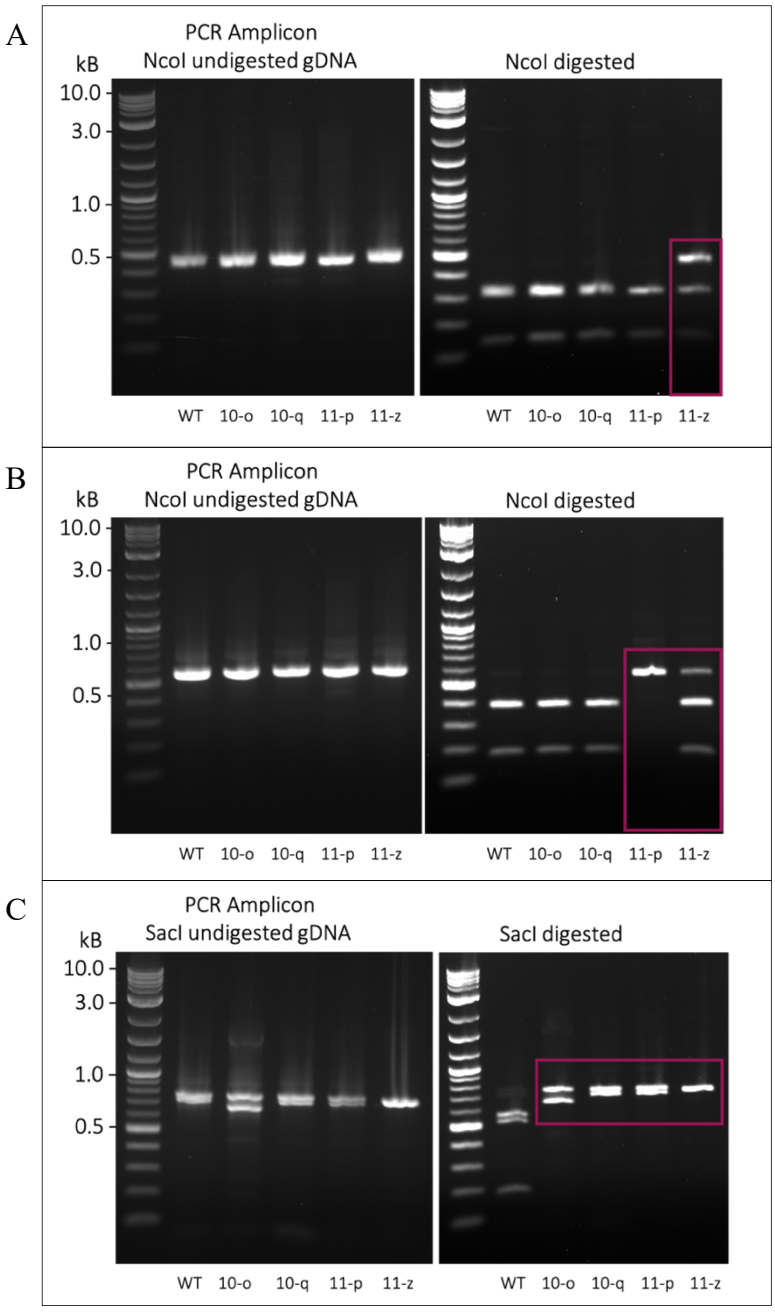
A
PCR Amplicon
NcoI undigested gDNA
NcoI digested
kB
10.0
3.0
1.0
0.5
WT 10-o 10-q 11-p 11-z
WT 10-o 10-q 11-p 11-z
B
PCR Amplicon
NcoI undigested gDNA
NcoI digested
kB
10.0
3.0
1.0
0.5
WT 10-o 10-q 11-p 11-z
WT 10-o 10-q 11-p 11-z
C
PCR Amplicon
SacI undigested gDNA
SacI digested
kB
10.0
3.0
1.0
0.5
WT 10-o 10-q 11-p 11-z
WT 10-o 10-q 11-p 11-z

Figure 5-9. Restriction enzyme site loss of representative transgenic lines were screened to detect chimeric or biallelic mutants of *UVR8* in INRA 717-IB4. Genomic DNA was prepared from the leaves of transgenic tissue culture plantlets by using CTAB and SDS as described in methods (Infante 2002). Regions of gDNA were amplified by PCR to include sequences targeted by gRNA (primers shown in Table 5-10). Undigested amplicons in each panel corresponds to the region targeted by (A) gRNA1, (B) gRNA2, (C) gRNA3. Red boxes in each panel highlight chimeric subcultures from Cas9 mutagenesis resulting in the loss of the restriction enzyme site. (A) Digestion of amplicon 1 with *Nco*I yielded fragments of 334 and 131 bp, indicative of wild-type DNA with no genomic mutation and only one chimeric variant, 11Z. (B) Digestion of amplicon 2 with *Nco*I yielded fragments 394 and 177 bp for wild-type DNA, however, a biallelic mutant was found in 11P, and variant 11Z suggests chimeric variants. (C) Digest of amplicon 3 with *Sac*I yields a 541 and 187 bp fragment for wild-type DNA and in all lines at or around band 728 bp show biallelic mutagenesis resulting from CRISPR.

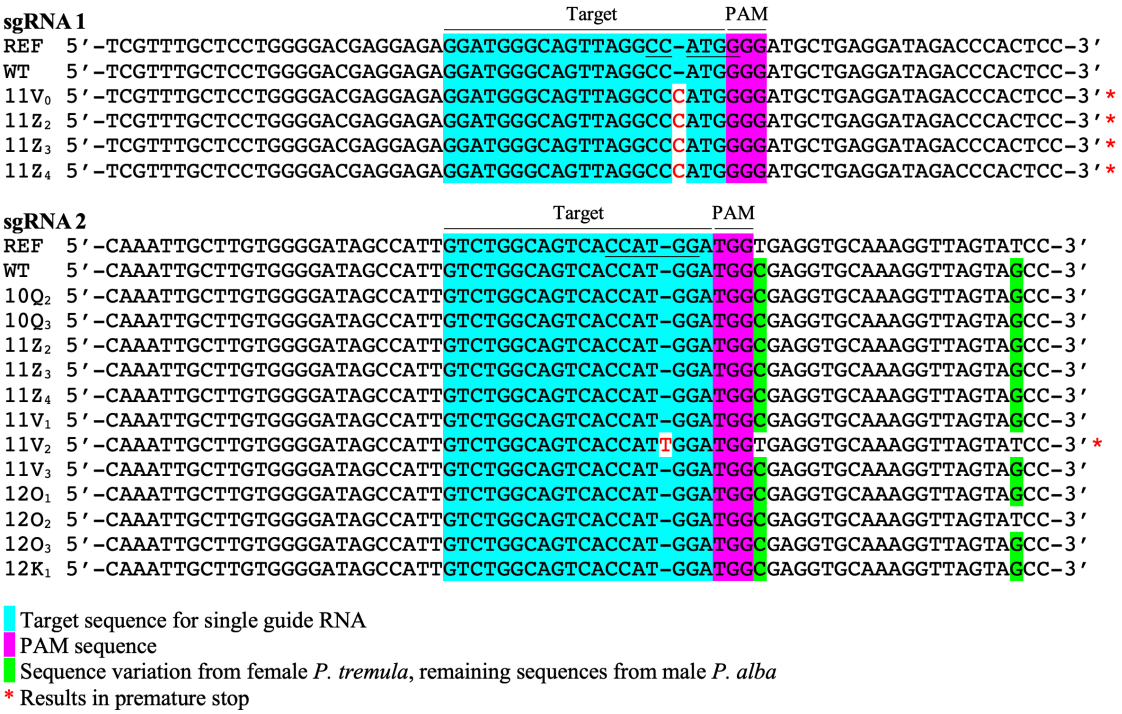

Figure 5-10. DNA sequence alignment from a subset of representative *UVR8* KO lines. The *UVR8* reference (REF) was obtained from Aspen DB (http://aspendb.uga.edu/) and the wild-type (WT) INRA 717-1B4 sequence was determined experimentally. Sequences are shown with the target site for gRNA1 and gRNA2 and highlighted in cyan with the protospacer adjacent motif (PAM) sequences highlighted in magenta. Underlined sequences in the gRNA target denote the restriction enzyme site, *Nco*I (CCATGG), that was used to assess site loss from biallelic mutation mediated by Cas9 regenerated INRA 717-1B4. Indels (in red) resulting in a premature stop occurs in lines denoted (*), which were selected for UV-B experimentation. Parental sequence variation was distinguished in the hybrid from the *P. tremula* (female) is highlighted in green while the majority of the sequences are from *P. alba*.

By contrast, the amplicon containing the gDNA binding region for gRNA3 shows that all of the lines screened contained disruptions to *UVR8*, with indels highlighted in red (Fig. 5-11). The sequences in yellow indicate regions upstream from the target site that resulted in large deletions. The asterisk denotes a frameshift that results in a premature stop. The indel alignment shows that the gRNA3 expression, driven by the *At*U3 promoter, yielded substantially higher mutagenesis efficiency compared to the *At*U6 promoter used for gRNA1 and gRNA2 expression, indicating that the *At*U3 promoter is optimal for use in poplar (Li et al. 2021). The nucleotide changes in the transgenic lines can be seen in sequencing chromatograms (Fig. 5-12) which compare the transgenic lines to wild-type to confirm the cleavage site to validate biallelic mutagenesis (Fig. 5-9c).

An alignment of the UVR8 protein sequence shows truncated sequences in several *UVR8* KO subcultures (Fig. 5-13a). Good efficiency of the Cas9 utilizing gRNA3 was seen in several subcultures including 10Q, 11Z, 12K, 30E, and 30F. However, the frameshift in subculture 10R did not result in a premature stop but rather, a seven amino acid (`WGRYGNL`) deletion in the chromophore perimeter. An examination of the *Arabidopsis* UVR8 x-ray crystal structure superimposed with the INRA 717-1B4 UVR8 amino acid deletions, revealed that the protein structure changes, shown as red spheres in 10R, occur mostly on chromophore perimeter and the periphery, which would likely affect dimer stabilization (Fig. 5-13b).

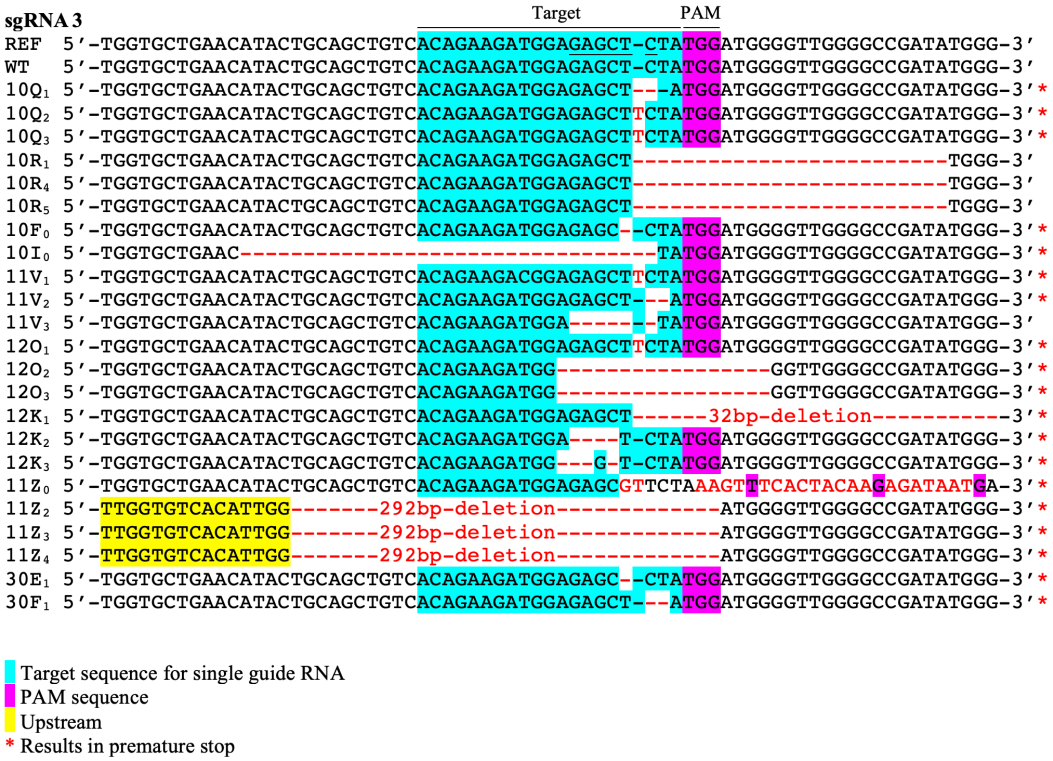

Figure 5-11. DNA sequence alignment from a subset of representative *UVR8* KO lines. The *UVR8* reference (REF) was obtained from Aspen DB (http://aspendb.uga.edu/) and the wild-type (WT) INRA 717-1B4 sequence was determined experimentally. Sequences are shown with the target site for gRNA3 and highlighted in cyan with the protospacer adjacent motif (PAM) sequences highlighted in magenta. Sequences highlighted in yellow are further upstream from the target site that resulted an unexpected large deletion. Underlined sequences in the gRNA target denote the restriction enzyme site, *Sac*I (GAGCTC), that was used to assess site loss from biallelic mutation mediated by Cas9 regenerated INRA 717-1B4. Indels (in red) resulting in a premature stop occurs in lines denoted (*), which were selected for UV-B experimentation. The alignment shows that gRNA3 expression cassette that is controlled by the *At*U3 promoter resulted in greater genome editing efficiency mediated by the Cas9 endonuclease compared to the *At*U6 promoter in gRNA1 and gRNA2.

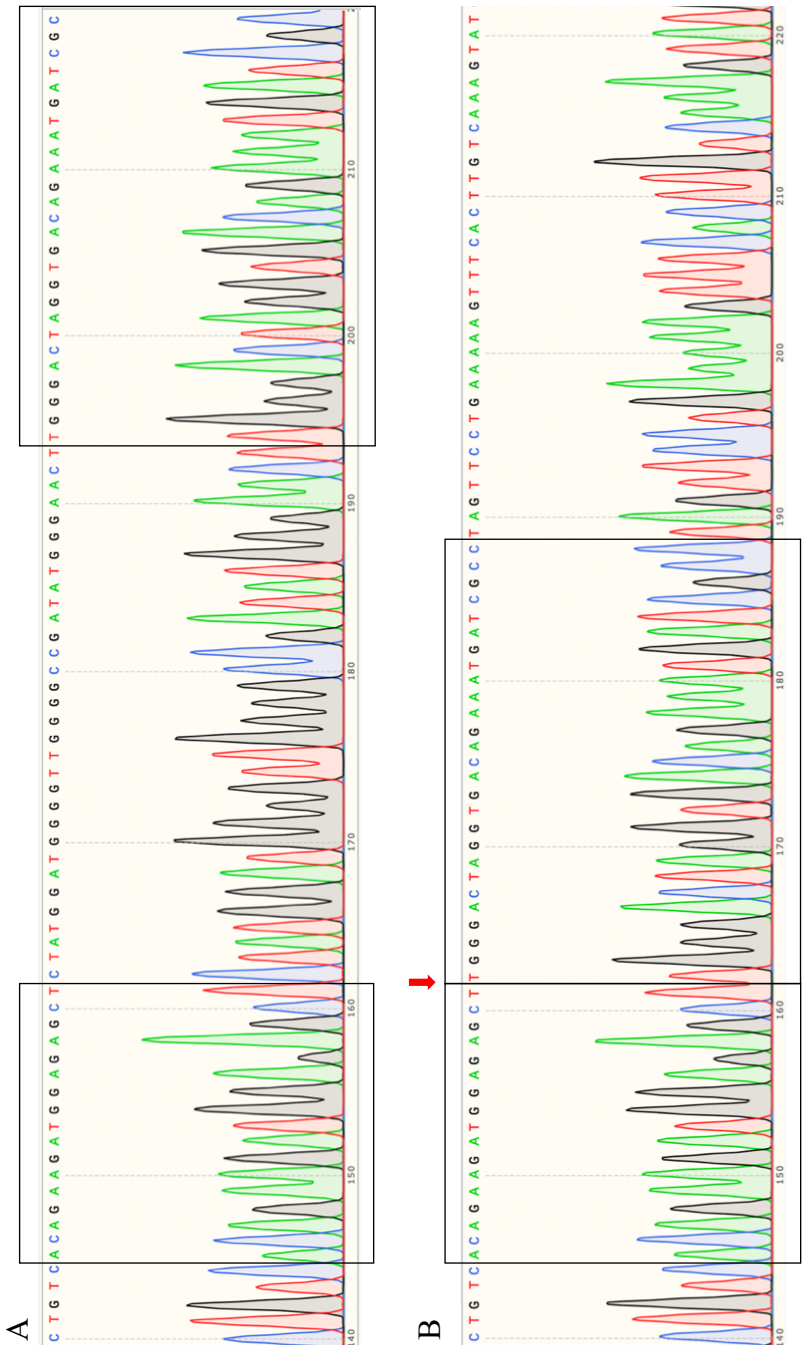
A
B

Figure 5-12. DNA sequencing chromatograms confirm mutagenesis in the fifth exon of *UVR8* stemming from cleavage by Cas9 localized with one of the gRNAs (ACAGAAGATGGAGAGCT). The sequence of *UVR8* deleted is upstream of the protospacer adjacent motif (PAM) sequence (TGG) in the CRISPR-Cas9 generated knockout lines. Sequences were determined by amplifying regions surrounding the gRNA targets by PCR and subsequent Sanger sequencing of fragments. (A) Homozygous wild-type control was compared with (B) CRISPR-Cas9 induced UVR8 mutation in INRA 717-1B4 with biallelic homozygous mutation. Red arrow indicates gRNA/Cas9 cleavage site.

A

```
REF - MAEDGRAASGSEVSGPIRQVILISAGASHSVALLSGNIVCSWGRGEDGQLGHGDAEDRPTPTQLSTLDGLD
10Q - MAEDGRAASGSEVSGPIRQVILISAGASHSVALLSGNIVCSWGRGEDGQLGHGDAEDRPTPTQLSTLDGLD
10R - MAEDGRAASGSEVSGPIRQVILISAGASHSVALLSGNIVCSWGRGEDGQLGHGDAEDRPTPTQLSTLDGLD
11Z - MAEDGRAASGSEVSGPIRQVILISAGASHSVALLSGNIVCSWGRGEDGQLGHGDAEDRPTPTQLSTLDGLD
12K - MAEDGRAASGSEVSGPIRQVILISAGASHSVALLSGNIVCSWGRGEDGQLGHGDAEDRPTPTQLSTLDGLD
30E - MAEDGRAASGSEVSGPIRQVILISAGASHSVALLSGNIVCSWGRGEDGQLGHGDAEDRPTPTQLSTLDGLD
30F - MAEDGRAASGSEVSGPIRQVILISAGASHSVALLSGNIVCSWGRGEDGQLGHGDAEDRPTPTQLSTLDGLD

REF - IISITCGADHTTAYSESRMEVYSWGWGDFGRLGHGNSSDLFTPQPIKALHSLKIRQIACGDSHCLAVTMDG
10Q - IISITCGADHTTAYSESRMEVYSWGWGDFGRLGHGNSSDLFTPQPIKALHSLKIRQIACGDSHCLAVTMDG
10R - IISITCGADHTTAYSESRMEVYSWGWGDFGRLGHGNSSDLFTPQPIKALHSLKIRQIACGDSHCLAVTMDG
11Z - IISITCGADHTTAYSESRMEVYSWGWGDFGRLGHGNSSDLFTPQPIKALHSLKIRQIACGDSHCLAVTMDG
12K - IISITCGADHTTAYSESRMEVYSWGWGDFGRLGHGNSSDLFTPQPIKALHSLKIRQIACGDSHCLAVTMDG
30E - IISITCGADHTTAYSESRMEVYSWGWGDFGRLGHGNSSDLFTPQPIKALHSLKIRQIACGDSHCLAVTMDG
30F - IISITCGADHTTAYSESRMEVYSWGWGDFGRLGHGNSSDLFTPQPIKALHSLKIRQIACGDSHCLAVTMDG

REF - EVQSWGRNQNGQLGLGTTEDSLVPQKIQAFQGVSIKMVAAGAEHTAAVTEDGELYGWGWGRYGNLGLGDRN
10Q - EVQSWGRNQNGQLGLGTTEDSLVPQKIQAFQGVSIKMVAAGAEHTAAVTEDGELWMGLGPIWELGTR*
10R - EVQSWGRNQNGQLGLGTTEDSLVPQKIQAFQGVSIKMVAAGAEHTAAVTEDGELYGWG-------GLGDRN
11Z - EVQSWGRNQNGQLGLGTTEDSLVPQKIQAFQMGLGPIWELGTR*
12K - EVQSWGRNQNGQLGLGTTEDSLVPQKIQAFQGVSIKMVAAGAEHTAAVTEDGELGTR*
30E - EVQSWGRNQNGQLGLGTTEDSLVPQKIQAFQGVSIKMVAAGAEHTAAVTEDGEPMDGVGADMGTWD*
30F - EVQSWGRNQNGQLGLGTTEDSLVPQKIQAFQGVSIKMVAAGAEHTAAVTEDGELWMGLGPIWELGTR*

REF - DRLVPEKVSLVKGDKMIMVACGWRHTISVSSSGGLYTYGWSKYGQLGHGDFEDHLTPHKVEALRDSYISLI
10Q -
10R - DRLVPEKVSLVKGDKMIMVACGWRHTISVSSSGGLYTYGWSKYGQLGHGDFEDHLTPHKVEALRDSYISLI
11Z -
12K -
30E -
30F -

REF - SGGWRHTMALASDGKLYGLGWNKFGQVGVGDNIDHCSPVQVKFPHEQKVVQISCGWRHTLAVTERQNVFSW
10Q -
10R - SGGWRHTMALASDGKLYGLGWNKFGQVGVGDNIDHCSPVQVKFPHEQKVVQISCGWRHTLAVTERQNVFSW
11Z -
12K -
30E -
30F -

REF - GRGTNGQLGHGESMDRNLPKIIEALSADGSGGHQIEASTVDPSLGKSWVSPSDRYAIVPDESGQTVSVGGN
10Q -
10R - GRGTNGQLGHGESMDRNLPKIIEALSADGSGGHQIEASTVDPSLGKSWVSPSDRYAIVPDESGQTVSVGGN
11Z -
12K -
30E -
30F -

REF - GNDASVPESDVKRIRI*
10Q -
10R - GNDASVPESDVKRIRI*
11Z -
12K -
30E -
30F -
```

UVR8 protein sequence length

REF – 443
10Q – 210
10R – 437
11Z – 186
12K – 200
30E – 209
30F – 210

Indel -
Tryptophan chromophore
Chromophore perimeter

B

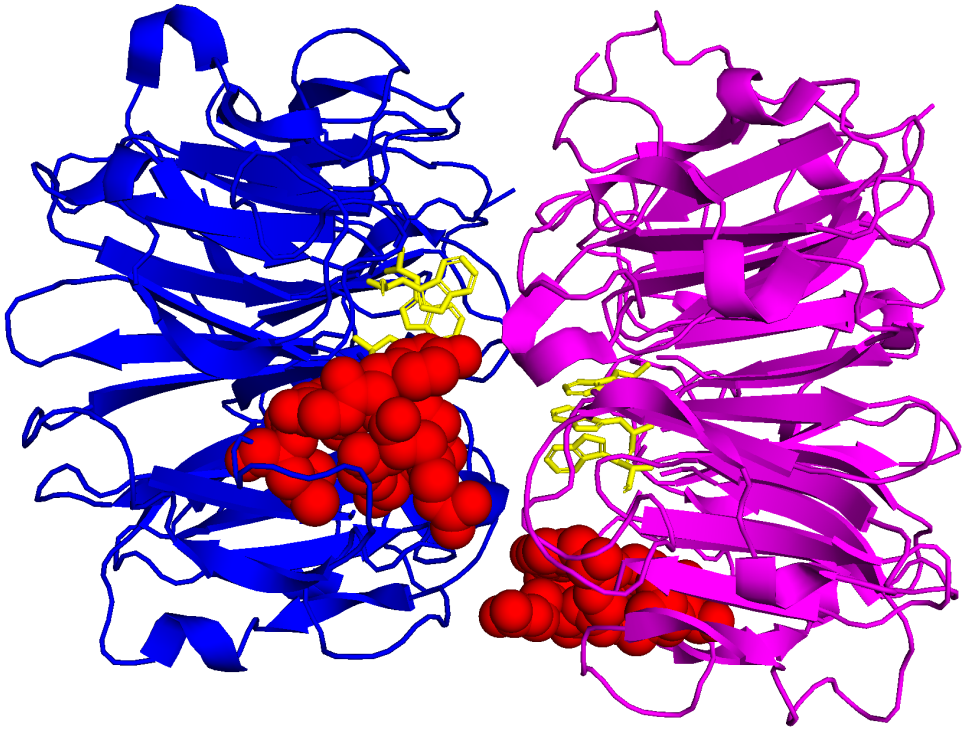

Figure 5-13. UVR8 protein alignment with *UVR8* KO subcultures. (A) *UVR8* KO subcultures with indels mediated by Cas9 in gRNA3 showed truncated amino acid sequences with corresponding sequence lengths. Highlighted in red indicates important residues that form the tryptophan pyramid chromophore that is essential for UV-B perception. Three aromatic pairs form the perimeter to protect the tryptophan pyramid are highlighted in cyan. (B) UVR8 dimer structure from *A. thaliana* with the *UVR8* KO subculture (10R) locations of the tryptophan chromophore as yellow sticks and the deleted sequences as red spheres that includes the chromophore perimeter. The location of the seven amino acid deletion could potentially result in destabilizing the UVR8 dimer.

Construction and Analysis of UVR8 Expression-Modulated Transgenic Populus Lines using CRISPRa and CRISPRi – In addition to *UVR8* knockout and overexpression transgenic poplar lines, it was of interest to modify *UVR8* expression by using CRISPRa and CRISPRi technology. CRISPRa utilizes the VP64 activation domain fused to a deactivated variant of Cas9 as a subunit to up-regulate gene expression, whereas CRISPRi uses a SRDX repressor domain fused to dCas9 to interfere with the binding of transcriptional machinery and down-regulate gene expression. However, several challenges persisted with these constructions and consequently they were not extensively used in my studies. As seen in my attempts to use RNAi to inhibit *CAD* expression and CRISPR/Cas9 to knockout the *UVR8* gene, no shoots were able to generate from experiments with CRISPRa and CRISPRi constructs in *Populus deltoides*. Thus, these candidates were not characterized. Alternatively, shoot formation was readily detected in INRA 717-1B4.

Ordinarily, the gRNAs used in CRSIPRa and CRISPRi constructs target the upstream control region of a gene. However, in this study, the same intragenic gRNAs as those used to construct the *UVR8* knockout lines were employed for the CRISPRi line. Although this situation might compromise the function of CRISPRa, the mechanism of the SRDX repressor suggests that it would still affect transcription by stalling transcriptional elongation (Moradpour and Abdulah 2020). Analysis of gene expression by RT-PCR in candidate lines revealed some complexities, however. Although expression levels of *UVR8* in the CRISPRa-treated line did increase slightly relative to the wild-type, the increased levels were not very substantial, and they were considerably less than that observed for

UVR8 in the 35S overexpression line (Fig. 5-14). By contrast, the relative transcript levels of *UVR8* in the CRISPRi-treated lines unexpectedly showed either no difference as compared to the wild-type, and even an increase in expression, to approximately the levels seen in lines constructed with CRISPRa (Fig. 5-15). Though possibly meriting further investigation, these lines were considered unusual enough that they were omitted from further investigation.

Generation and Analysis in INRA 717-1B4 Transgenic Lines Disrupted in Phenylpropanoid Biosynthesis and with Modulated UVR8 Expression – To understand how poplar reprograms metabolism to compensate for reduced lignin levels during acclimation to UV-B radiation, it was necessary to generate double mutants targeting *CAD* and *UVR8* expression in INRA 717-1B4 (Table 5-8). The RNAi-inhibited *CAD* transgenic line was used as the starting material for introducing modifications to *UVR8* expression. The same strategy employed for up-regulating UVR8 by using the 35S promoter to express the described UVR8-GFP fusion, and for down-regulating expression via gene knockout using CRISPR was used to construct double mutants.

Although one of the lines showed signs of contamination and was discarded, RT-PCR was used to evaluate relative transcripts in another single line (line 33) engineered for RNAi-inhibited expression of *CAD* and *UVR8:GFP* overexpression. The line showed a significant increase in transcript levels for *UVR8,* and a decrease in transcript levels for *CAD* compared to the wild-type (Fig. 5-16).

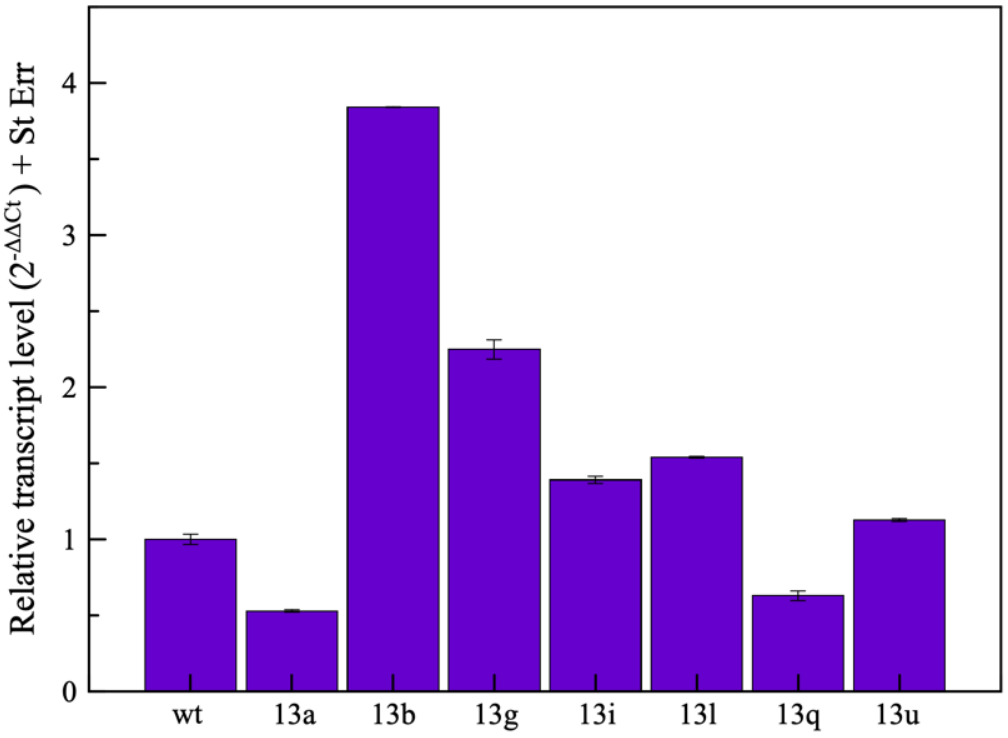

Figure 5-14. *UVR8* transcript levels in CRISPRa lines with dCas9 endonuclease were measured in INRA 717-1B4. OX lines using the VP64 activator in the control region of *UVR8* showed elevated transcript levels compared to the wild-type. Housekeeping genes, *CDC2* and *CYC063*, were used to normalize fold changes.

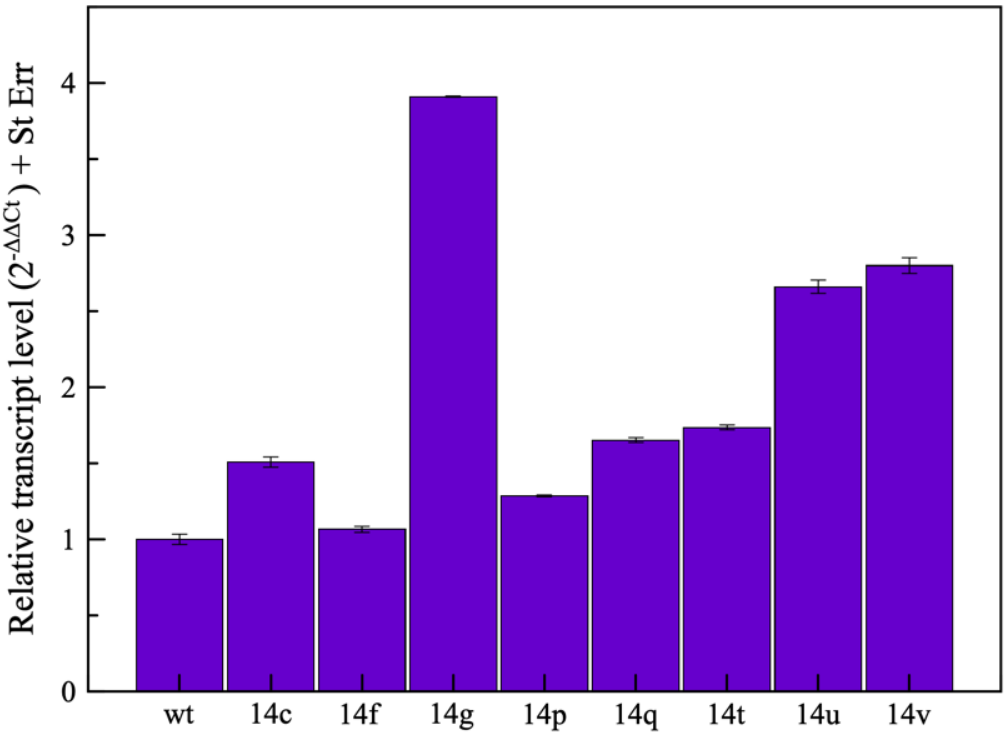

Figure 5-15. *UVR8* transcript levels in CRISPRi lines with dCas9 endonuclease were measured in INRA 717-1B4. Down-regulated *UVR8* using the SRDX repressor targeting the coding region showed no decrease in transcript levels and rather increased in gene expression of *UVR8* compared to the wild-type. Housekeeping genes, *CDC2* and *CYC063*, were used to normalize fold changes.

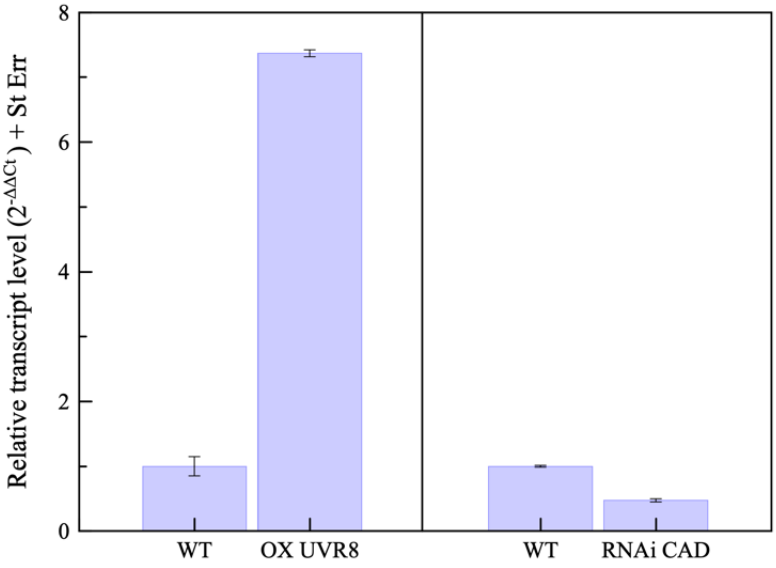

Figure 5-16. Relative transcript level of the low-lignin, *UVR8* OX line in INRA 717-1B4. *UVR8* transcript levels were increased significantly compared to the wild-type and the *CAD* transcript level was decreased. Reference genes, *CDC2* and *CYC063*, were used to normalize fold expression. This line was selected for UV-B experimentation based on transcript levels of both genes.

Three double mutant lines with RNAi-inhibited expression of *CAD* and a CRISPR-promoted disruption of *UVR8* were constructed in the same manner as previously described. Relative transcript levels determined by RT-PCR showed that all subcultures showed decreased levels of *CAD* expression, and that lines 30E and 30F expressed low levels of *UVR8* compared to the wild-type (Fig. 5-17). Further analysis of these two lines was performed to ascertain the disruption to *UVR8* in each subculture. Genomic DNA corresponding to regions containing the three gRNA binding sites was amplified and analyzed by Sanger sequencing. Indel alignments from the two subcultures analyzed were compared to the *UVR8* reference sequence from wild-type plants. Interestingly, one transgenic line (line 28) did not show any changes to *UVR8* in the vicinity of gRNA3 binding region. By contrast, sequence analysis of subcultures 30E and 30F showed deletions close to the PAM sequence of gRNA binding, resulting in a premature stop (Fig. 5-18). These lines were therefore selected for further characterization and UV-B experimentation.

Transient Expression Populus UVR8 in Nicotiana benthamiana – In order to confirm that the *35S::UVR8* construct did indeed overexpress the photoreceptor, *Agrobacterium* infiltration was used to transiently express *Populus deltoides UVR8* in *Nicotiana benthamiana*. The expression of *UVR8* or control sequences, was driven by CaMV 35S promoter and, since the *UVR8::GFP* was used in these studies, cellular localization within tobacco leaves was determined by light microscopy, via visualization of GFP fluorescence captured five days following Agro-infiltration. The empty vector negative control revealed no fluorescence (Fig. 5-19a), whereas the positive controls, GFP containing a C-terminal

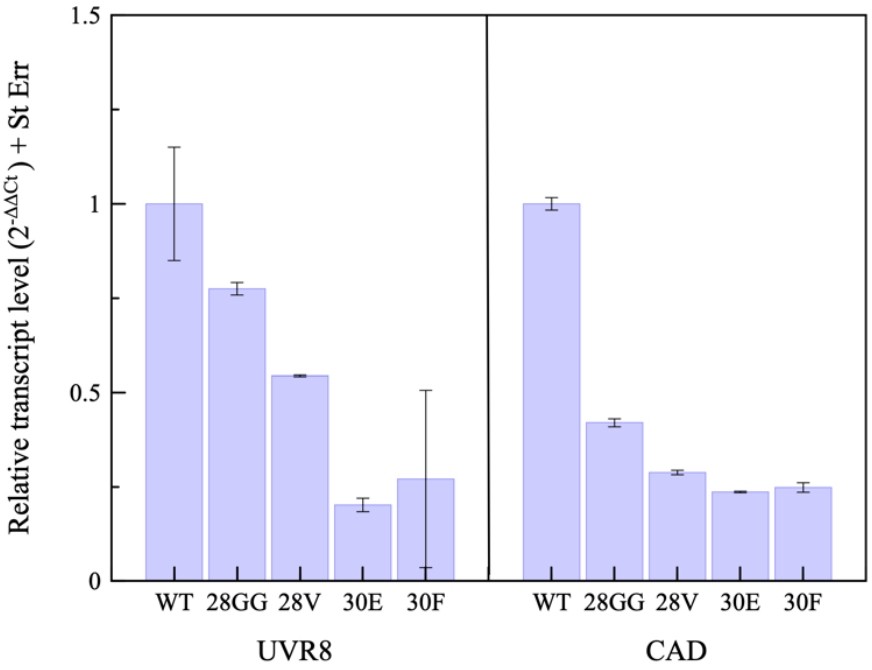

Figure 5-17. Relative transcript levels of *CAD* knockdown, *UVR8* KO and OX lines in INRA 717-1B4. *UVR8* and *CAD* transcript levels for 30E and 30F were selected for UV-B experimentation based on low transcript levels of both genes. Reference genes, *CDC2* and *CYC063*, were used to normalize fold expression. Subcultures 28GG and 28V were omitted from experimentation.

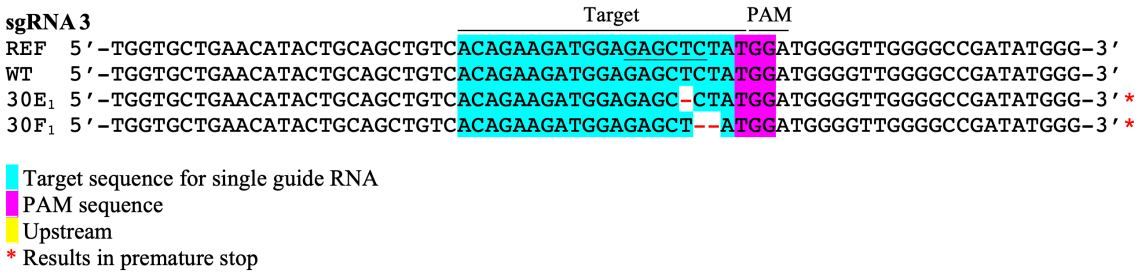

Figure 5-18. DNA sequence alignment of two subcultures from the *CAD* knockdown *UVR8* KO line. The *UVR8* reference (REF) was obtained from Aspen DB (http://aspendb.uga.edu/) and the wild-type (WT) INRA 717-1B4 sequence was determined experimentally. Sequences are shown with the target site for gRNA3 and highlighted in cyan with the protospacer adjacent motif (PAM) sequences highlighted in magenta. Sequences highlighted in yellow are further upstream from the target site that resulted an unexpected large deletion. Underlined sequences in the gRNA target denote the restriction enzyme site, *Sac*I (GAGCTC), that was used to assess site loss from biallelic mutation mediated by Cas9 regenerated INRA 717-1B4. Indels (in red) resulting in a premature stop occurs in lines denoted (*), which were selected for UV-B experimentation. The alignment shows that gRNA3 expression cassette that is controlled by the *At*U3 promoter resulted in greater genome editing efficiency mediated by the Cas9 endonuclease compared to the *At*U6 promoter in gRNA1 and gRNA2.

hemagglutinin (HA) tag and a *Melampsora larici-populina* candidate secreted effector gene with a GFP fusion, readily showed fluorescence in both the nucleus and the cytoplasm (Fig. 5-19b, c). Plants infiltrated with the *35S::UVR8:GFP* construct showed fluorescence in both the nucleus and cytoplasm (Fig. 5-19d), confirming successful expression of *UVR8*, and consistent with localization studies of *Arabidopsis* UVR8 (Kaiserli and Jenkins 2007, Tilbrook et al. 2013).

Localization of UVR8 in Transgenic Populus – In an effort to verify expression and proper localization of UVR8 in the constructed transgenic poplar lines, confocal microscopy was used to visualize the highly expressed *UVR8-GFP* fusion in transgenic INRA 717-1B4. Four images were captured for the analysis of each specimen: (A) autofluorescence of chloroplasts was measured at 680 nm to show the natural fluorescence emission from chlorophyll (B) GFP fluorescence at 395 nm; (C) white light field; (D) to distinguish natural and artificially added fluorescence markers (GFP), channels were merged to show autofluorescence and GFP fluorescence. Wild-type control plants are shown in Fig. 5-20. The *UVR8:GFP* overexpression line is shown in Fig. 5-21, with the chloroplast autofluorescence signal (Fig. 5-21a), fluorescence corresponding to the UVR8-GFP fusion localized in the nucleus and cytoplasm (Fig. 5-21b), white light field (Fig. 5-21c), and merged autofluorescence and GFP fluorescence channels to show localization of UVR8-GFP to the nucleus and cytoplasm (Fig. 5-21d). Transgenic poplar lines exhibiting both RNAi-inhibited *CAD* and *UVR8:GFP* overexpression were analyzed in the same manner, with the merged channels for autofluorescence and GFP fluorescence showing

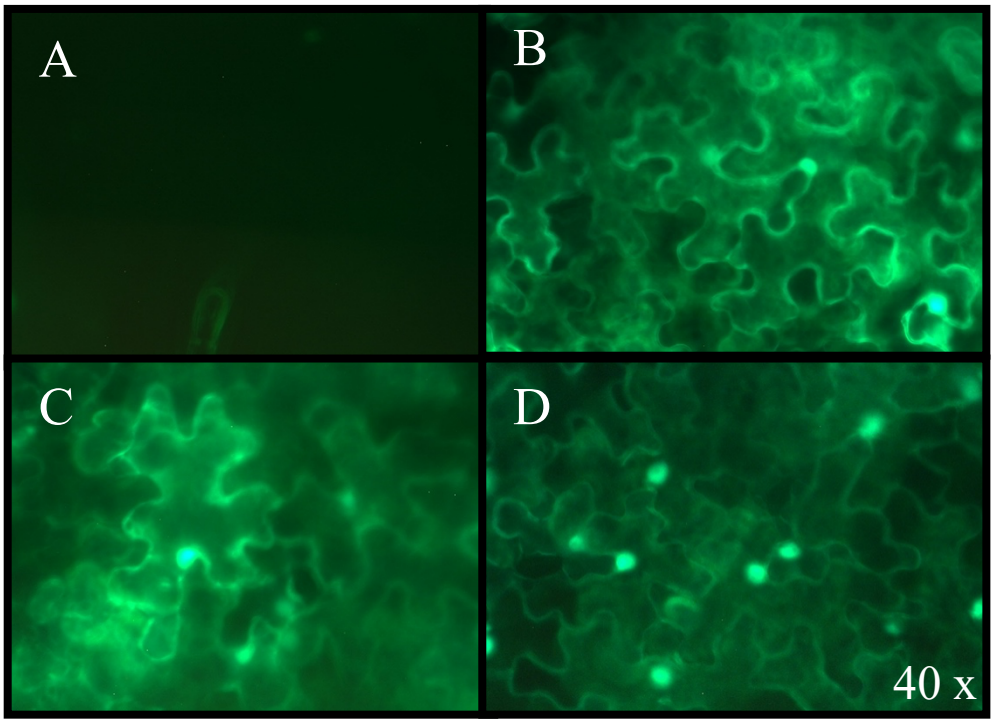

A. EV + TCV
B. *GFP*-HA + TCV
C. *MLP124017-GFP* + TCV
D. *UVR8-GFP* + TCV

Figure 5-19. Transient expression of *Populus deltoides UVR8* in *Nicotiana benthamiana*. Expression of *UVR8* and controls from the CaMV 35S promoter was used to confirm nuclear and cytoplasmic localization of *Populus deltoides UVR8* in *N. benthamiana*. Infiltration of *N. benthamiana* leaves with *Agrobacterium tumefaciens* (GV3101) containing *UVR8* or control sequences in pK7FWG2. A binary vector that allows for C-terminal fusion of *UVR8* with *GFP* via Gateway cloning, were visualized by light microscopy five days after infiltration. The turnip crinkle virus (TCV) suppressor of RNA silencing in *A. tumefaciens* was also co-infiltrated with experimental constructs. (A) pK7FWG2 empty vector control (no *GFP*). (B) Expression of *GFP*-HA from the CaMV 35S promoter with the HA epitope tag on the C-terminus. (C) *Melampsora larici-populina* gene *124017* fused at the C-terminus to *GFP*, localizes in the nucleus and cytoplasm. (D) *Populus deltoides UVR8* with *GFP* fused at the C-terminus is localized in both nucleus and cytoplasm.

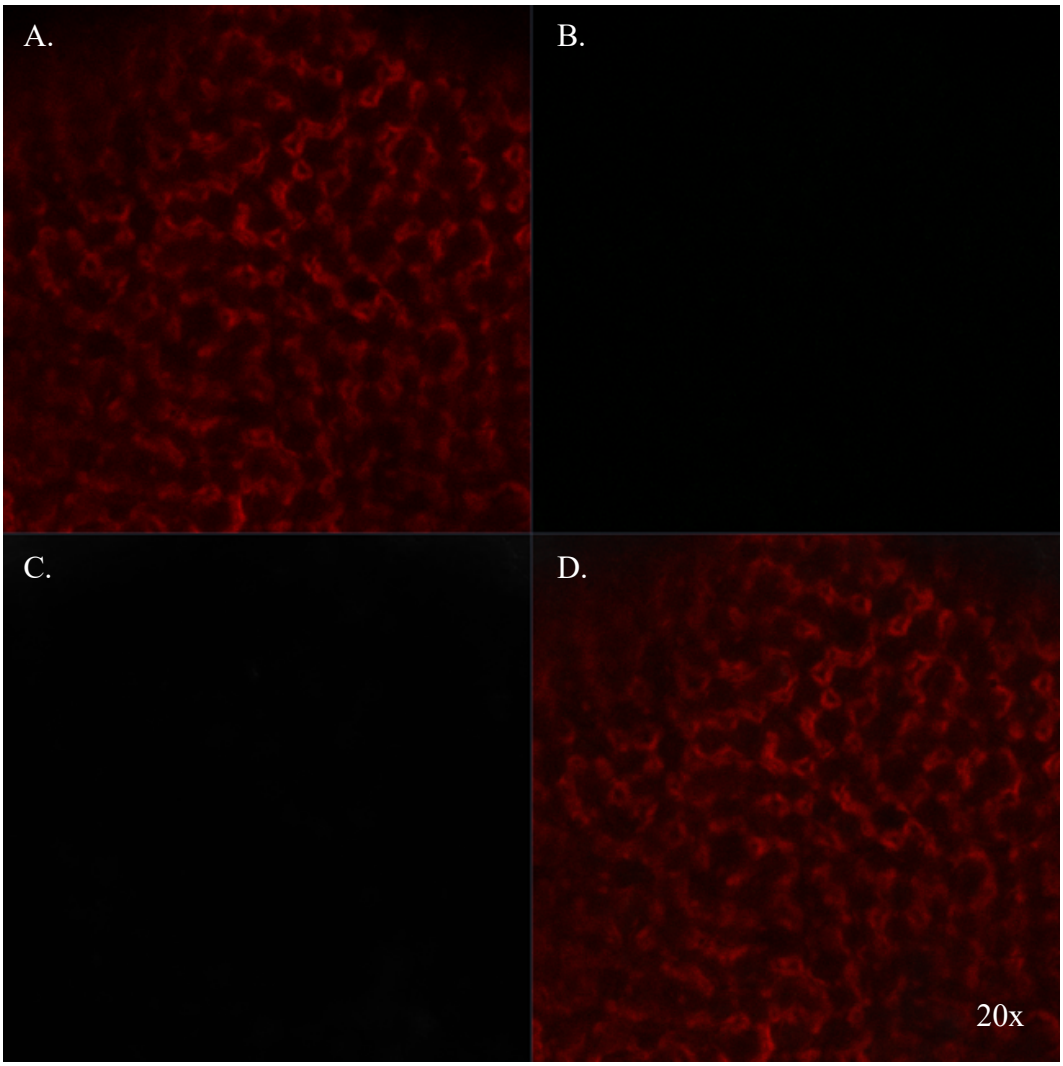

Figure 5-20. Confocal imaging with wild-type INRA 717-1B4 as the negative control. (A) chlorophyll fluorescence signal, (B) no GFP fluorescence, (C) bright-field, conventional optical illumination with white light, (D) merged channels.

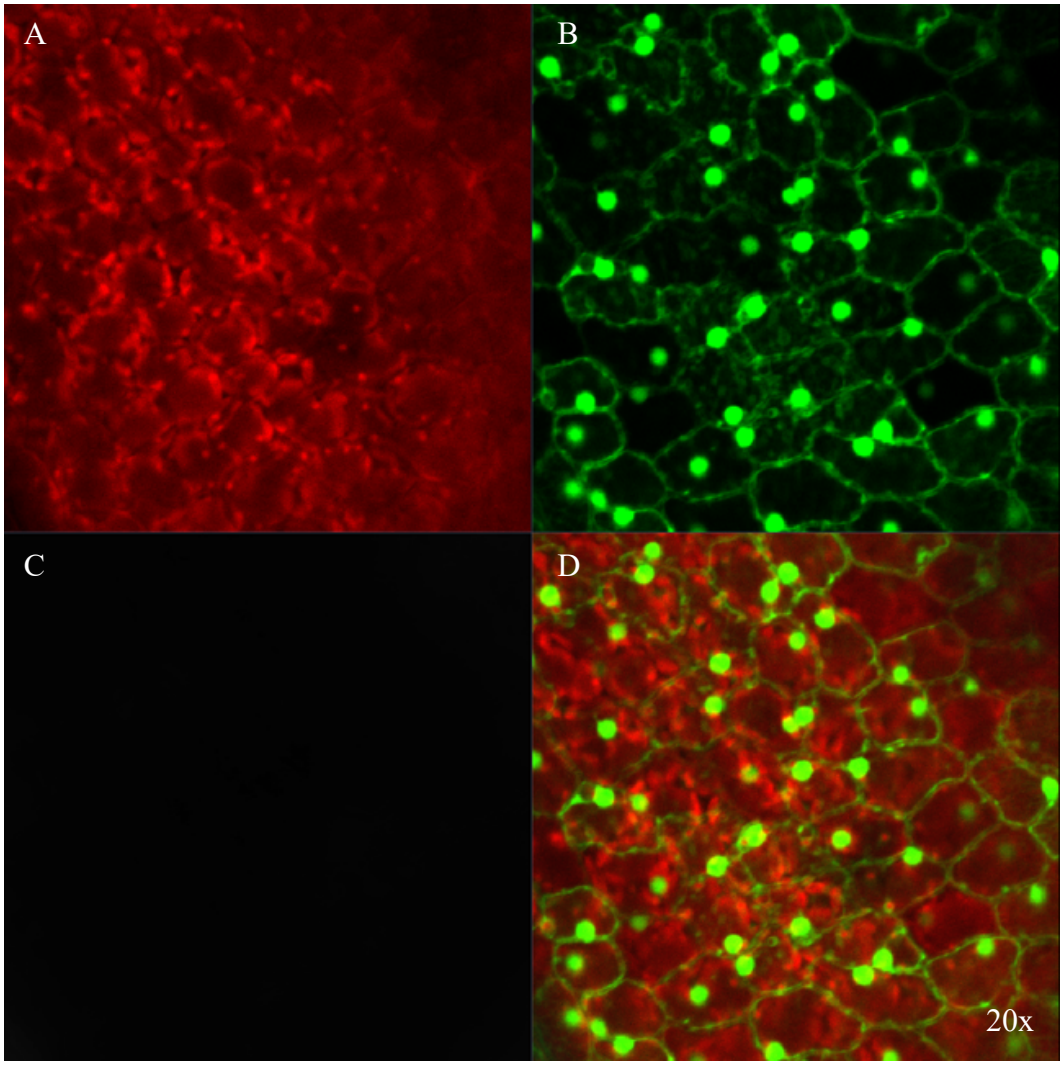

Figure 5-21. Confocal imaging with *UVR8* OX in INRA 717-1B4 to determine nuclear accumulation and localization UVR8 with GFP reporter in leaf epidermal tissue. (A) chlorophyll fluorescence signal, (B) GFP fluorescence observed in the nucleus and cytoplasm, (C) bright-field, conventional optical illumination with white light, (D) merged channels to indicate the localization of GFP fluorescence in the nucleus and cytoplasm.

nuclear and cytoplasmic accumulation of UVR8-GFP (Fig. 5-22). GFP fluorescence in *UVR8* OX poplar appear to be punctuated and localized in the plasma and nuclear membrane. However, these results establish consistency with those seen in tobacco, and conform to the current understanding of cytoplasmic and nuclear localization of UVR8 in *Arabidopsis* (Kaiserli and Jenkins 2007, Tilbrook et al. 2013).

Evaluation of the Effect of UV-B Radiation on CAD-Inhibited and UVR8-Regulated Transgenic Populus Lines – Little is known about the response of poplar UVR8 to various levels and dosages of UV-B radiation. Therefore, several rounds of exploratory experiments were undertaken with multiple biological specimens and replicates to narrow conditions that would enable a coherent interpretation of the genetic changes on UV-B acclimation and tolerance. Generally, because UVR8 promotes a photomorophogenic response in plants and acclimation to UV-B radiation, it was expected that *UVR8* knockout lines would be more susceptible to UV-B and would be unable to mount a metabolic response upon UV-B exposure. By contrast, the expectation was that the *UVR8* overexpression lines would be more resistant to UV-B radiation, and an increase in anthocyanins and flavonoids would be detected. The underlying goal was to evaluate these changes in *CAD*-inhibited transgenics, which presumably are defective in lignin formation (Yan et al. 2019).

Initial experiments were focused on single INRA 717-1B4 *UVR8* overexpression and knockout transgenic lines under conditions that approximated those used with the natural

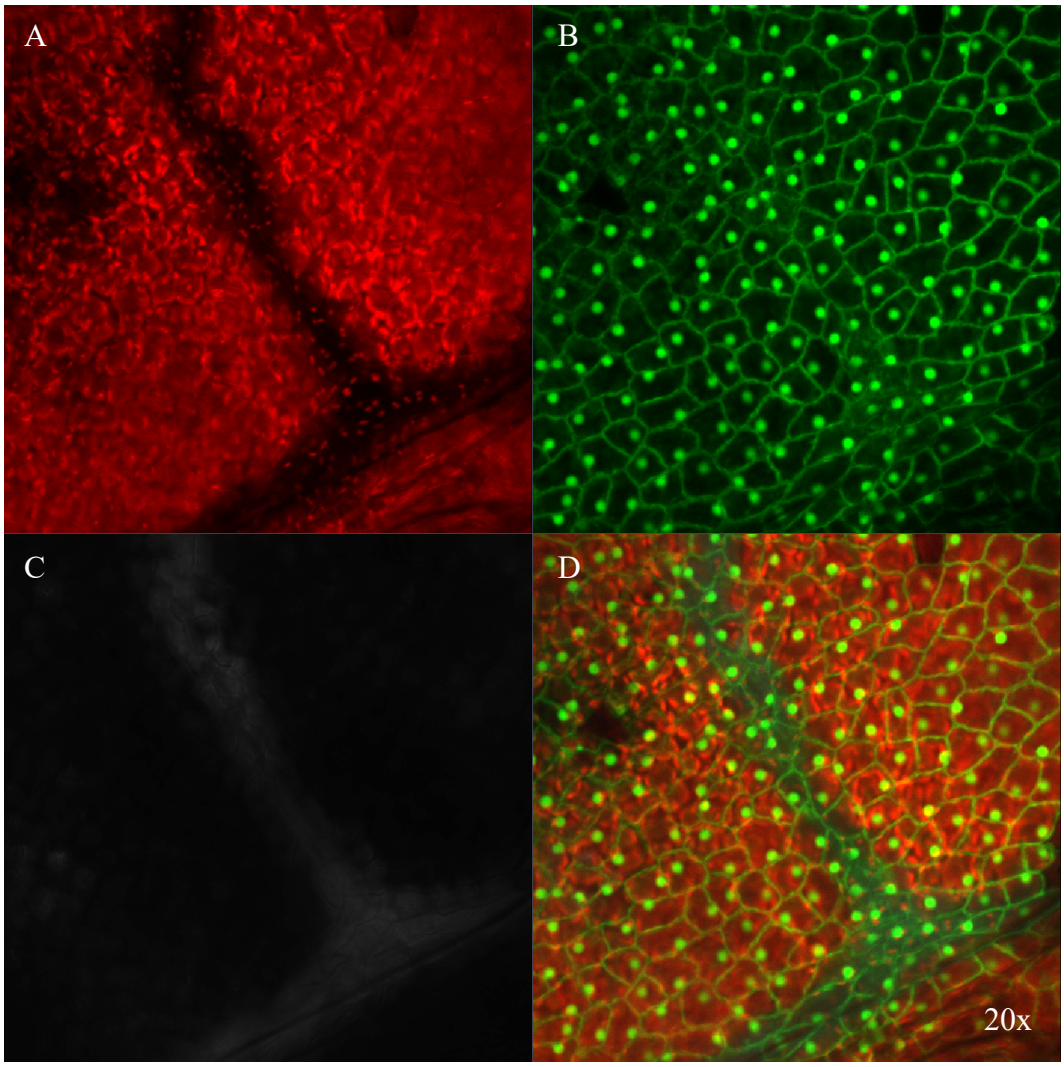

Figure 5-22. Confocal imaging with *CAD* knockdown, *UVR8* OX in INRA 717-1B4 to determine nuclear accumulation and localization UVR8 with GFP reporter in leaf epidermal tissue. (A) chlorophyll fluorescence signal, (B) GFP fluorescence observed in the nucleus and cytoplasm, (C) bright-field, conventional optical illumination with white light, (D) merged channels to indicate localization of GFP to the cytoplasm and nucleus.

variants described earlier. Wild-type and transgenic plants were grown for about 1.5 months grown beyond the tissue culture phase, then treated in the College Park greenhouse with 20 – 35 kJ m^{-2} of UV-B radiation for 8 h/day for 10 days. In this series of experiments, the plants, typically before and after UV-B treatment, where characterized in terms of growth height and leaf area, chlorophyll fluorescence, and total as well as selected aromatic (flavonoids and anthocyanins) metabolites.

The initial and perhaps most significant observation, was that the *UVR8* overexpression and *UVR8* knockout transgenic poplar lines apparently grow relatively normally, at least at a juvenile stage, when exposed to UV-B radiation (Table 5-11). This observation was in sharp contrast to that seen for *Arabidopsis*, for which *UVR8* mutants displayed dwarf phenotypes (Kliebenstein et al. 2002, Heijde et al. 2013). Untreated leaves are all similar in size and shape (Fig. 5-23a-c). After irradiation, leaves were compared to the control and wild-type (Fig. 5-23d). Interestingly, leaves harvested at LPI 7-8 from the wild-type and *UVR8* knockout and *UVR8* overexpression lines indicated that *UVR8* overexpression lines showed some difference in leaf area compared to the controls, with leaf area decreasing after UV-B treatments (Fig. 5-24). Alternatively, the *UVR8* KO lines did not show a difference in leaf area between treatments as compared to the wild-type except for the wavy leaf phenotype (Fig. 5-23e) and the *UVR8* overexpression line appeared smaller and darker in color (Fig. 5-23f, 24).

Table 5-11. Transgenic 717 modulated UVR8 treated with high intensity UV-B radiation 10 days

Transgenic line	**Treatment**	**Mean initial height (cm)**	**Std Err**	**Mean final height (cm)**	**Std Err**	**Mean growth (cm) per day**	**Mean initial F_v/F_m**	**Std Err**	**Mean final F_v/F_m**	**Std Err**	**Leaf area (cm^2)**	**Std Err**
WT	Control	8.20	0.70	23.25	0.25	1.50	0.8025	0.00	0.91	0.01	95.00	2.39
WT	UV-B	9.57	0.23	25.30	0.90	1.57	0.8005	0.01	0.91	0.01	108.64	6.79
UVR8 KO	Control	8.83	0.52	23.77	0.86	1.49	0.8055	0.00	0.91	0.01	107.15	1.68
UVR8 KO	UV-B	8.93	0.07	24.25	0.25	1.53	0.801	0.00	0.85	0.01	104.70	0.95
UVR8 OX	Control	10.35	0.65	22.90	1.00	1.26	0.7997	0.01	0.91	0.01	95.29	1.79
UVR8 OX	UV-B	8.95	0.55	22.65	0.35	1.37	0.8005	0.01	0.91	0.00	77.65	3.26

Table 5-11. Transgenic INRA 717-1B4 treated with UV-B radiation for 10 days. Initial and final measurements for height and chlorophyll fluorescence (F_v/F_m) were recorded in INRA 717-1B4. Leaves from LPI 3-4 were harvested on the final day of UV-B radiation treatments and to measure leaf area.

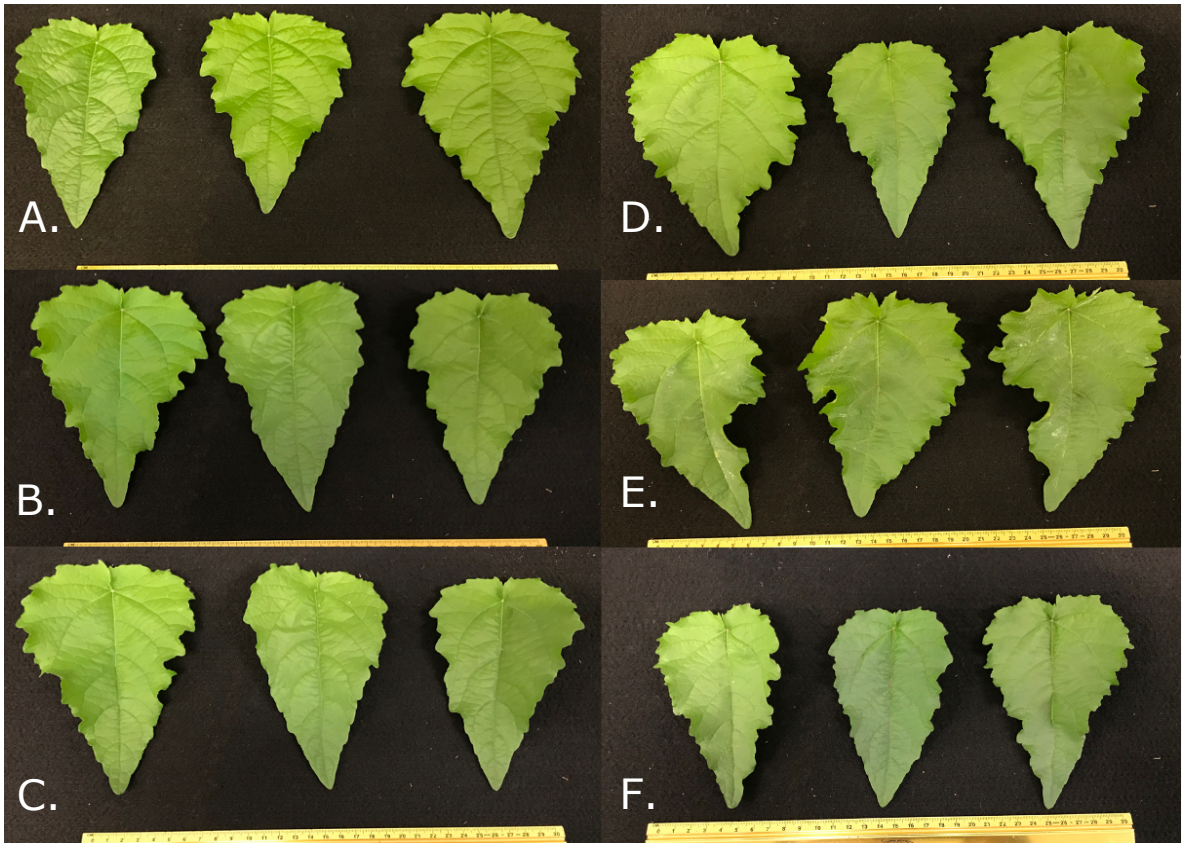

Figure 5-23. UV-B irradiated INRA 717-1B4 leaves were harvested at LPI 5 after 10 days of treatment. (A) Wild-type control leaves looked similar to the (D) wild-type treated with UV-B. (B) *UVR8* KO without UV-B treatment looked similar to the wild-type however, the (E) *UVR8* KO with UV-B developed with curling edges. (C) *UVR8* OX without UV-B treatment and (F) with UV-B were greener compared to the wild-type and the leaf area was slightly smaller. *UVR8* OX lines showed visible anthocyanin pigmentation at the veins and in the epidermis.

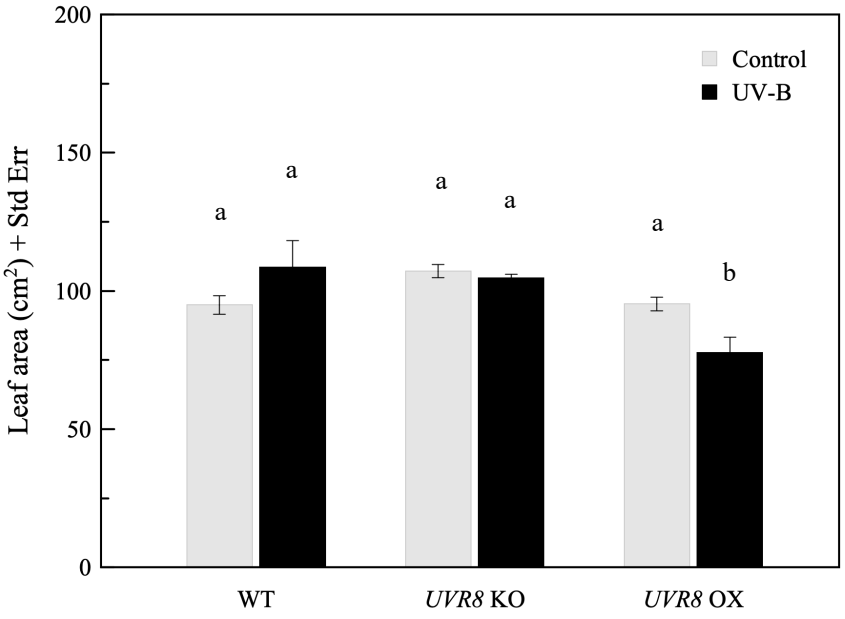

Figure 5-24. Leaf area was measured on LPI 7 or 8 from each treatment type from *UVR8* KO and *UVR8* OX. Leaf area from UV-B treated *UVR8* OX poplars (b) were smaller compared to the WT and *UVR8* KO in the controls and with UV-B treatment (a) (n = 3). Statistically significant differences in mean leaf area values between WT, *UVR8* KO, and *UVR8* OX lines are indicated by different letters (a and b: analysis of variance with post hoc Tukey's HSD test, $p < 0.05$). Inferential error bars denote the standard error in the variability of the mean.

Further analysis of the growth of the transgenic lines treated for approximately two weeks with UV-B radiation revealed additional surprises, however (Table 5-12, Fig 5-25). After two months following acclimation from tissue culture, or about three weeks after exposure to UV-B, the height of the *UVR8* knockout were taller than the wild-type (Fig. 5-26) and *UVR8* overexpressing lines were similar to the *UVR8* KO lines and taller than the wild-type (Fig. 5-27). When all lines were compared, the modulated *UVR8* lines showed striking increase in height compared to wild-type plants (Fig. 5-28).

It is generally agreed that plants respond to UV-B by producing aromatic compounds that accumulate in the epidermis to shield cells from the harmful effects of radiation. The effect of UV-B on F_v/F_m, a commonly used measurement of plant stress by chlorophyll fluorescence, were subtle in the transgenic lines, but consistent with expectations (Table 5-11). The *UVR8* knockout line shows smaller increases in chlorophyll fluorescence relative to the wild-type or the *UVR8* overexpressing line (Fig. 5-29). This observation was followed by an analysis of total anthocyanins and flavonoids. Anthocyanin levels in the wild-type and *UVR8* knockout lines showed little difference between control and UV-B treated plants. However, the *UVR8* overexpressing line showed a significant increase in total anthocyanin concentration treated with UV-B radiation when compared to controls (Fig. 5-30). Total flavonoid content showed similar trends. As expected, upon treatment with UV-B, wild-type poplar showed measurable increases in total flavonoid concentration (per quercetin equivalents (QE/g) (Fig. 5-31). As also expected, the *UVR8* knockout line showed little difference in flavonoid content after treatment with UV-B radiation.

Table 5-12. Transgenic INRA 717-1B4 growth after two months from tissue culture acclimation.			
Transgenic line	**Treatment**	**Mean height (cm)**	**SE**
WT	Control	33.49	0.53
UVR8 KO	Control	48.31	1.32
UVR8 OX	Control	47.91	1.65

Table 5-12. Transgenic 717 growth after two months from tissue culture acclimation. Transgenic lines *UVR8* KO and *UVR8* OX showed an increased height phenotype compared to WT.

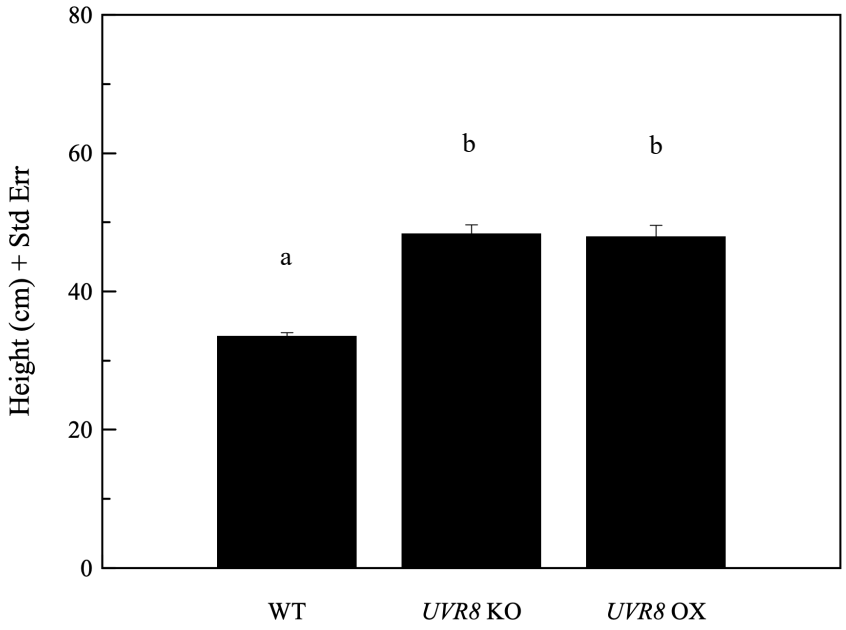

Figure 5-25. Height from transgenic INRA 717-1B4 were taller compared to WT control. Transgenic lines grown in potting media approximately two months out of tissue culture were untreated with UV-B radiation. The *UVR8* KO and *UVR8* OX lines (b) were taller compared to the WT (a) (n = 3). The *UVR8* KO and *UVR8* OX lines were similar in height. Statistical significance in mean height values between WT *UVR8* KO and *UVR8* OX lines are indicated by different letters (a and b: analysis of variance with post hoc Tukey's HSD test, $p < 0.05$, WT - *UVR8* KO ($p = 0.005$), WT - *UVR8* OX ($p = 0.004$), and *UVR8* KO - *UVR8* OX ($p = 1.0$). Inferential error bars denote the standard error in the variability of the mean.

UVR8 KO WT

Figure 5-26. A comparison of height difference in *UVR8* KO INRA 717-1B4 compared to the wild-type. Untreated transgenic *UVR8* KO line grown in potting media approximately two months out of tissue culture are taller compared to wild-type plants.

UVR8 OX WT

Figure 5-27. A comparison of height difference in *UVR8 OX* INRA 717-1B4 compared to the wild-type. Untreated transgenic *UVR8* OX line grown in potting media approximately two months out of tissue culture are taller compared to wild-type plants.

UVR8 OX *UVR8* KO WT

Figure 5-28. Representative *UVR8* OX and *UVR8* KO lines are similar in height and taller compared to wild-type.

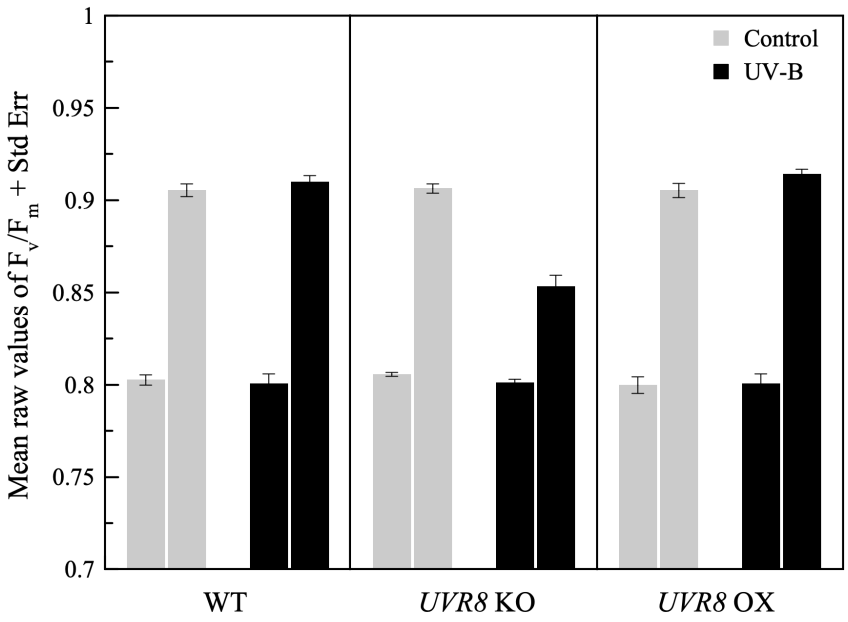

Figure 5-29. Initial and final F_v/F_m values were measured from each line and treatments. Final F_v/F_m measurement from the *UVR8* KO was lower than WT and *UVR8* OX suggesting lowered photosynthetic efficiency after UV-B treatment (n = 3).

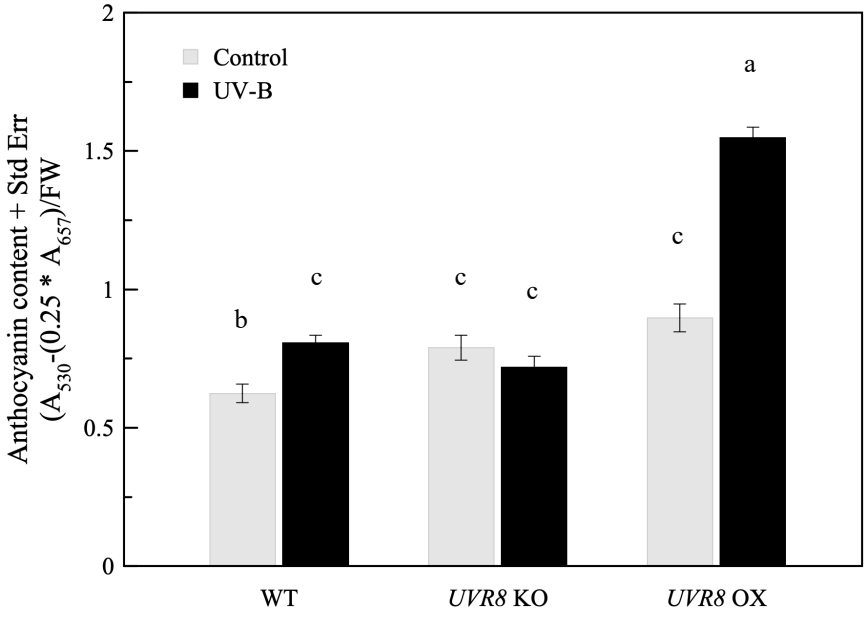

Figure 5-30. Determination of anthocyanin content was detected in leaf extracts using acidified MeOH (1% HCl v/v). Total anthocyanin content (TAC) was calculated from absorbance read at 530 and 657 nm and adjusted with the formula $A_{530} – (0.25 * A_{657})$ / fresh weight (Rabino and Mancinelli 1986). Anthocyanin levels were affected by UV-B treatments and increased in WT (c) and *UVR8* OX (a) lines except in the *UVR8* KO (c) lines that showed no change relative to the controls (c) (n = 3). Mean anthocyanin content between WT, *UVR8* KO, and *UVR8* OX lines are indicated as statistically significant by different letters (a, b, and c: analysis of variance with subsequent Tukey's HSD test, $p < 0.05$). Inferential error bars represent the standard error in the variability of the mean.

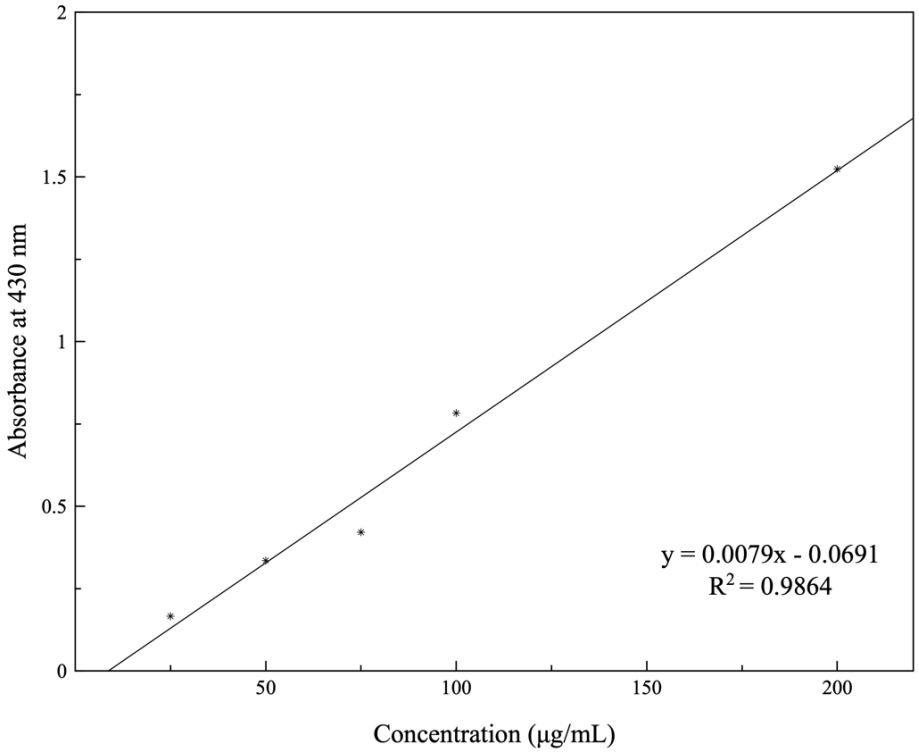

Figure 5-31. Bulk flavonoid content from methanol extracts of leaf tissue from INRA 717-1B4 was calculated by a standard curve of quercetin ($y = 0.0079x – 0.0691$, $R^2 = 0.9864$). The calibration curve was constructed from quercetin standard and dissolved in methanol with dilutions ranging from 25-200 µg/mL. 10% $AlCl_3$ (w/v) was added to diluted quercetin standard and absorbance was read with a spectrophotometer at 430 nm.

However, the *UVR8* overexpression line showed a significant increase in total flavonoid content when treated with UV-B, especially when compared to the wild-type and *UVR8* knockout lines (Fig. 5-32). To further probe the specific metabolites involved in UV-B acclimation in the transgenics, a targeted metabolomic analysis using LC-MS was performed in the *UVR8* knockout and *UVR8* overexpression poplar lines with samples obtained before and after 10 days of UV-B treatment. Compound retention times (t_R), exact and monoisotopic masses, and molecular formulas were used to identify metabolites that could be implicated with UV-B protection, and that may serve as branchpoints into other pathways (Table 5-13). Standard calibration curves were constructed using quercetin glucoside (Fig. 5-33) and salicin (Fig. 5-34) to calculate the estimated concentration of each metabolite and its related conjugates. As expected, increased levels of quercetin-3-O-glucoside were detected in the *UVR8* overexpression lines after UV-B treatment compared to the control or *UVR8* knockout line (Fig. 5-35), consistent with the increase seen for total flavonoids (Fig. 5-31). Interestingly, salicins and other phenolics have been shown to increase in poplar upon exposure to UV-B and thought to be involved in UV-B shielding as well as plant defense (Warren et al. 2003). In accord with those findings, levels of 2-acetylsalicin in the *UVR8* knockout line were greater than those seen in control plants, or in the *UVR8* overexpressing line, and the increase was even more pronounced after UV-B treatment (Fig. 5-36).

Based on the small but expected trends in parameters measured for plants treated with UV-B, the initial experiments focused on a broad set of transgenic lines that were able to withstand and tolerate a greater dosage of UV-B radiation, albeit for a short period of time.

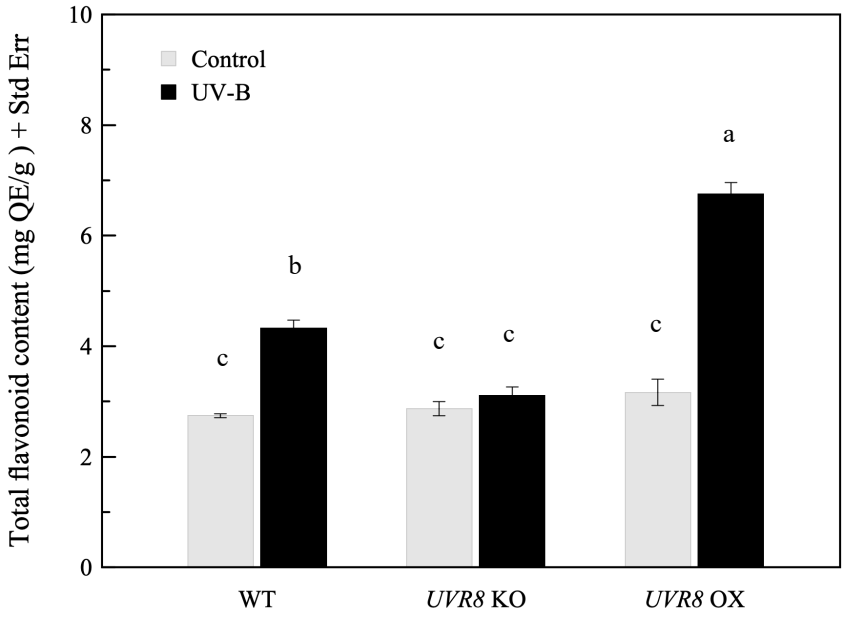

Figure 5-32. Total flavonoid content was determined in methanol extracts after UV-B exposure using an aluminum chloride assay and normalized to mg of quercetin equivalents (QE)/g. WT (b) and *UVR8* OX (a) increased in flavonoid content after UV-B exposure relative to no UV-B treatment (c) (n = 3). There was no change in flavonoid content was detected in the *UVR8* KO (c) line. Statistical significance in flavonoid content values between WT, *UVR8* KO, and *UVR8* OX lines are indicated by different letters (a, b, and c: analysis of variance with subsequent Tukey's HSD test, $p < 0.05$). Inferential error bars denote the standard error in the variability of the mean.

Table 5-13. Flavonoids and salicylates were identified and detected by LC-MS/TOF in *Populus.*

Compound name	**t_R**	**Exact Mass**	**[M-H]-**	**Molecular formula**
Vanillic acid	1.88	168.1467	167.0334	$C_8H_8O_4$
Flavonoids				
Quercetin-3-O-rutinoside	2.39	610.1534	609.1456	$C_{27}H_{30}O_{16}$
Quercetin-3-O-glucoside	2.48	464.0955	463.0877	$C_{21}H_{20}O_{12}$
Quercetin-3-O-glucuronide	2.47	478.0747	477.0669	$C_{21}H_{18}O_{13}$
Kaempferol-3-O-rutinoside	2.61	594.1585	593.1506	$C_{27}H_{30}O_{15}$
Kaempferol-glycuronide	2.71	462.0798	461.0720	$C_{21}H_{18}O_{12}$
Isorhamnetin-3-O-rutinoside	2.65	624.1690	623.1612	$C_{21}H_{32}O_{16}$
Isorhamnetin-glycuronide	2.79	492.0904	491.0826	$C_{22}H_{20}O_{13}$
Salicylates				
Salicin	1.44	286.1053	285.0974	$C_{13}H_{18}O_7$
2'-Acetylsalicin	1.93	328.1158	327.1080	$C_{15}H_{20}O_8$
Salicortin	2.53	424.1369	423.1291	$C_{20}H_{24}O_{10}$
2'-Acetylsalicortin	3.62	466.1475	465.1397	$C_{22}H_{26}O_{11}$

Table 5-13. Flavonoids and salicylates were identified and detected by LC-MS/TOF in *Populus.*

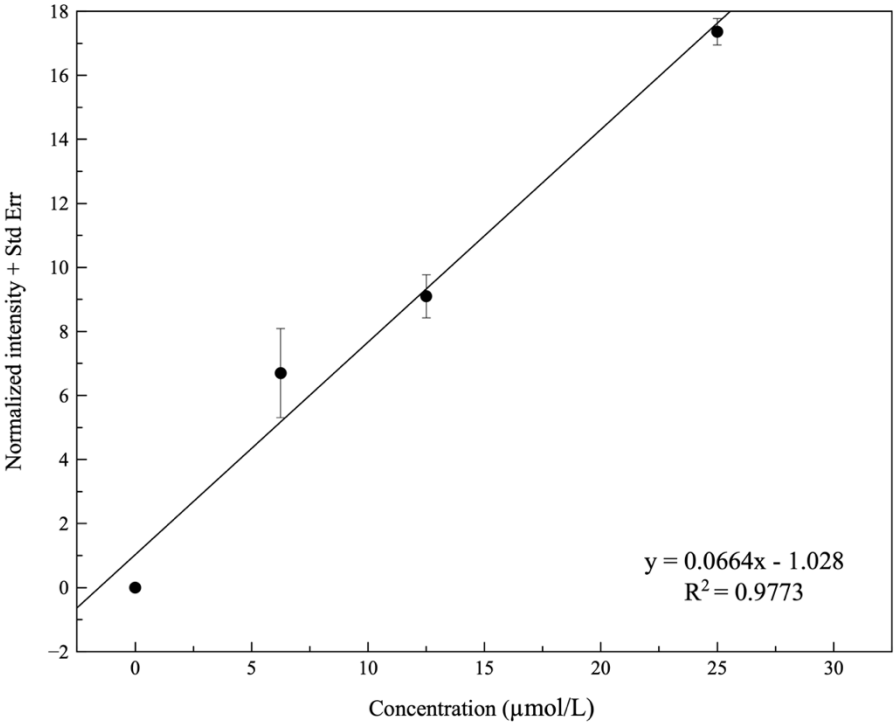

Figure 5-33. Standard calibration curve for the LC-MS analysis of quercetin glucoside. The correlation coefficient was calculated to be 0.9773 and the linear regression line y = 0.0664x – 1.028 was used to calculate quercetin concentration of UV-B treated samples.

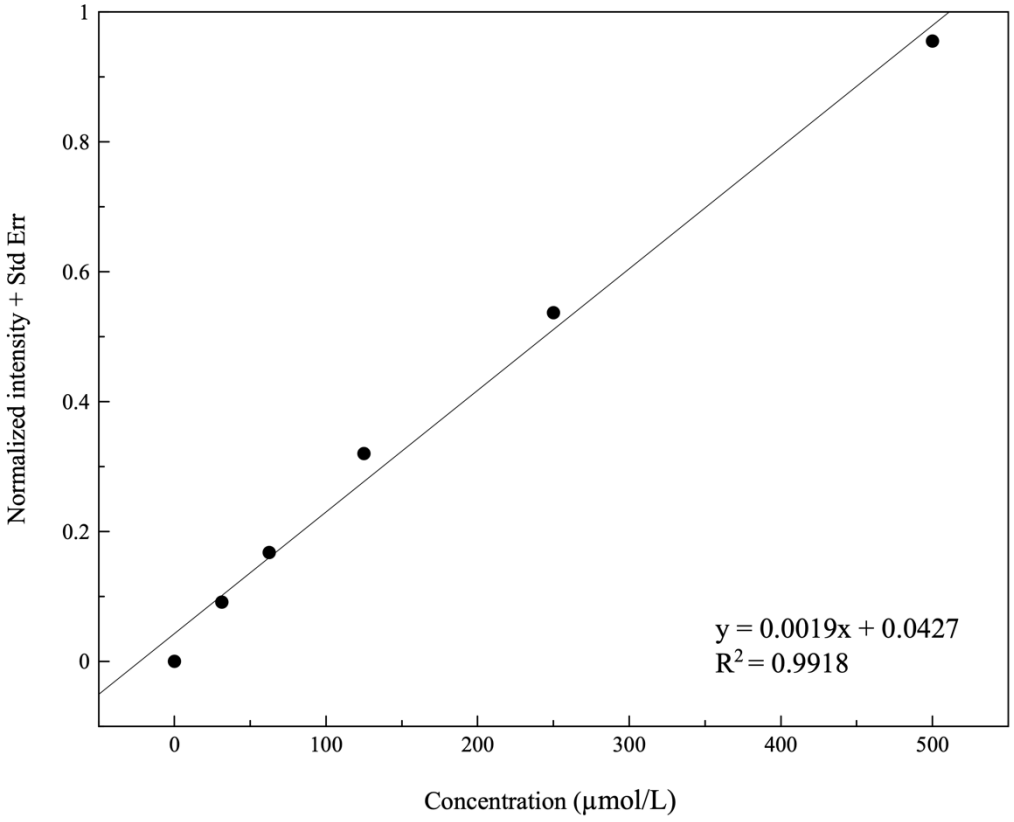

Figure 5-34. Standard calibration curve for the LC-MS analysis of salicin. The correlation coefficient was calculated to be 0.9918 and the linear regression line y = 0.0019x + 0.0427 was used to calculate salicylate concentration of UV-B treated samples.

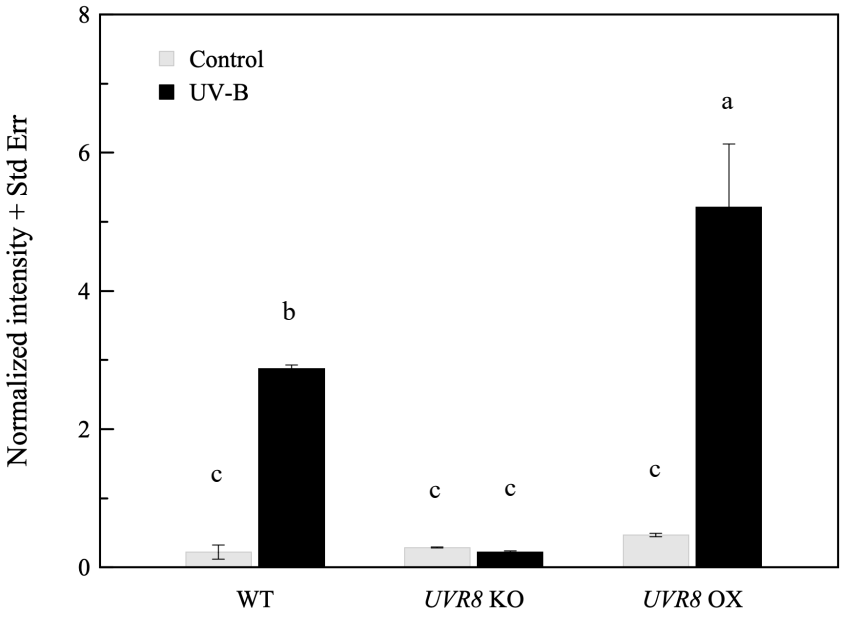

Figure 5-35. LC-MS measurement of quercetin-3-O-glucoside in transgenic INRA 717-1B4. *UVR8* KO and *UVR8* OX lines in INRA 717-1B4 were treated with UV-B radiation for 10 days (n = 3). The UV-B treated WT (b) and *UVR8* OX (a) poplars showed differences in quercetin levels compared to the *UVR8* KO (c) that was not different from the WT (c) and UVR8 OX (c) control. Statistical significance in normalized intensity values between WT, *UVR8* KO, and *UVR8* OX lines are indicated by different letters (a, b, and c: analysis of variance with post hoc Tukey's HSD test, $p < 0.05$). Inferential error bars denote the standard error in the variability of the mean.

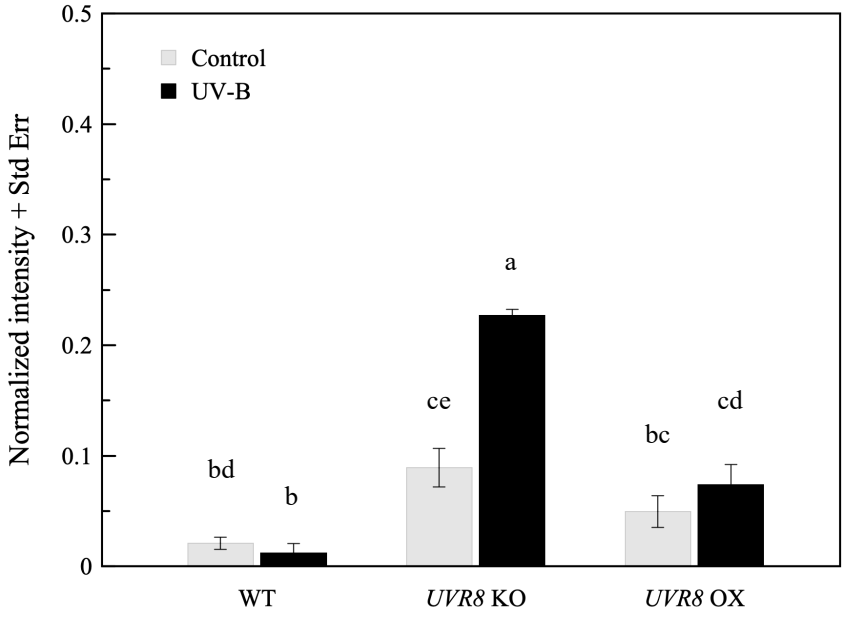

Figure 5-36. LC-MS measurement of 2-acetylsalicin in transgenic INRA 717-1B4. *UVR8* KO and *UVR8* OX lines in INRA 717-1B4 were treated with UV-B radiation for 10 days (n = 3). The WT (bd and b) or *UVR8* OX (bc and cd) line with and without UV-B were not significant but the UV-B treated WT (b) compared to the UV-B treated *UVR8* OX (cd) ($p < 0.05$) line showed differences in salicylate levels. The control *UVR8* KO (ce) was different from the WT (bd and b) poplars and the UV-B treated *UVR8* KO (a) was significantly different from the WT ($p < 0.00$) and *UVR8* OX ($p < 0.001$) line. Statistical significance in normalized intensity values between WT, *UVR8* KO, and *UVR8* OX lines are indicated by different letters (a, b, c, d, and e: analysis of variance with post hoc Tukey's HSD test, $p < 0.05$). Inferential error bars denote the standard error in the variability of the mean.

Therefore, RNAi-inhibited *UVR8*, *UVR8* knockout, and *UVR8* overexpressing transgenic lines were treated with a UV-B dosage of 35 kJ m^{-2} for 18 hours over a single day and then evaluated physiologically and metabolically. In the initial round of experiments, plant height, bud count, and internode length were determined, as well as F_v/F_m measurements. It was found that under one day under 18 h of intense UV-B exposure, an equal decrease in height change in the WT and *UVR8* OX lines was observed but not in the *UVR8* KO line (Table 5-14).

Metabolite measurements were also performed using LC-MS to detect any immediate response of the plants upon a brief but significant exposure to UV-B radiation. Analyses of quercetin-3-O-glucoside (Fig. 5-37) and 2-acetylsalicin (Fig. 5-38) in RNAi-inhibited *UVR8*, *UVR8* knockout, *UVR8* overexpressing, and RNAi-inhibited *CAD* transgenic INRA 717-1B4 lines showed considerable biological variation when treated with UV-B. Generally, quercetin-3-O-glucoside levels were lower in *UVR8* knockout lines than wild-type in the absence of UV-B, and there were little changes in the low levels upon treatment with UV-B (with the exception of 10F and 12I that showed increased levels in the absence of UV-B). By contrast, the *UVR8* overexpressing lines showed wild-type levels of quercetin-3-O-glucoside in the absence of UV-B, but significant increases in quercetin-3-O-glucoside were detected relative to controls when treated with UV-B radiation. Interestingly, RNAi-inhibited *CAD* lines showed a reduction in quercetin-3-O-glucoside relative to wild-type in the absence of UV-B, but levels were substantially increased upon UV-B treatment. Measurements of 2-acetylsalicin were also performed in the transgenic

Table 5-14. Transgenic INRA 717-1B4 with modulated *UVR8* treated with for a single day of high intensity UV-B for 18 hours.

Transgenic line	Treatment	Mean height change (cm)	SE	Mean initial F_v/F_m	SE	Mean final F_v/F_m	SE	Mean bud count	SE	Mean internode length (cm)	SE
WT	Control	0.67	0.17	0.8055	0.00	0.7997	0.00	12.00	2.00	0.74	0.19
WT	UV-B	0.33	0.17	0.8283	0.00	0.8078	0.00	12.00	1.15	0.73	0.19
UVR8 RNAi	Control	0.92	0.20	0.7889	0.01	0.7835	0.00	11.80	1.24	0.85	0.07
UVR8 RNAi	UV-B	0.42	0.19	0.8254	0.00	0.8006	0.01	12.33	0.76	0.71	0.11
UVR8 KO	Control	0.37	0.09	0.8023	0.00	0.7909	0.00	10.53	0.74	0.61	0.07
UVR8 KO	UV-B	0.36	0.08	0.8284	0.00	0.7977	0.00	10.06	0.64	0.76	0.10
UVR8 OX	Control	0.48	0.14	0.8098	0.00	0.7953	0.00	9.60	1.44	0.81	0.35
UVR8 OX	UV-B	0.17	0.04	0.8009	0.02	0.8022	0.00	10.40	0.75	0.52	0.27

Table 5-14. Transgenic INRA 717-1B4 with modulated *UVR8* treated with for a single day of high intensity UV-B for 18 hours. Initial height and chlorophyll fluorescence F_v/F_m measurements were recorded prior to UV-B treatment. After 18 hours of UV-B radiation, height, chlorophyll fluorescence, and bud count were measured. Approximate internode length was calculated by dividing final height and bud count.

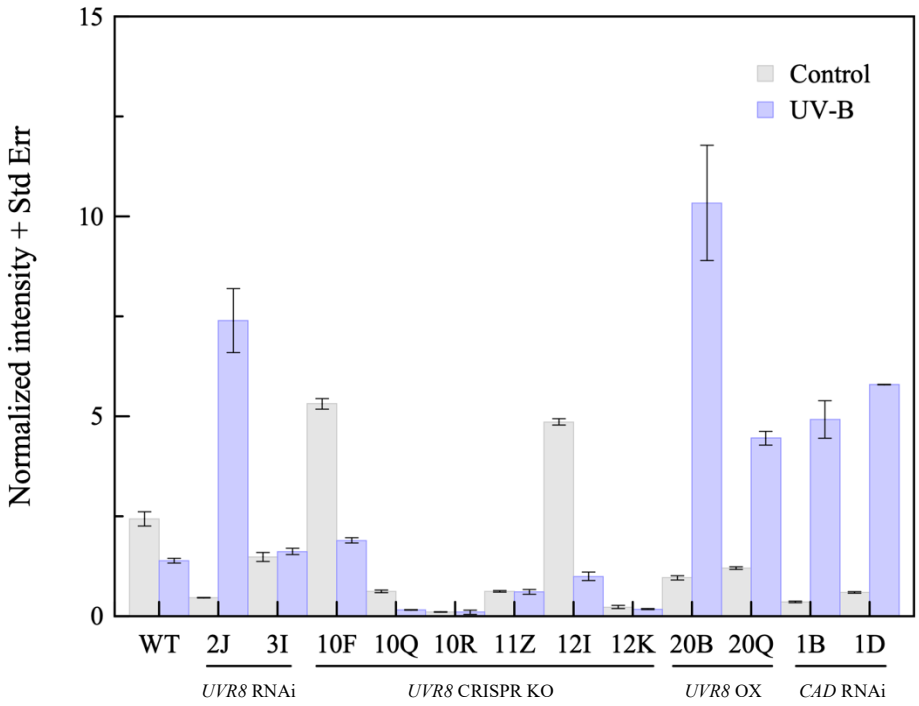

Figure 5-37. LC-MS measurement of quercetin-3-O-glucoside in transgenic INRA 717-1B4 with modulated *UVR8* or *CAD* treated with for a single day of high intensity UV-B for 18 hours. *UVR8* RNAi lines showed contrasting levels of quercetin-3-O-glucoside when treated with UV-B. In general, the *UVR8* KO lines showed a decrease in quercetin-3-O-glucoside with the exception of 10F and 12I that had increased levels without UV-B exposure. The *UVR8* OX line treated with UV-B radiation both showed an increase in quercetin-3-O-glucoside compared to the controls. Two *CAD* RNAi subcultures were included in this UV-B experiment, and both showed an increase in quercetin-3-O-glucoside compared to the wild-type.

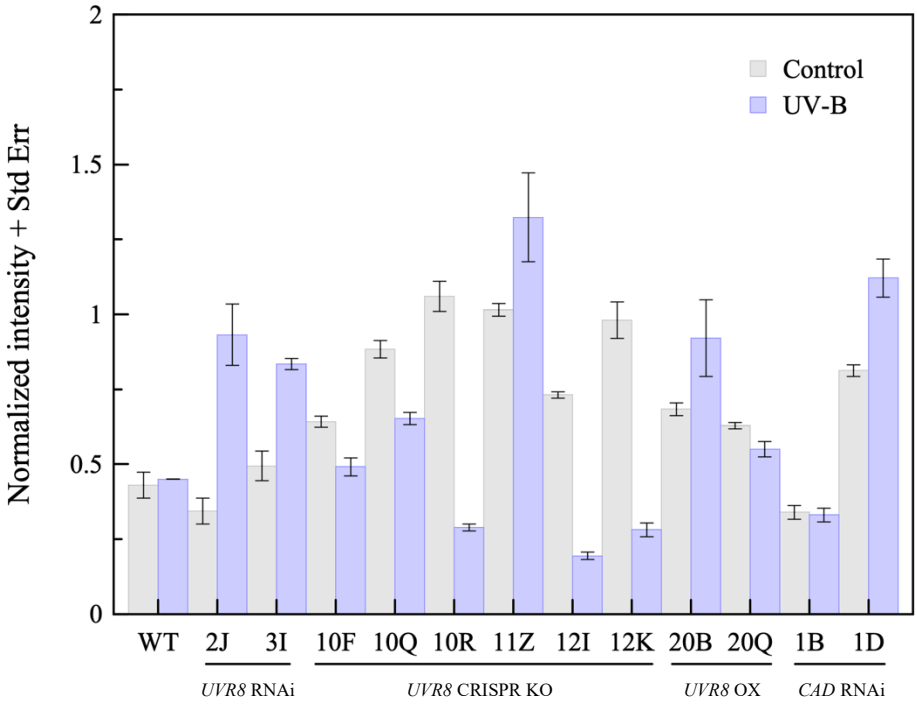

Figure 5-38. LC-MS measurement of 2-acetylsalicin in transgenic INRA 717-1B4 with modulated *UVR8* or *CAD* treated with for a single day of high intensity UV-B for 18 hours. *UVR8* RNAi lines showed an increase in 2-acetylsalicin after UV-B exposure compared to the wild-type. The *UVR8* KO lines showed greater variation in levels of 2-acetylsalicin but in general, several subcultures showed an increase compared to the controls. The *UVR8* OX showed increased levels of 2-acetylsalicin compared to the wild-type in either treatment. The *CAD* RNAi subcultures showed contrasting results in comparison to the wild-type in either treatment.

lines after a short period of intense exposure to UV-B radiation, and they too revealed biological variation among the lines (Fig. 5-38). RNAi-inhibited *UVR8* transgenics showed wild-type levels of 2-acetylsalicin before exposure to UV-B, but these increased significantly after exposure. Although a similar pattern was expected to be seen for the *UVR8* knockout lines, patterns of metabolite production were quite varied, proving difficult to compare with results in the RNAi-inhibited lines, though several lines showed an increase in 2-acetylsalicin compared to controls. Levels of 2-acetylsalicin were found to increase in the *UVR8* overexpression line, and maintained at high levels after treatment with UV-B. Finally, the RNAi-inhibited *CAD* lines, though varied, showed an increase in 2-acetylsalicin relative to wild-type, which increased after UV-B treatment. In previous studies, modified cell walls may elicit a stress phenotype that mimics wounding that would lead to alterations in secondary metabolite biosynthesis (Dauwe et al. 2007). Therefore, it is possible that the changes in metabolite levels in *CAD* knockdown *Populus* may be due to the alteration in the pathway and that the response may be exacerbated by UV-B radiation. Although some of the results from exposing the transgenics to a short, intensive regime of UV-B radiation are in line with expectations, the short period, and the relatively long exposure, was deemed unsatisfactory for detailed analysis of the double mutant lines, and further experiments on those plants utilized the exposure parameters similar to initial experiments.

With verified plants that exhibited RNAi-inhibited *CAD* expression and that also contained either a *UVR8* knockout or *UVR8* overexpression modification, as well as a reasonable experimental protocol to assess UV-B treatment in poplar, it was possible to address a

central question in this research: how do low-lignin poplar lines differ from wild-type poplar in their response to UV-B radiation? Thus, preliminary experiments to treat double mutant plants containing either the *UVR8* knockout in an RNAi-inhibited *CAD* background, or the 35S-overexpressed *UVR8* in an RNAi-inhibited *CAD* background, with a UV-B dosage of 35 kJ m^{-2} for 8 h/day for 7 days was performed. It is important to note that the wild-type specimens used in these experiments were approximately one month older than the RNAi-inhibited *CAD*, *UVR8* knockout lines or the RNAi-inhibited *CAD*, *UVR8* overexpression lines. Thus, because it is challenging to directly compare the results of the specimens, these results are preliminary and need to be reproduced with proper timing to accurately compare plant lines. As in previously described experiments, plant characteristics such as growth height and internodal length, shielding and selective metabolites were determined before and after UV-B treatment. Another interesting observation was made approximately two weeks after UV-B treatment in the *UVR8* knockout, RNAi-inhibited *CAD* background and the 35S-overexpressed *UVR8*, RNAi-inhibited *CAD* background (Fig. 5-39). The growth of the double mutants appears to be growing faster than the wild-type that is one month older.

The growth differences between expression modulated *UVR8* lines seen in previous experiments seems to maintain in the double mutant lines, though it is difficult to compare the differences reliably given the different maturities of the specimens at the start of the experiment, and the relatively short (seven days) growth period. In an effort to analyze with this characteristic, however, the changes in height for each line were calculated over the course of the UV-B treatment (Table 5-15). The main conclusion from these estimates

WT | *CAD* KD *UVR8* KO | *CAD* KD *UVR8* OX

Figure 5-39. Growth performance of double mutants compared to wild-type. The wild-type plants used for these measurements are about two months outside of tissue culture. The *CAD* KD, *UVR8* KO and OX double mutants have been transplanted out of tissue culture for about one month. The transgenic lines indicate increased growth performance compared to the wild-type.

is that there is negligible change in growth when plants are treated with UV-B radiation. Again, this was surprising for the poplar lines modulated for *UVR8* expression, in contrast to that seen for *Arabidopsis*. UV-B absorbing metabolites produced during UV-B treatment were also assessed for the double mutant lines. Chlorophyll fluorescence was measured before and after UV-B treatment to assess the extent of metabolite shielding in *CAD* knockdown, *UVR8* knockout lines relative to the *CAD* knockdown, *UVR8* overexpressing lines. Although the *CAD* knockdown lines, with either a *UVR8* knockout or overexpressed *UVR8*, showed slightly higher F_v/F_m values compared to the wild-type, these values did not appreciably change over the course of the experiment (Table 5-15). These values indicate that the *UVR8* knockout or *UVR8* overexpression seems to have little effect on short term changes in shielding metabolites. However, to probe more deeply into the potential metabolic changes that are initiated in these lines upon exposure to UV-B, metabolomics measurements were compared before and after UV-B treatment.

To simplify these preliminary analyses, total quercetins and total salicins are presented as aggregate values to get a perspective on the UV-B promoted metabolic changes. Interestingly, upon exposure to UV-B, quercetin levels were reduced in lines that contained the *UVR8* knockout (Fig. 5-40). By contrast, both the *CAD* knockdown, and *UVR8* overexpressing lines showed an increase in quercetin levels upon UV-B treatment (Fig. 5-41). These results are in general agreement with those seen in earlier experiments. Alternatively, whereas the absolute total salicin levels do not change appreciably from wild-type in any of the transgenic lines, there are only small or minor changes in salicins as a consequence of UV-B treatment. This is in contrast to that seen for plants treated with

Table 5-15. Transgenic double mutant INRA 717-1B4 treated with UV-B radiation for seven days

Transgenic line	**Treatment**	**Mean initial height (cm)**	**SE**	**Mean final height (cm)**	**SE**	**Mean height change (cm)**	**SE**	**Mean initial F_v/F_m**	**SE**	**Mean final F_v/F_m**	**SE**	**Mean internode length (cm)**	**SE**	**Mean bud count**	**SE**
WT*	Control	14.00	3.00	16.10	3.60	1.40	0.78	0.7957	0.00	0.7803	0.00	0.85	0.43	11.33	1.86
WT*	UV-B	15.05	2.65	17.25	2.75	1.47	0.74	0.7813	0.01	0.7837	0.00	0.88	0.44	12.00	1.15
cad/uvr8	Control	5.83	0.87	7.27	1.04	0.86	0.36	0.7990	0.00	0.7926	0.00	0.45	0.19	9.00	0.58
cad/uvr8	UV-B	6.34	1.03	7.68	1.25	0.96	0.29	0.8006	0.00	0.7927	0.00	0.58	0.18	9.50	1.19
cad/35S-UVR8:GFP	Control	6.45	0.65	8.20	0.90	1.75	0.25	0.7995	0.01	0.7920	0.01	0.91	0.10	9.00	0.00
cad/35S-UVR8:GFP	UV-B	6.13	0.41	7.50	0.46	1.37	0.09	0.8027	0.00	0.8090	0.00	0.75	0.05	10.00	0.58

*WT plants were approximately one month older than the transgenic lines at the time of experimentation due to lack of available materials.

Table 5-15. Transgenic double mutant INRA 717-1B4 with modulated *UVR8* treated with high UV-B radiation for seven days. Initial and final height was measured to calculate height change after 7 days of UV-B treatment. Initial and final measurements for chlorophyll were recorded and total bud count was used to calculate approximate internode length.

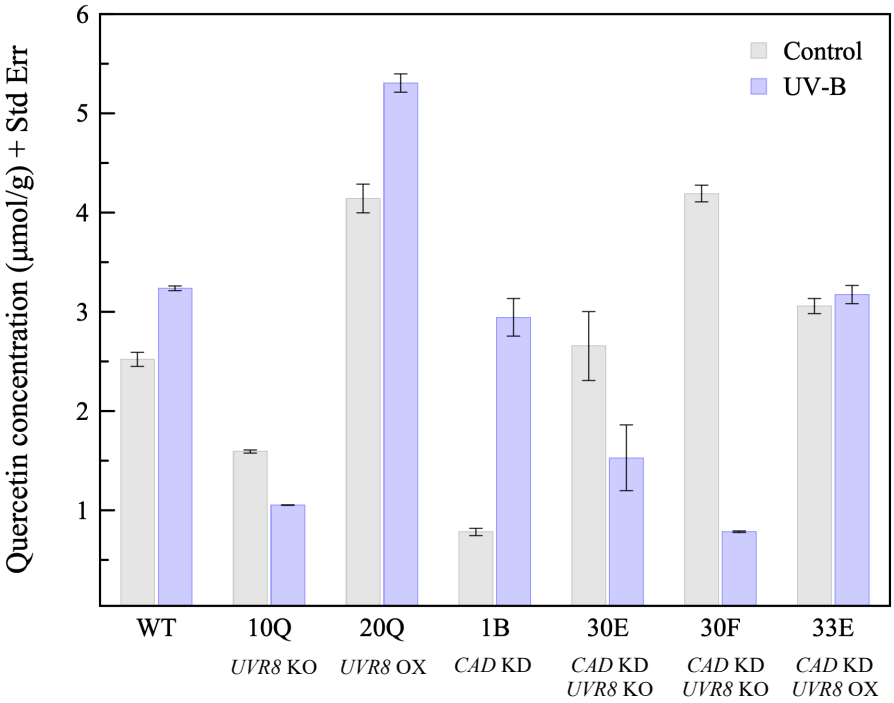

Figure 5-40. Metabolomic analysis of combined quercetins in transgenic INRA 717-1B4 were treated with UV-B for 8 h of high intensity UV-B radiation for seven days. Measurement of quercetins were combined to simply the results in the single and double mutants treated with UV-B radiation. Two *CAD* KD, *UVR8* KO subcultures were analyzed, and both decreased in quercetin levels compared to the wild-type after UV-B treatment. Quercetin concentration was about the same in the low-lignin *UVR8* OX line compared to the wild-type.

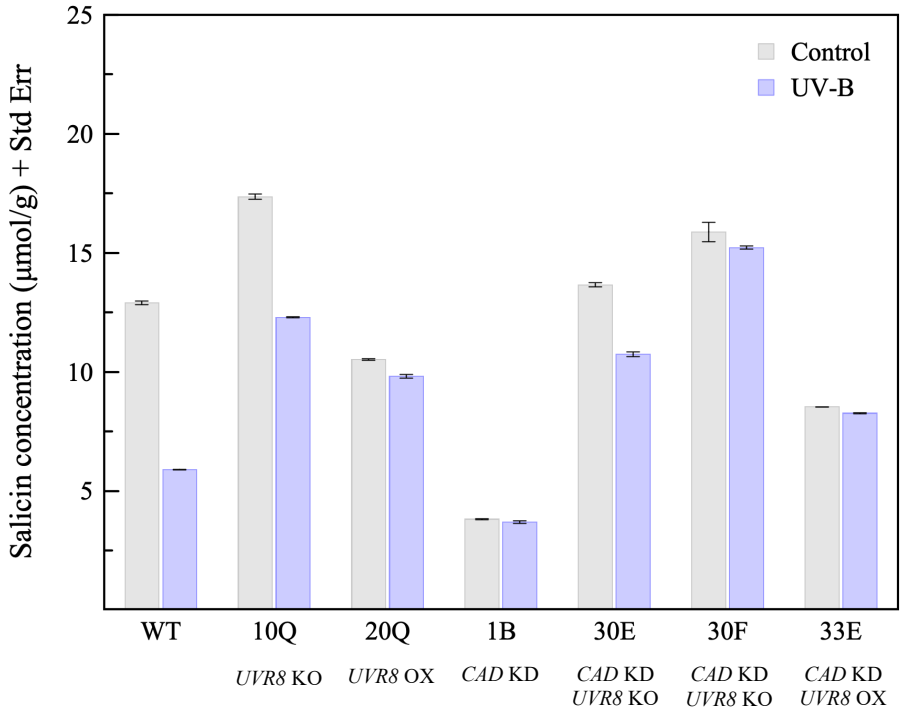

Figure 5-41. Metabolomic analysis of combined salicylate in transgenic INRA 717-1B4 were treated with UV-B for 8 h of high intensity UV-B radiation for seven days. The *CAD* KD, *UVR8* KO lines both had similar results to the *UVR8* KO line and increased in salicin after exposure to UV-B radiation. The *CAD* KD, *UVR8* OX line increased slightly after UV-B exposure compared to the wild-type and showed similar results as the single mutant, *UVR8* OX line.

a short, intensive period of UV-B, and may reflect time-dependent metabolic compensation during acclimation.

Discussion

The impact of UV-B radiation on transgenic poplar is an increasingly important problem with the extensive scientific effort in modifying plant cell walls to decrease the recalcitrance of lignocellulosic biomass for conversion to bioenergy and value-added bioproducts (Hu et al. 1999, Mansfield et al. 2012, Baxter and Stewart 2013). One approach to address this challenge that builds on modern genome engineering techniques is the construction of transgenic poplar lines with defined genotypes to carefully dissect the contributions of key metabolic branchpoints in controlling the production of aromatic compounds to protect against radiation damage. In this chapter, the construction and characterization of transgenic poplar lines with CRISPR-promoted alterations in the expression of UVR8, the key plant photoreceptor for UV-B radiation, is described. Additionally, double mutant transgenic lines were constructed that contained RNAi-mediated suppression of cinnamyl alcohol dehydrogenase (CAD), a key enzyme in the biosynthesis of phenylpropanoids, important precursor of lignin. Because *CAD* mutants show a reduction in transcript levels that would lead to a decrease in lignin content (Macaya-Sanz et al. 2017), it should be possible to examine the earliest steps in UV-B acclimation in *CAD*-defective, low lignin plants that possess altered expression levels of the UVR8 photoreceptor. It would be ideal to characterize lignin content in each subculture to further understand the response in *CAD* knockdown poplars to UV-B radiation.

However, accurate measurement of lignin content and composition of each plant would be a lengthy and exhaustive process that is beyond project objectives.

The construction of poplar transgenic lines was technically involved, though successful, and indicates great promise for the development of detailed genotype-phenotype relationships in a model tree of considerable economic importance. However, there remain some challenges to the broad application of genome engineering technology to poplar. For instance, in targeting CRSIPR/Cas9 modifications in poplar, two different *Arabidopsis* promoters, U3 and U6, were utilized to ascertain whether one promoter was more efficient in poplar than the other. Interestingly, gRNAs expressed from the *At*U6 promoter were much more efficient in generating *UVR8* genomic modifications than that compared to the *At*U3 promoter. Thus, the U6 promoter seems preferable for use in poplar, and in future work should rely preferentially on this promoter to express guide RNAs for Cas9 homing to a particular sequence in a genome. Similarly, three different codon-optimized variants of Cas9 were screened for mutagenesis efficiency in transgenic poplar lines transformed with CRISPR constructs. Cas9 with codons optimized for *Arabidopsis*, *Maize* or for generic expression in plants were equally effective in generating mutant lines, suggesting that any of the Cas9 sequences used would be effective in future studies with poplar. Finally, a comparison of the reduction of gene expression by RNAi versus CRISPR/Cas9 suggested more homogenous results were observed with the CRISPR system, which was also much easier to implement.

The INRA 717-1B4 hybrid (*P. tremula* x *P. alba*) was relatively transformed with ease and was found to be highly efficient for generating transgenic plants. On the other hand, significant challenges were experienced in generating transgenic plants using *Populus deltoides*. Although several experimental parameters were varied in attempted transformation of *P. deltoides*, including the use of various *Agrobacterium* strains, adjusting coculturing conditions, using different selection markers, and varying the composition of growth medium for propagation, none of the conditions yielded viable transformants. Clearly, developing improved tools for the routine transformation of *P. deltoides*, and *P. trichocarpa*, would significantly advance the field.

Once constructed, several experimental approaches were used for confirm that the intended genetic disruptions were indeed produced. Qualitative restriction enzyme screening of short regions of genomic DNA amplified by PCR were quite useful in quickly identifying transformed plantlets. These subcultures were further screened by RT-PCR to compare changes in gene expression in the biologically distinct lines. Though transcript levels in the *UVR8* KO line showed some variation relative to the wild-type, this may be accounted for trace expression of *UVR8* that is detected by the RT-PCR instrument as background noise. Further confirmation of knockout mutagenesis was validated by DNA sequencing of amplified genomic DNA to show the molecular basis for gene disruption. These approaches were applied to confirm the construction of the transgenic poplar lines used in this study, including RNAi-suppressed *CAD* lines, RNAi-suppressed *UVR8* lines, up- and down-regulated *UVR8* lines constructed with CRISPRa and CRISPRi, respectively, up-regulated *UVR8* expressed from the CaMV 35S promoter, and *UVR8* knockout lines

constructed with CRISPR/Cas9. The transgenic materials developed in this work will be useful for years to come by the collaborating laboratories involved in this project, as well as for colleagues in the field.

In devising the transgenic lines and their experimental characterization to help elucidate the molecular clues on the acclimation of *Populus* to UV-B radiation, several simple assumptions were adopted. Based on previous results in the literature (Lapierre et al. 2004, Dauwe et al. 2007, Baucher et al. 1996), it was anticipated that RNAi down regulated *CAD* would possess reduced lignin levels. UVR8 is expressed in shoots and leaves and even in roots that are not directly exposed to UV-B radiation and this may be associated with the range of UV-B tolerance throughout the plant (Tossi et al. 2019). Furthermore, lignin levels may be different in leaves versus stems, which may in turn show differences in UV-B sensitivity. Only the response in the leaves was evaluated in this work so it is difficult to fully assess the global response in these plants. Though lignin levels were not measured directly in *CAD*-regulated transgenic plants in this study, alterations would affect other precursors and metabolites in the phenylpropanoid pathway measured from UV-B treated leaves. Also, it was expected that up-regulation of *UVR8* expression would result in a more robust acclimation response, with plants exhibiting an increase in tolerance to UV-B radiation stemming from an increase in the production of anthocyanins and flavonoids. By contrast, it was expected that *UVR8* knockout lines would be more susceptible to UV-B radiation – if they survived at all. Interestingly, mutant *Arabidopsis* plants with disruptions to *UVR8* expression showed dwarf phenotypes, which were exacerbated when treated with UV-B radiation. In fact, those seminal observations with *Arabidopsis* resulted in some

hesitation at the design stage of the project since there was concern that considerable effort would be devoted to the construction of plants that would not survive. However, as described here, the phenotypes of up- and down-regulated *UVR8* expression in poplar were quite distinct from those seen in *Arabidopsis*, and very surprising.

Limited time permitted only the most general, initial characterization of the transgenic plant lines constructed. However, useful clues on the molecular basis for UV-B acclimation and tolerance in poplar were able to be gleaned from the findings. Despite the variation among the small set of biological replicates investigated, it was generally seen that the lines with reduced *UVR8* expression were less shielded based on chlorophyll fluorescence measurements, and were only able to synthesize lower levels of protective flavonoids compared to plants that overexpressed *UVR8*. When examined in a little more detail, metabolomics analyses demonstrated that quercetin levels were relatively low in *UVR8* knockout transgenic lines, but in *UVR8* overexpressing poplar lines, their production was significantly increased, consistent with the expectation that UVR8 enables plants to better acclimate to UV-B radiation. By contrast, the concentrations of salicylates were increased in *UVR8* knockout lines relative to wild-type and *UVR8* overexpression poplar lines, and the salicylate concentrations increased substantially in *UVR8* knockout lines treated with UV-B radiation. These changes may reflect the increased stress that may be experienced by *UVR8* knockout plants, especially in the presence of UV-B, or may relate to initial shifts in metabolite pools as the plant begins mobilization of resources to enable acclimation to UV-B as was noted previously with *Populus trichocarpa* (Mellway et al. 2009, Warren et al. 2003, Baucher et al. 1997, Dauwe et al. 2007).

The most surprising, and indeed, striking result observed with the *UVR8* modified transgenic poplar lines was the effect of the either overexpression or knockout of *UVR8* on the growth of plants. As mentioned above, *UVR8* knockout mutants, or *UVR8* overexpressing transgenic *Arabidopsis* lines, showed dwarf phenotypes, and exhibit even further growth inhibition in the presence of UV-B treatment. However, *UVR8* knockout and overexpressing *Populus* lines grew normally, at least at the juvenile stages used in these studies. Interestingly, however, was the effect of UV-B radiation on growth. Roughly three weeks after treatment of wild-type and *UVR8* modulated poplar with UV-B radiation, the mutant lines grew identically, and much faster to greater heights than wild-type poplar. This observation is intriguing, and potentially very important, not only for poplar, but perhaps for other plant species as well, especially if these observations hold true in economically important crops. A hypothesis for the effects seen in the UVR8 mutant lines is presented in Chapter 6.

A key question in this phase of the project was to examine the effect of modulating *UVR8* expression on the acclimation of poplar to UV-B radiation in order to provide clues on how low lignin plants might compensate for defects in an important protective component against radiation damage. Although some general clues were generated, which generally fit within existing models for the role of UVR8 in plants, the poplar system was quite complicated, presented several challenges for detailed analyses, and many good questions remain unresolved. For example, comprehensive system-wide metabolomics analyses would be very useful in resolving the changes to poplar metabolism that enable low lignin

plants to survive, and may yield additional information on perturbations that could be introduced into poplar to increase the response to UV-B and maintain fitness in the absence of extensive lignin.

Chapter 6: A Hypothesis for the Influence of Cellular UVR8 Concentration on the Rapid Growth Phenotype of Transgenic *Populus*

The motivation of this work was to investigate the molecular mechanisms for UV-B acclimation in a range of *Populus* variants with altered lignin levels to address one of the challenges in developing improved plant feedstocks for use as biofuel or in the development of bioproducts. A variety of approaches were employed to glean clues on the metabolic responses in poplar that are induced upon treatment to UV-B. Ecophysiological measurements were performed on natural poplar variants in an effort to correlate photo-shielding with growth elevation or with differing lignin content. Because of the considerable variation of responses to UV-B from the range of biological samples investigated, upstream factors in UV-B acclimation and tolerance were examined. The tremendous genomic sequencing resources available for *Populus* provided the impetus to look at variation in expression of the key UV-B photoreceptor in green plants, UVR8. Single nucleotide polymorphisms (SNPs) that might alter transcription, splicing of the 11 intron regions to generate mRNA, and photoreceptor structure and function, were examined. Interestingly, the analysis the *UVR8* gene locus revealed a paucity of SNPs that might promote deleterious effects on photoreceptor expression, structure or function, suggesting that its cellular concentration may be tightly regulated to coordinate for optimal responses to UV-B. These analyses, and the breathtaking advances in gene editing using

CRISPR based approaches, motivated a shift in direction to directly modulate the expression of *UVR8* in wild-type and in a poplar variant that was defective in the biosynthesis of phenylpropanoids, key precursors of lignin. This effort led to the construction and analysis of several useful poplar transgenic lines. Analysis of these plants conformed to expectations with respect to the role of UVR8 in enhancing acclimation to UV-B by activating flavonoid biosynthesis, which may be important in low-lignin poplars. These resources will continue to be of value to the collaborating laboratories that are engaged with this research, as well as to the field in general.

The most striking, and surprising observation of the constructed *Populus* transgenic lines involved the rate and extent of growth relative to wild-type plants. However, results on *UVR8* knockout plants as well as constitutively active UVR8 variants in *Arabidopsis* initially limited enthusiasm for this line of research. In *Arabidopsis*, *UVR8* knockout and constitutively active UVR8 lines exhibited a dwarf phenotype and look compromised relative to wild-type plants (Heijde et al. 2013). These differences were exacerbated when plants are treated with UV-B radiation. Thus, there was concern that despite investing considerable effort to construct transgenic poplar lines in which *UVR8* expression was modulated, the plants would not survive subculturing and experimental exposure conditions. However, that turned out not to be the case.

Both the *UVR8* knockout (48.31 cm $\pm$ 1.32) and *UVR8* overexpression (47.91 cm $\pm$ 1.65) transgenic poplar lines appear to grow faster and to greater heights than similarly reared and treated wild-type (33.49 cm $\pm$ 0.53) plants. Thus, not only was the dwarf phenotype

described for *Arabidopsis* not observed, but the transgenic poplar lines looked healthy. This unexpected observation was surprising and warrants further investigation, not only in poplar, but in a range of agriculturally important crops.

In order to account for the unexpected observations of the *UVR8* knockout and overexpression lines constructed in this study, it is useful to review the groundbreaking results on UVR8 using *Arabidopsis*, where the genetics and the relative ease of constructing and propagating stable transgenic lines, and using them in subsequent constructions, has significantly advanced our understanding. It is in this light that an interpretation of the influence of cellular UVR8 concentrations can be considered.

UVR8 Plays a Central Role in the Proposed Molecular Mechanisms of UV-B Acclimation – Ever since the striking discovery that UVR8 plays a key role in mediating responses to UV-B radiation in plants (Kliebenstein et al. 2002, Rizzini et al. 2011), tremendous effort has been focused to elucidate two key components concerning the molecular mechanism for photomorphogenesis and UV-B acclimation. First, significant progress has been made in elucidating the perception of UV-B radiation by UVR8, and second, ongoing research continues to reveal a growing repertoire of factors that signal significant changes in a host of physiological responses. The significant body of work, mainly undertaken in the tractable plant model *Arabidopsis thaliana*, has laid a useful foundation to dissect the role of UVR8 in *Populus*, a useful model for trees.

A consensus has emerged for UVR8 perception and signaling of UV-B radiation in plants. UVR8 is a homodimer, and its cytoplasmic concentration seems unaffected by light, although UV-B radiation promotes a redistribution of UVR8 to the nucleus. When UVR8 absorbs UV-B radiation, it readily dissociates to monomers, which have been shown to interact with a number of regulatory factors involved in light signaling. Early research identified COP1 (CONSTITUTIVELY PHOTOMORPHOGENIC 1) as a key target. COP1 is an E3 ubiquitin ligase, which functions in photomorphogenesis by targeting HY5 (ELONGATED HYPOCOTYL 5), a transcription factor for genes involved in the initiation of photomorphogenesis, for ubiquitinoylation and proteolysis. Thus, COP1-mediated degradation of HY5 results in attenuated growth, and a repression of photomorphogenesis. When COP1 binds to monomeric UVR8, COP1 is unavailable to target HY5, thereby promoting photomorphogenesis. Among the genes activated by UV-B irradiation of plants are the *RUP* (REPRESSOR OF UV-B PHOTOMORPHOGENESIS) genes, RUP1 and RUP2. The RUP1 and RUP2 proteins are thought to provide negative feedback to the UV-B response by facilitating the dissociation of UVR8-COP1 complexes, allowing UVR8 monomers to reform into dimers. This simple model is illustrated in Fig. 6-1.

Research on UV acclimation in *Arabidopsis* has been indispensable as it enabled the construction mutant lines and the heterologous expression of modified *UVR8* variants to further characterize the mechanisms of UV-B promoted photomorphogenesis and signal transduction. The first breakthrough was realized by Kliebenstein et al. (2002) in the generation of a mutant *Arabidopsis* line that was hypersensitive to chronic UV-B irradiation that contained a 15 bp deletion in a gene with similarity to the human Regulator

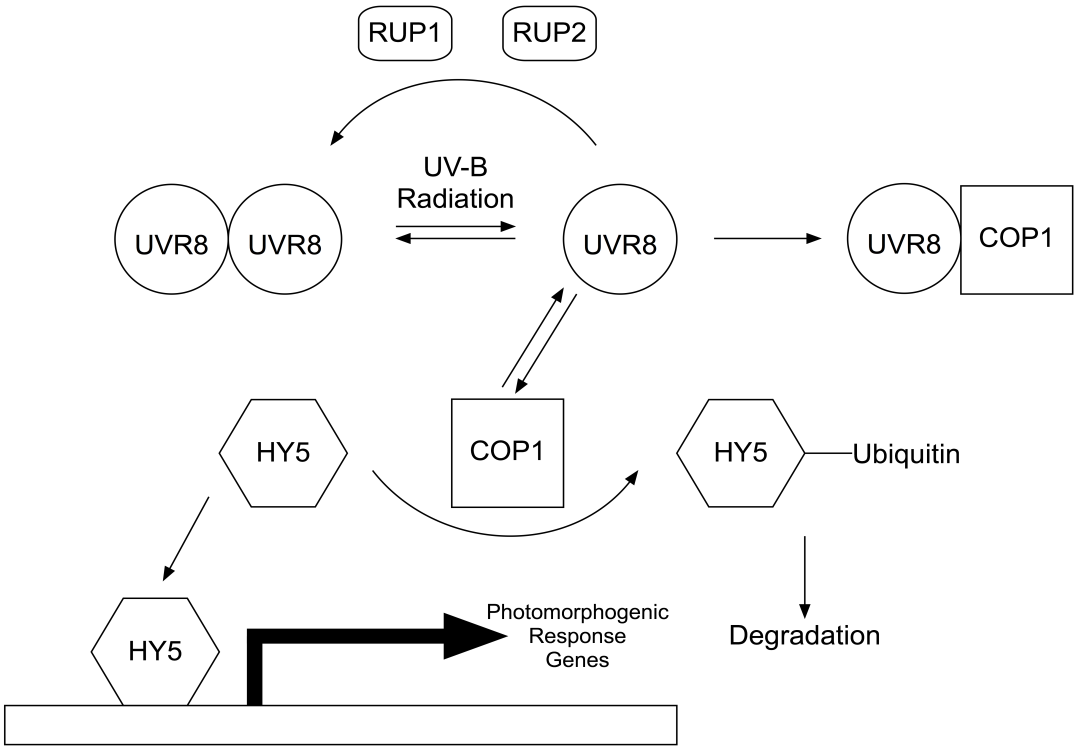

Figure 6-1. Simplified model of the UVR8 signal transduction in *Arabidopsis*. The UVR8 photoreceptor is linked to a molecular signaling pathway that leads to acclimation to UV-B radiation via positive and negative regulation of transcription factors.

of Chromatin Condensation 1 (RCC1), which was designated *UVR8* (Rizzini et al. 2011, Duanmu et al. 2017, Kliebenstein et al. 2002). Interestingly, the *uvr8-1* mutant line was identified in a chalcone synthase-knockdown, *tt4 Arabidopsis* line, that was already UV-B hypersensitive in that it showed decreased accumulation of flavonoids (Li et al. 1993, Landry et al. 1995).

However, the *uvr8-1* mutant was distinguished phenotypically by necrosis on the youngest leaves, reductions of up to 50% in accumulation of flavonoids relative to wild-type plants, and the lack of induction of the chalcone synthase gene, *CHS*, as evidenced by a decrease in *CHS* mRNA upon UV-B treatment. Additional *UVR8* mutant lines were constructed using reporter lines with luciferase fused to either the *CHS* promoter (Brown et al. 2005), or the *HY5* promoter (Favory et al. 2009), which recapitulated the original findings and extended them to highlight the essential role of HY5 in mediating UV-B responses.

The identification of the *UVR8* gene in *Arabidopsis* spawned several additional genetic studies that resulted in gene knockout and over-expressed *UVR8* variants, as well as the introduction of mutant *UVR8* alleles into stable lines, to probe tenets of working models for molecular mechanisms of UV-B acclimation (Paul and Gwynn-Jones, 2003, Rizzini et al. 2011, Christie et al. 2012, O'Hara and Jenkins 2012, Wu et al. 2012, Heijde et al. 2013, Huang et al. 2014, Heilmann et al. 2016, Podolec et al. 2021). Of particular interest are single amino acid replacements, constructed either by site-directed mutagenesis or discovered by genetic selection. For example, a W285F substitution in one of the key tryptophan residues of *Arabidopsis* UVR8 was found to be a relatively stable dimer that

was primarily an inactive homodimer, and thus was unresponsive to UV-B treatment (O'Hara and Jenkins 2012). By contrast, the W285A mutation results in a monomeric variant of UVR8, which interacts constitutively with COP1. Although an N-terminal GFP fusion of UVR8-W285A did not display an altered phenotype under normal growth conditions, it lacked a UV-B response (O'Hara and Jenkins 2012). However, expression of the un-complexed UVR8-W285A variant in *Arabidopsis* plants exhibited constitutive photomorphogenesis and enhanced acclimation-independent UV-B tolerance, suggesting that the N-terminus of UVR8 contributes to activity, and is impaired in N-terminal fusions. Two additional variants of UVR8, UVR8-D96N, D107N (Heilmann et al. 2016) and UVR8-G101S (*uvr8-17D*) (Podolec et al. 2021) are also stabilized as monomers, yet require UV-B to promote physiological responses. Perhaps most striking are the *Arabidopsis* phenotypes observed when *UVR8* null mutants are compared to either wild-type, C-terminal GFP fusions, or mutant *UVR8* alleles that are overexpressed using the cauliflower mosaic virus 35S promoter. Interestingly, both *UVR8* null mutants, and overexpression of wild-type, or active variants of UVR8, show pronounced dwarf growth phenotypes. These observations have been explained by the apparent high-sensitivity of the UVR8 photoreceptor system. These observations are in sharp contrast to what was observed in this study with poplar variants with modulated UVR8 expression.

The described genetic studies in *Arabidopsis* were enabled by another breakthrough in UVR8 research: the elucidation of the three-dimensional structure of the receptor (Wu et al. 2012, Zeng et al. 2015). The x-ray crystal structure of the core domain of *Arabidopsis* UVR8 is dimeric and belongs to the family of seven-bladed β-propeller proteins.

Interestingly, the dimer interface is mediated by a network of salt bridges, which must be disrupted to promote the formation of monomers for signaling. Of additional interest was the realization that a specific group of tryptophan residues were arranged in a pyramid conformation at the dimer interface. These residues are thought to capture UV-B radiation and upon electronic excitation, promote disruption of the interfacial salt bridges to promote the formation of monomers, which are the active units of the photoreceptor as they are capable of binding to host factors involved in photomorphogenesis.

Recently it has been recognized that UVR8 interacts with a host of other proteins that initiate a wide range of responses within the so-called photomorphogenic response. And several previously characterized transcription factors have been identified as targets of UVR8. For example, it has been shown in *Arabidopsis* that UVR8 monomers bind to WRKY36 (Yang et al. 2018). WRKY36 binds to the HY5 promoter to repress transcription. Thus, interaction of UVR8 monomers with WRKY36 result in an increase in HY5, and therefore promote expression of photomorphogenic response genes. Additionally, BIM1 and BES1 are transcription factors that mediate brassinosteroid signaling and stimulate growth. The binding of monomeric UVR8 to these factors results in the suppression of brassinosteroid responsive genes and, consequently, a suppression of plant growth (Liang et al. 2018). Finally, the transcription factors MYB73 and MYB77 regulate genes involved in auxin-controlled responses. A competition between the binding of these factors to monomeric UVR8 and their promoters results in an attenuation of gene activation and thus an inhibition of auxin-stimulated growth (Yang et al. 2020).

Studies with purified protein suggest that UVR8 monomers reassociate to form dimers over many hours. However, *in vivo* the process is thought to occur much more rapidly with the facilitation of RUP1 and RUP2. By promoting dimerization of UVR8, the RUP proteins attenuate responses triggered by UVR8 monomers. Additionally, the expression of RUP genes is stimulated by UV-B, mediated by UVR8, COP1 and HY5, providing negative feedback. RUP proteins may also comprise components of an E3 ubiquitin ligase that targets HY5 for degradation. Furthermore, by binding to the same 27-amino acid sequence in the intrinsically disordered domain at the C-terminus of UVR8, COP1 antagonizes the action of the RUP proteins by mediating their proteolysis (Cloix et al. 2012, Lin et al. 2020). In fact, the same 27-residue region of UVR8 is also thought to mediate UVR8 binding to WRKY36, BIM1 and BES1 (Liang et al. 2018, Yang et al. 2018, Lin et al. 2020, Yang et al. 2020).

Despite the relative complexity and some unexpected observations with mutants of UVR8, the vast majority of data on its role in photomorphogenesis and UV-B acclimation is readily explained by the simple model described above. However, very recent observations, and work described here, suggest a more elaborate model may be operative.

Unusual Phenotypes of Transgenic Populus Lines with Modulated UVR8 Expression – It was surprising that both the UVR8 knockout and the UVR8 overexpression transgenic poplar lines exhibited robust growth relative to wild-type plants. Based on the literature summarized above, it was expected that poplar variants with modulated *UVR8* expression would display properties similar to *Arabidopsis*: *UVR8* knockout lines would exhibit a

dwarf phenotype which would be relatively unaffected by UV-B treatment, and that *UVR8* overexpressing lines would also exhibit a dwarf growth phenotype, but which would be exacerbated by UV-B treatment (Heijde et al. 2013).

Based on the previous work in *Arabidopsis*, a dramatic growth phenotype was observed in the modulated *UVR8* transgenic poplars and may be difficult to explain. However, it is worthwhile to consider that UVR8 may function quite differently in other plants since some species contain multiple copies containing conserved regions crucial for UV-B perception (Fernandez et al. 2016). Also, the responses seen in different plants may reflect contributions from UV-B acclimation to low levels of supplementary radiation or may stem from UV-B promoted stress (Czégény et al. 2016). More extensive analysis of poplar, at various stages of growth and under a variety of illumination conditions, would help clarify the distinction between these two UVR8-promoted adaptations. It is possible, as described recently, that in addition to the role of UV-B in dissociating UVR8 dimers to monomers, UV-B may also act directly on monomers to effect a conformational change of UVR8 into a more extended, activated state, that more binds more strongly to host factors to activate physiological effects (Camacho et al. 2019, Liao et al. 2020). On the other hand, the molecular mechanism of UVR8 action could be more complex than the simple model described above. First, UVR8 may not be exclusively dimeric in UV-B acclimated plants, and the dimer may not be completely converted to monomers when exposed to elevated levels of UV-B radiation. This 'photo-equilibrium' is also dependent on RUP proteins, and it is thought that the rate of UV-B promoted dissociation of dimers is balanced by RUP-mediated dimerization of monomers. Thus, it is possible that UVR8 does not

function as a simple dimer-to-monomer on/off switch in mature, light-grown, UV-B acclimated plants (Liao et al. 2020).

A Simple, Photo- and Chemical-Equilibrium Hypothesis for UVR8 in Photomorphogenesis in Populus – It is assumed that UVR8 in *Populus* is generally analogous to *Arabidopsis* UVR8 in that it is active as a monomer, then the growth phenotypes seen with the transgenic lines suggest that UVR8 monomers play an additional, significant role to constrain poplar growth due to considerations involving chemical equilibria. Thus, it is hypothesized that in poplar, UVR8 may operate according to a photo-chemical-equilibrium, in which both UV-B promoted dissociation of dimeric UVR8, and concentration-dependent dissociation (and re-association) of UVR8 monomers play a role in physiological activation. The photomorphogenic effects could certainly be mediated by interaction of UVR8 monomers with transcription factors homologous to those described above. Thus, in the absence of UVR8, as is the case in CRISPR-promoted knockout variants, an increase in growth is seen relative to wild-type plants because there are no UVR8 monomers to compete for binding with growth-stimulating transcription factors bound to their promoter sites. And that when UVR8 is overexpressed in poplar, the increase in protein concentration drives the assembly equilibrium significantly in the direction of dimer, thereby decreasing monomeric UVR8 concentration. These considerations suggest that if UVR8 monomers are able to bind factors to promote transcription regulation, then adjusting concentrations of UVR8 would re-configure the linked equilibria to control the function of these effectors and their physiological outputs. Based on the observed growth phenotypes for the UVR8-modulated poplar lines described

here, it is possible that the absence of active UVR8 monomers precludes an interaction with a transcription factor regulating growth, which is unattenuated in the absence of a functional unit of UVR8.

The basis for this simple photo-chemical-equilibrium hypothesis is that all oligomeric proteins dissociate to monomers at some, albeit in many cases, low protein concentrations. This can be seen from the simple equilibrium considerations below to express the fraction monomer and dimer relative to the total protein concentration[1].

For a dimerization reaction (like that for UVR8):

$$2\,M \leftrightarrow D$$

In which a dissociation constant, K_d, can be defined as:

$$K_d = [M]^2 / [D]$$

Where [M] is the concentration of monomeric UVR8 and [D] is the concentration of dimeric UVR8.

Let α = the fraction of monomer, so:

$$[M] = \alpha * C_{total}$$

[1] Not the free protein concentration as is customary in binding analyses.

Where C_{total} is the total protein concentration (the concentration of dimers and monomers) and by substitution therefore:

$$[D] = (1 - \alpha)\, C_{total}$$

Substituting [M] and/or [D] into the expression for K_d, one obtains:

$$K_d = \alpha^2 * C_{total}^2 / ((1 - \alpha) * C_{total}) = \alpha^2 / (1 - \alpha) * C_{total}$$

When there is an equivalent concentration of monomers and dimers, then the fraction monomer, α, is 0.5, and therefore:

$$K_d = \alpha^2 / (1 - \alpha) * C_{total}$$

or

$$C_{total}/K_d = (1 - \alpha) / \alpha^2$$

Where C_{total}/K_d is the total protein concentration normalized to the dissociation constant. Therefore, letting $\alpha = 0.5$:

$$C_{total}/K_d = 0.5 / (0.5)^2 = 2$$

Thus, the total protein concentration at which there is an equal mixture of monomers and dimers occurs at:

$$C_{total} = 2 * K_d$$

The total protein concentration dependence of monomer or dimer can be seen in the Fig. 6-2.

According to Le Chatelier's Principle, at protein concentrations well below the dissociation constant, the vast majority of protein is in a monomeric state, whereas at higher concentrations, the dimeric state predominates. This is likely the case for UVR8, which at physiological levels is doubtless present in 100- to even 1000-fold higher concentrations relative to the dimer-monomer dissociation constant. But even at these concentrations, measurable monomer is present, and this species may interact with a factor to regulate growth of poplar. When UVR8 is deleted, obviously, there are no monomers to interact with factors that regulate growth, and therefore the line is unable to sustain growth inhibition and grows more robustly than wild-type poplar. By contrast, when the expression of UVR8 is increased 50- to 100-fold by transcription from the 35S promoter, there would be a significant increase in the total UVR8 concentration, thereby increasing dimer concentration while concomitantly reducing monomer concentration. The reduction of monomers would again deplete any UVR8 complexes that required to manage growth, and similarly to the knockout lines, the variants grow more robustly than wild-type poplar. The simple photo- chemical- equilibrium hypothesis is summarized in Fig. 6-3.

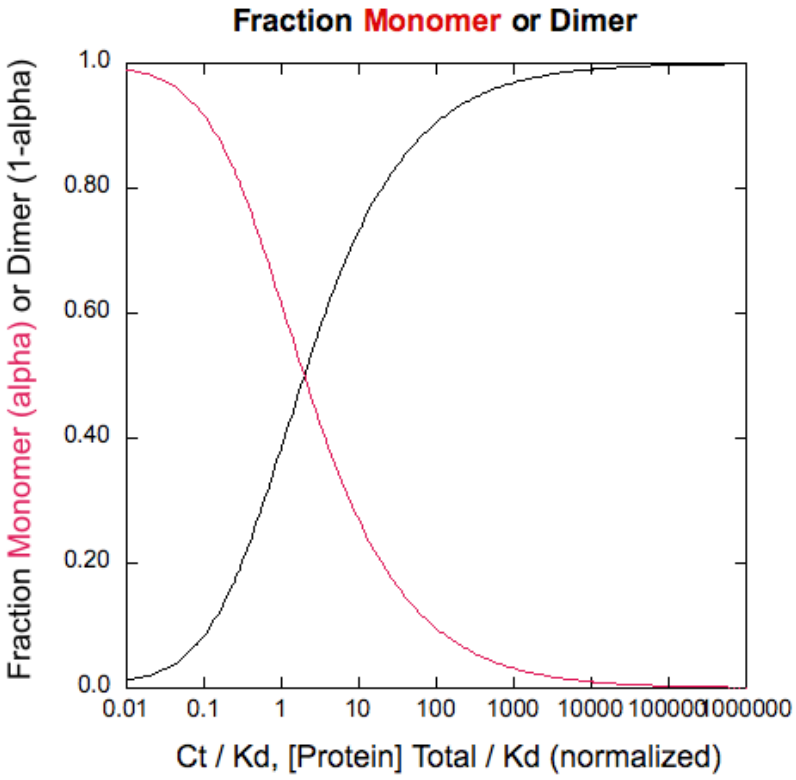

Figure 6-2. The total protein concentration dependence of monomer or dimer.

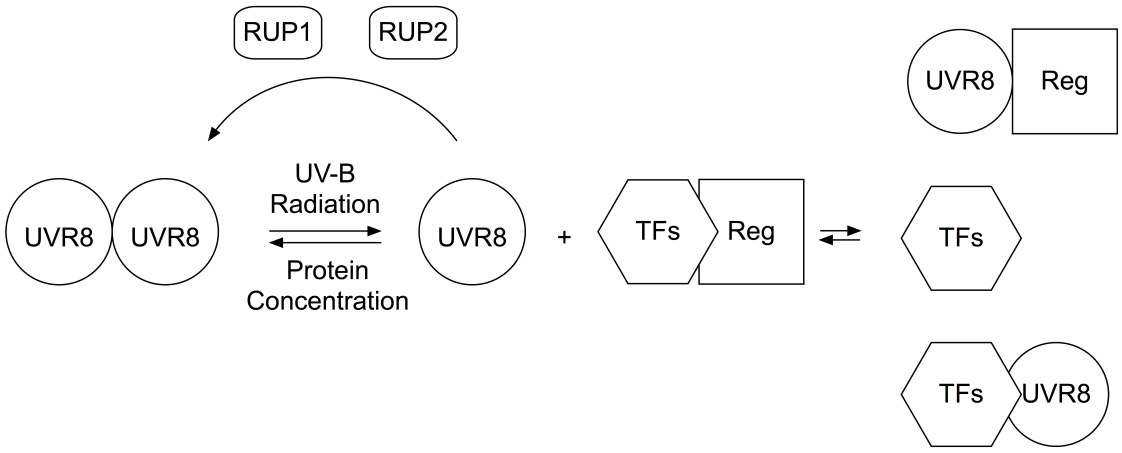

Figure 6-3. A photo- chemical- equilibrium hypothesis for the transcriptional control by UVR8. At rest, UVR8 dimers can be converted to monomers by UV-B radiation, and reconverted to dimers by the action of RUP proteins, but the monomer-dimer interconversion is also governed by Le Chatelier's principle. In this way, at high total protein concentrations, above the dissociation constant, the dimeric species would predominate, and low, dilute total protein concentrations, the monomeric species would predominate. The monomer is considered the 'active' species in that it interacts with a number of factors that control transcription, either by up- or down-regulating gene expression. Thus, UVR8 can bind negative regulators (shown as squares labeled Reg) to free transcription factors (shown as hexagons labeled TFs) for gene activation (as in the case with COP1 binding to UVR8 to stabilize HY5 for transcription activation) or UVR8 can bind directly to transcription factors such as in the case of WRKY36, BIM1 and BES1, or MYB73 and MYB77, to derepress the transcription of HY5, suppress brassinosteroid response genes, or attenuation of auxin-stimulated growth.

Additional research is needed to test this hypothesis, and new findings may yield novel approaches to enhance plant growth, not only for poplar, but for other plants as well. Indeed, there are many approaches that could, and should be considered in evaluating the photo-chemical equilibrium hypothesis for UVR8 action in poplar. For instance, as a simple extension to the present studies, it may be possible using newer, more precise CRISPR activation systems (Pan et al. 2021), to incrementally adjust the expression (and inhibition) level of UVR8 in transgenic poplar. It would be of interest to examine dose-response effects of UVR8 on the various UV-B promoted responses. Alternatively, direct measures of UVR8 protein concentrations could be made using mass spectrometry. Although this approach is outside the current expertise of collaborating laboratories, the question is worthy of study and new collaborations could therefore be established. Finally, large-scale genomic studies could be pursued to establish the transcriptional profiles of poplar that are modulated for *UVR8* expression under UV-B challenges, to characterize the genes involved in photomorphogenesis and stress to see if these responses play a role in the observed growth phenotypes.

References

Abramowicz, A. and M. Gos (2018). "Splicing mutations in human genetic disorders: examples, detection, and confirmation." Journal of applied genetics **59**(3): 253-268.

Abreu, I.N., M. Ahnlund, T. Moritz and B. R. Albrectsen (2011). "UHPLC-ESI/TOFMS determination of salicylate-like phenolic glycosides in Populus tremula leaves." Journal of chemical ecology **37**(8): 857-870.

Albert, K. R., T. N. Mikkelsen, H. Ro-Poulsen, A. Michelsen, M. F. Arndal, L. Bredahl, K. B. Håkansson, K. Boesgaard and N. M. Schmidt (2010). "Improved UV-B screening capacity does not prevent negative effects of ambient UV irradiance on PSII performance in High Arctic plants. Results from a six year UV exclusion study." Journal of Plant Physiology **167**(18): 1542-1549.

Allwright, M. R. and G. Taylor (2016). "Molecular Breeding for Improved Second Generation Bioenergy Crops." Trends Plant Sci **21**(1): 43-54.

Altpeter, F., N. M. Springer, L. E. Bartley, A. E. Blechl, T. P. Brutnell, V. Citovsky, L. J. Conrad, S. B. Gelvin, D. P. Jackson, A. P. Kausch, P. G. Lemaux, J. I. Medford, M. L. Orozco-Cardenas, D. M. Tricoli, J. Van Eck, D. F. Voytas, V. Walbot, K. Wang, Z. J. Zhang and C. N. Stewart, Jr. (2016). "Advancing Crop Transformation in the Era of Genome Editing." Plant Cell **28**(7): 1510-1520.

An, Y., Y. Geng, J. Yao, C. Fu, M. Lu, C. Wang and J. Du (2020). "Efficient Genome Editing in Populus Using CRISPR/Cas12a." Front Plant Sci **11**: 593938.

Appenzeller, T. (1993). "Filling a hole in the ozone argument." Science **262**(5136): 990-991.

Armarego-Marriott, T., O. Sandoval-Ibanez and L. Kowalewska (2020). "Beyond the darkness: recent lessons from etiolation and de-etiolation studies." J Exp Bot **71**(4): 1215-1225.

Ayabe, S. I. and T. Akashi (2006). "Cytochrome P450s in flavonoid metabolism." Phytochemistry Reviews **5**(2-3): 271-282.

Azeez, A. and V. Busov (2021). "CRISPR/Cas9-mediated single and biallelic knockout of poplar STERILE APETALA (PopSAP) leads to complete reproductive sterility." Plant Biotechnol J **19**(1): 23-25.

Babst, B. A., H. Y. Chen, H. Q. Wang, R. S. Payyavula, T. P. Thomas, S. A. Harding and C. J. Tsai (2014). "Stress-responsive hydroxycinnamate glycosyltransferase modulates phenylpropanoid metabolism in Populus." J Exp Bot **65**(15): 4191-4200.

Bae, E. K., H. Choi, J. W. Choi, H. Lee, S. G. Kim, J. H. Ko and Y. I. Choi (2021). "Efficient knockout of the phytoene desaturase gene in a hybrid poplar (Populus alba x Populus glandulosa) using the CRISPR/Cas9 system with a single gRNA." Transgenic Res.

Bais, A. F., R. L. McKenzie, G. Bernhard, P. J. Aucamp, M. Ilyas, S. Madronich and K. Tourpali (2015). "Ozone depletion and climate change: impacts on UV radiation." Photochem Photobiol Sci **14**(1): 19-52.

Baker, N. R. (2008). "Chlorophyll fluorescence: a probe of photosynthesis in vivo." Annu Rev Plant Biol **59**: 89-113.

Ballare, C. L. (2003). "Stress under the sun: spotlight on ultraviolet-B responses." Plant Physiol **132**(4): 1725-1727.

Ballare, C. L., M. M. Caldwell, S. D. Flint, S. A. Robinson and J. F. Bornman (2011). "Effects of solar ultraviolet radiation on terrestrial ecosystems. Patterns, mechanisms, and interactions with climate change." Photochem Photobiol Sci **10**(2): 226-241.

Barber, J. and B. Andersson (1992). "Too much of a good thing: light can be bad for photosynthesis." Trends in Biochemical Sciences **17**(2): 62-66.

Barnes, P. W., C. L. Ballare and M. M. Caldwell (1996). "Photomorphogenic Effects of UV-B Radiation on Plants: Consequences for Light Competition." Journal of Plant Physiology **148**(1-2): 15-20.

Barnes, P. W., S. D. Flint, J. R. Slusser, W. Gao and R. J. Ryel (2008). "Diurnal changes in epidermal UV transmittance of plants in naturally high UV environments." Physiol Plant **133**(2): 363-372.

Barnes, P. W., M. A. Tobler, K. Keefover-Ring, S. D. Flint, A. E. Barkley, R. J. Ryel and R. L. Lindroth (2016). "Rapid modulation of ultraviolet shielding in plants is influenced by solar ultraviolet radiation and linked to alterations in flavonoids." Plant cell and environment **39**(1): 222-230.

Basioumy, P. M. and R. H. Biggs (1975). Photosynthetic and carbonic anhydrase activities in Zn-deficient peach seedlings exposed to UV-B radiation. Impacts of Climate Change on the Biosphere Washingtoin, DC, Department of Transportation. **DOT-TST-75-55**.

Basu, S., V. Ramegowda, A. Kumar and A. Pereira (2016). "Plant adaptation to drought stress." F1000Res **5F1000** Faculty Rev-1554.

Baucher, M., B. Chabbert, G. Pilate, J. Van Doorsselaere, M. T. Tollier, M. Petit-Conil, D. Cornu, B. Monties, M. Van Montagu, D. Inzé and L. Jouanin (1996). "Red xylem and higher lignin extractability by down-regulating a cinnamyl alcohol dehydrogenase in poplar." Plant physiology **112**(4): 1479-1490.

Baxter, H. L. and C. N. Stewart, Jr. (2013). "Effects of altered lignin biosynthesis on phenylpropanoid metabolism and plant stress." Biofuels **4**(6): 635-650.

Beerli, R. R., D. J. Segal, B. Dreier and C. F. Barbas, 3rd (1998). "Toward controlling gene expression at will: specific regulation of the erbB-2/HER-2 promoter by using polydactyl zinc finger proteins constructed from modular building blocks." Proc Natl Acad Sci U S A **95**(25): 14628-14633.

Beggs, C. J., U. Schneider-Ziebert and E. Wellmann (1986). UV-B radiation and adaptive mechanisms in plants. Stratospheric Ozone Reduction, Solar Ultraviolet Radiation and Plant Life. R. C. Worrest and M. M. Caldwell. Berlin, Heidelberg, Springer-Verlag**:** 235-250.

Belén, F. M., L. Lorenzo and C. Raúl (2019). "Functional analysis of the UVR8 photoreceptor from the monocot Zea mays." bioRxiv: 649905.

Bennett, P. V., M. Hada, J. Hidena, A. M. Lepre, L. C. Pope, F. E. Quaite, J. H. Sullivan, S. Takayangi, J. C. Sutherland and B. M. Sutherland (2001). "Isolation of high molecular length DNA: alfalfa, pea, rice, sorghum, soybean and spinach." Crop Science **41**: 167-172.

Berkey, R., Y. Zhang, X. Ma, H. King, Q. Zhang, W. Wang and S. Xiao (2017). "Homologues of the RPW8 Resistance Protein Are Localized to the Extrahaustorial Membrane that Is Likely Synthesized De Novo." Plant Physiol **173**(1): 600-613.

Bewg, W. P., D. Ci and C. J. Tsai (2018). "Genome Editing in Trees: From Multiple Repair Pathways to Long-Term Stability." Front Plant Sci **9**: 1732.

Bhuiyan, N. H., G. Selvaraj, Y. Wei and J. King (2009). "Role of lignification in plant defense." Plant Signal Behav **4**(2): 158-159.

Bilger, W., T. Johnsen and U. Schreiber (2001). "UV-excited chlorophyll fluorescence as a tool for the assessment of UV-protection by the epidermis of plants." Journal of Experimental Botany **52**(363): 2007-2014.

Bilger, W., M. Veit, L. Schreiber and U. Schereiber (1997). "Measurement of leaf epidermal transmittance of UV radiation by chlorophyll fluorescence." Physiol Plant **101**(754-763).

Boerjan, W., J. Ralph and M. Baucher (2003). "Lignin biosynthesis." Annu Rev Plant Biol **54**: 519-546.

Bogenrieder, A. and R. Klein (1982). Does solar UV influence the competitive relationship in higher plants? . The role of solar ultraviolet radiation in marine ecosystems. J. Calkins. New York, Plenum**:** 641-649.

Bornman, J.F. (1989). "New trends in photobiology: Target sites of UV-B radiation in photosynthesis of higher plants." Journal of Photochemistry and Photobiology B: Biology **4**(2): 145-158.

Brenna, H., S. Kutterolf and K. Kruger (2019). "Global ozone depletion and increase of UV radiation caused by pre-industrial tropical volcanic eruptions." Sci Rep **9**(1): 9435.

Britt, A. B. (1996). "DNA Damage and Repair in Plants." Annu Rev Plant Physiol Plant Mol Biol **47**: 75-100.

Brown, B. A., C. Cloix, G. H. Jiang, E. Kaiserli, P. Herzyk, D. J. Kliebenstein and G. I. Jenkins (2005). "A UV-B-specific signaling component orchestrates plant UV protection." Proc Natl Acad Sci U S A **102**(50): 18225-18230.

Brown, B. A. and G. I. Jenkins (2008). "UV-B signaling pathways with different fluence-rate response profiles are distinguished in mature Arabidopsis leaf tissue by requirement for UVR8, HY5, and HYH." Plant Physiol **146**(2): 576-588.

Burchard, P., W. Bilger and G. Weissenböck (2000). "Contribution of hydroxycinnamates and flavonoids to epidermal shielding of UV-A and UV-B radiation in developing rye primary leaves as assessed by ultraviolet-induced chlorophyll fluorescence measurements." Plant Cell and Environment **23**(12): 1373-1380.

Butelli, E., L. Titta, M. Giorgio, H. P. Mock, A. Matros, S. Peterek, E. G. Schijlen, R. D. Hall, A. G. Bovy, J. Luo and C. Martin (2008). "Enrichment of tomato fruit with health-promoting anthocyanins by expression of select transcription factors." Nat Biotechnol **26**(11): 1301-1308.

Caffarri, S., T. Tibiletti, R. C. Jennings and S. Santabarbara (2014). "A comparison between plant photosystem I and photosystem II architecture and functioning." Curr Protein Pept Sci **15**(4): 296-331.

Caldwell, M. M. (1968). "Solar Ultraviolet Radiation as an Ecological Factor for Alpine Plants." Ecological Monographs **38**(3): 243-268.

Caldwell, M. M., R. Robberecht and S. D. Flint (1983). "Internal filters: prospects for UV-acclimation in higher plants." Physiologia Plantarum **58**(3): 445-450.

Camacho, I. S., A. Theisen, L. O. Johannissen, L. A. Diaz-Ramos, J. M. Christie, G. I. Jenkins, B. Bellina, P. Barran and A. R. Jones (2019). "Native mass spectrometry reveals the conformational diversity of the UVR8 photoreceptor." Proc Natl Acad Sci U S A **116**(4): 1116-1125.

Casati, P. and V. Walbot (2004). "Rapid transcriptome responses of maize (Zea mays) to UV-B in irradiated and shielded tissues." Genome Biol **5**(3): R16.

Caseys, C., G. Glauser, K. N. Stölting, C. Christe, B. R. Albrectsen and C. Lexer (2012). "Effects of interspecific recombination on functional traits in trees revealed by metabolomics and genotyping-by-resequencing." Plant Ecology and Diversity **5**(4): 457-471.

Chang, C.-C., M.-H. Yang, H.-M. Wen and J.-C. Chern (2002). "Estimation of total flavonoid content in propolis by two complementary colorimetric methods." Journal of food and drug analysis **10**(3).

Chang, S., E. L. Mahon, H. A. MacKay, W. H. Rottmann, S. H. Strauss, P. M. Pijut, W. A. Powell, V. Coffey, H. Lu, S. D. Mansfield and T. J. Jones (2018). "Genetic engineering of trees: progress and new horizons." In Vitro Cellular & Developmental Biology - Plant **54**: 341-376.

Chen, F., C. J. Liu, T. J. Tschaplinski and N. Zhao (2009). "Genomics of secondary metabolism in Populus: interactions with biotic and abiotic environments." Critical Reviews in Plant Science **28**(5): 375-392.

Chen, K., Y. Wang, R. Zhang, H. Zhang and C. Gao (2019). "CRISPR/Cas Genome Editing and Precision Plant Breeding in Agriculture." Annu Rev Plant Biol **70**: 667-697.

Chen, Z., J. Wang, M. X. Ye, H. Li, L. X. Ji, Y. Li, D. Q. Cui, J. M. Liu and X. M. An (2013). "A novel moderate constitutive promoter derived from poplar (Populus tomentosa Carrière)." International Journal of Molecular Sciences **14**(3): 6187-6204.

Christie, J. M., A. S. Arvai, K. J. Baxter, M. Heilmann, A. J. Pratt, A. O'Hara, S. M. Kelly, M. Hothorn, B. O. Smith, K. Hitomi, G. I. Jenkins and E. D. Getzoff (2012). "Plant UVR8 photoreceptor senses UV-B by tryptophan-mediated disruption of cross-dimer salt bridges." Science **335**(6075): 1492-1496.

Clayton, W. A., N. W. Albert, A. H. Thrimawithana, T. K. McGhie, S. C. Deroles, K. E. Schwinn, B. A. Warren, A. R. G. McLachlan, J. L. Bowman, B. R. Jordan and K. M. Davies (2018). "UVR8-mediated induction of flavonoid biosynthesis for UVB tolerance is conserved between the liverwort Marchantia polymorpha and flowering plants." Plant J **96**(3): 503-517.

Cloix, C., E. Kaiserli, M. Heilmann, K. J. Baxter, B. A. Brown, A. O'Hara, B. O. Smith, J. M. Christie and G. I. Jenkins (2012). "C-terminal region of the UV-B photoreceptor UVR8 initiates signaling through interaction with the COP1 protein." Proc Natl Acad Sci U S A **109**(40): 16366-16370.

Cooper, J. P. (1975). Photosynthesis and productivity in different environments, No. 3, Cambridge University Press.

Cronk, Q. C. (2005). "Plant eco-devo: the potential of poplar as a model organism." New Phytol **166**(1): 39-48.

Czégény, G., A. Mátai, and É. Hideg (2016). "UV-B effects on leaves—Oxidative stress and acclimation in controlled environments." Plant Science **248**: 57-63.

Czégény, G., M. Wu, A. Der, L. A. Eriksson, A. Strid and E. Hideg (2014). "Hydrogen peroxide contributes to the ultraviolet-B (280-315 nm) induced oxidative stress of plant leaves through multiple pathways." FEBS Lett **588**(14): 2255-2261.

D'Archivio, M., C. Filesi, R. Di Benedetto, R. Gargiulo, C. Giovannini and R. Masella (2007). "Polyphenols, dietary sources and bioavailability." Ann Ist Super Sanita **43**(4): 348-361.

Dai, Q., B. Yan, S. Huang, X. Liu, S. Peng, M. L. L. Miranda, A. Q. Chavez, B. S. Vergara, and D. M. Olszyk (1997). "Response of oxidative stress defense systems in rice (Oryza sativa) leaves with supplemental UV-B radiation." Physiologia Plantarum **101**(2): 301-308.

Dale, J. E. (1988). "The Control of Leaf Expansion." Annual Review of Plant Physiology and Plant Molecular Biology **39**: 267-295.

Dauwe, R., K. Morreel, G. Goeminne, B. Gielen, A. Rohde, J. Van Beeumen, J. Ralph, A. M. Boudet, J. Kopka, S. F. Rochange and C. Halpin (2007). "Molecular phenotyping of lignin-modified tobacco reveals associated changes in cell-wall metabolism, primary metabolism, stress metabolism and photorespiration." The Plant Journal **52**(2): 263-285.

Day, T. A. (1993). "Relating UV-B radiation screening effectiveness of foliage to absorbing-compound concentration and anatomical characteristics in a diverse group of plants." Oecologia **95**: 542-550.

Day, T. A., B. S. Howells and W. J. Rice (1994). "Ultraviolet absorption and epidermal-transmittance spectra in foliage." Physiologia Plantarum **92**: 207-218.

De Smet, R., K. L. Adams, K. Vandepoele, M. C. Van Montagu, S. Maere and Y. Van de Peer (2013). "Convergent gene loss following gene and genome duplications creates single-copy families in flowering plants." Proc Natl Acad Sci U S A **110**(8): 2898-2903.

de Vries, L., M. Brouckaert, A. Chanoca, H. Kim, M. R. Regner, V. I. Timokhin, Y. Sun, B. De Meester, J. Van Doorsselaere, G. Goeminne, V. L. Chiang, J. P. Wang, J. Ralph, K. Morreel, R. Vanholme and W. Boerjan (2021). "CRISPR-Cas9 Editing of CAFFEOYL SHIKIMATE ESTERASE 1 and 2 Shows Their Importance and Partial Redundancy in Lignification in Populus tremula x P. alba." Plant Biotechnol J.

Dean, J. C., R. Kusaka, P. S. Walsh, F. Allais and T. S. Zwier (2014). "Plant sunscreens in the UV-B: ultraviolet spectroscopy of jet-cooled sinapoyl malate, sinapic acid, and sinapate ester derivatives." J Am Chem Soc **136**(42): 14780-14795.

DeLucia, E.H., T. A. Day, and T. C. Vogelman (1992). "Ultraviolet-B and visible light penetration into needles of two species of subalpine conifers during foliar development." Plant, Cell & Environment **15**(8): 921-929.

Demarsy, E., M. Goldschmidt-Clermont and R. Ulm (2018). "Coping with 'Dark Sides of the Sun' through Photoreceptor Signaling." Trends Plant Sci **23**(3): 260-271.

Demmig-Adams, B. and W. W. Adams, 3rd (2000). "Harvesting sunlight safely." Nature **403**(6768): 371, 373-374.

Dickson, R. E., P. Larson and J. Isebrands (1974). Differences in cell-wall chemical composition among eighteen three-year-old Populus hybrid clones. Proceedings of the 9 th Central States Tree Improve Conf., Ames, IA.

Diffey, B. L. (2002). "Sources and measurement of ultraviolet radiation." Methods **28**(1): 4-13.

Dillenburg, L. R., J. H. Sullivan and A. H. Teramura (1995). "Leaf expansion and development of photosynthetic capacity and pigments in Liquidambar styraciflua (Hamamelidaceae)—effects of UV-B radiation." American Journal of Botany **82**(7): 878-885.

Dogan, R. I., L. Getoor, W. J. Wilbur and S. M. Mount (2007). "SplicePort—an interactive splice-site analysis tool." Nucleic acids research **35**(suppl_2): W285-W291.

Doudna, J. A. and E. Charpentier (2014). "Genome editing. The new frontier of genome engineering with CRISPR-Cas9." Science **346**(6213): 1258096.

Duanmu, D., N. C. Rockwell and J. C. Lagarias (2017). "Algal light sensing and photoacclimation in aquatic environments." Plant, cell & environment **40**(11): 2558-2570.

Duarte, J. M., P. K. Wall, P. P. Edger, L. L. Landherr, H. Ma, J. C. Pires, J. Leebens-Mack and C. W. dePamphilis (2010). "Identification of shared single copy nuclear genes in Arabidopsis, Populus, Vitis and Oryza and their phylogenetic utility across various taxonomic levels." BMC Evol Biol **10**: 61.

Ehleringer, J. and I. Forseth (1980). "Solar tracking by plants." Science **210**(4474): 1094-1098.

Emerson, R. (1958). "The quantum yield of photosynthesis." Annual Review of Plant Physiology **9**(1): 1-24.

Evans, L. M., G. T. Slavov, E. Rodgers-Melnick, J. Martin, P. Ranjan, W. Muchero, A. M. Brunner, W. Schackwitz, L. Gunter, J. G. Chen, G. A. Tuskan and S. P. DiFazio (2014). "Population genomics of Populus trichocarpa identifies signatures of selection and adaptive trait associations." Nat Genet **46**(10): 1089-1096.

Fan, D., T. Liu, C. Li, B. Jiao, S. Li, Y. Hou and K. Luo (2015). "Efficient CRISPR/Cas9-mediated Targeted Mutagenesis in Populus in the First Generation." Sci Rep **5**: 12217.

Favory, J. J., A. Stec, H. Gruber, L. Rizzini, A. Oravecz, M. Funk, A. Albert, C. Cloix, G. I. Jenkins, E. J. Oakeley, H. K. Seidlitz, F. Nagy and R. Ulm (2009). "Interaction of COP1 and UVR8 regulates UV-B-induced photomorphogenesis and stress acclimation in Arabidopsis." EMBO J **28**(5): 591-601.

Fernandez, M. B., V. Tossi, L. Lamattina and R. Cassia (2016). "A Comprehensive Phylogeny Reveals Functional Conservation of the UV-B Photoreceptor UVR8 from Green Algae to Higher Plants." Front Plant Sci **7**: 1698.

Findlay, K. M. and G. I. Jenkins (2016). "Regulation of UVR8 photoreceptor dimer/monomer photo-equilibrium in Arabidopsis plants grown under photoperiodic conditions." Plant Cell Environ **39**(8): 1706-1714.

Fraser, C. M. and C. Chapple (2011). "The phenylpropanoid pathway in Arabidopsis." Arabidopsis Book **9**: e0152.

Frederick, J. K., H. E. Snell and E. K. Haywood (1989). "Solar ultraviolet radiation at the earth's surface." Photochem Photobiol **50**: 443-450.

Frohnmeyer, H. and D. Staiger (2003). "Ultraviolet-B radiation-mediated responses in plants. Balancing damage and protection." Plant Physiol **133**(4): 1420-1428.

Fromm, M., L. P. Taylor and V. Walbot (1985). "Expression of genes transferred into monocot and dicot plant cells by electroporation." Proc Natl Acad Sci U S A **82**(17): 5824-5828.

Fu, W., A. Chaiboonchoe, B. Khraiwesh, M. Sultana, A. Jaiswal, K. Jijakli, D. R. Nelson, A. Al-Hrout, B. Baig, A. Amin and K. Salehi-Ashtiani (2017). "Intracellular spectral recompositioning of light enhances algal photosynthetic efficiency." Sci Adv **3**(9): e1603096.

Gallego-Giraldo, L., Y. Jikumaru, Y. Kamiya, Y. Tang and R. A. Dixon (2011). "Selective lignin downregulation leads to constitutive defense response expression in alfalfa (Medicago sativa L.)." New Phytol **190**(3): 627-639.

Gamon, J. and J. Surfus (1999). "Assessing leaf pigment content and activity with a reflectometer." The New Phytologist **143**(1): 105-117.

Gao, W., Y. Zheng, J. R. Slusser, G. M. Heisler, R. H. Grant, J. Xu and D. He (2004). "Effects of supplementary ultraviolet-B irradiance on maize yield and qualities: a field experiment." Photochem Photobiol **80**: 127-131.

Giese, A. C. (1964). Studies on ultraviolet radiation action upon animal cells. Photophysiology. A. C. Giese. NY-London, Academic Press. **2:** 203-245.

Goldman, N. and Z. Yang (1994). "A codon-based model of nucleotide substitution for protein-coding DNA sequences." Molecular biology and evolution **11**(5): 725-736.

Goodstein, D. M., S. Shu, R. Howson, R. Neupane, R. D. Hayes, J. Fazo, T. Mitros, W. Dirks, U. Hellsten, N. Putnam and D. S. Rokhsar (2012). "Phytozome: a comparative platform for green plant genomics." Nucleic Acids Res **40**(Database issue): D1178-1186.

Gourlay, G. and C.P. Constabel (2019). "Condensed tannins are inducible antioxidants and protect hybrid poplar against oxidative stress." Tree Physiology **39**: 345–355.

Graham, T. L. (1998). "Flavonoid and flavonol glycoside metabolism in Arabidopsis." Plant Physiology and Biochemistry **36**(1-2): 135-144.

Gruber, H., M. Heijde, W. Heller, A. Albert, H. K. Seidlitz and R. Ulm (2010). "Negative feedback regulation of UV-B-induced photomorphogenesis and stress acclimation in Arabidopsis." Proc Natl Acad Sci U S A **107**(46): 20132-20137.

Gupta, P. K., S. Rustgi and P. L. Kulwal (2005). "Linkage disequilibrium and association studies in higher plants: present status and future prospects." Plant Mol Biol **57**(4): 461-485.

Halliwell, B. (2007). "Dietary polyphenols: good, bad, or indifferent for your health?" Cardiovasc Res **73**(2): 341-347.

Hammond, S. M. (2005). "Dicing and slicing: the core machinery of the RNA interference pathway." FEBS Lett **579**(26): 5822-5829.

Hara, M., J. Furukawa, A. Sato, T. Mizoguchi and K. Miura (2012). Abiotic Stress and Role of Salicylic Acid in Plants. Abiotic Stress Responses in Plants. New York, Springer**:** 235-251.

Heijde, M., M. Binkert, R. Yin, F. Ares-Orpel, L. Rizzini, E. Van De Slijke, G. Persiau, J. Nolf, K. Gevaert, G. De Jaeger and R. Ulm (2013). "Constitutively active UVR8 photoreceptor variant in Arabidopsis." Proc Natl Acad Sci U S A **110**(50): 20326-20331.

Heilmann, M., C. N. Velanis, C. Cloix, B. O. Smith, J. M. Christie and G. I. Jenkins (2016). "Dimer/monomer status and in vivo function of salt-bridge mutants of the plant UV-B photoreceptor UVR8." Plant J **88**(1): 71-81.

Herman, J. R. (2010). "Global increase in UV irradiance during the past 30 years (1979–2008) estimated from satellite data." Journal of Geophysical Research: Atmospheres, **115**(D4).

Hicke, J. A., D. B. Lobell and G. P. Asner (2004). "Cropland area and net primary production computed from 30 years of USDA agricultural harvest data." Earth Interactions **8**(10): 1-20.

Hideg, E., M. A. Jansen and A. Strid (2013). "UV-B exposure, ROS, and stress: inseparable companions or loosely linked associates?" Trends Plant Sci **18**(2): 107-115.

Hideg, É. and Å. Strid (2017). The effects of UV-B on the biochemistry and metabolism in plants. UV-B radiation and plant life: molecular biology to ecology. B. R. Jordan, CAB International**:** 90-110.

Hideg, É. and I. Vass (1996). "UV-B induced free radical production in plant leaves and isolated thylakoid membranes." Plant Science **115**(2): 251-260.

Hu, W. J., S. A. Harding, J. Lung, J. L. Popko, J. Ralph, D. D. Stokke, C. J. Tsai and V. L. Chiang (1999). "Repression of lignin biosynthesis promotes cellulose accumulation and growth in transgenic trees." Nat Biotechnol **17**(8): 808-812.

Huala, E., A. W. Dickerman, M. Garcia-Hernandez, D. Weems, L. Reiser, F. LaFond, D. Hanley, D. Kiphart, M. Zhuang, W. Huang, L. A. Mueller, D. Bhattacharyya, D. Bhaya, B. W. Sobral, W. Beavis, D. W. Meinke, C. D. Town, C. Somerville and S. Y. Rhee (2001). "The Arabidopsis Information Resource (TAIR): a comprehensive database and web-based information retrieval, analysis, and visualization system for a model plant." Nucleic Acids Res **29**(1): 102-105.

Huang, X., X. Ouyang, P. Yang, O. S. Lau, L. Chen, N. Wei and X. W. Deng (2013). "Conversion from CUL4-based COP1-SPA E3 apparatus to UVR8-COP1-SPA complexes underlies a distinct biochemical function of COP1 under UV-B." Proc Natl Acad Sci U S A **110**(41): 16669-16674.

Huang, X., P. Yang, X. Ouyang, L. Chen and X. W. Deng (2014). "Photoactivated UVR8-COP1 module determines photomorphogenic UV-B signaling output in Arabidopsis." PLoS Genet **10**(3): e1004218.

Huq, M. A., S. Akter, I. S. Nou, H. T. Kim, Y. J. Jung and K. K. Kang (2016). "Identification of functional SNPs in genes and their effects on plant phenotypes." Journal of Plant Biotechnology **43**(1): 1-11.

Hurst, L. D. (2002). "The Ka/Ks ratio: diagnosing the form of sequence evolution." Trends Genet **18**(9): 486.

Impa, S. M., S. Nadaradjan and S. V. K. Jagadish (2012). Drought stress induced reactive oxygen species and anti-oxidants in plants. Abiotic Stress Responses in Plants New York, Springer**:** 131-147.

Infante, D. (2002). "A rapid and simple method for small-scale DNA extraction inAgavaceae and other tropical plants." Plant Molecular Biology Reporter **20**: 299a-299e.

Jackson, M. B. and T. D. Colmer (2005). "Response and adaptation by plants to flooding stress." Ann Bot **96**(4): 501-505.

Jaganathan, D., K. Ramasamy, G. Sellamuthu, S. Jayabalan and G. Venkataraman (2018). "CRISPR for Crop Improvement: An Update Review." Front Plant Sci **9**: 985.

James, A. M., D. Ma, R. Mellway, A. Gesell, K. Yoshida, V. Walker, L. Tran, D. Stewart, M. Reichelt, J. Suvanto and J. P. Salminen (2017). "Poplar MYB115 and MYB134 Transcription Factors Regulate Proanthocyanidin Synthesis and Structure." Plant Physiology **174**: 154–171.

Jansen, M. A., T. S. Babu, D. Heller, V. Gaba, A. K. Mattoo and M. Edelman (1996). "Ultraviolet-B effects on Spirodela oligorrhiza: induction of different protection mechanisms." Plant Science **115**(2): 217-223.

Jansen, M. A., V. Gaba and B. M. Greenberg (1998). "Higher plants and UV-B radiation: balancing damage, repair and acclimation." Trends in Plant Science **3**(4): 131-135.

Jansen, M. A. K. (2002). "Ultraviolet-B radiation effects on plants: induction of morphogenic responses." Physiologia Plantarum **116**: 423-429.

Jansen, M. A. K., W. Bilger, E. Hideg, A. Strid, U. V. P. W. Participants and O. Urban (2019). "Editorial: Interactive effects of UV-B radiation in a complex environment." Plant Physiol Biochem **134**: 1-8.

Jansson, S. and C. J. Douglas (2007). "Populus: a model system for plant biology." Annu Rev Plant Biol **58**: 435-458.

Jenkins, G. I. (2009). "Signal transduction in responses to UV-B radiation." Annu Rev Plant Biol **60**: 407-431.

Jenkins, G. I. (2017). "Photomorphogenic responses to ultraviolet-B light." Plant Cell Environ **40**(11): 2544-2557.

Jia, X. L., G. L. Wang, F. Xiong, X. R. Yu, Z. S. Xu, F. Wang and A. S. Xiong (2015). "De novo assembly, transcriptome characterization, lignin accumulation and anatomic characteristics: novel insights into lignin biosynthesis during celery leaf development." Scientific reports **5**(1): 1-14.

Jiang, X., J. Xu, R. Lin, J. Song, S. Shao, J. Yu and Y. Zhou (2020). "Light-induced HY5 Functions as a Systemic Signal to Coordinate the Photoprotective Response to Light Fluctuation." Plant Physiol **184**(2): 1181-1193.

Joshi, C. P. (1987). "An inspection of the domain between putative TATA box and translation start site in 79 plant genes." Nucleic acids research **15**(16): 6643-6653.

Kaiserli, E. and G. I. Jenkins (2007). "UV-B promotes rapid nuclear translocation of the Arabidopsis UV-B specific signaling component UVR8 and activates its function in the nucleus." Plant Cell **19**(8): 2662-2673.

Kanehisa, M. (2016). "KEGG bioinformatics resource for plant genomics and metabolomics." Plant Bioinformatics 55-70. Humana Press, New York, NY.

Karimi, M., D. Inze and A. Depicker (2002). "GATEWAY vectors for Agrobacterium-mediated plant transformation." Trends Plant Sci **7**(5): 193-195.

Karve, A. A., S. S. Jawdy, L. E. Gunter, S. M. Allen, X. Yang, G. A. Tuskan, S. D. Wullschleger and D. J. Weston (2012). "Initial characterization of shade avoidance response suggests functional diversity between Populus phytochrome B genes." New Phytol **196**(3): 726-737.

Kaufmann, M. R. (1978). The effects of ultraviolet radiation on Engelmann spruce and lodgepole pine seedlings. Research Report on the Impacts of Ultraviolet-B Radiation on Biological Systems: A study related to atmospheric ozone depletion. Washington, DC. **EPA-IAG-DG-0168**.

Keren, N. and A. Krieger-Liszkay (2011). "Photoinhibition: molecular mechanisms and physiological significance." Physiologia Plantarum **142**(1): 1-5.

Kerr, J. B. and C. T. McElroy (1993). "Evidence for large upward trends of ultraviolet-B radiation linked to ozone depletion." Science **262**(5136): 1032-1034.

Kharabian, A. (2010). "An efficient computational method for screening functional SNPs in plants." J Theor Biol **265**(1): 55-62.

Kim, B. C., D. J. Tennessen and R. L. Last (1998). "UV-B-induced photomorphogenesis in Arabidopsis thaliana." Plant J **15**(5): 667-674.

Kliebenstein, D. J., J. E. Lim, L. G. Landry and R. L. Last (2002). "Arabidopsis UVR8 regulates ultraviolet-B signal transduction and tolerance and contains sequence similarity to human regulator of chromatin condensation 1." Plant Physiol **130**(1): 234-243.

Klobas, J. E., D. M. Wilmouth, D. K. Weisenstein, J. G. Anderson and R. J. Salawitch (2017). "Ozone depletion following future volcanic eruptions." Geophysical Research Letters **44**(14): 7490-7499.

Knobloch, K. H. and K. Hahlbrock (1977). "4-Coumarate:CoA ligase from cell suspension cultures of Petroselinum hortense Hoffm. Partial purification, substrate specificity, and further properties." Arch Biochem Biophys **184**(1): 237-248.

Kolb, C. A., J. Kopecky, M. Riederer and E. E. Pfundel (2003). "UV screening by phenolics in berries of grapevine (Vitis vinifera) " Functional Plant Biology **30**: 1177-1186.

Kolb, C. A. and E. E. Pfundel (2005). "Origins of non-linear and dissimilar relationships between epidermal UV absorbance and UV absorbance of extracted phenolics in leaves of grapevine and barley." Plant cell and environment **25**: 580-590.

Kootstra, A. (1994). "Protection from UV-B-induced DNA damage by flavonoids." Plant Molecular Biology **26**(2): .771-774.

Kossuth, S. V. and R. H. Biggs (1981). "Ultraviolet-B radiation effects on early seedling growth of Pinaceae species." Canadian Journal of Forestry Research **11**: 243-248.

Kranner, I., F. V. Minibayeva, R. P. Beckett and C. E. Seal (2010). "What is stress? Concepts, definitions and applications in seed science." New Phytol **188**(3): 655-673.

Krizek, D. T., R. M. Mirecki and S. J. Britz (1997). "Inhibitory effects of ambient levels of solar UV-A and UV-B radiation on growth of cucumber." Physiologia Plantarum **100**: 886-893.

Laakso, K., J. H. Sullivan and S. Huttunen (2000). "The effects of UV-B radiation on epidermal anatomy in loblolly pine (Pinus taeda L.) and Scots pine (Pinus sylvestris L.)." Plant, Cell and Environmnent **23**(5): 461-472.

Landry, L. G., C. C. Chapple and R. L. Last (1995). "Arabidopsis mutants lacking phenolic sunscreens exhibit enhanced ultraviolet-B injury and oxidative damage." Plant Physiol **109**(4): 1159-1166.

Lapierre, C., G. Pilate, B. Pollet, I. Mila, J.-C. Leple, L. Jouanin, H. Kim and J. Ralph (2004). "Signatures of cinnamyl alcohol dehydrogenase deficiency in poplar lignins." Phytochemistry **65**(3): 313-321.

Lapierre, C., R. Sibout, F. Laurans, M.C. Lesage-Descauses, A. Déjardin, and G. Pilate (2021). "p-coumaroylation of poplar lignins impacts lignin structure and improves wood saccharification." Plant Physiol **kiab359**.

León-Chan, R. G., M. López-Meyer, T. Osuna-Enciso, J. A. Sañudo-Barajas, J. B. Heredia and J. León-Félix (2017). "Low temperature and ultraviolet-B radiation affect chlorophyll content and induce the accumulation of UV-B-absorbing and antioxidant compounds in bell pepper (Capsicum annuum) plants." Environmental and Experimental Botany **139**: 143-151.

Leple, J. C., A. C. Brasileiro, M. F. Michel, F. Delmotte and L. Jouanin (1992). "Transgenic poplars: expression of chimeric genes using four different constructs." Plant Cell Rep **11**(3): 137-141.

Levitt, J. (1980). Responses of Plants to Environmental Stress. Volume 1: Chilling, Freezing, and High Temperature Stresses. New York, Academic Press.

Li, G., S. Sretenovic, E. Eisenstein, G. Coleman and Y. Qi (2021). "Highly efficient C-to-T and A-to-G base editing in a Populus hybrid." Plant Biotechnol J **19**(6): 1086-1088.

Li, J., T. M. Ou-Lee, R. Raba, R. G. Amundson and R. L. Last (1993). "Arabidopsis Flavonoid Mutants Are Hypersensitive to UV-B Irradiation." Plant Cell **5**(2): 171-179.

Li, J. F., J. E. Norville, J. Aach, M. McCormack, D. Zhang, J. Bush, G. M. Church and J. Sheen (2013). "Multiplex and homologous recombination-mediated genome editing in Arabidopsis and Nicotiana benthamiana using guide RNA and Cas9." Nat Biotechnol **31**(8): 688-691.

Li, X., N. D. Bonawitz, J. K. Weng and C. Chapple (2010). "The growth reduction associated with repressed lignin biosynthesis in Arabidopsis thaliana is independent of flavonoids." Plant Cell **22**(5): 1620-1632.

Liakoura, V., M. Stefanou, Y. Manetas, C. Cholevas and G. Karabourniotis (1997). "Trichome density and its UV-B protective potential are affected by shading and leaf position on the canopy." Environmental and Experimental Botany **38**(3): 223-229.

Liang, T., S. Mei, C. Shi, Y. Yang, Y. Peng, L. Ma, F. Wang, X. Li, X. Huang, Y. Yin and H. Liu (2018). "UVR8 Interacts with BES1 and BIM1 to Regulate Transcription and Photomorphogenesis in Arabidopsis." Dev Cell **44**(4): 512-523 e515.

Liao, X., W. Liu, H. Q. Yang and G. I. Jenkins (2020). "A dynamic model of UVR8 photoreceptor signalling in UV-B-acclimated Arabidopsis." New Phytol **227**(3): 857-866.

Lin, L., H. Dong, G. Yang and R. Yin (2020). "The C-terminal 17 amino acids of the photoreceptor UVR8 is involved in the fine-tuning of UV-B signaling." J Integr Plant Biol **62**(9): 1327-1340.

Lindroth, R. L. (2001). Adaptations of quaking aspen for defense against damage by herbivores and related environmental agents. Sustaining aspen in western landscapes, Grand Junction, CO, US Department of Agriculture, Forest Service, Rocky Mountain Research Station.

Lindroth, R. L. and S. Y. Hwang (1996). Diversity, redundancy, and multiplicity in chemical defense systems of aspen, Springer.

Liu, L., D. C. Gitz and J. W. McClure (1995). "Effects of UV-B on flavonoids, ferulic acid, growth and photosynthesis in Barley primary leaves." Plant Physiol **93**: 725-733.

Liu, T. T., D. Fan, L. Y. Ran, Y. Z. Jiang, R. Liu and K. M. Luo (2015). "Highly efficient CRISPR/Cas9-mediated targeted mutagenesis of multiple genes in Populus." Yi Chuan **37**(10): 1044-1052.

Liu, W., M. Mazarei, Y. Peng, M. H. Fethe, M. R. Rudis, J. Lin, R. J. Millwood, P. R. Arelli and C. N. Stewart Jr (2014). "Computational discovery of soybean promoter cis-regulatory elements for the construction of soybean cyst nematode-inducible synthetic promoters." Plant biotechnology journal **12**(8): 1015-1026.

Liu, W. and C. N. Stewart Jr (2016). "Plant synthetic promoters and transcription factors." Current opinion in biotechnology **37**: 36-44.

Livak, K. J. and T. D. Schmittgen (2001). "Analysis of relative gene expression data using real-time quantitative PCR and the 2(-Delta Delta C(T)) Method." Methods **25**(4): 402-408.

Lowder, L. G., D. Zhang, N. J. Baltes, J. W. Paul, 3rd, X. Tang, X. Zheng, D. F. Voytas, T. F. Hsieh, Y. Zhang and Y. Qi (2015). "A CRISPR/Cas9 Toolbox for Multiplexed Plant Genome Editing and Transcriptional Regulation." Plant Physiol **169**(2): 971-985.

Mabry, T. J., K. R. Markham and M. B. Thomas (1970). The ultraviolet spectra of flavones and flavonols. The Systematic Identification of Flavonoids. Berlin, Heidelberg, Springer**:** 41-164.

Macaya-Sanz, D., J. G. Chen, U. C. Kalluri, W. Muchero, T. J. Tschaplinski, L. E. Gunter, S. J. Simon, A. K. Biswal, A. C. Bryan, R. Payyavula, M. Xie, Y. Yang, J. Zhang, D. Mohnen, G. A. Tuskan and S. P. DiFazio (2017). "Agronomic performance of Populus deltoides trees engineered for biofuel production." Biotechnol Biofuels **10**: 253.

Mach, J. (2016). "How Plants Take the Bad with the Good: Conserved UV-B Perception and Signaling in Chlamydomonas." The Plant Cell **28**(4): 825.

Mader, M., M.-C. Le Paslier, R. Bounon, A. Bérard, P. Faivre-Rampant, M. Fladung, J.-C. Leplé and B. Kersten (2016). "Whole-genome draft assembly of Populus tremula x P. alba clone INRA 717-1B4." Silvae Genetica **65**(2): 74-79.

Manetas, Y., Y. Petropoulou, K. Stamatakis, D. Nikolopoulou, E. Levizou, G. Psaras and G. Karabourniotis (1997). "Beneficial effects of enhanced UV-B radiation under field conditions: improvement of needle water relations and survival capacity of Pinus pinea L. seedlings during the Mediterranean summer." Plant Ecology and Diversity **128**: 100-108.

Mansfield, S. D., K. Y. Kang and C. Chapple (2012). "Designed for deconstruction--poplar trees altered in cell wall lignification improve the efficacy of bioethanol production." New Phytol **194**(1): 91-101.

Markstädter, C., I. Queck, J. Baumeister, M. Riederer, U. Schreiber and W. Bilger (2001). "Epidermal transmittance of leaves of Vicia faba for UV radiation as determined by two different methods." Photosynthesis research **67**(1): 17-25.

Martin, M.E. and J. D. Aber (1994). "Analyses of forest foliage III: Determining nitrogen, lignin and cellulose in fresh leaves using near infrared reflectance data." Journal of Near Infrared Spectroscopy **2**(1): 25-32.

Mazza, C.A., P. I. Giménez, A. G. Kantolic, and C. L. Ballaré (2013). "Beneficial effects of solar UV-B radiation on soybean yield mediated by reduced insect herbivory under field conditions." Physiologia Plantarum **147**(3): 307-315.

McCree, K. J. (1971). "The action spectrum, absorptance and quantum yield of photosynthesis in crop plants." Agricultural Meteorology **9**: 191-216.

McKenzie, R., B. Connor and G. Bodeker (1999). "Increased summertime UV radiation in New Zealand in response to ozone loss." Science **285**(5434): 1709-1711.

Mellway, R.D., L. T. Tran, M. B. Prouse, M. M. Campbell and C. P. Constabel (2009). "The wound-, pathogen-, and ultraviolet B-responsive MYB134 gene encodes an R2R3 MYB transcription factor that regulates proanthocyanidin synthesis in poplar." Plant Physiology **150**: 924–941.

Miller, Z. D., P. N. Peralta, P. Mitchell, V. L. Chiang, C. W. Edmunds and I. M. Peszlen (2018). "Altered lignin content and composition in transgenic Populus trichocarpa results in a decrease of modulus of elasticity." Bioresources **13**(4): 7698-7708.

Mittler, R. (2002). "Oxidative stress, antioxidants and stress tolerance." Trends Plant Sci **7**(9): 405-410.

Molina, M. J. and F. S. Rowland (1974). "Stratospheric sink for chlorofluoromethanes: chlorine atom-catalysed destruction of ozone." Nature **249**: 810-812.

Moradpour, M. and S. N. A. Abdulah (2020). "CRISPR/dCas9 platforms in plants: strategies and applications beyond genome editing." Plant Biotechnol J **18**(1): 32-44.

Muhr, M., M. Paulat, M. Awwanah, M. Brinkkotter and T. Teichmann (2018). "CRISPR/Cas9-mediated knockout of Populus BRANCHED1 and BRANCHED2 orthologs reveals a major function in bud outgrowth control." Tree Physiol **38**(10): 1588-1597.

Naidu, S. L., J. H. Sullivan, A. H. Teramura, and E. H. DeLucia (1993). “The effects of ultraviolet-B radiation on photosynthesis of different aged needles in field-grown loblolly pine.” Tree Physiology **12**(2): 151-162.

Nasti, R. A. and D. F. Voytas (2021). "Attaining the promise of plant gene editing at scale." Proc Natl Acad Sci U S A **118**(22).

Nawkar, G. M., P. Maibam, J. H. Park, V. P. Sahi, S. Y. Lee and C. H. Kang (2013). "UV-Induced cell death in plants." Int J Mol Sci **14**(1): 1608-1628.

Neale, P. J., V. R. Goodrich and W. R. Ririnley (2004). The Smithsonian-NIST-USDA-FPL Network for Monitoring Solar Ultraviolet Irradiance: Comparison of Radiometer Measurements and Radiative Transfer Model Calculations. Proceedings of the 3rd International Symposium on Service Life Prediction. Federation of Societies for Coatings Technology, Oxford, Elsevier.

Neale, R.E., P. W. Barnes, T. M. Robson, P. J. Neale, C. E. Williamson, R. G. Zepp, S. R. Wilson, S. Madronich, A. L. Andrady, A. M. Heikkilä, and G. H. Bernhard (2021). “Environmental effects of stratospheric ozone depletion, UV radiation, and interactions with climate change: UNEP Environmental Effects Assessment Panel, Update 2020.” Photochemical & Photobiological Sciences **20**(1): 1-67.

Neugart, S. and M. Schreiner (2018). "UVB and UVA as eustressors in horticultural and agricultural crops." Scientia Horticulturae **234**: 370-381.

Novaes, E., M. Kirst, V. Chiang, H. Winter-Sederoff and R. Sederoff (2010). "Lignin and biomass: a negative correlation for wood formation and lignin content in trees." Plant Physiol **154**(2): 555-561.

O'Hara, A., L. R. Headland, L. A. Diaz-Ramos, L. O. Morales, A. Strid and G. I. Jenkins (2019). "Regulation of Arabidopsis gene expression by low fluence rate UV-B independently of UVR8 and stress signaling." Photochem Photobiol Sci **18**(7): 1675-1684.

O'Hara, A. and G. I. Jenkins (2012). "In vivo function of tryptophans in the Arabidopsis UV-B photoreceptor UVR8." Plant Cell **24**(9): 3755-3766.

ONeill, C. M., A. Kazantzidis, M. J. Ryan, N. Barber, C. T. Sempos, R. A. Durazo-Arvizu, R. Jorde, G. Grimnes, G. Eiriksdottir, V. Gudnason and M. F. Cotch (2016). "Seasonal changes in vitamin D-effective UVB availability in Europe and associations with population serum 25-hydroxyvitamin D." Nutrients **8**(9): 533.

Osakabe, Y., S. S. Sugano and K. Osakabe (2016). "Genome engineering of woody plants: past, present and future." Journal of Wood Science **62**(3): 217-225.

Palancar, G. G., B. L. Lefer, S. R. Hall, W. J. Shaw, C. A. Corr, S. C. Herndon, J. R. Slusser and S. Madronich (2013). "Effect of aerosols and NO2 concentration on ultraviolet actinic

flux near Mexico City during MILAGRO: measurements and model calculations." Atmos. Chem. Phys. **13**(2): 1011–1022.

Pan, C., S. Sretenovic and Y. Qi (2021). "CRISPR/dCas-mediated transcriptional and epigenetic regulation in plants." Curr Opin Plant Biol **60**: 101980.

Pan, C., X. Wu, K. Markel, A. A. Malzahn, N. Kundagrami, S. Sretenovic, Y. Zhang, Y. Cheng, P. M. Shih and Y. Qi (2021). "CRISPR-Act3.0 for highly efficient multiplexed gene activation in plants." Nat Plants.

Park, S. H., N. Yi, Y. S. Kim, M. H. Jeong, S. W. Bang, Y. D. Choi and J. K. Kim (2010). "Analysis of five novel putative constitutive gene promoters in transgenic rice plants." J Exp Bot **61**(9): 2459-2467.

Pascual, J., M. Rahikainen and S. Kangasjärvi (2017). Plant Light Stress. eLS. Chichester, John Wiley & Sons, Ltd.

Paul, N. D. and D. Gwynn-Jones (2003). "Ecological roles of solar UV radiation: towards an integrated approach." Trends in Ecology and Evolution **18**(1): 48-55.

Peer, W. A., D. E. Brown, B. W. Tague, G. K. Muday, L. Taiz and A. S. Murphy (2001). "Flavonoid accumulation patterns of transparent testa mutants of arabidopsis." Plant Physiol **126**(2): 536-548.

Petropoulou, Y., A. Kyparissis, D. Nikolopoulos and Y. Manetas (1995). "Enhanced UV-B radiation alleviates the adverse effects of summer drought in two Mediterranean pines under field conditions." Physiologia Plantarum **94**: 37-44.

Pettengill, E. A., C. Parmentier-Line and G. D. Coleman (2012). "Evaluation of qPCR reference genes in two genotypes of Populus for use in photoperiod and low-temperature studies." BMC Res Notes **5**: 366.

Podolec, R., E. Demarsy and R. Ulm (2021). "Perception and Signaling of Ultraviolet-B Radiation in Plants." Annu Rev Plant Biol **72**: 793-822.

Podolec, R., K. Lau, T. B. Wagnon, M. Hothorn and R. Ulm (2021). "A constitutively monomeric UVR8 photoreceptor confers enhanced UV-B photomorphogenesis." Proc Natl Acad Sci U S A **118**(6).

Porto, M. S., M. P. N. Pinheiro, V. G. L. Batista, R. C. dos Santos, P. de Albuquerque Melo Filho and L. M. de Lima (2014). "Plant promoters: an approach of structure and function." Molecular biotechnology **56**(1): 38-49.

Prince, S. D., J. Haskett, M. Steininger, H. Strand and R. Wright (2001). "Net primary production of US Midwest croplands from agricultural harvest yield data." Ecological Applications **11**(4): 1194-1205.

Programme, W. U. W. M. O. U. N. E. (2014). Scientific Assessment of Ozone Depletion: 2014. Global Ozone Research and Monitoring Project Report No. 55. Geneva, Switzerland**:** 416.

Qu, F., T. Ren and T. J. Morris (2003). "The coat protein of turnip crinkle virus suppresses posttranscriptional gene silencing at an early initiation step." J Virol **77**(1): 511-522.

Rabino, I. and A. L. Mancinelli (1986). "Light, temperature, and anthocyanin production." Plant Physiol **81**(3): 922-924.

Ralph, J., K. Lundquist, G. Brunow, F. Lu, H. Kim, P. F. Schatz, J. M. Marita, R. D. Hatfield, S. A. Ralph, J. H. Christensen and W. Boerjan (2004). "Lignins: Natural polymers from osicative coupleing of 4-hydroxyphenyl-propanoids." Phytochemistry Reviews **3**(29-60).

Rasmussen, S. and R. A. Dixon (1999). "Transgene-mediated and elicitor-induced perturbation of metabolic channeling at the entry point into the phenylpropanoid pathway." Plant Cell **11**(8): 1537-1552.

Razzaq, A., F. Saleem, M. Kanwal, G. Mustafa, S. Yousaf, H. M. Imran Arshad, M. K. Hameed, M. S. Khan and F. A. Joyia (2019). "Modern Trends in Plant Genome Editing: An Inclusive Review of the CRISPR/Cas9 Toolbox." Int J Mol Sci **20**(16).

Reifenrath, K. and C. Müller (2007). "Species-specific and leaf-age dependent effects of ultraviolet radiation on two Brassicaceae." Phytochemistry **68**(6): 875-885.

Ries, G., W. Heller, H. Puchta, H. Sandermann, H. K. Seidlitz and B. Hohn (2000). "Elevated UV-B radiation reduces genome stability in plants." Nature **406**(6791): 98-101.

Rizzini, L., J. J. Favory, C. Cloix, D. Faggionato, A. O'Hara, E. Kaiserli, R. Baumeister, E. Schafer, F. Nagy, G. I. Jenkins and R. Ulm (2011). "Perception of UV-B by the Arabidopsis UVR8 protein." Science **332**(6025): 103-106.

Rousseaux, M. C., C. L. Ballare, C. V. Giordano, A. L. Scopel, A. M. Zima, M. Szwarcberg-Bracchitta, P. S. Searles, M. M. Caldwell and S. B. Diaz (1999). "Ozone depletion and UVB radiation: impact on plant DNA damage in southern South America." Proc Natl Acad Sci U S A **96**(26): 15310-15315.

Rozema, J., P. Blokker, M. A. Mayoral Fuertes and R. Broekman (2009). "UV-B absorbing compounds in present-day and fossil pollen, spores, cuticles, seed coats and wood: evaluation of a proxy for solar UV radiation." Photochem Photobiol Sci **8**(9): 1233-1243.

Ruuhola, T. M. and M. R. K. Julkunen-Tiitto (2000). “Salicylates of intact Salix myrsinifolia plantlets do not undergo rapid metabolic turnover.” Plant Physiology **122**(3): 895-906.

Sadeghifar, H. and A. Ragauskas (2020). "Lignin as a UV Light Blocker-A Review." Polymers (Basel) **12**(5).

Schreiber, U. (2004). Pulse-Amplitude-Modulation (PAM) Fluorometry and Saturation Pulse Method: An Overview. Chlorophyll a Fluorescence: A Signature of Photosynthesis. G. C. Papageorgiou and Govindjee. Dordrecht, Springer Netherlands**:** 279-319.

Schumaker, M. A., J. H. Bassman, R. Robberecht and G. K. Radamaker (1997). "Growth, leaf anatomy, and physiology of Populus clones in response to solar ultraviolet-B radiation." Tree Physiol **17**(10): 617-626.

Searles, P. S., S. D. Flint, and M. M. Caldwell (2001). "A meta-analysis of plant field studies simulating stratospheric ozone depletion." Oecologia, **127**(1): 1-10.

Searles, P. S., S. D. Flint, S. B. Diaz, M. C. Rousseaux, C. L. Ballare and M. M. Caldwell (1999). "Solar ultraviolet-B radiation influence on Sphagnum bog and Carex fen ecosystems: first field season findings in Tierra del Fuego, Argentina." Global Change Biology **5**(2): 225-234.

Semeniuk, P. (1978). Biological effects of ultraviolet radiation on plant growth and development in florist and nursery crops. Research report on the impacts of ultraviolet-B radiation on biological systems: A study related to stratospheric ozone depletion. Washington, DC, US EPA. **EPA-IAG-DG-0168:** SIRA File 142.210.

Shames, L. (2007). USDA: Information on Classical Plant and Animal Breeding Activities. Washington DC, US GAO**:** 34.

Sharma, A., V. Kumar, B. Shahzad, M. Ramakrishnan, G. P. S. Sidhu, A. S. Bali, N. Handa, D. Kapoor, P. Yadav, K. Khanna and P. Bakshi (2019). "Photosynthetic response of plants under different abiotic stresses: a review." Journal of Plant Growth Regulation: 1-23.

Sharma, S. S. and K. J. Dietz (2006). "The significance of amino acids and amino acid-derived molecules in plant responses and adaptation to heavy metal stress." Journal of Experimental Botany **57**(4): 711-726.

Sigoillot, F. D. and R. W. King (2011). "Vigilance and validation: Keys to success in RNAi screening." ACS chemical biology **6**(1): 47-60.

Singh, S., R. Kumari, M. Agrawal and S. B. Agrawal (2011). "Modification in growth, biomass and yield of radish under supplemental UV-B at different NPK levels." Ecotoxicol Environ Saf **74**(4): 897-903.

Smillie, R. M. and R. Nott, (1982). "Salt tolerance in crop plants monitored by chlorophyll fluorescence in vivo." Plant Physiology **70**(4): 1049-1054.

Solomon, S., D. J. Ivy, D. Kinnison, M. J. Mills, R. R. Neely, 3rd and A. Schmidt (2016). "Emergence of healing in the Antarctic ozone layer." Science **353**(6296): 269-274.

Staehelin, J., N. R. Harris, C. Appenzeller, and J. Eberhard (2001). "Ozone trends: A review." Reviews of Geophysics **39**(2): 231-290.

Stapleton, A. E. (1992). "Ultraviolet radiation and plants: burning questions." The Plant Cell **4**(11): 1353.

Stommel, J. R., G. J. Lightbourn, B. S. Winkel and R. J. Griesbach (2009). "Transcription factor families regulate the anthocyanin biosynthetic pathway in Capsicum annuum." Journal of the American Society for Horticultural Science **134**(2): 244-251.

Strid, A., W. S. Chow and J. M. Anderson (1994). "UV-B damage and protection at the molecular level in plants." Photosynth Res **39**(3): 475-489.

Studer, M. H., J. D. DeMartini, M. F. Davis, R. W. Sykes, B. Davison, M. Keller, G. A. Tuskan and C. E. Wyman (2011). "Lignin content in natural Populus variants affects sugar release." Proc Natl Acad Sci U S A **108**(15): 6300-6305.

Suetsugu, N. and M. Wada (2007). "Chloroplast photorelocation movement mediated by phototropin family proteins in green plants." Biol Chem **388**(9): 927-935.

Sullivan, J. H. (2005). "Possible impacts of changes in UV-B radiation on North American trees and forests." Environmental Pollution **137**(3): 380-389.

Sullivan, J. H., D. C. Gitz, III , M. S. Peek and A. J. McElrone (2003). "Response of three eastern tree species to supplemental UV-B radiation: leaf chemistry and gas exchange." Agricultural and Forest Meteorology **120**(1-4): 219-228.

Sullivan, J. H., D. C. Gitz, III , L. Liu-Gitz, C. Wu, W. Gao and J. Slusser (2007). "Coupling short-term changes in ambient UV-B levels with induction of UV-screening compounds." Photochem Photobiol **83**: 863-870.

Sullivan, J. H., B. S. Howells, C. T. Ruhland and T. A. Day (1996). "Changes in leaf expansion and epidermal screening effectiveness in Liquidambar styraciflua and Pinus taeda in response to UV-B radiation " Physiologia Plantarum **98**: 349-357.

Sullivan, J. H., L. C. Pope, B. M. Sutherland, P. V. Bennett, J. E. Blum, A. Stapleton and D. C. I. Gitz (2010). Assessment of DNA damage as a tool to measure UV-B tolerance. in soybean lines differing in foliar flavonoid composition. UV Radiation in Global Climate Change: Measurements, Modeling and Effects on Ecosystems. W. Gao, D. Smoltz and J. Slusser, Springer-Verlag and Tsinghua University Press**:** 437-457.

Sullivan, J. H. and J. Rozema (1999). UV-B effects on terrestrial plant growth and photosynthesis. Stratospheric Ozone Depletion: The effects of enhanced UV-B radiation on terrestrail ecosystems. J. Rozema. The Netherlands, Backays Publishers**:** 39-57.

Sullivan, J. H. and A. H. Teramura (1988). "Effects of ultraviolet-B irradiation on seedling growth in the Pinaceae." American Journal of Botany **75**: 225-230.

Sullivan, J. H. and A. H. Teramura (1992). "The effects of ultraviolet-B radiation on loblolly pines 2. Growth of field-grown seedlings." Trees **6**: 115-120.

Sullivan, J. H. and A. H. Teramura (1994). "The effects of ultraviolet-B radiation on loblolly pine. 3. Interaction with CO2 enhancement." Plant Cell & Environment **17**: 311-317.

Sullivan, J. H., A. H. Teramura and L. H. Ziska (1992). "Variation in UV-B sensitivity in plants from a 3,000-m elevational gradient in Hawaii." American Journal of Botany **79**: 737-743.

Sutherland, B. M., T. Shinnosuke, J. H. Sullivan and J. C. Sutherland (1996). "Plant responses to changing environmental stress: Cyclobutyl pyrimidine dimer repair in soybean leaves." Photochem Photobiol **64**: 464-468.

Suyama, M., D. Torrents and P. Bork (2006). "PAL2NAL: robust conversion of protein sequence alignments into the corresponding codon alignments." Nucleic acids research **34**(suppl_2): W609-W612.

Takahashi, S. and M. R. Badger (2011). "Photoprotection in plants: a new light on photosystem II damage." Trends Plant Sci **16**(1): 53-60.
Taylor, G. (2002). "Populus: arabidopsis for forestry. Do we need a model tree?" Ann Bot **90**(6): 681-689.

Tegelberg, R. and R. Julkunen-Tiitto (2001). "Quantitative changes in secondary metabolites of dark-leaved willow (Salix myrsinifolia) exposed to enhanced ultraviolet-B radiation." Physiologia Plantarum **113**(4): 541-547.

Teramura, A. H. and M. M. Caldwell (1981). "Effects of ultraviolet-B irradiances on soybean. IV. Leaf ontogeny as a factor in evaluating ultraviolet-B irradiance effects on net photosynthesis." American Journal of Botany **68**(7): 934-941.

Tevini, M. and A. H. Teramura (1989). "UV-B effects on terrestrial plants." Photochemistry and Photobiology **50**(4): 479-487.

Thimijan, R. W. and R. D. Heins (1983). "Photometric, radiometric, and quantum light units of measure: a review of procedures for interconversion." HortScience **18**(6): 818-822.

Tian, J. and J. H. Sullivan (1999). "UV-B radiation effects on leaf anatomy and development of Pinus taeda and Liquidambar styraciflua." Bulletin of the Ecological Society of America: 314.

Tian, J. and J. H. Sullivan (2000). "Field studies on the effects of UV-B radiation on foliar anatomy and morphology in Liquidambar styraciflua and Pinus taeda." Bulletin of the Ecological Society of America: 346.

Tilbrook, K., A. B. Arongaus, M. Binkert, M. Heijde, R. Yin and R. Ulm (2013). "The UVR8 UV-B Photoreceptor: Perception, Signaling and Response." Arabidopsis Book **11**: e0164.

Tohge, T., Y. Nishiyama, M. Y. Hirai, M. Yano, J. Nakajima, M. Awazuhara, E. Inoue, H. Takahashi, D. B. Goodenowe, M. Kitayama, M. Noji, M. Yamazaki and K. Saito (2005). "Functional genomics by integrated analysis of metabolome and transcriptome of Arabidopsis plants over-expressing an MYB transcription factor." Plant J **42**(2): 218-235.

Tossi, V. E., J. J. Regalado, J. Iannicelli, L. E. Laino, H. P. Burrieza, A. S. Escandon and S. I. Pitta-Alvarez (2019). "Beyond Arabidopsis: Differential UV-B Response Mediated by UVR8 in Diverse Species." Front Plant Sci **10**: 780.

Tran, M. H., D.-P. Phan and E. Y. Lee (2021). "Review on lignin modifications toward natural UV protection ingredient for lignin-based sunscreens." Green Chemistry **23**(13): 4633-4646.

Triozzi, P., H. W. Schmidt, C. Dervinis, M. Kirst and D. Conde (2021). "Simple, efficient and open-source CRISPR/Cas9 strategy for multi-site genome editing in Populus tremula x alba." Tree Physiol **tpab066**: 1-12.

Tsai, C.J., W. Guo, B. Babst, B. Nyamdari, Y. Yuan, R. Payyavula, H. Y. Chen, X. Liangjiao, K. Tay, V. Michelizzi and S. Harding (2011). “Salicylate metabolism in Populus.” BMC Proceedings **5**(7): 1-2.

Tsai, C. J., S. A. Harding, T. J. Tschaplinski, R. L. Lindroth and Y. Yuan (2006). "Genome-wide analysis of the structural genes regulating defense phenylpropanoid metabolism in Populus." New Phytol **172**(1): 47-62.

Turnbull, J. D. and S. A. Robinson (2009). "Accumulation of DNA damage in Antarctic mosses: correlations with ultraviolet-B radiation, temperature and turf water content vary among species." Global Change Biology **15**(2): 319-329.

Turunen, M. and K. Latola (2005). "UV-B radiation and acclimation in timberline plants." Environmental Pollution **137**(3): 390-403.

Tuskan, G. A., S. Difazio, S. Jansson, J. Bohlmann, I. Grigoriev, U. Hellsten, N. Putnam, S. Ralph, S. Rombauts, A. Salamov, J. Schein, L. Sterck, A. Aerts, R. R. Bhalerao, R. P. Bhalerao, D. Blaudez, W. Boerjan, A. Brun, A. Brunner, V. Busov, M. Campbell, J. Carlson, M. Chalot, J. Chapman, G. L. Chen, D. Cooper, P. M. Coutinho, J. Couturier, S. Covert, Q. Cronk, R. Cunningham, J. Davis, S. Degroeve, A. Dejardin, C. Depamphilis, J. Detter, B. Dirks, I. Dubchak, S. Duplessis, J. Ehlting, B. Ellis, K. Gendler, D. Goodstein, M. Gribskov, J. Grimwood, A. Groover, L. Gunter, B. Hamberger, B. Heinze, Y. Helariutta, B. Henrissat, D. Holligan, R. Holt, W. Huang, N. Islam-Faridi, S. Jones, M. Jones-Rhoades, R. Jorgensen, C. Joshi, J. Kangasjarvi, J. Karlsson, C. Kelleher, R. Kirkpatrick, M. Kirst, A. Kohler, U. Kalluri, F. Larimer, J. Leebens-Mack, J. C. Leple, P. Locascio, Y. Lou, S. Lucas, F. Martin, B. Montanini, C. Napoli, D. R. Nelson, C. Nelson, K. Nieminen, O. Nilsson, V. Pereda, G. Peter, R. Philippe, G. Pilate, A. Poliakov, J. Razumovskaya, P. Richardson, C. Rinaldi, K. Ritland, P. Rouze, D. Ryaboy, J. Schmutz, J. Schrader, B. Segerman, H. Shin, A. Siddiqui, F. Sterky, A. Terry, C. J. Tsai, E. Uberbacher, P. Unneberg, J. Vahala, K. Wall, S. Wessler, G. Yang, T. Yin, C. Douglas, M. Marra, G. Sandberg, Y. Van de Peer and D. Rokhsar (2006). "The genome of black cottonwood, Populus trichocarpa (Torr. & Gray)." Science **313**(5793): 1596-1604.

Van Acker, R., J. C. Leplé, D. Aerts, V. Storme, G. Goeminne, B. Ivens, F. Légée, C. Lapierre, K. Piens, M. C. Van Montagu, and N. Santoro (2014). “Improved saccharification and ethanol yield from field-grown transgenic poplar deficient in cinnamoyl-CoA reductase.” Proceedings of the National Academy of Sciences **111**(2): 845-850.

Vanholme, R., B. Demedts, K. Morreel, J. Ralph and W. Boerjan (2010). "Lignin biosynthesis and structure." Plant Physiol **153**(3): 895-905.

Vanholme, R., K. Morreel, C. Darrah, P. Oyarce, J. H. Grabber, J. Ralph and W. Boerjan (2012). "Metabolic engineering of novel lignin in biomass crops." New Phytol **196**(4): 978-1000.

Vinyard, D. J., G. M. Ananyev and G. C. Dismukes (2013). "Photosystem II: the reaction center of oxygenic photosynthesis." Annu Rev Biochem **82**: 577-606.

Voelker, S. L., B. Lachenbruch, F. C. Meinzer and S. H. Strauss (2011). "Reduced wood stiffness and strength, and altered stem form, in young antisense 4CL transgenic poplars with reduced lignin contents." New Phytol **189**(4): 1096-1109.

Vogel, J. M. (1994). Identifying and Characterizing the TATA Box Promoter Sequence Element in a Maize Nuclear Gene. The Maize Handbook, Springer**:** 630-633.

Vogt, T. (2010). "Phenylpropanoid biosynthesis." Mol Plant **3**(1): 2-20.

Volkov, V. and M. J. Beilby (2017). "Editorial: Salinity Tolerance in Plants: Mechanisms and Regulation of Ion Transport." Front Plant Sci **8**: 1795.

Wada, N., R. Ueta, Y. Osakabe and K. Osakabe (2020). "Precision genome editing in plants: state-of-the-art in CRISPR/Cas9-based genome engineering." BMC Plant Biol **20**(1): 234.

Waese, J. and N. J. Provart (2016). "The Bio-Analytic Resource: data visualization and analytic tools for multiple levels of plant biology." Current Plant Biology **7**: 2-5.

Wang, D., C. Zhang, B. Wang, B. Li, Q. Wang, D. Liu, H. Wang, Y. Zhou, L. Shi, F. Lan and Y. Wang (2019). "Optimized CRISPR guide RNA design for two high-fidelity Cas9 variants by deep learning." Nat Commun **10**(1): 4284.

Wang, J., H. Wu, Y. Chen and T. Yin (2020). "Efficient CRISPR/Cas9-Mediated Gene Editing in an Interspecific Hybrid Poplar With a Highly Heterozygous Genome." Front Plant Sci **11**: 996.

Wang, Q. W., J. Hidema and K. Hikosaka (2014). "Is UV-induced DNA damage greater at higher elevation?" Am J Bot **101**(5): 796-802.

Wargent, J. J. and B. R. Jordan (2013). "From ozone depletion to agriculture: understanding the role of UV radiation in sustainable crop production." New Phytol **197**(4): 1058-1076.

Warren, J. M., J. H. Bassman, J. K. Fellman, D. S. Mattinson and S. Eigenbrode (2003). "Ultraviolet-B radiation alters phenolic salicylate and flavonoid composition of Populus trichocarpa leaves." Tree Physiol **23**(8): 527-535.

Wei, N., L. Zhang, H. Huang, Y. Chen, J. Zheng, X. Zhou, F. Yi, Q. Du and Z. Liang (2012). "siRNA has greatly elevated mismatch tolerance at 3'-UTR sites." PLoS One **7**(11): e49309.

Weselake, R. J., S. D. Singer and G. Chen (2018). Introduction to plant biomolecules and cellular metabolism Plant Bioproducts. New York, Springer**:** 9-25.

Winkel-Shirley, B. (2002). "Biosynthesis of flavonoids and effects of stress." Curr Opin Plant Biol **5**(3): 218-223.

Wojcik, E. Z., C. Singleton, L. N. Chapman, D. A. Parker, and J. Love (2001). "Plant Biomass as Biofuels." eLS 1-11.

Woodward, F. I. (2007). "Global primary production." Curr Biol **17**(8): R269-273.

Wu, D., Q. Hu, Z. Yan, W. Chen, C. Yan, X. Huang, J. Zhang, P. Yang, H. Deng, J. Wang, X. Deng and Y. Shi (2012). "Structural basis of ultraviolet-B perception by UVR8." Nature **484**(7393): 214-219.

Xiong, F. S. and T. A. Day (2001). "Effect of Solar Ultraviolet-B Radiation during Springtime Ozone Depletion on Photosynthesis and Biomass Production of Antarctic Vascular Plants." Plant Physiol **123**(2): 738–751.

Xu, C., S. Natarajan and J. H. Sullivan (2008). "Impact of Solar Ultraviolet-B radiation on the antioxidant defense system in soybean lines differing in flavonoids biosynthesis." Environmental and Experimental Botany **63**: 39-48.

Xu, C., J. H. Sullivan and S. Natarajan (2010). Ultraviolet-B induced oxidative stress: Flavonoids as an antioxidant defense system in plants. Oxidative stress: Role of Antioxidants in Plants. P. Ahmad and S. Umar, Stadium Press LLD.

Yan, X., J. Liu, H. Kim, B. Liu, X. Huang, Z. Yang, Y. J. Lin, H. Chen, C. Yang, J. P. Wang, D. C. Muddiman, J. Ralph, R. R. Sederoff, Q. Li and V. L. Chiang (2019). "CAD1 and CCR2 protein complex formation in monolignol biosynthesis in Populus trichocarpa." New Phytol **222**(1): 244-260.

Yang, Y., T. Liang, L. Zhang, K. Shao, X. Gu, R. Shang, N. Shi, X. Li, P. Zhang and H. Liu (2018). "UVR8 interacts with WRKY36 to regulate HY5 transcription and hypocotyl elongation in Arabidopsis." Nat Plants **4**(2): 98-107.

Yang, Y., L. Zhang, P. Chen, T. Liang, X. Li and H. Liu (2020). "UV-B photoreceptor UVR8 interacts with MYB73/MYB77 to regulate auxin responses and lateral root development." EMBO J **39**(2): e101928.

Yokawa, K., T. Kagenishi and F. Baluska (2015). "UV-B Induced Generation of Reactive Oxygen Species Promotes Formation of BFA-Induced Compartments in Cells of Arabidopsis Root Apices." Front Plant Sci **6**: 1162.

Zaidi, S. S., M. S. Mukhtar and S. Mansoor (2018). "Genome Editing: Targeting Susceptibility Genes for Plant Disease Resistance." Trends Biotechnol **36**(9): 898-906.

Zeng, X., Z. Ren, Q. Wu, J. Fan, P. P. Peng, K. Tang, R. Zhang, K. H. Zhao and X. Yang (2015). "Dynamic Crystallography Reveals Early Signalling Events in Ultraviolet Photoreceptor UVR8." Nat Plants **1**.

Zerefos, C. S., D. S. Balis, A. F. Bais, D. Gillotay, P. C. Simon, B. Mayer and G. Seckmeyer (1997). "Variability of UV-B at four stations in Europe." Geophysical Research Letters **24**(11): 1363-1366.

Zhang, Y., E. Butelli, S. Alseekh, T. Tohge, G. Rallapalli, J. Luo, P. G. Kawar, L. Hill, A. Santino, A. R. Fernie and C. Martin (2015). "Multi-level engineering facilitates the production of phenylpropanoid compounds in tomato." Nat Commun **6**: 8635.

Zhang, Y., A. A. Malzahn, S. Sretenovic and Y. Qi (2019). "The emerging and uncultivated potential of CRISPR technology in plant science." Nat Plants **5**(8): 778-794.

Zheng, G., B. O. Tian, F. Zhang, F. Tao and W. Li (2011). "Plant adaptation to frequent alterations between high and low temperatures: remodelling of membrane lipids and maintenance of unsaturation levels." Plant, cell and environmnent **34**(9): 1431-1442.

Zhou, X., T. B. Jacobs, L. J. Xue, S. A. Harding and C. J. Tsai (2015). "Exploiting SNPs for biallelic CRISPR mutations in the outcrossing woody perennial Populus reveals 4-coumarate:CoA ligase specificity and redundancy." New Phytol **208**(2): 298-301.

Zhu, H., C. Li and C. Gao (2020). "Applications of CRISPR-Cas in agriculture and plant biotechnology." Nat Rev Mol Cell Biol **21**(11): 661-677.

Ziska, L. H., A. H. Teramura and J. H. Sullivan (1992). "Physiological sensitivity of plants along an elevational gradient to UV-B radiation." Am J Bot **79**(8): 863-871.

Zwaenepoel, A. and Y. Van de Peer (2019). "wgd—simple command line tools for the analysis of ancient whole-genome duplications." Bioinformatics **35**(12): 2153-2155.